Hydro-morphodynamics of open-channel confluences with low discharge ratio and dominant tributary sediment supply

PAR

Sebastián GUILLÉN LUDEÑA

ÉCOLE POLYTECHNIQUE
FÉDÉRALE DE LAUSANNE

Suisse
2015

Abstract

Hydro-morphodynamics of open-channel confluences with low discharge ratio and dominant tributary sediment supply

River confluences in which the tributary supplies the dominant sediment load, and the flow discharge is abundantly provided by the main river, are typically observed in mountain-river basins. In the Upper-Rhone river basin in Switzerland, confluences are also characterized by highly channelized rivers as a result of the river training works, which were performed in the last two centuries for flood safety reasons and urban and agricultural development. These works impoverished the fluvial ecosystem and resulted in steep and narrow tributaries that join the main river at high junction angles.

The existent knowledge on the hydrodynamic, morphodynamic and sedimentary processes involved in mountain-river confluences is sparse, since most of the studies on confluence dynamics focus on low land confluences. However, the understanding of the dynamics involved in this type of confluence constitutes an essential tool for recovering total or partially the degraded ecosystems by means of restoration projects. In this context, the present research study aims to deepen the knowledge on the hydro-morphodynamics and sedimentology of mountain-river confluences inspired in those of the Upper-Rhone river basin.

For that purpose twelve laboratory experiments were conducted in two experimental facilities: one located at the Laboratory of Hydraulic Constructions of the École Polytechnique Fédérale de Lausanne (LCH-EPFL), and the other one located at the Instituto Superior Técnico de Lisboa (IST-UL). The experimental setup covered a wide range of configurations including three unit-discharge ratios ($q_r = q_t/q_m = 0.37$, 0.50, and 0.77), two junction angles ($\alpha = 90°$ and 70°), two sediment mixtures with different gradation coefficients ($\sigma = 4.51$ and 1.35), and two width ratios ($B_t/B_m = 0.30$ and 0.15). The experiments were performed under movable bed conditions and with continuous sediment supply to both flumes, which represents a novelty in the study of this type of confluence. The sediment rates were $Q_{st} = 0.5$ *kg/min* for tributary and $Q_{sm} = 0.3$ or 0.6 *kg/min* for the main channel, depending on the width ratio.

Systematic surveys of bed topography and water surface were recorded at different instants during the experiments and at equilibrium condition. This condition was attained when the outgoing sediment transport rate was similar to the incoming rate and the bed topography had attained a quasi-steady state. Additionally and also at equilibrium, point velocities were measured and the spatial and grain size distribution of the bed sediments were analyzed. These measurements allowed the analysis of the influence of the discharge ratio, junction angle, sediment gradation and width ratio on the hydro-morphodynamics of open channel confluences.

The bed morphology and hydrodynamics displayed some common features in all the experiments. The main morphological features were: i) a bank-attached bar along the inner bank of the main channel downstream of the confluence, ii) a scour hole which

extended from the tributary mouth to the opposite bank flanking the bar, and iii) a tributary-mouth bar which produced a marked bed discordance between the tributary and main channel. Regarding the hydrodynamics, the following features were observed in all the experiments: i) a M1-type backwater curve induced by the tributary inflow in the upstream reach of the main channel, ii) stagnation zone characterized by a local increase of the water surface and eventually by sediment deposition at the upstream junction corner, iii) a zone of reduced flow velocities which promoted deposition at the downstream junction corner, iv) flow upwelling associated with a low pressure zone at the downstream junction corner, v) a zone of flow deflection where each flow deviated each other to become aligned with the post-confluence channel, vi) a shear layer which separated the flows coming from the tributary and main channel at the post-confluence, vii) a zone of flow acceleration downstream of the confluence, and viii) a recovery zone downstream of the confluence, where the flow tended to uniform conditions by adopting a nearly constant flow-depth.

The bed discordance together with the bank-attached bar and the flow deflection zone played an essential role in the hydro-morphodynamics of the confluence that, in general terms, can be described as follows: the near-surface flow of the main channel was deflected toward the outer bank by the tributary inflow, whereas the near-bed fraction flowed unimpeded downstream, protected by the bed discordance, until reaching the bank-attached bar. This bar steered the near-bed flow towards the outer bank where both deflected flows converged and accelerate eroding the bed. In addition, the continuous supply of sediment to the main channel inhibited the bed armoring and contributed to the bed erosion along the outer bank.

The dynamics of the confluence were influenced by each of the tested parameters. For instance, increasing discharge ratios resulted in deeper scour holes at the tributary mouth, less penetration of the tributary-mouth bar into the main channel, and lower bed slopes in the upstream reach of the tributary. The size of the bank-attached bar increased with the discharge ratio with uniform sediments, whereas with non-uniform sediments the size of the bar decreased as the discharge ratio increased. Regarding hydrodynamics, increasing discharge ratios increased the distance to where the post-confluence flow becomes uniform. The energy loss induced by the tributary inflow in the main channel and the geomorphic work made by the flow resulting from the junction also increased with the discharge ratio.

The junction angle was also a major control of the hydro-morphodynamics of the confluence. With a junction angle of $\alpha = 70°$, the alignment of tributary and main stream was enhanced, which in turn favored the penetration of the tributary-mouth bar into the main channel with respect to $\alpha = 90°$. The further penetration of the tributary-mouth bar eased the transference of the tributary sediment load to the main stream and increased the size of the bank-attached bar compared to $\alpha = 90°$. On the one side, the larger bank-attached bar increased the outward flow deflection and concentration at the outer bank, which resulted in deeper erosion at that location. On the other side, the eased delivery of the tributary sediment load in the main channel led to a lower bed elevation in the tributary with $\alpha = 70°$ with respect to $\alpha = 90°$. In contrast, with $\alpha = 90°$

the hydro-morphodynamics of the confluence evolved to increase the available sediment transport capacity of the tributary to convey the imposed sediment load to the main channel. This evolution resulted in higher bed elevations and lower flow depths in the tributary, which together with the steep bed slope led to critical or supercritical flows, depending on the discharge ratio. With $\alpha = 90°$, a hydraulic jump occurred at the tributary mouth when the flow regime was supercritical. This hydraulic jump reduced the velocity of the tributary flow before it entered the main channel and consequently reduced the tributary-induced energy loss in the main channel. Therefore, for those discharge ratios in which the tributary flow regime was supercritical with $\alpha = 90°$, the tributary-induced energy loss in the main channel was lower than with $\alpha = 70°$.

The sediment gradation was another influential parameter on the hydro-morphodynamics of the confluence. The experiments performed with sediments with high gradation coefficient (σ) presented higher gradients in the bed morphology and water surface in comparison with the experiments performed with sediments with low σ. With non-uniform sediments (high σ) the hydro-morphodynamics needed to evolve to convey the wide range of particle sizes of the sediment mixture. This evolution resulted in larger bank-attached bars, deeper scour holes, steeper tributary bed slopes, and steeper slopes of the water surface in comparison to the experiments performed with uniform sediments (low σ). In addition, the high gradation of the non-uniform sediment mixtures promoted the bed armoring and inhibited the formation of bedforms. With uniform sediments (low σ), the bed morphology and water surface exhibited attenuated features with respect to those observed with non-uniform sediments. Also, the relative excess of sediment transport capacity together with the low gradation of the sediment mixture promoted the formation of migrating dunes, which masked some morphological features such as the scour hole and the bank-attached bar.

The influence of the ratio between the width of tributary and the width of the main channel (B_t/B_m) on the confluence morphodynamics was also analyzed in this research study. With $B_t/B_m = 0.15$ the size of the bank attached bar and the depth of the scour hole increased with respect to the results obtained with $B_t/B_m = 0.30$. These patterns may be related to the unit-momentum flux ratio ($m_r = m_t/m_m$), which was higher with $B_t/B_m = 0.15$ than with $B_t/B_m = 0.30$. In addition, a meandering flow was observed downstream of the confluence with $B_t/B_m = 0.30$ but not for $B_t/B_m = 0.15$, which may indicate that the larger width ratio promoted such a perturbation of the flow.

In summary, this research study presents a broad analysis of the hydrodynamic, morphodynamic and sedimentary processes involved in confluences characterized by low discharge ratios, and where the dominant sediment load is supplied by the tributary. This analysis contributes to widen the existent knowledge on the dynamics of this type of confluence and constitutes a benchmark for further studies, as well as a valuable tool for restoration projects.

Keywords: open-channel confluences, discharge ratio, junction angle, sediment gradation, width ratio, sediment transport, bed armoring, bedforms, energy loss, geomorphic work, hydraulic jump.

Résumé

Hydro-morphodynamique des confluences en canaux ouverts avec de faibles ratios de débits et une fourniture sédimentaire dominante de l'affluant

Les confluences de rivières dans lesquelles la charge principale de sédiments est fournie par l'affluant et le débit majoritaire par la rivière principale sont usuellement observées dans les bassins montagneux. Dans le bassin du Haut Rhône, en Suisse, les confluences sont également caractérisées par des rivières très canalisées de par les travaux réalisés les deux derniers siècles pour des raisons sécuritaires ainsi que pour le développement urbain et agricole. Ces transformations ont appauvri l'écosystème fluvial et il en résulte des affluents étroits et à forte pente rejoignant la rivière principale avec de grands angles de jonction.

L'état des connaissances sur l'hydrodynamique, la morphodynamique et les processus sédimentaires des confluences de rivières de montagne est épars. En effet, la plupart des études sur la dynamique des confluences portent sur les rivières de plaines. La compréhension des dynamiques impliquées dans les confluences en régions montagneuses est donc un outil essentiel pour recouvrer—partiellement ou totalement— les écosystèmes dégradés, de par des projets de restauration. Dans ce contexte, cette étude a pour but d'approfondir la compréhension de l'hydro-morphodynamique et la sédimentologie des confluences de rivières en montagne, notamment dans le cas du bassin du Haut Rhône.

Dans cet objectif, douze expériences de laboratoire ont été conduites dans deux installations expérimentales : l'une située au Laboratoire de Constructions Hydrauliques de l'Ecole Polytechnique Fédérale de Lausanne (LCH-EPFL), et l'autre à l'Instituto Superior Técnico de Lisboa (IST-UL). Ces installations ont permis la couverture d'un grand nombre de configurations incluant trois ratios de débits unitaires ($q_r = q_t/q_m$ = 0.37, 0.50, et 0.77), deux angles de jonction (α = 90° et 70°), deux mélanges de sédiments avec des coefficients de gradation différents (σ = 4.15 et 1.35), et deux ratios de largeurs (B_t/B_m = 0.30 et 0.15). Les expériences ont été réalisées dans des conditions de lit mobile et un apport continu en sédiments dans les deux canaux, cette dernière caractéristique représentant une innovation importante dans l'étude de ce type de confluence. Les flux de sédiments qui ont été testés sont Q_{st} = 0.5 *kg/min* pour l'affluant et Q_{sm} = 0.3 ou 0.6 *kg/min* pour le canal principal, dépendant du ratio des largeurs.

Des relevés systématiques de la topographie du lit ainsi que de la surface libre ont été enregistrés à différents instants pendant les expériences, et une fois la situation d'équilibre atteinte. Cette condition était satisfaite lorsque les flux sédimentaires à l'entrée et la sortie étaient quasi-identiques, et lorsque la topographie du lit devenait quasi-invariable. De plus et toujours en situation d'équilibre, des mesures de vélocité ponctuelles ont été effectuées et les distributions spatiales et granulométriques des

sédiments du lit ont été analysées. Ces mesures ont permis d'étudier l'influence du ratio de débits, de l'angle de jonction, de la gradation sédimentaire et du ratio de largeurs sur l'hydro-morphodynamique des confluences de canaux à surface libre.

La morphologie et l'hydrodynamique du lit ont montrés des particularités communes dans toutes les expériences. Les caractéristiques morphologiques principales ont été : i) un banc latéral le long de la rive intérieure à l'aval de la confluence ; ii) une zone d'affouillement s'étendant de l'embouchure de l'affluent jusqu'à la rive opposée, traversant le banc attaché à la rive intérieure ; et iii) une barre traversant l'embouchure de l'affluent qui produit une remarquable discordance de lits entre le canal principal et l'affluent. Concernant l'hydrodynamique, les caractéristiques principales suivantes ont été observées dans toutes les expériences : i) une courbe de remous de type M1 induite par l'écoulement de l'affluent dans le canal principal ; ii) une zone de stagnation dans le coin amont de la jonction, caractérisée par une augmentation locale du niveau d'eau, et occasionnellement par une déposition de sédiments ; iii) une zone de vélocités réduites favorisant la déposition dans le coin aval de la jonction ; iv) un écoulement ascendant associé à une zone de réduction de pression dans le coin aval de la jonction ; v) une de déflection des écoulements où chaque écoulement se détourne de l'autre avant de se réaligner dans la zone post-confluence ; vi) une couche de séparation des écoulements venant de l'affluent et du canal principal à la post-confluence ; vii) une zone d'accélération à l'aval de la confluence ; and viii) une zone de recouvrement à l'aval de la confluence, où l'écoulement tend vers des conditions uniformes en adoptant une hauteur d'écoulement quasi-constante.

La discordance du lit, le banc attaché à la rive et la zone de déflection de l'écoulement jouent un rôle essentiel dans l'hydrodynamique de la confluence qui, en termes généraux, peut être écrite comme suit : l'écoulement superficiel du canal principal est dévié vers la rive extérieure par l'écoulement de l'affluent, tandis que la fraction de l'écoulement plus proche du lit coule librement vers l'aval, protégée par les discordances du lit, jusqu'à atteindre le banc attaché à la rive intérieure. Là, le banc dirige l'écoulement proche du lit vers l'autre rive où les deux écoulements séparés convergent et accélèrent, érodant le lit. De plus, l'apport continu de sédiment dans le canal principal empêche le développement d'une couche de pavage et contribue à l'érosion du lit le long de la rive extérieure.

La dynamique de la confluence a été influencée par chacun des paramètres testés. Par exemple, augmenter le ratio des débits a résulté en une zone d'affouillement plus profonde à l'embouchure de l'affluent, une réduction de la pénétration de la barre d'embouchure dans le canal principal, et des pentes de lit plus faibles à l'arrivée amont de l'affluent. La taille du banc latéral a augmenté avec le ratio de débits avec des sédiments uniformes, tandis qu'avec des sédiments non-uniformes la taille du banc a diminué avec l'augmentation du ratio. Concernant l'hydrodynamique, l'augmentation du ratio de débits a augmenté la distance à laquelle l'écoulement post-confluence devient uniforme. Les pertes d'énergie provoquée par l'écoulement de l'affluent dans le

canal principal et le travail géo-morphique effectué par l'écoulement résultant de la jonction ont également augmenté avec l'augmentation du ratio des débits.

L'angle de jonction a également eu un effet important sur l'hydro-morphodynamique de la confluence. Avec un angle $\alpha = 70°$, l'alignement des lignes de courant de l'affluent et du canal principal a été meilleur, favorisant la pénétration de la barre de l'embouchure de l'affluent dans le canal principal, par rapport à $\alpha = 90°$. La pénétration plus conséquente de la barre d'embouchure de l'affluent a facilité le transfert de la charge de sédiment de l'affluent vers le courant principal, augmentant la taille du banc latéral sur la rive intérieure comparé à $\alpha = 90°$. D'un côté, un banc latéral sur la rive intérieure plus important a renforcé la déflection de l'écoulement sortant et sa concentration vers la rive extérieure, favorisant une plus grande érosion à cet endroit. D'un autre côté, l'apport favorisé de la charge en sédiments de l'affluent dans le canal principal a conduit à une plus basse élévation du lit de l'affluent avec $\alpha = 70°$ par rapport à $\alpha = 90°$. Au contraire, avec $\alpha = 90°$ l'hydro-morphodynamique de la confluence a évolué afin d'augmenter la capacité de transport sédimentaire de l'affluent permettant de transférer la charge imposée au canal principal. Cette évolution a conduit des élévations du lit plus élevées et des hauteurs d'écoulement plus faibles dans l'affluent. Cela ajouté à une pente de lit plus raide a conduit à des écoulements critiques ou torrentiels, dépendant du ratio de débits. Avec $\alpha = 90°$, un ressaut hydraulique s'est mis en place à l'embouchure lorsque le régime était torrentiel. Ce ressaut a réduit la vélocité de l'écoulement affluent avant qu'il n'entre dans le canal principal, réduisant ainsi la perte d'énergie dans ce dernier due à l'affluent. En conséquence, pour les ratios de débit pour lesquels l'écoulement dans l'affluent était torrentiel avec $\alpha = 90°$, les pertes d'énergie induites dans le canal principal étaient plus faibles qu'avec $\alpha = 70°$.

La gradation des sédiments a également été un autre paramètre influent sur l'hydro-morphodynamique de la confluence. Les expériences conduites avec des sédiments avec un grand coefficient de gradation (σ) ont présenté de plus grands gradients dans la morphologie du lit et la hauteur d'eau en comparaison avec les expériences conduites avec un faible σ. Avec des sédiments non-uniformes (grand σ) l'hydro-morphodynamique avait besoin d'évoluer pour transporter un large intervalle de diamètres de particules du mélange sédimentaire. Cette évolution a conduit à de plus importants bancs latéraux sur la rive intérieure, de plus profonds affouillements, des pentes plus raides du lit de l'affluent, et des pentes de surface d'écoulement plus raides plus raides en comparaison avec les expériences conduites avec des sédiments uniformes (faible σ). De plus, la grande gradation de mélange non-uniforme de sédiments a favorisé le développement d'une couche de pavage, défavorisant ainsi la formation de dunes. Avec des sédiments uniformes (faible σ), la morphologie du lit et la surface d'écoulement ont été moins affectés par les processus précédemment décrits avec des sédiments non-uniformes. Enfin, l'excès relatif de la capacité de transport en sédiments associé à une faible gradation du mélange en sédiments a favorisé la formation de dunes migratoires, masquant certains aspects morphologiques tels l'affouillement et le banc latéral.

L'influence du ratio des largeurs de l'affluent et du canal principal (B_t/B_m) sur la morphodynamique de la confluence a également été étudiée dans ce projet de recherche. Avec $B_t/B_m = 0.15$ la taille du banc latéral sur la rive intérieure et la profondeur de l'affouillement a augmenté par rapport aux résultats obtenus avec $B_t/B_m = 0.30$. Ces tendances peuvent être dues au ratio des quantités de mouvement unitaires des écoulements ($m_r = m_t/m_m$), qui était supérieurs avec $B_t/B_m = 0.15$ qu'avec $B_t/B_m = 0.30$. De plus, un écoulement en méandres a été observé à l'aval de la confluence avec $B_t/B_m = 0.30$, mais non avec $B_t/B_m = 0.15$, ceci pouvant indiquer qu'un ratio de largeurs plus grand favorise une telle perturbation de l'écoulement.

En résumé, ce projet de recherche présente une analyse étendue de l'hydrodynamique, la morphodynamique et des processus sédimentaires qui ont lieu dans les confluences caractérisées par de faibles ratios de débits, et ou la charge dominante en sédiments est apportée par l'affluent. Cette analyse contribue à élargir l'état des connaissances sur la dynamique de ce type de confluence et constitue non seulement une référence pour de futures études, mais également un outil important pour des projets de restauration.

Mots-clés: Confluences dans canaux ouverts, ratio de décharge, angle de jonction, gradation de sédiments, ratio de largeur, transport de sédiment, perte d'énergie, travaux géo-morphiques, resaut hydraulique.

Resumen

Hidro-morfodinámica de confluencias en canales abiertos con bajo ratio de caudal y con un aporte de sedimentos dominante desde el afluente.

Confluencias fluviales en las que la carga de sedimentos dominante es suministrada por los afluentes, y el flujo de agua es proporcionado de manera abundante por el rio principal, son comunes en cuencas de montaña. En Suiza, en la cuenca del alto Ródano, las confluencias fluviales están caracterizadas además por afluentes fuertemente canalizados como resultado de encauzamientos, que fueron realizados durante los últimos doscientos años para la protección contra inundaciones y para el desarrollo agrario y urbanístico. Estas canalizaciones empobrecieron el ecosistema fluvial y dieron lugar a estrechos afluentes con fuertes pendientes y a pronunciados ángulos en la confluencia.

El conocimiento existente sobre procesos hidrodinámicos, morfodinámicos y sedimentarios involucrados en la dinámica de confluencias de ríos de montaña es escaso, puesto que la mayoría de los estudios sobre la dinámica de confluencias están enfocados a confluencias de ríos de planicie. No obstante, el conocimiento de la dinámica de este tipo de confluencias constituye una herramienta fundamental para la recuperación total o parcial de los ecosistemas degradados por medio de proyectos de rehabilitación.

Con este propósito, doce experimentos fueron realizados en dos instalaciones experimentales: una situada en el Laboratoire de Constructions Hydrauliques de la École Polytechnique Fédérale de Lausanne (LCH-EPFL), y la otra situada en el Instituto Superior Técnico de la Universidad de Lisboa (IST-UL). Estos experimentos cubren un amplio rango de configuraciones que incluyen tres ratios de caudal unitario ($q_r = q_t/q_m = 0.37$, 0.50, and 0.77), dos ángulos de confluencia (α = 90° and 70°), dos mezclas de sedimentos con diferentes coeficientes de gradación (σ = 4.51 and 1.35), y dos ratios de anchura (B_t/B_m = 0.30 and 0.15). Los experimentos fueron realizados con lecho móvil y con suministro continuo de sedimentos en ambos canales, lo que representa una novedad en el estudio de este tipo de confluencias. Las tasas de suministro de sedimentos fueron para el Q_{st} = 0.5 *kg/min* afluente y Q_{sm} = 0.3 or 0.6 *kg/min* para el principal, en función del ratio de anchura.

Las topografías del fondo y de la superficie del agua fueron medidas sistemáticamente en diferentes instantes del experimento y en condición de equilibrio. Esta condición consiste en que la tasa de sedimentos saliente es próxima a la tasa total suministrada y la topografía del fondo alcanza un estado quasi-estacionario. Adicionalmente y también en equilibrio, la velocidad del flujo fue medida en varios puntos de la confluencia y la granulometría del fondo fue analizada. Estas mediciones permitieron analizar la influencia del ratio de caudal, del ángulo de confluencia, de la gradación de los sedimentos y del ratio de anchura sobre la hidro-morfodinámica de confluencias de canales abiertos.

La morfología del lecho e hidrodinámica presentaron formas comunes en todos los experimentos. Las principales formas morfológicas eran: i) una barra de deposición a lo largo de la pared interior del canal principal aguas abajo de la confluencia, ii) una socavación que se extendía desde la boca del afluente hasta la pared exterior flaqueando la

barra, y iii) una barra en la boca del afluente que producía una discordancia acusada de nivel entre el fondo del afluente y el del canal principal. Respecto a la hidrodinámica, las siguientes formas fueron observadas en todos los experimentos: i) una curva de remanso tipo M1 inducida por el influjo afluente aguas arriba de la confluencia, ii) una zona de estagnación caracterizada por un incremento local de la superficie de agua y eventualmente por una deposición en la esquina aguas arriba de la confluencia, iii) una zona de velocidad reducida que favorecía la deposición en la esquina aguas abajo de la confluencia, iv) flujo vertical ascendente asociado con una zona de baja presión en la esquina aguas abajo, v) una zona de deflexión del flujo donde ambos flujos confluentes se desviaban recíprocamente para quedar alineados con el canal aguas abajo de la confluencia, vi) una capa de esfuerzo cortante que separaba los flujos provenientes del afluente y del principal aguas abajo de la confluencia, vii) una zona de aceleración del flujo aguas abajo de la confluencia, y viii) una zona de recuperación, donde el flujo tendía a ser uniforme adoptando un calado constante.

La discordancia de nivel de fondo junto con la barra de deposición y la zona de deflexión de flujo jugaron un papel fundamental en la hidro-morfodinámica de la confluencia, que en términos generales puede ser descrita como sigue: la parte superior del flujo del canal principal era desviada hacia la pared exterior del canal por el influjo afluente, mientras que la parte inferior fluía sin impedimento hacia aguas abajo, protegida por la discordancia de fondo, hasta alcanzar la barra de deposición. Esta barra deflectaba el flujo inferior hacia la pared exterior del canal principal, donde convergía con el flujo superior y aceleraba erosionando el fondo. Adicionalmente, el suministro continuo de sedimentos al canal principal evitó el armado del lecho y contribuyó a la erosión de este a lo largo de la pared exterior.

La dinámica de la confluencia fue afectada por cada uno de los parámetros ensayados. Por ejemplo, el incremento del ratio de caudal dio lugar a socavaciones más profundas, a menores penetraciones de la barra del afluente en el canal principal, y a pendientes de fondo menos pronunciadas en el afluente. El tamaño de la barra de deposición incrementó con el ratio de caudal en los experimentos realizados con sedimentos uniformes (baja gradación), mientras que en aquellos realizados con sedimentos no uniformes (alta gradación) el tamaño de la barra decreció para ratios de caudal crecientes. En cuanto a la hidrodinámica, el incremento del ratio de caudal aumentó la distancia, aguas abajo de la confluencia, a la que el flujo pasaba a ser uniforme. La pérdida de energía inducida por el influjo del afluente en el canal principal y el trabajo geomorfológico realizado por el flujo resultante de la confluencia también aumentaron con el ratio de caudal.

El ángulo de confluencia fue también un factor influyente en la hidro-morfodinámica de la confluencia. Con $\alpha = 70°$, el alineamiento del afluente con el canal principal fue mejorado, lo que a vez favoreció la penetración de la barra del afluente en el canal principal con respecto a $\alpha = 90°$. Esta mayor penetración facilitó la transferencia de la carga de sedimentos del afluente al canal principal e incrementó el tamaño de la barra de deposición comparado con $\alpha = 90°$. Por un lado, la mayor barra de deposición incrementó la deflexión del flujo hacia la pared exterior y su concentración, dando lugar a mayores socavaciones en esta zona. Por otro lado, la transferencia mejorada de la carga de sedimentos llevó a un nivel de fondo en el afluente menos elevado con $\alpha = 70°$ que con $\alpha = 90°$. En cambio, con $\alpha = 90°$ la hidro-morfodinámica de la confluencia tuvo que evolucionar para incrementar la capacidad del afluente para transportar la carga de sedimentos impuesta al canal principal.

Esta evolución dio lugar a un fondo más elevado y a un menor calado en el afluente, que junto con la pronunciada pendiente del fondo derivó en regímenes de flujo críticos o supercríticos, dependiendo del ratio de caudal. Con α = 90°, un resalto hidráulico fue observado en la boca del afluente cuando el flujo era supercrítico. Este resalto redujo la velocidad del flujo del afluente antes de entrar en el canal principal y consecuentemente redujo la pérdida de energía inducida por el afluente en el canal principal. Por lo tanto, para aquello ratios de caudal en los que el régimen de flujo del afluente era supercrítico con α = 90°, la pérdida de energía en el canal principal fue menor que con α = 70°.

La gradación de los sedimentos fue otro parámetro influyente en la hidro-morfodinámica de la confluencia. Los experimentos realizados con sedimentos con alta coeficiente de gradación (σ) presentaron grandes variaciones en la morfología del fondo y la superficie del agua, en comparación con los experimentos realizados con sedimentos con bajo coeficiente de gradación. Con sedimentos no uniformes (bajo σ) la hidro-morfodinámica evolucionó para transportar el amplio rango de tamaños de partículas de la mezcla de sedimentos. Esta evolución derivó en mayores barras de deposición en la pared interior del canal principal, mayores socavaciones, pendientes de fondo más pronunciadas en el afluente y en la superficie del agua, en comparación con los experimentos realizados con sedimentos uniformes (bajo σ). Además, la alta gradación de los sedimentos favoreció el armado del lecho y evitó la formación de formas de fondo. Con sedimentos uniformes (bajo σ), la morfología del fondo y la superficie del agua presentaron formas más atenuadas en comparación con las obtenidas con sedimentos no uniformes. El exceso relativo de capacidad de transporte junto con la baja gradación de los sedimentos dio lugar a la formación de dunas que enmascararon algunas de las formas morfodinámicas como la barra de deposición y la socavación.

La influencia del ratio entre las anchuras del afluente y del canal principal (B_t/B_m) sobre la morfodinámica de la confluencia fue analizada también en este estudio. Con $B_t/B_m = 0.15$ el tamaño de la barra de deposición y la profundidad de socavación era mayor que con $B_t/B_m = 0.30$. Estas diferencias pueden ser relacionadas con el ratio de momento unitario $m_r = m_t/m_m$, que era mayor con $B_t/B_m = 0.15$ que con $B_t/B_m = 0.30$. Adicionalmente, con $B_t/B_m = 0.30$ se observó una tendencia a la formación de meandros aguas abajo de la confluencia, que no fue observada con $B_t/B_m = 0.15$. Esto puede indicar que un incremento en el ratio de anchura puede inducir inestabilidades en la configuración planimétrica del flujo.

En resumen, este estudio presenta un amplio análisis de los procesos hidrodinámicos, morfodinámicos y sedimentarios implicados en confluencias caracterizadas por bajos ratios de caudal, y en las que la carga dominante de sedimentos es suministrada por el afluente. Este análisis contribuye a ampliar el conocimiento existente en este tipo de confluencias y constituye un punto de partida para futuros estudios, además de ser una valiosa herramienta para proyectos de rehabilitación.

Palabras clave: confluencias canales abiertos, ratio de caudal, ángulo de confluencia, gradación de sedimentos, ratio de anchuras, transporte de sedimentos, armado de lecho, formas de fondo, pérdida de energía, trabajo geomorfológico, resalto hidráulico.

List of symbols and acronyms

Roman capital cases

B_m	Width of the main channel upstream of the confluence	[m]
$B_{p\text{-}c}$	Width of the main channel downstream of the confluence	[m]
B_t	Width of the tributary	[m]
B_t/B_m	Width ratio	[-]
C'	Chezy coefficient	$[\text{m}^{0.5}\,\text{s}^{-1}]$
D	Maximum depth of the scour hole at the tributary mouth	[m]
D_*	Particle size parameter of van Rijn	[-]
D_{*dw}	Particle size parameter of van Rijn downstream of the confluence	[-]
D_{*up}	Particle size parameter of van Rijn upstream of the confluence	[-]
Fr	Froude number	[-]
Fr_t	Characteristic Froude number of the tributary	[-]
Fr_{up}	Characteristic Froude number of the main channel upstream of the confluence	[-]
Fr_{dw}	Characteristic Froude number of the main channel downstream of the confluence	[-]
H	Total energy	[m]
H_d	Total energy at the downstream end of the main channel	[m]
J_b	Bed slope	[-]
J_H	Total energy slope	[-]
Jwl	Water surface slope	[-]
K_{st}	Strickler friction coefficient	$[\text{m}^{1/3}\,\text{s}^{-1}]$
L	Lengh of the bank-attached bar	[m]
M	Total momentum	[N]
M_d	Total momentum at the downstream end of the main channel	[N]
M_m	Momentum flux of the main channel upstream of the confluence	[N]
M_r	Momentum flux ratio	[-]
M_t	Momentum flux of the tributary upstream of the confluence	[N]
Q_m	Flow discharge of the main channel upstream of the confluence	$[\text{m}^3\,\text{s}^{-1}]$
Q_r	Discharge ratio between the tributary and main channel discharges	[-]
Q_t	Flow discharge of the tributary upstream of the confluence	$[\text{m}^3\,\text{s}^{-1}]$
$Q_{p\text{-}c}$	Flow discharge downstream of the confluence	$[\text{m}^3\,\text{s}^{-1}]$
Q_{sm}	Sediment flux rate supplied to the main channel	$[\text{kg min}^{-1}]$
Q_{sm}	Sediment flux rate supplied to the tributary	$[\text{kg min}^{-1}]$
R	Resultant force acting on the flow	[N]
R_h	Hydraulic radius	[m]
T	Transport stage parameter of van Rijn	[-]
T_{dw}	Transport stage parameter of van Rijn downstream of the confluence	[-]
T_{up}	Transport stage parameter of van Rijn upstream of the confluence	[-]
U	Mean flow velocity	$[\text{m s}^{-1}]$
U_d	Mean flow velocity at the downstream end of the main channel	$[\text{m s}^{-1}]$
U_m	Characteristic mean flow velocity of the main channel upstream of the confluence	$[\text{m s}^{-1}]$
U_t	Characteristic mean flow velocity of the tributary	$[\text{m s}^{-1}]$
W	Maximum width of the bank-attached bar	[m]
W_g	Geomorphic work	[N m]

Z	Elevation	[m]

Roman lower cases

d_m	Mean particle diameter by weight	[m]
d_{16}, d_{84}, d_{90}	Characteristic particle diameters by weight	[m]
d_{50}	Median particle diameter by weight	[m]
g	Gravitational acceleration	[m/s^2]
h	Normal flow depth	[m]
m_m	Unit-momentum flux of the main channel upstream of the confluence	[N m^{-1}]
m_r	Unit-momentum flux ratio	[-]
m_t	Unit-momentum flux of the tributary upstream of the confluence	[N m^{-1}]
q_m	Unit-discharge of the main channel upstream of the confluence	[m² s^{-1}]
q_r	Unit-dicharge ratio	[-]
q_t	Unit-discharge of the tributary upstream of the confluence	[m² s^{-1}]
s	Specific density	[-]
t	Time	[h]
u^*	Shear velocity	[m s^{-1}]
$u_{*,cr}$	Critical shear velocity	[m s^{-1}]
y	Local flow depth	[m]
y_c	Critical flow depth	[m]
y_{md}	Characteristic flow depth of the main channel downstream of the confluence	[m]
y_{mu}	Characteristic flow depth of the main channel upstream of the confluence	[m]
y_t	Characteristic flow depth of the tributary	[m]

Greek symbols

α	Junction angle	[°]
γ	Specific weight of the water	[N m^{-3}]
Δ	Height of dunes	[m]
ΔH	Energy loss per unit specific weight of the water	[m]
λ	Wave-length of dunes	[m]
λ_M	Wave-length of meandering	[m]
σ	Sediment gradation coefficient	[-]
ν	Kinematic viscosity	[m²/s]

Acronyms

CSA	Cross Sectional Average
GSD	Grain Size Distribution
EPFL	Ecole Polytechnique Fédérale de Lausanne
FCT	Fundação para a Ciência e a Tecnologia
HR	High discharge Ratio
IST	Instituto Superior Técnico
IR	Intermediate discharge Ratio
LCH	Laboratory of Hydraulic Constructions
LR	Low discharge Ratio
UL	Universidade de Lisboa

Este trabajo está dedicado

a mis padres: Sebastián y Ruperta

Table of Contents

List of Figures

List of Tables

<div style="text-align: right">

1

</div>

Introduction

1.1 River confluences

River confluences comprise a main river (or channel) into which one or more tributaries flow. Within the fluvial network, confluences are considered as environmental hot spots, which contribute to the river ecosystem by providing ecological connectivity and heterogeneity in flow, water quality and bed substrate (Benda *et al.*, 2004; Leite Ribeiro *et al.*, 2015). Confluences play also a major role in fluvial transport at the network scale, since it is through the confluence of tributaries with main rivers that the flow and sediment are provided to the latter. In river confluences, the flow and sediment dynamics are characterized by complex three-dimensional patterns. It is through these patterns that the flow dynamics and bed morphology closely interact to accommodate the step changes in flow and sediment transport that occur therein (Gutierrez *et al.*, 2014)

The focus of this research is on river confluences of mountain river basins since this constitutes a gap in existing knowledge of confluence morphodynamics. In this type of confluence, steep and narrow tributaries supply the dominant sediment load to the confluence, whereas the flow discharge is abundantly provided by the main channel. In addition, in the particular case of the Upper-Rhone river basin that inspires this research study, the confluences are characterized by highly channelized tributaries which join the main channel at high junction angles. These tributaries are environmentally disconnected from the main river due to river training works performed in the last two centuries, mainly motivated by agricultural and urban purposes and flood safety reasons (Figure 1.1).
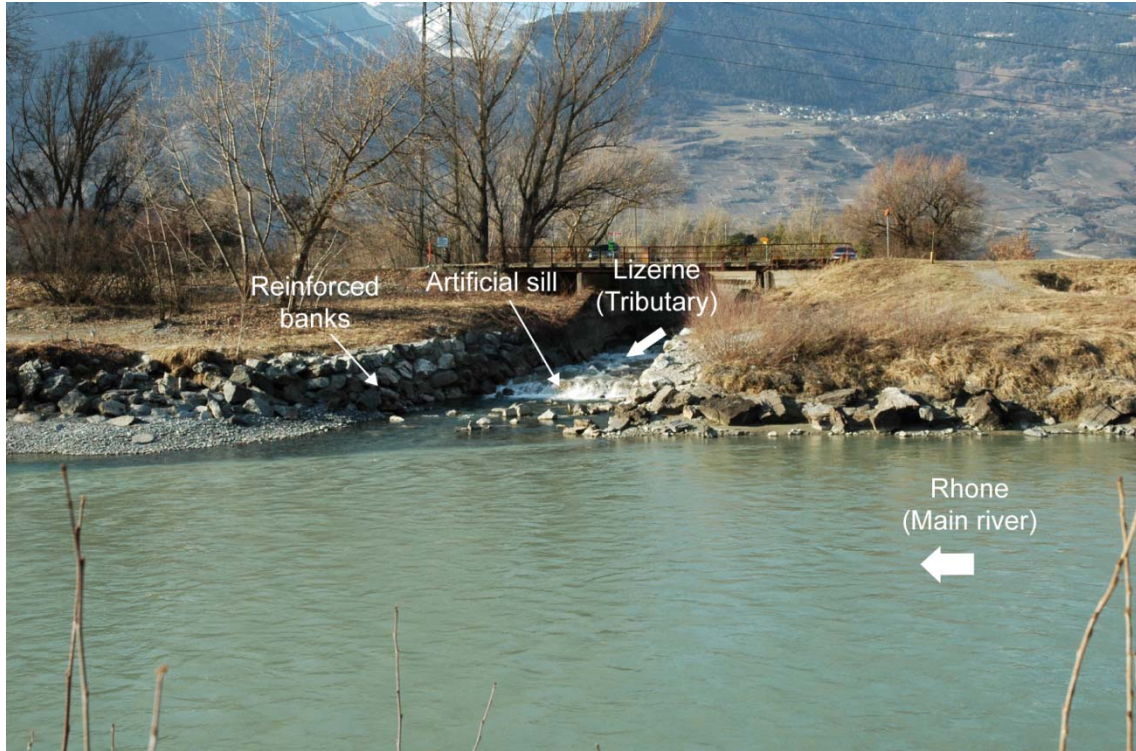
Figure 1.1 Confluence between the Lizerne and Rhone rivers in Switzerland. Source: Rusconi (2012).

From the end of the 20th century, authorities and environmental professionals have become aware of the restoration requirements of rivers that were degraded by human interventions (Bernhardt *et al*., 2005; Reichert *et al*., 2007). The aim of restoration consists of recovering the vital space required by rivers to maintain the quantity and quality of water in the fluvial ecosystem (Havinga *et al*., 2005; Nakamura *et al*., 2006). Restoration projects must therefore pay attention to the complex processes involved in fluvial dynamics and their interaction with environmental and flood protection issues (Peter, 2006).

1.2   Objectives and methods

This thesis builds on the work of Leite Ribeiro (2011), which was one of the first investigations on the Upper-Rhone river confluences based on systematic laboratory experiments. The goal of this thesis was to deepen the knowledge about the hydrodynamic, morphodynamic and sedimentary processes involved in mountain river confluences.

This research study presents the results of twelve laboratory experiments conducted in two experimental facilities, one located at the Laboratory of Hydraulic Constructions (LCH) of the École Polytechnique Fédérale de Lausanne (EPFL), and the other one at the Instituto Superior Técnico of the University of Lisbon (IST-UL). The aim of these experiments was analyzing the influence of several influent parameters on the dynamics of mountain river confluences.

For that purpose, the experimental setup covered a wide range of representative parameters of the Upper-Rhone river basin, such as three discharge ratios, two junction

angles, two sediment mixtures, and two width ratios. The experiments were performed under movable bed conditions and with continuous sediment supply to both flumes, tributary and main channel, which is novel compared to earlier studies. Bed topography and water surface surveys were systematically recorded at different times during the experiments. Additionally, the flow velocity was measured at different points of the confluence and the bed sediments were characterized by their grain size distribution, when the experiments reached equilibrium.

1.3 Structure of the report

This thesis report is organized in three parts with a total of eight chapters, as outlined in Figure 1.2

- In Part I, the context, motivation, objectives, background and methods of the thesis are presented in three chapters:

    - ✓ Chapter 1 highlights the importance of river confluences within the fluvial network, with especial emphasis on confluences of mountain river basins. In this chapter, the main objectives of this study, the methodology undertaken and the structure of this report are presented.

    - ✓ Chapter 2 compiles existing knowledge of the dynamics of river confluences and points out the gaps to be filled by this study. The literature review is made by focusing on the hydrodynamic, morphological and sedimentary processes of river confluences.

    - ✓ Chapter 3 outlines the experimental facilities, measurement equipment and experimental setup.

- Part II presents the results of this research study. It is composed of four complementary studies that correspond to chapters 4 to 7 of this report. Chapters 4 to 6 were written as scientific articles. Chapter 4 was recently published and chapters 5 and 6 have been submitted to peer-reviewed journals. A brief description of Chapters 4 to 7 is given below:

    - ✓ Chapter 4. In this study the evolution of the bed morphology and hydrodynamics of the confluence is described and analyzed. Both hydrodynamics and morphodynamics are characterized by their main features. At equilibrium, the texture of the bed surface is analyzed highlighting the main sediment patterns. In addition, the effects of the sediment supply to the main channel are discussed by comparison with the results of Leite Ribeiro *et al.* (2012a), who only supplied sediment to the tributary.

    - ✓ Chapter 5 focuses on the analysis of the influence of the discharge ratio and the junction angle on the hydro-morphodynamics at equilibrium and on the evolution of the bed morphology. The results correspond to six

experiments in which two junction angles were tested for three discharge ratios.

✓ Chapter 6 analyzes the influence of the sediment gradation on the hydro-morphodynamics of the confluence. This chapter presents the results of six experiments in which two different sediment mixtures were tested for three discharge ratios.

✓ Chapter 7 analyzes the influence of the width ratio on the confluence morphodynamics. The results of six experiments in which three unit-discharge ratios are tested for two width ratios, are presented and discussed.

• In Part III, the main conclusions together with some recommendations for future research on mountain river confluences are given in Chapter 8.

The annexes at the end of the document contain the graphical representation of the measurements made for each experiment.
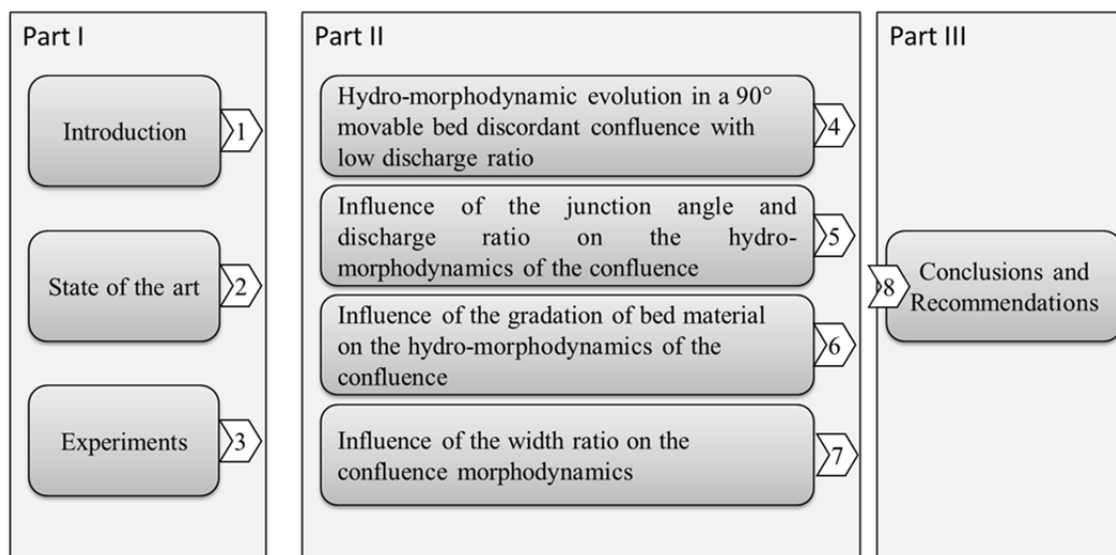
Figure 1.2 Outline of this research study.

2

State of the art

Open-channel confluences are systems characterized by complex hydrodynamic, morphodynamic and sediment transport patterns. These patterns are predominantly influenced by parameters such as the junction angle, the discharge and momentum flux ratios, the ratio between the width of the tributary and the main channel, the gradation of the bed sediment mixtures, the Froude number of each channel, and the ratio between the sediment transport rate and the flow discharge of each channel. This chapter provides a literature review focused on the aforementioned dynamic processes involved in open-channel confluences. Although these processes are strongly related, they are analyzed independently herein for a better understanding of each process. In the end of the chapter, a general assessment of the state of the art based on the literature review is drawn.

2.1   General aspects of open-channel confluences

River confluences are singularities within the fluvial network, where two or more streams converge in a single channel downstream. Depending on the planform geometry, confluences are asymmetrical when the tributaries join laterally a main channel (Figure 2.1a). They can also be symmetrical (Y-shaped) (Figure 2.1b) when the confluent channels join and form a new channel downstream (Mosley, 1976). Channel confluences are characterized by parameters such as the junction angle, denoted by α, and the discharge and momentum flux ratios, defined respectively as:

$$Q_r = \frac{Q_t}{Q_m} \tag{2.1}$$

$$M_r = \frac{\rho Q_t U_t}{\rho Q_m U_m} \tag{2.2}$$

Where Q, U, and ρ denote the flow discharge, mean flow velocity and density of water respectively, and the sub-indexes t and m refer to the tributary and main channel, respectively.
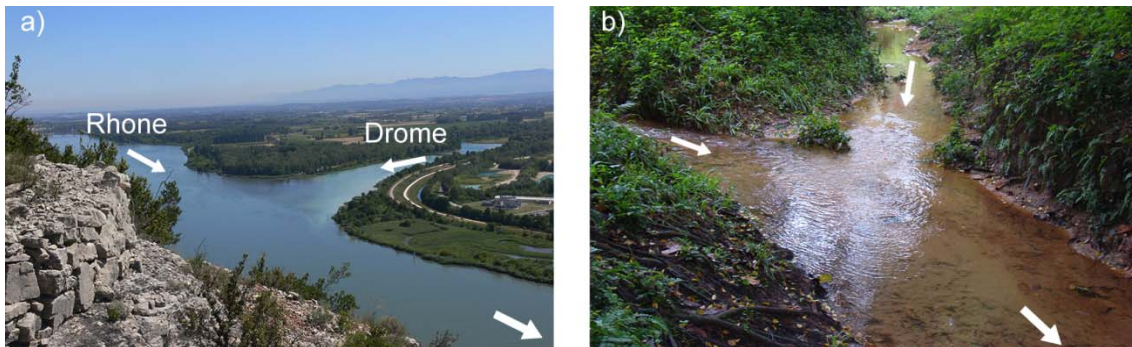
Figure 2.1 a) Asymmetric confluence between Rhone and Drome rivers (Source: www.wikipedia.com). b) Symmetrical (Y-shaped) confluence (Source: www.flickr.com)

Since Taylor (1944) performed the first investigation on channel confluences, many studies have been developed in this field deepening the knowledge of the complex hydrodynamic, morphodynamic and sedimentary processes involved in river confluences. Most of the existent knowledge regarding channel confluences was thoroughly compiled by Rice *et al*. (2008) in an extensive bibliographic review.

2.2   Hydrodynamics in open-channel confluences

The first existent studies on confluence hydrodynamics are those by Taylor (1944) and Webber and Greated (1966), based on one-dimensional approaches. These authors carried out experiments with different junction angles to estimate the relationship between the upstream and downstream flow depths and the energy head-losses in the confluence. Subsequently, Lin and Soong (1979), Ramamurthy *et al*. (1988), Hager (1989), Hsu *et al*. (1998a, b) and Shabayek *et al*. (2002) developed one-dimensional models to determine the flow depth upstream and downstream of the confluence, the energy head losses caused by the confluence, and the momentum transferred from the

tributary to the main channel for different junction angles, discharge ratios, channel widths and flow regimes. All these one-dimensional approaches are based on mass and momentum conservation and neglect wall-friction roughness. The highly three-dimensional character of the flow in the confluence makes necessary the use of empirical correction coefficients in these models.

Best (1987) developed a conceptual hydrodynamic model based on experimental results obtained from an asymmetric confluence with fixed and flat bed. This model consists of six hydrodynamic features (Figure 2.2), which are:

- A stagnation zone at the upstream corner of the confluence. This zone is linked to flow deflection of both streams and it is associated with an increase of pressure and flow depth, and with a decrease of the flow velocity and shear stress.

- A flow deflection zone, where the tributary flow deviates the main stream towards the outer bank of the main channel.

- A zone of flow separation at the downstream junction corner originated by the change of direction experienced by the tributary flow. This zone is associated with flow detachment from the inner bank of the main channel, low pressures, and flow recirculation.

- A maximum velocity or acceleration zone located downstream of the confluence, between the separation zone and the outer bank of the main channel. Here, the flow accelerates reaching a maximum velocity and increasing the shear stress. This zone is created both by the reduction of the effective flow section due to the separation zone, and by the flow concentration at the outer half of the main channel due to the flow deflection.

- Shear layers caused by the strong velocity gradients: one between the recirculation zone and the surrounding flow, and another which separates the flows coming from the tributary and main channel. The latter is referred herein as external shear layer, and it is characterized by high turbulence intensity and shear stress.

- A flow recovery zone where the post-confluence flow restores from the influence of the confluence hydrodynamics.
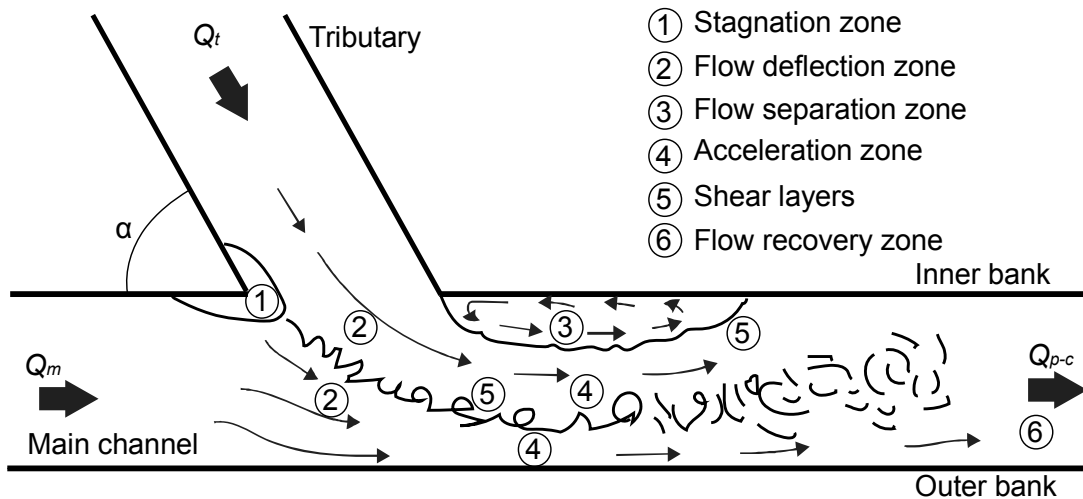
Figure 2.2 Hydrodynamics at open-channel confluences (modified from Best's, 1987).

According to Best (1987), the dominant controls of the confluence hydrodynamics are the discharge ratio and the junction angle. As these parameters increase, the separation zone grows and increasingly dominates the flow dynamics (Best and Reid, 1984; Weber *et al*., 2001; Biron and Lane, 2008; Shakibainia *et al*., 2010; Liu *et al*., 2012).

Best (1987) highlighted as well the importance of the external shear layer as a relevant feature of the confluence, as it is responsible for increased shear stress within the junction. Boyer *et al*. (2006) documented good correlation between the shear stress associated with the shear layer and patterns of sediment transport. The turbulent flow structure associated with the external shear layer and the mixing patterns were studied in natural confluences by Rhoads and Kenworthy (1995), De Serres *et al*. (1999), Rhoads and Sukhodolov (2001, 2004), Sukhodolov and Rhoads (2001); in a laboratory fixed-bed confluence by Weber *et al*. (2001), in a laboratory movable-bed confluence by Leite Ribeiro *et al*. (2012a); and numerically simulated by Lane *et al*. (1999), Bradbrook *et al*. (2001), and Biron *et al*. (2004).

The difference in height between the bed levels of the tributary and main channel, the so-called bed discordance, highly influences the hydrodynamics of confluences. In discordant confluences, the tributary flow deflects the near-surface flow of the main stream towards the outer bank, whereas the near-bed flow is protected by the bed discordance from the tributary inflow (Biron *et al*., 1993, 1996a; Leite Ribeiro *et al*., 2012a). Biron *et al*. (1993) suggested that the bed discordance in the Bayonne-Berthier confluence (in Canada), may be responsible for the absence of separation zone at the downstream junction corner. This statement was verified latter in experimental studies by Biron *et al*. (1996a, b), which reported the following characteristics of the flow dynamics for discordant confluences:

- Absence of deflection of the near-bed flow.

- Presence of flow upwelling and absence of flow recirculation at the downstream junction corner.

- Lack of marked flow acceleration at the post-confluence.

- Enhancement of the turbulent shear stress associated with the external shear layer.

De Serres *et al.* (1999) and Boyer *et al.* (2006) studied the Bayonne-Berthier confluence in Canada for different momentum flux ratios, corroborating the influence of the bed discordance on the confluence hydrodynamics. These studies emphasize the relation between the momentum flux ratio and the position of the external shear layer within the confluence. Low momentum flux ratios ($M_r < 1$) yield a shear layer close to the inner bank of the main channel, whereas high momentum flux ratios ($M_r > 1$) lead to a shift of the shear layer towards the outer bank.

Apart from the hydrodynamic features described by Best (1987), Mosley (1976) reported the presence of two counter-rotating helical flow cells downstream of the confluence, generated by the converging flows and separated by a shear layer. This secondary circulation was widely investigated in the field (Ashmore *et al.*, 1992; Rhoads and Kenworthy, 1995, 1998; Rhoads, 1996; Rhoads and Sukhodolov, 2001; Riley *et al.*, 2015), in the laboratory (Mosley, 1976; Ashmore, 1982; Ashmore and Parker, 1983; McLelland *et al.*, 1996; Weber *et al.*, 2001; Liu *et al.*, 2012) and by means of numerical models (Bradbrook *et al.*, 1998, 2000; Lane *et al.*, 2000).

Rhoads and Kenworthy (1995) argued that these flow structures are comparable to flow through meander bends, since the curvature adopted in the flow deflection zone induces helical cells downstream of the confluence. In asymmetrical confluences, the greater curvature adopted by the tributary inflow entering the main channel, compared with the minor deflection experienced by the main stream, leads to a more developed helical cell on the tributary side of the shear layer (Rhoads and Kenworthy, 1995; Rhoads, 1996; Bradbrook et al., 2000; Rhoads and Sukhodolov, 2001). In contrast, the helical cells in symmetrical confluences were observed to be weak or inexistent by Rhoads and Sukhodolov (2001).

Secondary circulation is influenced by the momentum flux ratio, since the higher this is, the larger is the cell on the tributary side to the detriment of that on the main stream side (Rhoads and Kenworthy, 1995; Rhoads, 1996; Riley *et al.*, 2015). The secondary circulation is also enhanced by bed discordance, planform curvature and junction angle (Lane *et al.*, 1999b; Bradbrook *et al.*, 2000, 2001; Biron *et al.*, 2002; Riley *et al.*, 2015). The numerical study by Bradbrook *et al.* (1998) demonstrates that for specific combinations of depth and velocity ratio, the secondary circulation is generated in absence of planform curvature. Parsons *et al.* (2007) attributed the absence of secondary flow cells in a natural confluence in the Río Paraná (Argentina), to the high form roughness and the high width to depth ratio.

Various studies address the numerical simulation of channel confluences using two-dimensional approaches either for research purposes (Lane and Richards, 1998; Khan *et al.*, 2000; Ghostine *et al.*, 2010), or for case studies (Duan and Schwar, 2003; D'Oria and Tanda, 2006; Roca *et al.*, 2009). Although they report good agreement between numerical results and field or experimental measurements, three-dimensional

models were recommended by Lane *et al.* (1999a) to simulate the confluence hydrodynamics, especially if the two-dimensional numerical model does not implement any correction for the influence of the secondary circulation on the flow structure. Also Lane *et al.* (1999a) argue that three-dimensional models provide more reliable results of bed shear stress and flow field.

Nowadays, the use of three-dimensional models to simulate confluence hydrodynamics is more generalized (Bradbrook *et al.*, 2000, 2001; Huang *et al.*, 2002; Biron *et al.*, 2004; Shakibainia *et al.*, 2010). For these simulations, Lane *et al.* (2000), Parsons (2003), and Baranya and Józsa (2007) recommend the use of unsteady turbulence models to fully capture the intermittent or periodic flow structures due to the presence of shear layers.

2.3 Morphodynamics of open-channel confluences

The morphodynamics of open channel confluences are characterized by complex erosion and deposition processes, resulting from the close interaction between flow dynamics, bed morphology and sediment transport. Best and Rhoads (2008) described the bed morphology of river confluences by means of a conceptual model which consists of five morphological features (Figure 2.3):

- Scour hole that often extends from the tributary mouth to the outer bank of the post-confluence channel. The alignment of this scour approximately bisects the junction angle. This feature is associated with increased velocities and turbulence intensity within the junction and the sediment transport patterns.

- Tributary-mouth bars that form at the mouth of one or both confluent channels. The avalanche slope created at the downstream end of these bars usually dips into the scour hole.

- A mid-channel bar, mostly observed in symmetric confluences (not shown in Figure 2.3).

- A bank-attached bar at the inner bank of the post-confluence channel. It is associated with regions of flow recirculation or reduced flow velocities.

- Sediment accumulation at the upstream junction corner, which may be associated with flow stagnation (not shown in Figure 2.3).
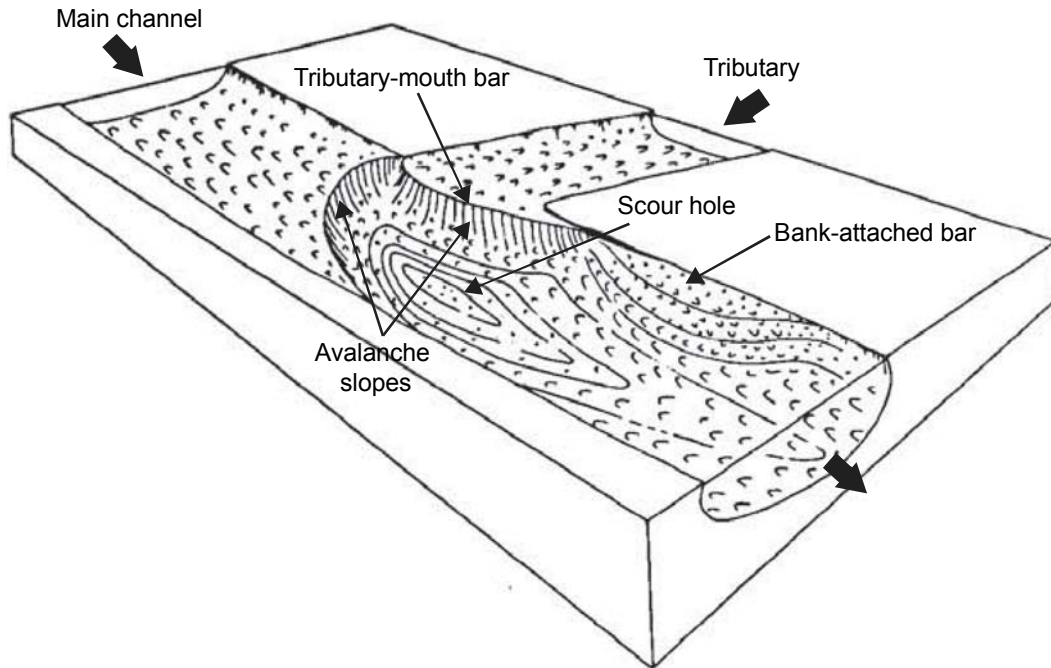
Figure 2.3 Bed morphology at asymmetrical confluences (modified from Bristow *et al.*, 1993)

This model was built on the morphological conceptual model proposed by Best (1988) and compiles most of the existent knowledge on confluence morphodynamics provided by experimental and field studies.

Best's (1988) morphological model is based on laboratory experiments, in which five junction angles (15°, 45°, 70°, 90° and 105°) and three discharge ratios (0.53, 1.02, and 1.53) were tested. The experiments were performed with a movable bed composed of well-sorted sand, while sediments were continuously supplied to both channels during the experiments. The results obtained from the experiments were contrasted with field measurements from the confluence of the Ure and Widdale Beck rivers in United Kingdom.

Apart from the study of Best (1988), few studies have examined confluence morphodynamics by means of systematic laboratory experiments. For instance, the study by Mosley (1976) presents the results of laboratory experiments performed both in symmetrical and asymmetrical confluences with different discharge ratios ($0.33 < Q_r < 1.00$) and junction angles ($15° < \alpha < 90°$). The experiments were carried out under movable bed conditions, with erodible banks, and with continuous supply of sediments during the experiments. The study by Ashmore and Parker (1983) describes the bed morphology of confluences formed by braided streams (mostly symmetrical), based on laboratory experiments with movable bed, continuous sediment feeding during the experiments and erodible banks. Ghobadian and Bejestan (2007), Bejestan and Hemmati (2008), and Liu *et al.* (2012) studied the bed morphology in a laboratory confluence for different angles (60°, 75° and 90°) and discharge ratios ($0.18 < Q_r < 1.25$). These experiments were performed with fixed lateral banks, with movable bed but without sediment feeding during the experiments. Leite Ribeiro *et al.* (2012a, b, 2015) analyzed the morphodynamics of the Upper-Rhone river confluences

in an experimental facility for three discharge ratios (0.11, 0.15, 0.23), and different geometries of the tributary mouth, with a junction angle of $\alpha = 90°$. The experiments were performed with a movable bed and by supplying a poorly-sorted sand-gravel mixture only to the tributary.

The most relevant field studies of confluence morphodynamcs were carried out either in the confluence formed by the Kaskaskia and Cooper Slough rivers in USA (Rhoads and Kenworthy, 1995; Rhoads, 1996, 2006; Rhoads *et al*., 2009), or in that formed by the Bayonne and Bethier rivers in Canada (Biron *et al*., 1993; Leclair and Roy, 1997; De Serres *et al*., 1999; Boyer *et al*., 2006). According to Leite Ribeiro *et al*. (2012a), these field studies analyze the hydrodynamic, morphodynamic and sedimentary processes of the confluence under varying flow conditions, which cover a broad range of discharge and momentum flux ratios ($0.20 < Q_r < 6.64$; $0.18 < M_r < 54$).

The aforementioned field and experimental studies identify the junction angle together with the momentum-flux and discharge ratios as key parameters in the bed morphology of open-channel confluences. Experimental studies report deeper scour holes and larger bank-attached bars both for increasing discharge ratios and junction angles (Mosley, 1976; Ashmore and Parker, 1983; Best, 1988; Ghobadian and Bejestan, 2007; Bejestan and Hemmati, 2008; Liu *et al*., 2012). Furthermore, for increasing momentum-flux ratios, the tributary mouth-bar of the dominant tributary penetrates further into the confluence and the scour hole is forced to shift towards the outer bank of the post-confluence channel (Ashmore and Parker, 1983; Best, 1988; Biron *et al*., 1993; Leclair and Roy, 1997; Rhoads, 2006; Rhoads *et al*., 2009; Riley *et al*., 2015).

Bed discordance was observed to be a common feature in natural confluences by Kennedy (1984), and its existence and characteristics are associated with the different ratios between sediment transport rate and flow discharge of the tributary and main channel (Kennedy, 1984; Leite Ribeiro *et al*., 2012a). As reported previously in Section 2.1, this feature has a significant influence in the flow dynamics of the confluence and consequently, it also influences the bed morphology and sediment transport (Section 2.4). Biron *et al*. (1993) highlighted the absence of marked scour in the natural discordant Bayonne-Berthier confluence. Later, Leclasir and Roy (1997) and Boyer *et al*. (2006) corroborated the lack of substantial scour hole in this confluence, and observed a protruding tributary-mouth bar highly depending on M_r. Furthermore, Leite Ribeiro *et al*. (2012, 2015), who also studied discordant confluences in the laboratory, reported only weak erosion at the outer bank of the post-confluence channel.

2.4   Sediment transport

Sediment transport, especially bedload transport, is the key linkage between confluence flow dynamics and the bed morphology. In confluences, the bedload transport patterns are highly two-dimensional due to the turbulent three-dimensional flow structure. In the laboratory, where the flow and bed morphology evolve towards equilibrium conditions, the sediment flux tends to a steady state needed to maintain a constant bed morphology. In nature, where the flow conditions change continuously, the

bed morphology dynamically evolves due to spatio-temporal variations in transport capacity (Best and Rhoads, 2008).

The study of sediment transport at open-channel confluences begins with the study by Mosley (1976), which describes the sediment transport patterns observed in symmetrical laboratory confluences. In these experiments, the sediments moved predominantly along the flanks of the scour hole due to the presence of helical flow cells, which sweep the sediments outwards the scour. Downstream of the confluence, the sediment transport converged, yielding the highest transport rates in the center of the channel. Also, Mosley (1976) related the depth of the scour hole to the total sediment load, concluding that the depth of the scour decreases as the total sediment load increases. This was later corroborated by Rezaur *et al*. (1999).

Best (1988) studied the sediment transport patterns in asymmetrical confluences by means of laboratory experiments. Based on these, Best (1988) reported segregation between the sediment loads provided by each confluent channel. Additionally, Best (1988) observed that segregation increases with the junction angle and with the mutual flow deflection at the confluence. Converse to the observations by Mosley (1976), a lack of sediment transport was observed in the center of the post-confluence channel for high junction angles (Best, 1988). Particle-tracking experiments at natural confluences such as at the Ure and Widdale Beck rivers in United Kingdom, confirmed that in asymmetrical confluences, the sediments move along the bank-attached bar, flanking the scour hole (Best, 1988). In contrast with Best (1988), Roy and Bergeron (1990) document gravel particle movement through the scour hole and mixing of sediments pathways within a small asymmetrical confluence in Canada.

Rhoads (1996) reported segregation at the junction, high sediment transport through the scour and sediment mixing downstream of the Kaskaskia-Cooper Slough confluence for $M_r < 1$. Later, Rhoads *et al*. (2009) observed different sediment transport patterns for $M_r > 1$. In these conditions, the sediments move flanking the scour hole and they are well mixed within the confluence.

Biron *et al*. (1993), in the discordant Bayonne-Berthier confluence, observed an abrupt change in the alignment of migrating ripples between the tributary-mouth bar and the bed of the main channel, revealing the influence of the bed discordance on sediment transport patterns. This natural discordant confluence is characterized by a lack of marked scour hole and a dynamic protruding of the tributary-mouth bar, which affects the patterns of sediment transport (Boyer *et al*., 2006). In this confluence, the highest rates of bedload transport were measured near the edges of the shear layer that, in addition, impinges the tributary-mouth bar, contributing to the high sediment transport rates. Boyer *et al*. (2006) related the sediment transport rates to the variations in momentum flux ratio (M_r), which affect to the position of the shear layer and its interaction with the bed morphology. Contrary to the observations made by Rhoads (1996), Boyer *et al*. (2006) reported sediment mixture within the confluence.

Leite Ribeiro *et al*. (2012a) identified two sediment corridors in their experiments: one of fine sediments on top of the bank-attached bar, and another of coarse sediments

at the lateral slope of the bar. The high gradation of the sediments supplied to the tributary ($\sigma \approx 4.51$) promoted the armoring of the tributary bed, and the lateral slope of the bank-attached bar. In addition, the lack of sediment supply to the main channel together with the high gradation of the bed sediments ($\sigma \approx 3.15$) result in an armored bed in the main channel upstream of the confluence.

2.5 Concluding remarks

In open-channel confluences there is a strong interaction between flow dynamics, bed morphology and sediment transport. Previous authors such as Mosley (1976), Best (1987; 1988) and Leite Ribeiro (2011) identified the discharge and momentum flux ratios (Q_r and M_r, respectively), the Froude number of each channel (Fr), the junction angle (α), the ratio between the width of the tributary and main channel (B_t/B_m), the gradation coefficient of the bed sediment mixtures (σ), and the ratio between the sediment transport rate and the flow discharge of each channel (Q_s/Q), where Q_s stands for the sediment discharge and Q for the flow discharge, as controllers of the hydro-morphodynamic and sedimentary processes of open channel confluences.

The flow dynamics in open-channel confluences have been thoroughly investigated in laboratory, field and by means of numerical models. These studies provide, on the one side, very valuable insights in the general understanding of the confluence hydrodynamics and, on the other side, an extensive database for the future development of numerical models.

The existent knowledge regarding confluence morphodynamics comes mainly from the exhaustive study of two natural confluences: i) the asymmetrical concordant confluence between the Kaskaskia and Cooper Slough rivers in USA, and ii) the asymmetrical discordant confluence between the Bayonne and Berthier rivers in Canada. Both confluences are characterized by a low sediment transport activity.

With the exceptions of Mosley (1976) and Best (1988), there is a lack of morphodynamic studies based on systematic laboratory experiments, carried out under movable bed conditions and with continuous sediment supply to both channels throughout the experiments.

Solely Leite Ribeiro *et al*. (2012a, b, 2015) studied the hydro-morphodynamics and sediment patterns of the Upper-Rhone river confluences, by means of systematic laboratory experiments in which the sediment transport of the main channel was neglected, since sediments were only supplied to the tributary.

3

Experiments

In this chapter, the experimental setup and the methodology adopted for the present research study are described. The experiments are inspired by the confluences of the Upper-Rhone river basin. There, a wide main channel provides the dominant discharge, while the sediments are abundantly supplied by narrow steep tributaries. In these confluences, the sediment load is composed of poorly sorted sand-gravel mixtures, and the tributaries join the main channel at high junction angles. The effects induced on the hydro-morpho-sedimentary processes of the confluence by the discharge ratio (Q_r), the junction angle (α), the sediment gradation (σ), and the width ratio between the tributary and main channel (B_t/B_m), are studied herein. Twelve experiments divided into four sets of three, were conducted in two experimental facilities:

- The first experimental facility was located at the Laboratory of Hydraulic Constructions of the École Polytechnique Fédérale de Lausanne (LCH-EPFL). In this facility two sets of experiments were performed, the so-called set I and set II. These experimental sets covered two junction angles (one per set), which were tested for three discharge ratios. The sediments supplied in these experimental sets consisted of non-uniform mixtures with high values of σ.

- The second experimental facility was located at the hydraulic laboratory of the Instituto Superior Técnico of the University of Lisbon (IST-UL). In this facility were conducted the so-called experimental set III and set IV. These sets covered two width ratios (one per set), each one tested for three discharge ratios. The sediments consisted of a uniform mixture with low value of σ; and the junction angle was constant for these sets of experiments.

3.1 Experimental facility at LCH-EPFL

The experimental facility at the Laboratory of Hydraulic Constructions of the Ecole Polytechnique Fédérale de Lausanne (LCH-EPFL) was the same used by Leite Ribeiro (2011) (Figures 3.1 to 3.2), and it consisted of:

- A 8.50 m long and 0.50 m wide straight rectangular glass-wall main channel.

- A 4.90 m long and 0.15 m wide straight rectangular PVC tributary.

Figure 3.1 sketches the geometry of the confluence in its two configurations. For the first set of experiments, the tributary connected the main channel at a distance of 3.15 m from the main channel inlet, with an angle of $\alpha = 90°$ (Figure 3.1a). For the second set, the junction was at 4.50 m from the inlet of the main channel, with an angle of $\alpha = 70°$ (Figure 3.1b). The results obtained in this facility were referred to the reference axes X, Y and Z as indicated in Figure 3.1. The inlet of the main channel was composed of a V-notch weir and a block of honeycomb, placed downstream of the weir (Figure 3.1c). At the outlet of the main channel there were a sediment trap to recover the transported sediments and an adjustable tailgate to control the downstream flow depth (Figure 3.1c).
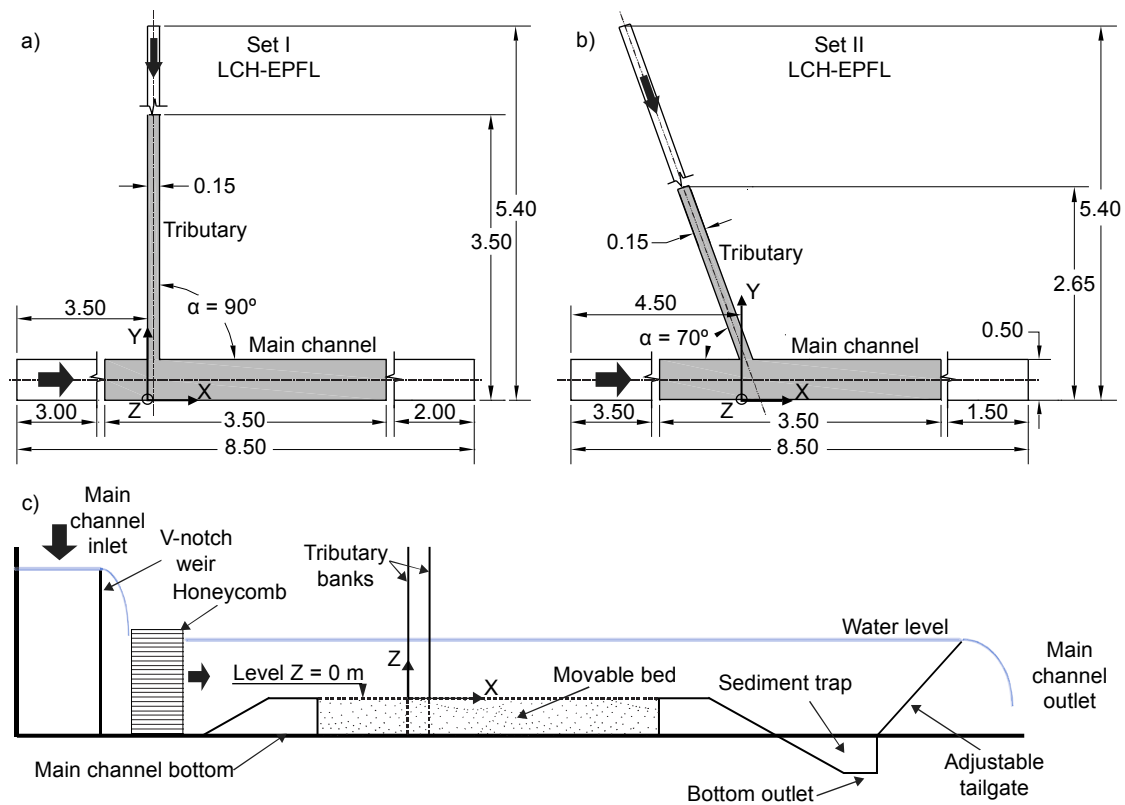
Figure 3.1 Sketch of the experimental facility at LCH/EPFL with units in meters. a) Plan view with $\alpha = 90°$ for the experimental set I, b) plan view with $\alpha = 70°$ for the experimental set II, and c) Schematic side view of the main channel. The grey-shaded areas represent the measurement domains for each experimental set.

Figure 3.2 shows the two configurations of the experimental facility at LCH-EPFL; i.e. with a junction angle of $\alpha = 90°$ (experimental set I), and with an angle of $\alpha = 70°$ (experimental set II).

Figure 3.2 Experimental facility at LCH-EPFL. a) Upstream view of the main channel with $\alpha = 90°$. b) Upstream view of the tributary with $\alpha = 90°$. c) Upstream view of the main channel with $\alpha = 70°$. d) Upstream view of the tributary with $\alpha = 70°$.

3.2 Experimental facility at IST-UL

The experimental facility at the hydraulic laboratory of the Instituto Superior Técnico (IST) of the University of Lisbon (Figure 3.3 and Figure 3.4) was composed of the following items:

- A 12.00 m long and 1.00 m wide straight rectangular channel with glass and concrete walls.

- A 4.50 m long and 0.15 m wide straight rectangular tributary with PVC-walls, which connected to the main channel with an angle of $\alpha = 70°$, at a distance of 5.00 m from the main channel inlet.

Figure 3.3 depicts the geometry of the second experimental facility in its two configurations. For the third set of experiments, only half of the width of the main channel was used ($B_m = 0.50$ m), to obtain a width ratio $B_t/B_m = 0.30$ (Figure 3.3a). For the fourth set, the width of the main channel was increased to $B_m = 1.00$ m, yielding a width ratio of $B_t/B_m = 0.15$ (Figure 3.3b). The results obtained in this facility were referred to the reference axes X, Y and Z as indicated in Figure 3.3. The inlet of the main channel was composed of a submerged pipe which supplies the water flow and a rock filter, placed downstream of the pipe (Figure 3.3c). At the outlet of the main channel there were a sediment trap to recover the transported sediments and an adjustable tailgate to control the downstream flow depth (Figure 3.3c).
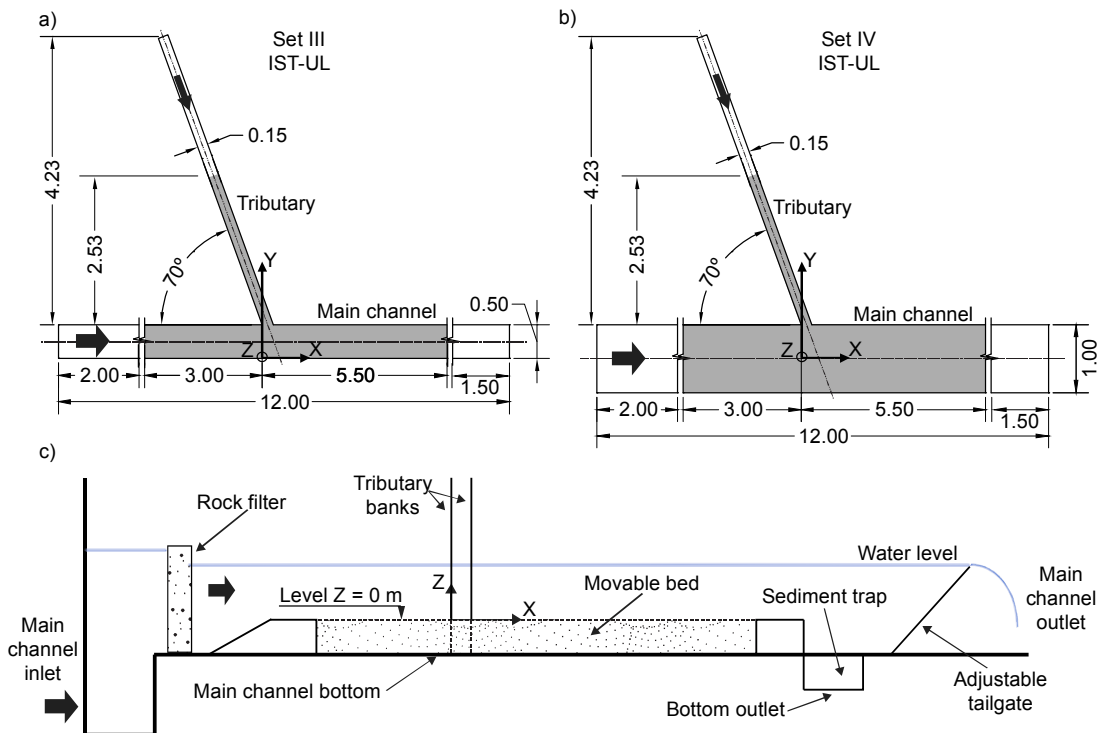
Figure 3.3 Sketch of the experimental facility at IST-UL with units in meters. a) Plan view with $B_t/B_m = 0.30$ for the experiemencal set III, b) Plan view with $B_t/B_m = 0.15$ for the experimental set IV, and c) Schematic side view of the main channel. The grey-shaded areas represent the measurement domain for each experimental set.

Figure 3.4 depicts the two configuration of the main channel; i. e. with $B_m = 0.50$ m for the experimental set III, and with $B_m = 1.00$ m for the experimental set IV.
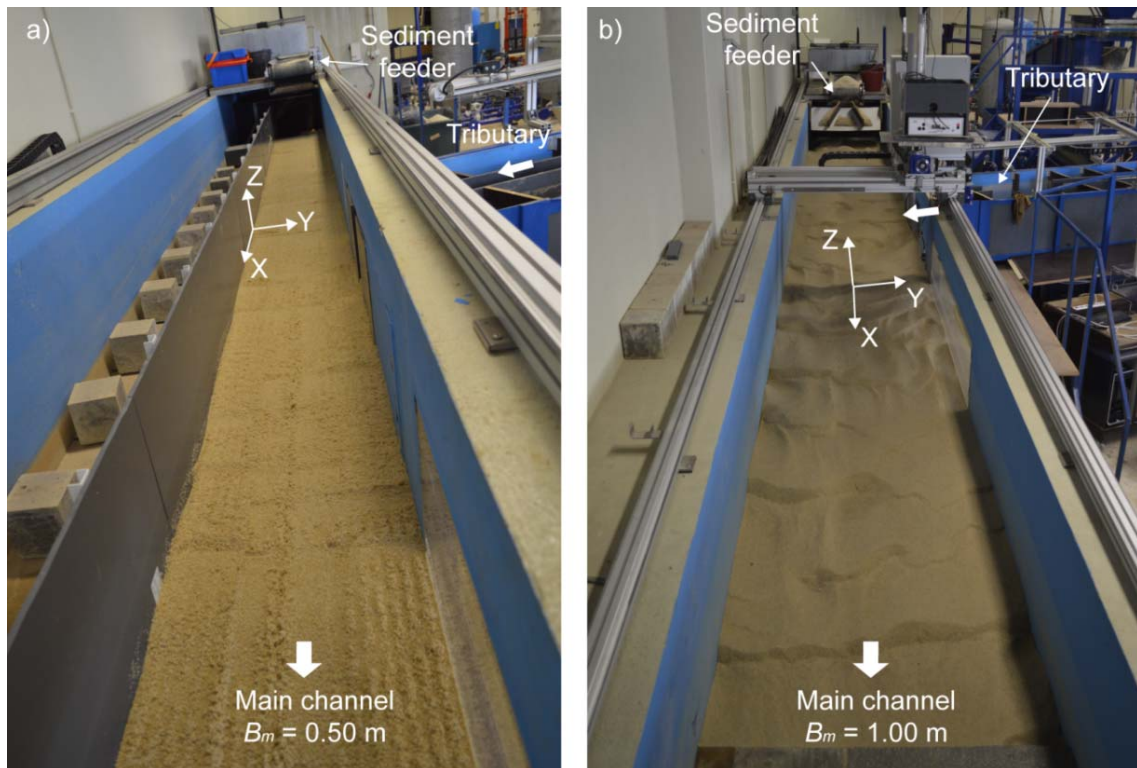
Figure 3.4. Experimental facility at IST- Lisbon. a) Upstream view of the main channel with $B_m = 0.50$ m for the experimental set III. b) Upstream view of the main channel with $B_m = 1.00$ m for the experimental set IV.

3.3 Measuring instrumentation and equipment of the experimental facility at LCH-EPFL

The experimental facility at LCH-EPFL was equipped as follows:

• A V-notch weir installed at the inlet of the main channel to control the supplied flow discharge with ± 0.1 *l/s* accuracy (Figure 3.5a).

• An electromagnetic flowmeter to control the supplied flow discharge to the tributary with ± 0.1 *l/s* accuracy (Figure 3.5b).

• An adjustable tailgate at the downstream end of the main channel to control the downstream water level with ± 0.005 m accuracy (Figure 3.5c).

• A sediment recovery system at the downstream end of the main channel to assess the outgoing sediment rate. This system is composed of a sediment trap, a botton outlet, a recovery tank and a digital scale with ± 0.5 *kg* accuracy (Figure 3.5c-d).

• An arquimedes screw acting as sediment feeder for the main channel (Figure 3.5e).

Figure 3.5 Measuring instrumentation and equipment of the experimental facility at LCH-EPFL. a) V-notch weir at the main channel inlet. b) Water supply system for the tributary. c) Sediment recovery system. d) Digital scale. e) Sediment feeder of the main channel. f) Sediment feeder of the tributary. g) Adquisition data box of the Mini-EchoSounder. h) Mini-EchoSounder probe.

- A 5 m long and 0.5 m wide conveyor belt as sediment feeder for the tributary (Figure 3.5f).

- A Mini-EchoSounder probe (UltraLab UWS) that works with an ultrasonic-impulse-run time procedure to measure the bed topography in both flumes, with ± 1 mm accuracy (Kantoush *et al*., 2008) (Figure 3.5g-h)

- An ultrasonic limnimeter to measure the water surface in both flumes with ± 1 mm accuracy.

- A micro-propeller Schiltknecht to measure point flow velocities with ± 0.01 m/s accuracy.

- A movable frame where the Mini-EchoSounder and the limnimeter probes were installed. This frame covered 3.50 m in the main channel, and 3.00 m in the tributary for the experimental set I ($\alpha = 90°$). For the experimental set II ($\alpha = 70°$), the frame covered ≈ 2.30 m of the tributary length (Figure 3.1). This frame allowed automatic displacements in the X direction, and manual displacements in the Y direction (Figure 3.6).
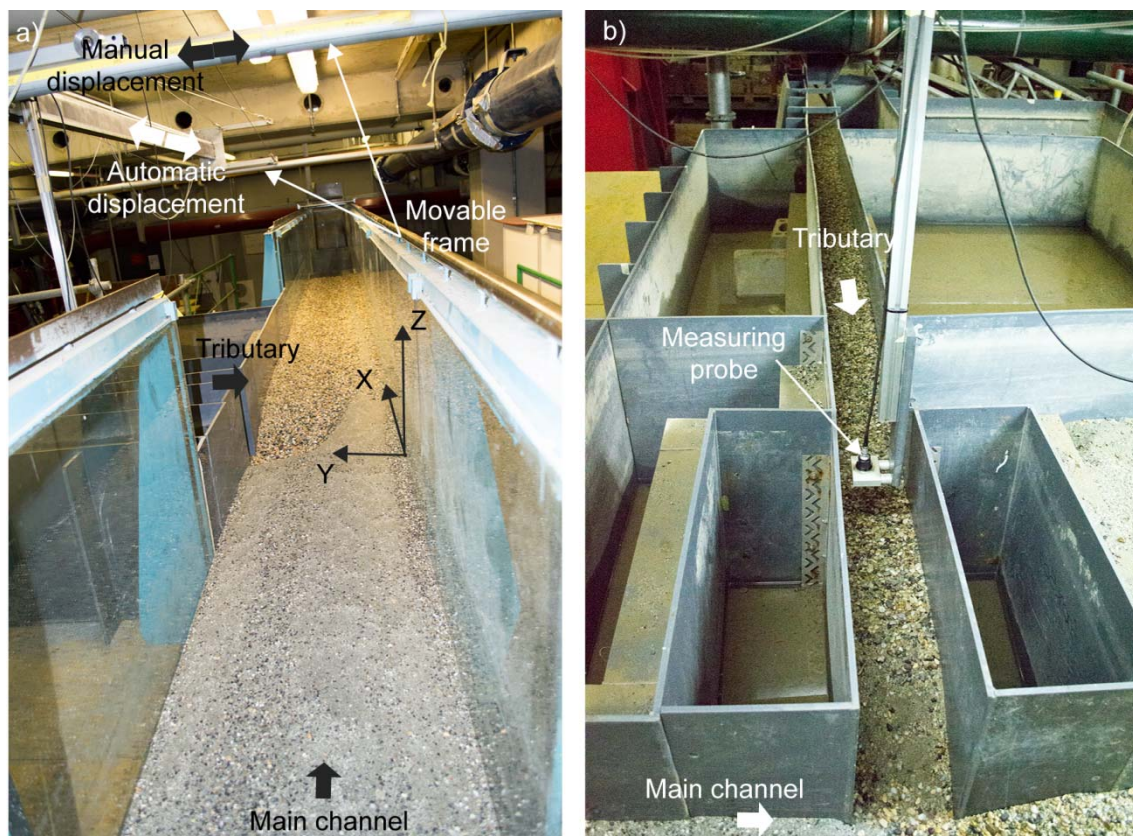
Figure 3.6 a) Movable frame for measuring of the experimental facility at LCH-EPFL. b) Measuring probe installed in the movable frame of the experimental facility at LCH-EPFL.

3.4 Measuring instrumentation and equipment of the experimental facility at IST-Lisbon

The experimental facility at IST-Lisbon was equipped as follows:

- An electromagnetic flowmeter to control the supplied flow discharge to the main channel with ± 0.1 *l/s* accuracy (Figure 3.7a).

- A V-notch weir at the tributary inlet to control the supplied flow discharge with ± 0.1 *l/s* accuracy (Figure 3.7b).

- An adjustable tailgate at the downstream end of the main channel to control the water level with ± 0.005 m accuracy (Figure 3.7c).

- A sediment recovery system at the downstream end of the main channel to assess the outgoing sediment rate. This system consisted of a sediment trap, a bottom outlet, a sediment recovery tank, and a digital scale with ± 0.5 *Kg* accuracy (Figure 3.7d-e).

- Two conveyor belts to supply sediments to the main channel and the tributary. The conveyor belt of the main channel was 1.5 m long and 0.5 m wide; whereas for the tributary it was 3.5 m long and 0.3 m wide (Figure 3.7f-g).

- Two Mini-EchoSounder probes (UltraLab UWS) to measure the bed topography in each flume with ± 1 mm accuracy (see Figure 3.7h).

- Two ultrasonic limnimeters to measure the water surface in each flume with ± 1 mm accuracy (Figure 3.7i).

- Two robotic arms, one for the main channel and one for the tributary, where the Mini-EchoSounder and the limnimeter probes were installed. In the main channel, the robotic arm moved automatically in the *X Y* and *Z* directions (Figure 3.8a). This system covered 8.50 m in the *X* direction and 0.80 m in the *Y* direction. In the tributary, the automatic arm was able to move along the tributary axis for a length of 2.70 m (Figure 3.8b).
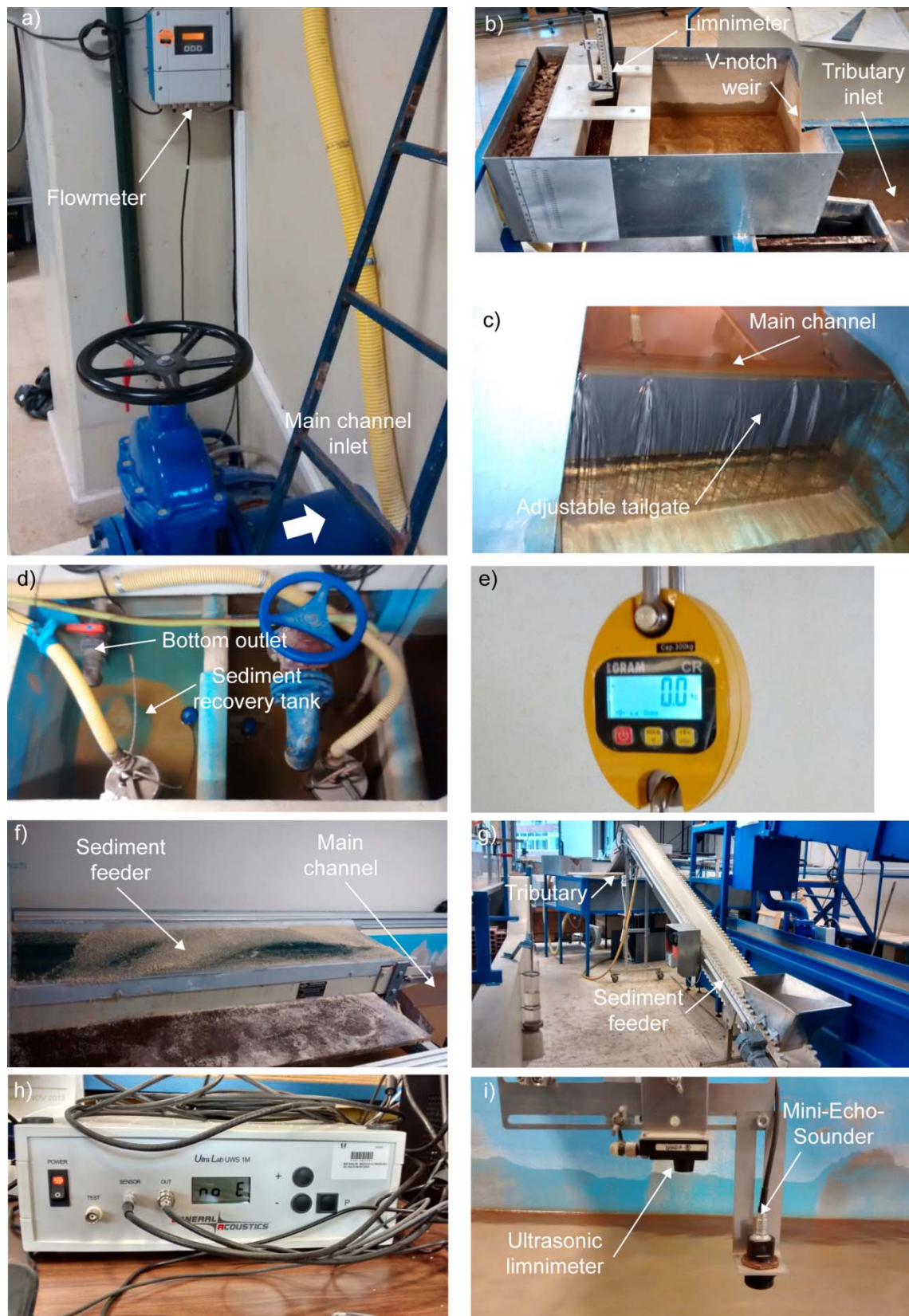
Figure 3.7 Measuring instrumentation and equipment of the experimental facility at the IST-UL. a) Electromagnetic flowmeter at the main channel inlet. b) V-notch weir at the tributary inlet. c) Adjustable tailgate at the downstream end of the main channel. d) Sediment recovery tank and bottom outlet. e) Digital scale. f) Sediment feeder of the main channel. g) Sediment feeder of the tributary. h) Adquisition data box of the Mini-EchoSounder. i) Ultrasonic limnimeter and MiniEchoSounder.

23
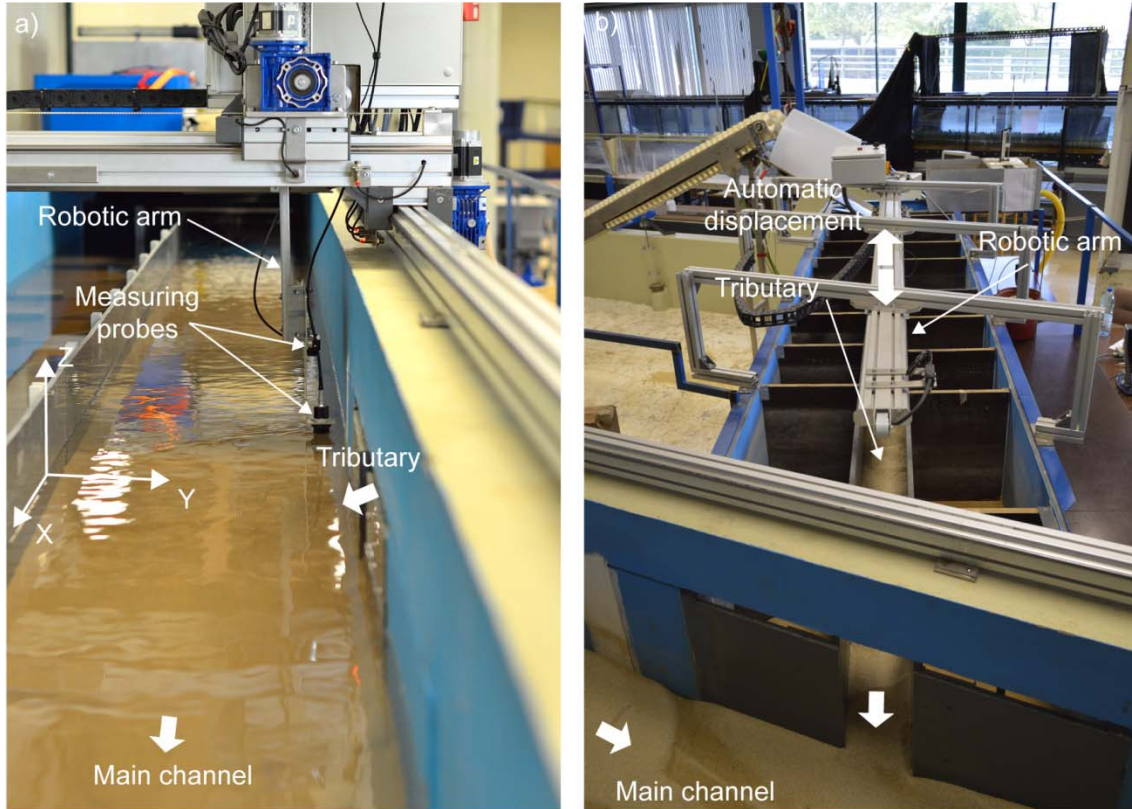
Figure 3.8 a) Robotic arm of the experimental facility at IST-UL for measuring in the main channel. b) Robotic arm of the experimental facility at IST-UL for measuring in the tributary.

3.5 Experimental parameters

The bed morphology and flow dynamics of open-channel confluences are controlled by parameters such as the junction angle (α), the ratio between the width of the tributary and main channel (B_t/B_m), the discharge and momentum flux ratios (Q_r and M_r, respectively), the Froude number of each channel (Fr), the gradation coefficient of the bed sediment mixtures (σ), and the ratio between the sediment transport rate and the flow discharge of each channel (Q_s/Q) (Mosley, 1976; Best, 1987, 1988; Leite Ribeiro, 2011). In this section, the values of these parameters adopted for the experiments are presented.

3.5.1 Junction angle (α)

The adopted values for the junction angle were:

- $\alpha = 90°$ for the experimental set I, carried out in the facility of the LCH-EPFL.

- $\alpha = 70°$ for the rest of experiments; i.e. set II (LCH-EPFL), set III (IST-UL) and set IV (IST-UL).

These angles are consistent with the observations made by Leite Ribeiro (2011) in the Upper-Rhone river basin, where the tributaries join the main river at high junction angles due to previous channelization works. Also, these angles are within the range of the values observed by Miller (1958) in the Sangre de Cristo Range at the Rocky

mountains in USA. Moreover, the studies of Devauchelle *et al.*, (2012) and Gutierrez *et al.* (2014) suggest that in nature, the junction angles respond to a normal distribution with means of $\alpha \approx 72°$ and $82°$, respectively.

3.5.2 Width ratio (B_t/B_m)

The width ratio is defined as the relation between the widths of the tributary and main channel B_t/B_m, where the sub-indexes t and m refer to the tributary and main channel, respectively. The values adopted in this research study were:

- $B_t/B_m = 0.30$ for the experimental set I (LCH-EPFL), set II (LCH-EPFL) and set III (IST-UL).

- $B_t/B_m = 0.15$ for the experimental set IV (IST-UL).

These values are within the ratios observed in the Upper-Rhone river confluences by Leite Ribeiro (2011).

3.5.3 Flow discharge scenarios

In this research study, three discharge scenarios were tested in each experimental set. Each discharge scenario is defined by a discharge ratio value, which is defined as the relation between the flow discharges of the tributary and main channel measured upstream of the confluence $Q_r = Q_t/Q_m$. In this research study, the following discharge ratios were tested:

- $Q_r = 0.11, 0.15, 0.23$ for the experimental sets performed with a width ratio of $B_t/B_m = 0.30$; set I (LCH-EPFL), set II (LCH-EPFL) and set III (IST-UL). These values are referred in this study as "low discharge ratio" (LR), "intermediate discharge ratio" (IR), and "high discharge ratio" (HR), and they are representative of the Upper-Rhone river confluences (Leite Ribeiro, 2011).

- $Q_r = 0.06, 0.07, 0.11$ for the experimental set IV (IST-UL), performed with a width ratio of $B_t/B_m = 0.15$. These values keep the same unit-discharge ratio as those defined for sets I to III. The unit-discharge ratio is defined as $q_r = q_t/q_m$ (Table 3.1)

The post-confluence flow discharge $Q_{p-c} = Q_t + Q_m$ was established at 30 l/s for all the experiments of the sets I, II, and III. This value is higher than the discharge of 20 *l/s* adopted by Leite Ribeiro (2011), with the purpose of guaranteeing sediment transport all along the main channel. In the case of set IV, Q_{p-c} varies for each discharge ratio from 54.4 *l/s* to 57.0 *l/s* (Table 3.1).

Table 3.1 contains the values of the tributary flow discharge (Q_t), main channel flow discharge (Q_m), post-confluence flow discharge (Q_{p-c}), discharge ratio (Q_r), and unit-discharge ratio (q_r), for each experimental set.

Table 3.1. Discharge values for each experimental set.

Experimental set	Q_t [l/s]	Q_m [l/s]	$Q_{p\text{-}c}$ [l/s]	Q_r [-]	q_r [-]
	3.0	27.0		0.11	0.37
Set I, II and III	3.9	26.1	30.0	0.15	0.50
	5.6	24.4		0.23	0.77
	3.0	54.0	57.0	0.06	0.37
Set IV	3.9	52.2	56.1	0.07	0.50
	5.6	48.8	54.4	0.11	0.77

3.5.4 Sediment mixtures and sediment rates

The sediment mixtures used in this research study are characterized by the median diameter (d_{50}), the mean diameter (d_m), and the gradation coefficient (σ). The gradation coefficient is defined herein as:

$$\sigma = \frac{1}{2}\left(\frac{d_{84}}{d_{50}} + \frac{d_{50}}{d_{16}}\right)$$

(3.1)

Where d_{84}, d_{50}, d_{16} are the particle sizes coarser than the 84%, 50% and 16% by weight of the sediment mixture, respectively. The sediment mixtures supplied to the tributary and main channel were different in each experimental facility:

- In the facility of the LCH-EPFL (sets I and II), the sediments supplied to the tributary were the same used by Leite Ribeiro (2011). This mixture consisted of an 80% of poorly-sorted 0.1 – 4.0 mm sand-gravel mixture, and a 20% of 4.0 – 8.0 mm gravel, which yields $d_{50} = 0.82$ mm, $d_m = 2.3$ mm, and $\sigma = 4.51$. For the main channel, the sediments were composed of the 0.1 - 4.0 mm sand-gravel mixture supplied to the tributary, which means that the coarser part (4.0 – 8.0 mm gravel) was removed. The latter mixture was characterized by $d_{50} = 0.82$ mm, $d_m = 1.4$ mm, and $\sigma = 4.51$. Both sediment mixtures are representative, after scaling, of the sediments found in the Upper-Rhone river confluences, as justified by Leite Ribeiro (2011).

- At IST - UL (sets III and IV), a uniform 0.4 – 2.0 mm sand with $d_{50} = 0.85$ mm, $d_m = 0.85$ mm, and $\sigma = 1.35$ was supplied to both the tributary and main channel during the experiments. The grain size distribution of this mixture is rather representative of low land confluences in alluvial valleys. The use of uniform sediments with nearly equal d_{50} to the non-uniform mixtures, allows independent analysis of the effect of the grain size distribution on the hydrodynamics and morphodynamics of open-channel confluences.

The grain size distribution (GSD) of the supplied sediment mixtures is depicted in Figure 3.9, while Table 3.2 contains the values of the grain density (ρ_S), the gradation coefficient (σ), and the characteristic grain diameters of each mixture (d_{16}, d_{50}, d_m, d_{84}, and d_{90}).
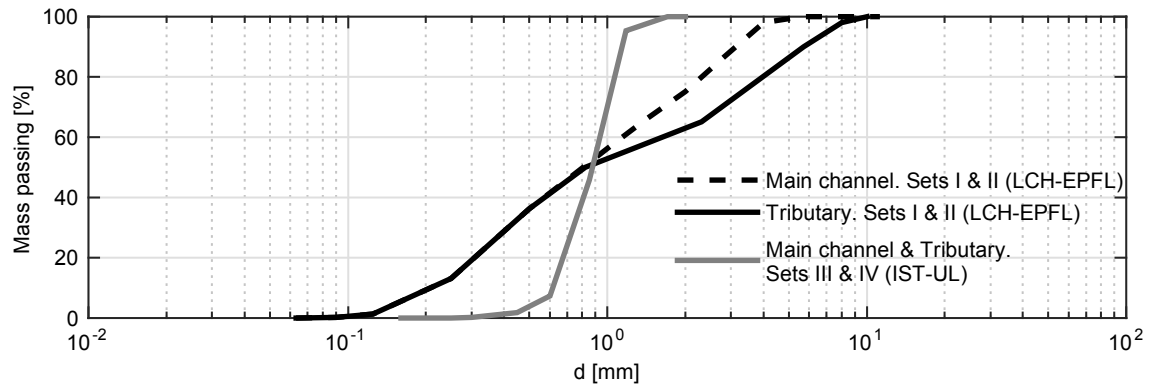
Figure 3.9 Grain size distribution (GSD) of the supplied sediment mixtures.

Table 3.2 Main characteristics of the supplied sediment mixtures

Experimental set	Channel	ρ_s [kg/m³]	d_{16} [mm]	d_{50} [mm]	d_m [mm]	d_{84} [mm]	d_{90} [mm]	σ [-]
Set I & II (LCH-EPFL)	Main channel		0.26	0.82	1.40	2.60	3.00	3.15
	Tributary	2650	0.26	0.82	2.30	4.82	5.70	4.51
Sets III & IV (IST-UL)	Main channel & Tributary		0.64	0.85	0.85	1.17	1.40	1.35

ρ_s is the grain density, σ is the gradation coefficient, and d_x are the characteristic grain diameters of the mixtures, where the sub-index x represents the percentage of sediment mixture by weight, which have smaller diameters

The sediment rates for the tributary (Q_{st}) and main channel (Q_{sm}) were defined by assuming, as initial hypothesis, that the longitudinal bed slope and grain size distributions are in the range of those observed in the Upper-Rhone river confluences. Hence, the hypothetical bed slopes under equilibrium conditions were assumed to be approximately 1.0% for the tributary and within the range of 0.3% – 0.4% for the main channel. By assuming uniform flow in both channels for such slopes, and for the defined discharge ratios, the sediment rates to be supplied during the experiments to both channels were estimated through the Smart's (1984) sediment transport formula, developed for gravel bed rivers. The sediment rates adopted for the main channel (Q_{sm}) and the tributary (Q_{st}) are thus:

- For the experimental sets performed with a width ratio of B_t/B_m = 0.30 (sets I, II, and III), Q_{sm} = 0.3 *kg/min* for the main channel, and Q_{st} = 0.5 *kg/min* for the tributary.

- For the experimental set IV, performed with a width ratio of B_t/B_m = 0.15, Q_{sm} = 0.6 *kg/min* for the main channel, and Q_{st} = 0.5 *kg/min* for the tributary. The reason for a higher sediment rate of the main channel with respect to the other experimental sets, was to keep the same unit sediment rate in the main channel.

3.5.5 Downstream boundary condition

At the downstream end of the main channel, the flow depth (y_d) was imposed by means of the adjustable tailgate. The value of y_d was estimated by means of the Manning-Strickler formula, considering uniform flow in the main channel, a bed slope of about 0.4%, and a Strickler roughness coefficient of $K_{st} \approx 72$ m$^{1/3}$ s^{-1}. This estimation yielded a downstream flow depth of $y_d \approx 0.08$ m (*Froude* ≈ 0.85), which was imposed in all the experiments performed at EPFL (sets I and II). For sets III and IV, the downstream flow depth was increased up to 0.10 m for practical reasons, since for lower values the sediment transport was so high that the movable bed was rapidly washed out.

3.6 Comparison between experimental parameters and Rhone river's physical parameters

The experimental parameters adopted in this study are inspired by those observed in the Upper-Rhone river confluences. To characterize these confluences, the twenty main confluences between Brig and Lake Geneva have been analyzed. These confluences present high junction angles that are either imposed by river training works or naturally formed as typical for mountainous areas. Figure 3.10 illustrates the angles measured nearby the confluences by means of aerial photography (www.maps.google.com).
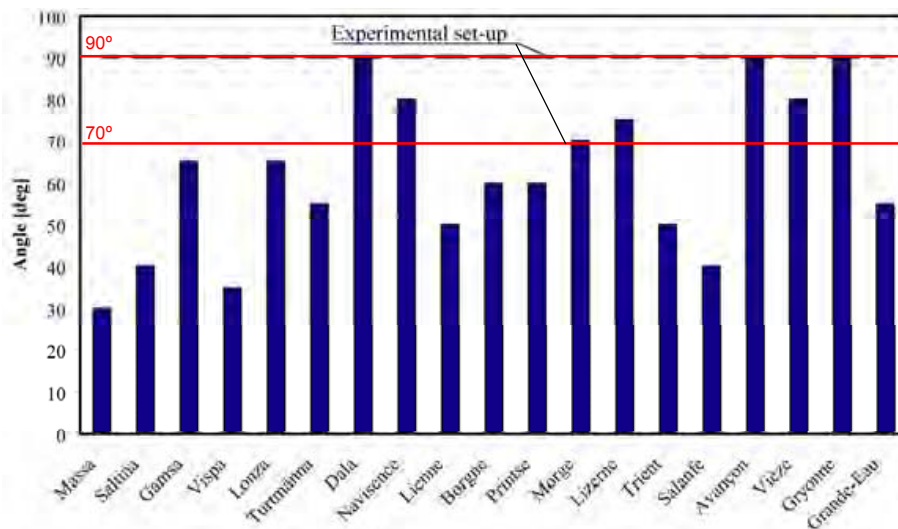
Figure 3.10 Junction angle of the main confluences in the basin of the Upper Rhone river. Horizontal solid lines indicate the adopted values for the experimental setup.

Because of previous river training works, the Rhone river is characterized by a monotonous linear prismatic profile that derives in a lack of structural diversity such as gravel banks, islands or bars. The Rhone river's width is fixed between 30 and 60 m. Due to this width constraint, the ratio between the width upstream of the confluence and the width at the post-confluence (B_m/B_{p-c}) is close to 1 in most of the analyzed confluences (Figure 3.11). Considering the ratio between the tributaries and the main channel widths (B_t/B_m), Figure 3.11 shows that with the exception of the Vispa river ($B_t/B_m = 0.54$), the range of the width ratio (B_t/B_m) is between 0.15 and 0.30.
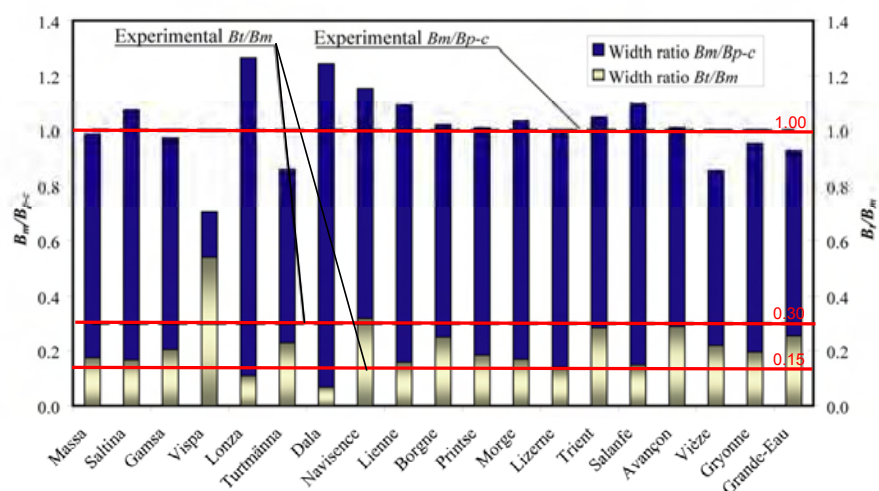
Figure 3.11 Ratio between the widths of the Rhone river upstream of the confluence and at the post-confluence (B_m/B_{p-c}), and ratio between the widths of the tributaries and the Rhone river (B_t/B_m). Horizontal solid lines indicate the values adopted for the experimental setup.

Figure 3.12 shows that the Upper Rhone river basin is characterized by steep tributaries, with the exception of some such as the Turtmanna, Dala, Morge and Grand-Eau River that present low bed slopes.
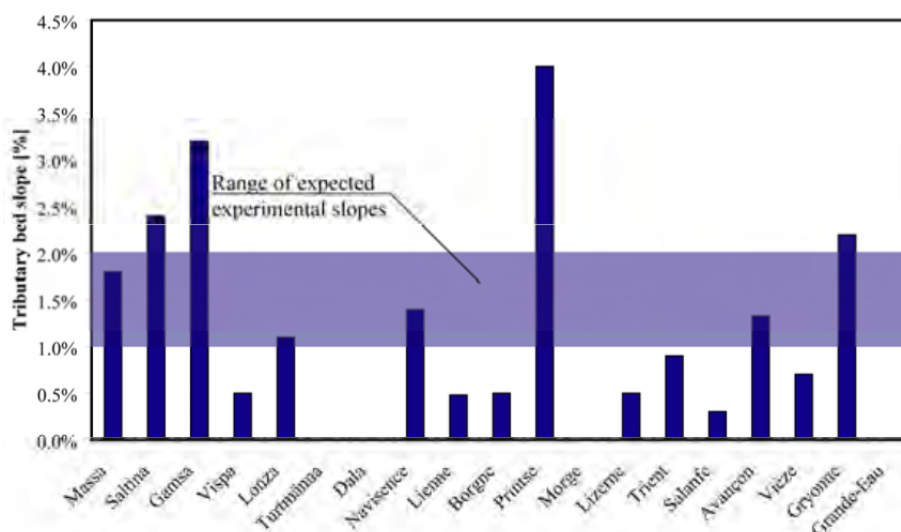
Figure 3.12 Bed slope of the tributaries at the downstream reach before the confluence with the Rhone (Source: "Valais river's database" and "BD-Eaux"). Shaded area indicate the range of self-forming bed slopes during the experiments

In the basin of the Rhone river, the flow regime varies depending on glaciers and snow melting periods combined with hydropeakings. In general, flood events between 2 and 5 years return period (Q_2 and Q_5) can be considered as determinant for the size and shape of a river channel. In addition, these discharges are also responsible for the main morphological and ecological development of fluvial systems over very long time-scales. Figure 3.13 shows the ratio between the discharge of the tributaries and the Rhone during flood events with a return period of 2 and 5 years and the discharge ratios adopted in the experimental setup. In the confluences of the upper part of the basin, the

discharge ratios are about 0.2 and 0.3. In the middle reach of the basin, the discharge ratios are about 0.1 and 0.15. For the confluences near the Lake Geneva, the discharge ratios present very low values ($Q_r < 0.05$). Discharge values of the Dala, Printse, Morge, Lizerne and Salanfe are missing.
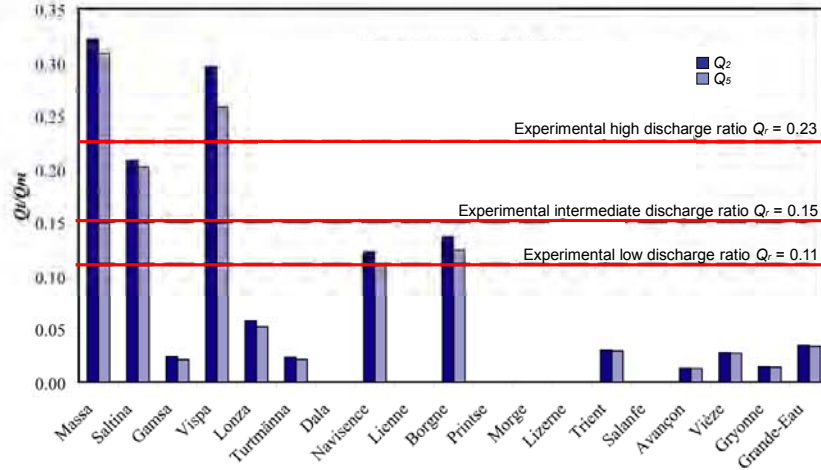
Figure 3.13 Discharge ratio between tributaries and the Rhone river for different flood events with return periods of 2 and 5 years (Source: FOEN). Horizontal solid lines indicate the experimental discharge ratios.

The flow regime of the tributaries has been analyzed by considering the 2 and 5 years return period discharges (Q_2 and Q_5 respectively) and assuming uniform flow. The Manning-Strickler equation was used to determine the uniform flow depth (h). The energy gradient was assumed equal to the bed slope. A Manning coefficient of 0.03 m$^{1/3}$ s^{-1} was adopted (d_{90} of tributaries bed surface is around 0.10 m) and the cross-section was considered rectangular. Figure 3.14 reveals that the flow regime is transcritical ($Fr > 0.70$) for most of the tributaries. Some tributaries (Saltina, Gamsa, Navisance and Gryonne) present supercritical flow regimes ($Fr > 1$) and others present subcritical regimes ($Fr < 1$, Vispa, Lonza, Borge, Trient and Vièze). The extremely low Froude numbers of Turtmanna and Grande-Eau are due to their low bed slopes.
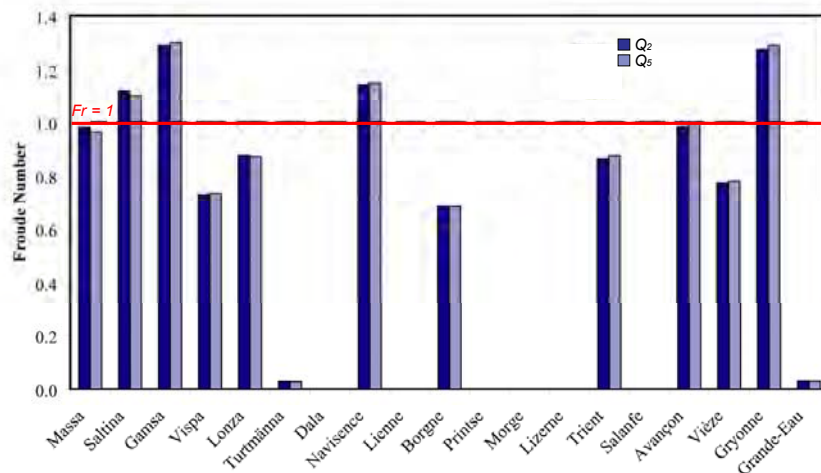
Figure 3.14 Froude number of the main tributaries of the Rhone river. The horizontal solid line indicates $Fr = 1$.

Figure 3.15 shows the dimensionless grain size distribution with respect to the mean diameter (d_m) of the bed surface of the Rhone River at different locations and those of the sediment mixtures used for the experiments.
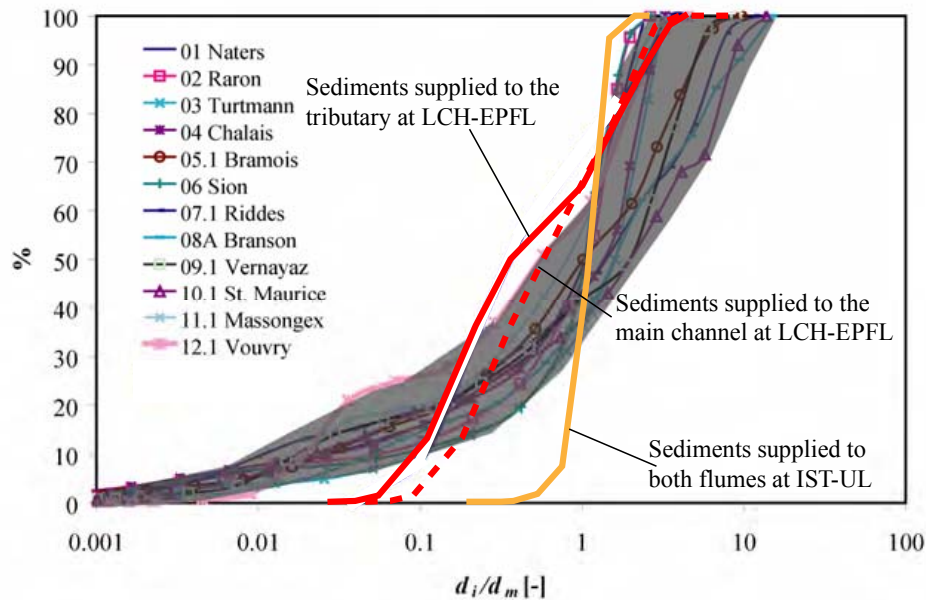
Figure 3.15 Dimensionless grain size distribution of the Rhone river at different locations and those of the used sediment mixtures for the experiments.

Figure 3.15 reveals that the size of the sediment mixtures supplied to the main channel and tributary for the experiments conducted at the LCH-EPFL are in the range of those found in the basin of the Upper Rhone river.

3.7 Experimental procedure and measurements

Each experiment was performed following the same procedure. Before each experiment, the initial movable bed was prepared by using the same sediment mixtures that subsequently were supplied to each channel. The bed of the main channel was roughly flat (Figure 3.16a-c). In the tributary, to accelerate the bed topography evolution, a small bed discordance of approximately 0.03 m was imposed at the tributary mouth, together with a bed slope of about 0.5% (Figure 3.16b-d). This initial bed morphology did not affect the final topography because, as verified later, the initial slope and the initial discordance were smaller than those reached at equilibrium.

Once the channel beds were prepared, the flumes were slowly filled with water, and both bed topographies (for the tributary and for the main channel) were recorded before the beginning of the experiment.

Latter, the tributary and main channel flow discharges and the sediment rates were adjusted to the required values. After that, the downstream tailgate was slowly lowered until the y_d value established for each experimental set was reached. This instant was considered the beginning of the experiments, and it is identified as $t = 0\ h$.
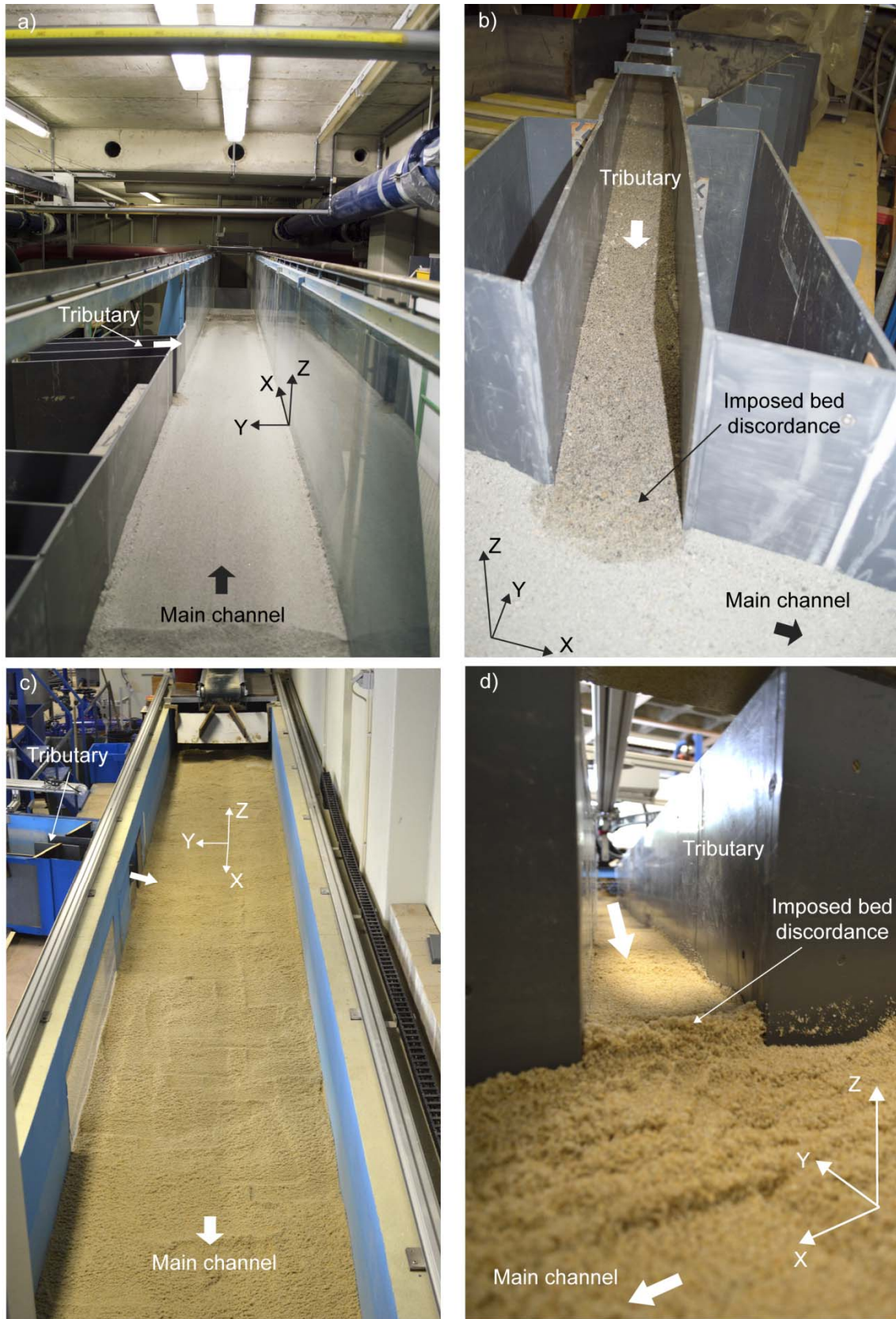
Figure 3.16 a) Initial bed of the main channel of the experimental facility at LCH-EPFL. b) Initial bed of the tributary of the experimental facility at LCH-EPFL. c) Initial bed of the main channel of the experimental facility at IST-UL. d) Initial bed of the tributary of the experimental facility at IST-UL.

The experiments were run until equilibrium was reached, which means that the bed topography attained a quasi-steady state, and the outgoing sediment rate was equal to the incoming rate. To determine when the experiments were in equilibrium, the sediment transport was evaluated at the downstream end of the main channel by weighing the volume of sediments collected in the sediment-recovery tank (Figures 3.5c and Figure 3.7d). The outgoing sediments were weighed with the digital scales of each experimental facility. Additionally, in the experimental sets I and II the evolution of the bed topography was controlled during the experiments at five check points distributed throughout the confluence (Figure 3.17).
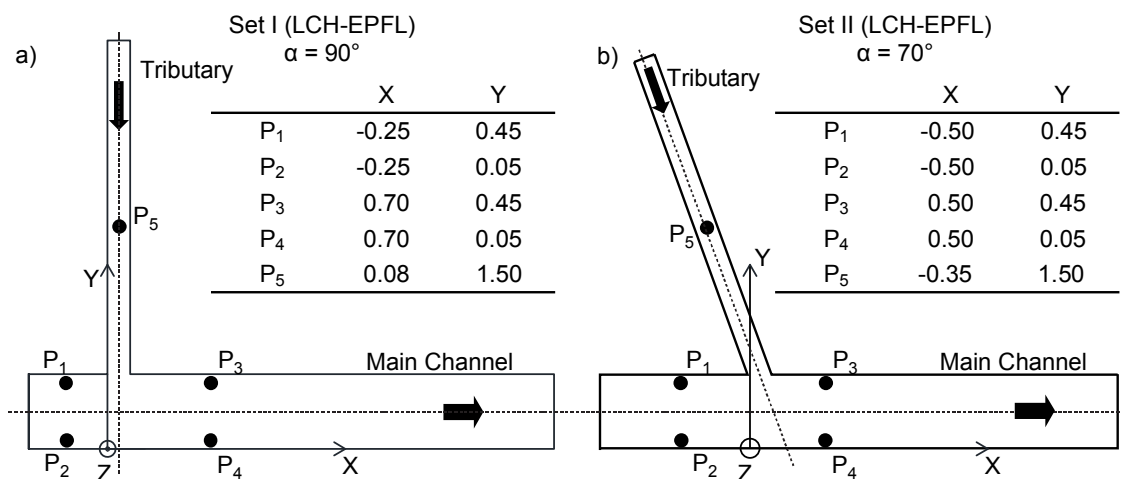
Figure 3.17 Checkpoints to control the bed topography evolution with a) $\alpha = 90°$ and b) $\alpha = 70°$

Bed topography and water surface surveys were systematically recorded during the experiments at $t = 1\ h$, at $t = 7\ h$ and at equilibrium. The time to reach equilibrium varied from 14 to 16 hours, depending on the experimental setup. Bed topography was measured with Mini-Echo-Sounder probes. Since the Mini-Echo-Sounder is an intrusive device that needs to be slightly submerged for measuring, to perform topography surveys the downstream tailgate was raised to increase the water level and to stop the sediment transport by decreasing the flow velocity. Tributary and main channel discharges were reduced and the sediment feeders were switched off. Under these conditions, the bed topography was measured. To restart the experiment, the discharges were adjusted according to the set values, the downstream water level was established, and the sediment feeders were turned on. The stop and re-start processes were shown not to affect the bed topography.

For the instants $t = 1\ h$ and $t = 7\ h$, the water surface was measured immediately after re-starting the experiment, whereas at equilibrium ($t = 14\ h$ to $16\ h$) the water surface was measured just before stopping the experiment. The water surface was measured with the ultrasonic limnimeters, with an adquisition frequency of 100 Hz. For each point, an average value was considered for the analysis.

Both bed topography and water surface measurements were performed as follows in each experimental facility:

- In the facility of the LCH-EPFL, the topographic and water surface surveys consisted of nine longitudinal profiles along the main channel ($Y = 0.05$ to 0.45 m), laterally spaced by $\Delta Y = 0.05$ m with a longitudinal resolution of $\Delta X = 0.01$ m; and one profile along the tributary axis. The tributary profiles were measured every 0.05 m along the flume.

- In the facility of the IST-UL, the topographic and water surface surveys consisted of twenty two longitudinal profiles along the main channel. These profiles were laterally spaced by $\Delta Y = 0.02$ m for set III and $\Delta Y = 0.04$ m for set IV. The longitudinal resolution was of $\Delta X = 0.01$ m. In the tributary, one longitudinal profile along the axis was recorded, with a longitudinal resolution of 0.02 m.

At equilibrium, in the experimental set I, the flow velocity was measured at 12 points distributed throughout the confluence (V_1 to V_{12} in Figure 3.18). These measurements were taken at half flow depth by means of a micro-propeller Schiltknecht with ± 0.01 m/s accuracy.

Points	X [m]	Y [m]
V_1	1.70	0.45
V_2	1.70	0.25
V_3	1.70	0.05
V_4	0.30	0.45
V_5	0.30	0.25
V_6	0.30	0.05
V_7	-0.12	0.45
V_8	-0.12	0.25
V_9	-0.12	0.05
V_{10}	0.08	1.50
V_{11}	0.08	1.00
V_{12}	0.08	0.60
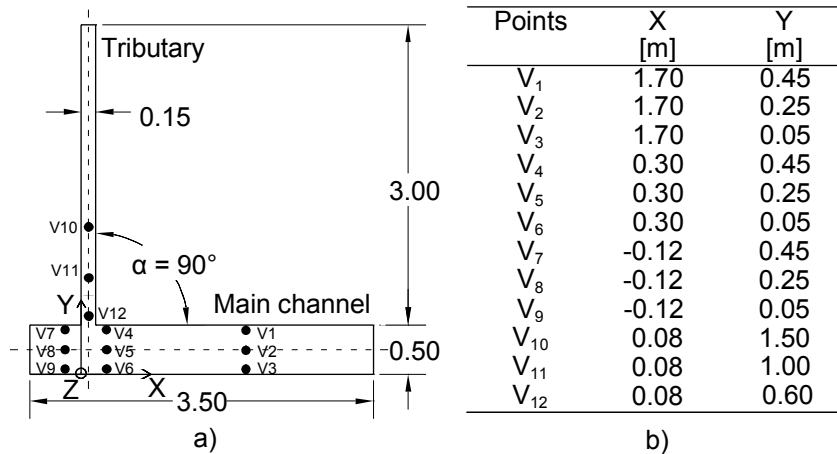
Figure 3.18 Positions of the point-velocity measurements. a) Plan view. b) Coordinates.

At the end of the experiments, the channels were slowly emptied through the bottom outlet, keeping intact the bed topography. In the experimental sets I and II (LCH-EPFL), four samples of the bed sediments were taken to analyze the GSD of the bed surface (Figure 3.19). The samples were obtained by using an adhesive paper to which the surficial bed sediments were glued. These samples were weighed and sieved to obtain the GSD of each one. The four samples corresponded to: i) the main channel upstream of the confluence (S1), ii) the tributary bed upstream of the confluence (S2), iii) the top of the bank-attached bar in the main channel downstream of the confluence (S3), and iv) the lateral slope of the bank-attached bar in the main channel downstream of the confluence (S4). This analysis was not required for sets III and IV, since the supplied sediments were uniform and equal in both flumes.

Figure 3.19 Positions of the bed sediment samples.

3.8 Summary

Table 3.3 contains the main values of the experimental setup. For every set of experiments, the junction angle (α), the width ratio (B_t/B_m), the sediment gradation coefficient (σ), the discharge ratio (Q_r), the unit discharge ratio (q_r), the sediment rates for the main channel and tributary (Q_{sm} and Q_{st}, respectively), the performed measurements, and the chapters where the results are discussed, are given in Table 3.3.

Table 3.3 Summary of the experimental setup and measurements for each experimental set.

Experimental facility	Experimental set	α [°]	B_t/B_m [-]	σ [-]	Q_r [-]	q_r [-]	Q_{sm} [Kg/min]	Q_{st} [Kg/min]	Measurements	Results in chapter
LCH - EPFL	Set I	90°	0.30	3.15; 4.51	0.11 (LR) 0.15 (IR) 0.23 (HR)	0.37, 0.50, 0.77	0.3	0.5	Bed topo at t = 0, 1, 7 h & equilibrium Water surf. at t = 1 h, & equilibrium Point velocities at equilibrium GSD of bed surface	4 – 5 – A1
	Set II	70°	0.30	3.15; 4.51	0.11 (LR) 0.15 (IR) 0.23 (HR)	0.37, 0.50, 0.77	0.3	0.5	Bed topo at t = 0, 1, 7 h & equilibrium Water surf. at t = 1, 7 h & equilibrium.	5 – 6 – A2
IST - UL	Set III	70°	0.30	1.35	0.11 (LR) 0.15 (IR) 0.23 (HR)	0.37, 0.50, 0.77	0.3	0.5	Bed topo at t = 0, 1, 7 h & equilibrium Water surf. at t = 1, 7 h & equilibrium	6 – 7 – A3
	Set IV	70°	0.15	1.35	0.06 (LR) 0.07 (IR) 0.11 (HR)	0.37, 0.50, 0.77	0.6	0.5	Bed topo at t = 0, 1, 7 h & equilibrium Water surf. at t = 1, 7 & equilibrium	7 – A4

4

Hydro-morphodynamic evolution in a 90° movable bed discordant confluence with low discharge ratio

This chapter presents the evolution of the bed morphology and hydrodynamics as observed in an experimental facility with a movable bed. For that purpose, one experiment was carried out in a laboratory right-angled confluence with low discharge ratio, where constant sediment rates were supplied to both flumes. During the experiment, bed topography and water surface elevations were systematically recorded. When the bed topography reached a steady state (so-called equilibrium) and the outgoing sediment rate approximated the incoming rate, flow velocity was measured at 12 different points distributed throughout the confluence, and the grain size distribution of the bed surface was analyzed. Typical morphodynamic features of discordant confluences such as a bank-attached bar and a flow deflection zone are identified in this study. Nevertheless, the presence of a marked scour hole in the discordant confluence and distinct flow regimes for the tributary and main channel, differ from results obtained in previous studies. Strong acceleration of the flow along the outer bank of the main channel is responsible for the scour hole. This erosion is facilitated by the sediment discharge into the confluence from the main channel which inhibits bed armoring in this region. The supercritical flow regime observed in the tributary is a hydrodynamic response to the imposed sediment rate in the tributary.

4.1 Introduction

Alpine river confluences are system characterized by low discharge and momentum ratios. In this type of confluence, the main stream provides the dominant discharge and the sediments are predominantly and abundantly supplied by the tributaries, whose bed level is higher than the bed of the main channel (bed discordance). Tributaries are narrower but steeper than the main stream, and such steep slopes and sediment loads often result in supercritical flows in the tributaries. The sediment provided by the tributaries is coarser than that supplied by the main stream and consists of poorly sorted gravel with high gradation coefficients.

To examine such conditions, Leite Ribeiro *et al.* (2012a, b, 2015) carried out experiments with low discharge and momentum ratios ($Q_r = 0.11$ and $M_r = 0.22$) in a laboratory right-angled confluence where sediment was supplied to only the tributary. The lack of sediment discharge in the main channel induced an artificial bed armoring that may not occur in nature. According to Leite Ribeiro *et al.* (2012a, b, 2015) the morphodynamic of this type of confluence is characterized by a pronounced bed discordance between the tributary and main channel, an absence of marked bed erosion, and critical or supercritical flow regime in the tributaries.

With the aim of increasing existing knowledge of the hydro-morpho-sedimentary processes found in river confluences, an experimental study was carried out in a laboratory right-angled confluence with low discharge and momentum ratios ($Q_r = 0.11$ and $M_r = 0.16$). To build on the work by Leite Ribeiro *et al.* (2012a) and to better approximate conditions observed in nature, sediments were supplied to both the tributary and the main channel during the experiment. Systematic bed topography and water surface surveys illustrate the main morphological and hydrodynamic features, the flow velocity was measured at 12 different points distributed throughout the confluence. Sediment patterns and bed material texture at equilibrium were also analyzed. The results of this study are contrasted with previous studies concerning the hydraulics, morphology and sedimentology of river confluences.

4.2 Experimental setup

The results presented herein correspond to one experiment performed with $Q_r = 0.11$ (LR) and $\alpha = 90°$ in the experimental facility of the LCH-EPFL. The experimental setup is summarized in Table 4.1 and described in detail in Chapter 3.

Table 4.1 Overview of the experimental setup

Experimental set	α [°]	B_t/B_m [-]	σ [-]	Q_r [-]	Q_{sm} [Kg/min]	Q_{st} [Kg/min]	Measurements
Set I	90°	0.30	3.15 (main) 4.51 (trib)	0.11	0.3	0.5	Bed topo at t = 0, 1, 7 h, & eq W. surf at t = 1 h & eq Point velocities at equilibrium GSD of bed surface at equilibrium

4.3 Results

4.3.1 Bed morphology and water surface evolution

The bed morphology and the water surface evolved from the beginning of the experiment until reaching equilibrium. At the beginning ($t = 0$ h), the bed was fairly horizontal in the main channel, whereas the tributary bed had a slight slope and a small step at the mouth (see Figures 4.1 and 4.2).

After one hour ($t = 1$ h), a scour hole formed at the tributary mouth while the eroded material deposited downstream at about $X = 2.00$ m (cf. Figures 4.1b and 4.2a). The maximum depth of the scour hole was $Z = -0.04$ m located at $X = 0.20$ m, $Y = 0.45$ m.
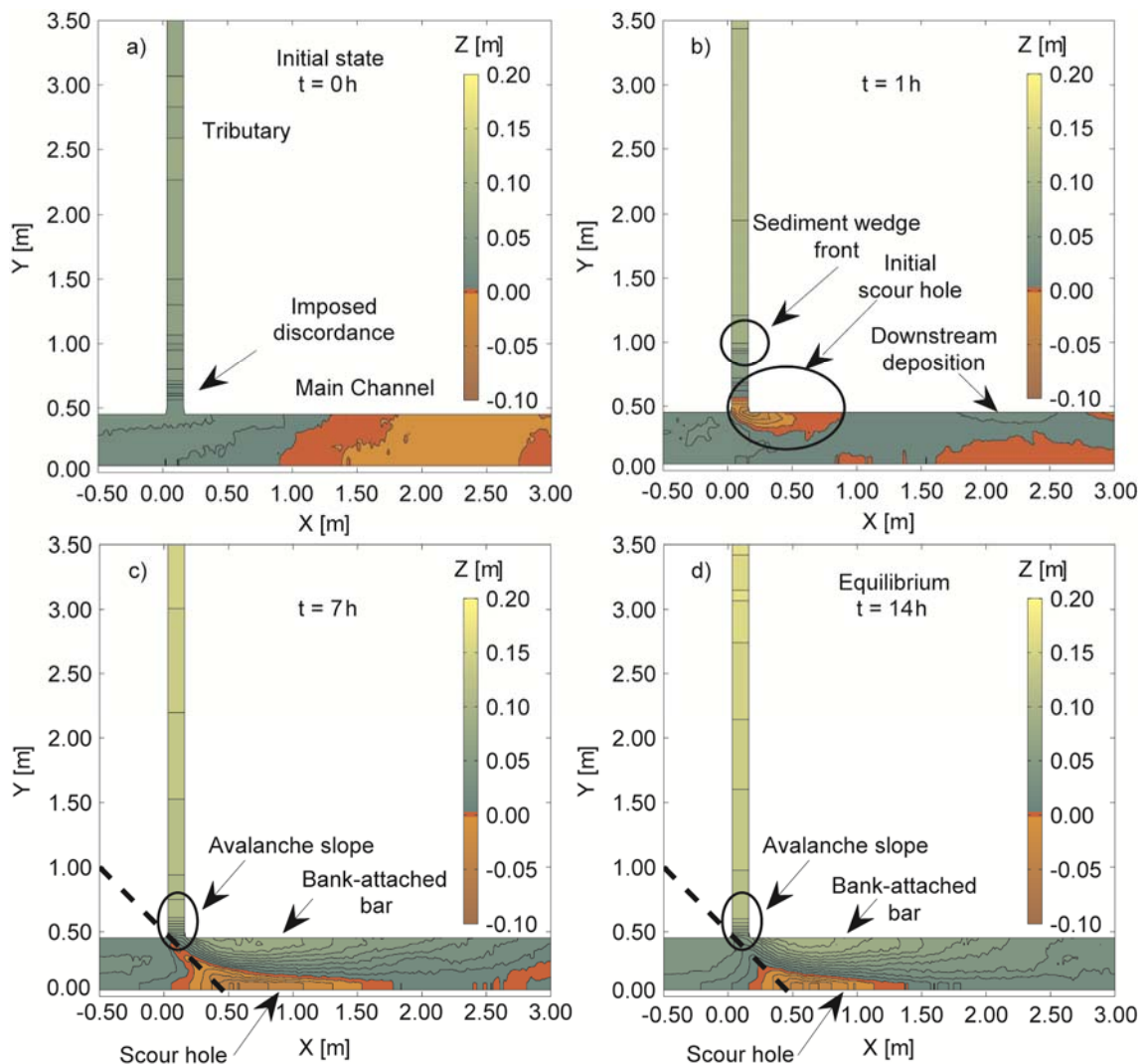
Figure 4.1 Bed topography with bed-level contours spaced $\Delta Z = 0.01$ m: a) at the initial state ($t = 0$ h); b) after one hour ($t = 1$ h); c) after 7 hours ($t = 7$ h); and d) at equilibrium ($t = 14$ h).

In the tributary, during the first hour, the supplied sediment formed a wedge that gradually progressed downstream (cf. Figures 4.1b and 4.2c), raising the level of the bed. At $t = 1$ h, the front of this wedge was located at $Y \sim 1.00$ m (cf. Figures 4.1b and

4.2c). The position of this wedge at $t = 1$ h reveals that the scour hole was excavated in the initial bed of the main channel.

The water surface gradient at $t = 1$ h was relatively mild in both channels (Figure 4.2). In the main channel and at the inner bank, an abrupt increase in water-surface elevation related to the tributary inflow was measured at the confluence (cf. Figure 4.2a). In the tributary, the water level profile rose from $Y = 2.00$ m to $Y = 0.50$ m, which revealed the presence of an M1-type backwater curve (Chow, 1959) imposed by the elevated water level in the main channel (Figure 4.2c).
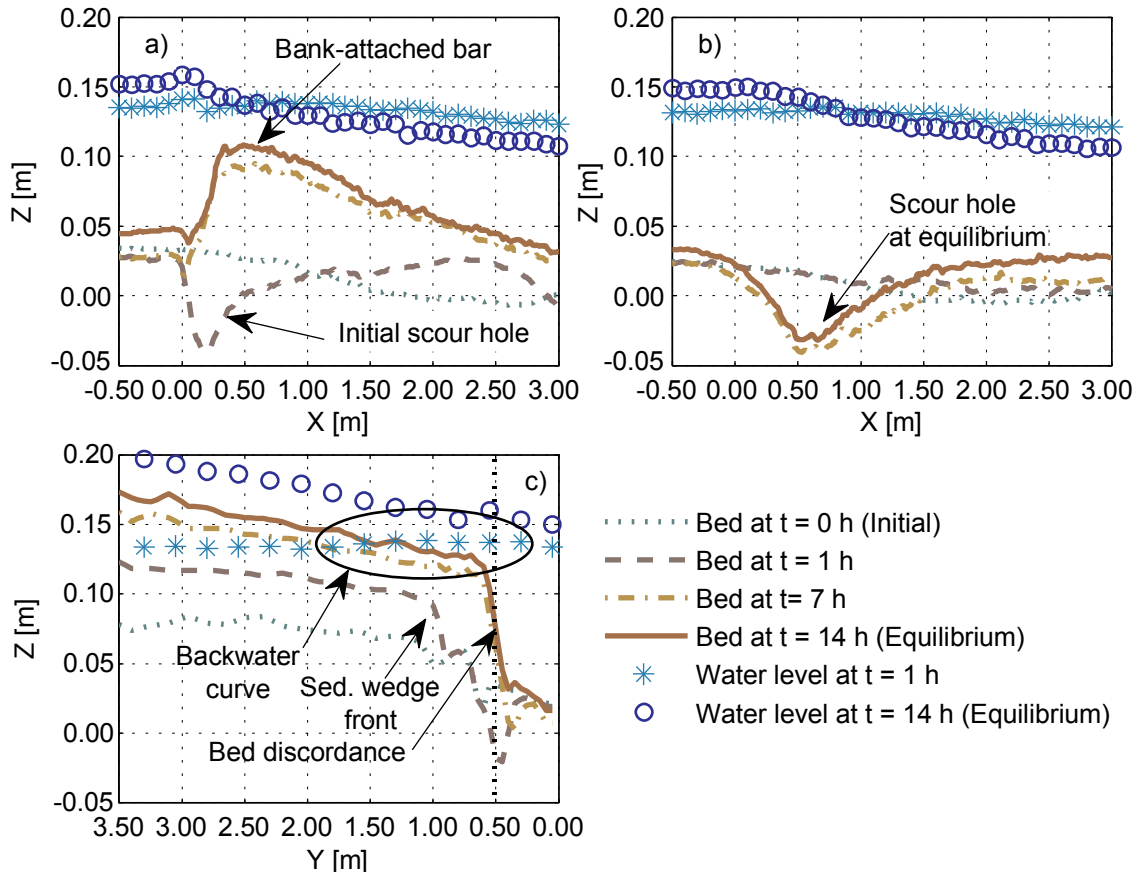
Figure 4.2 Longitudinal profiles of channel bed and water surface: a) at the inner bank of the main channel, b) at the outer bank of the main channel, and c) at the tributary axis.

After 7 hours ($t = 7$ h), the tributary attained a quasi-equilibrium bed morphology consisting of a steep bed slope, a raised bed elevation and a well-developed bed discordance with the main channel (see Figures 4.1c and 4.2c).

At the inner bank of the main channel (cf. Figure 4.2a), downstream of the confluence, the sediment coming from the tributary in the form of a migrating wedge filled the initial scour hole and created a bar (Figure 4.3a), commonly termed as a bank-attached bar (Best and Rhoads, 2008). In addition, a new scour hole extended from the tributary mouth to the outer bank of the main channel, flanking the bar (Figure 4.3a). The alignment of the new scour bisected the junction angle until reaching the outer bank, at which point it paralleled the orientation of the outer bank (cf. Figures 4.1c, 4.2b, and 4.3a). From seven hours ($t = 7$ h) until reaching equilibrium ($t = 14$ h), the

bed morphology in both channels experienced only minor changes, including a small increase in the height of the bank-attached bar (cf. Figure 4.2).
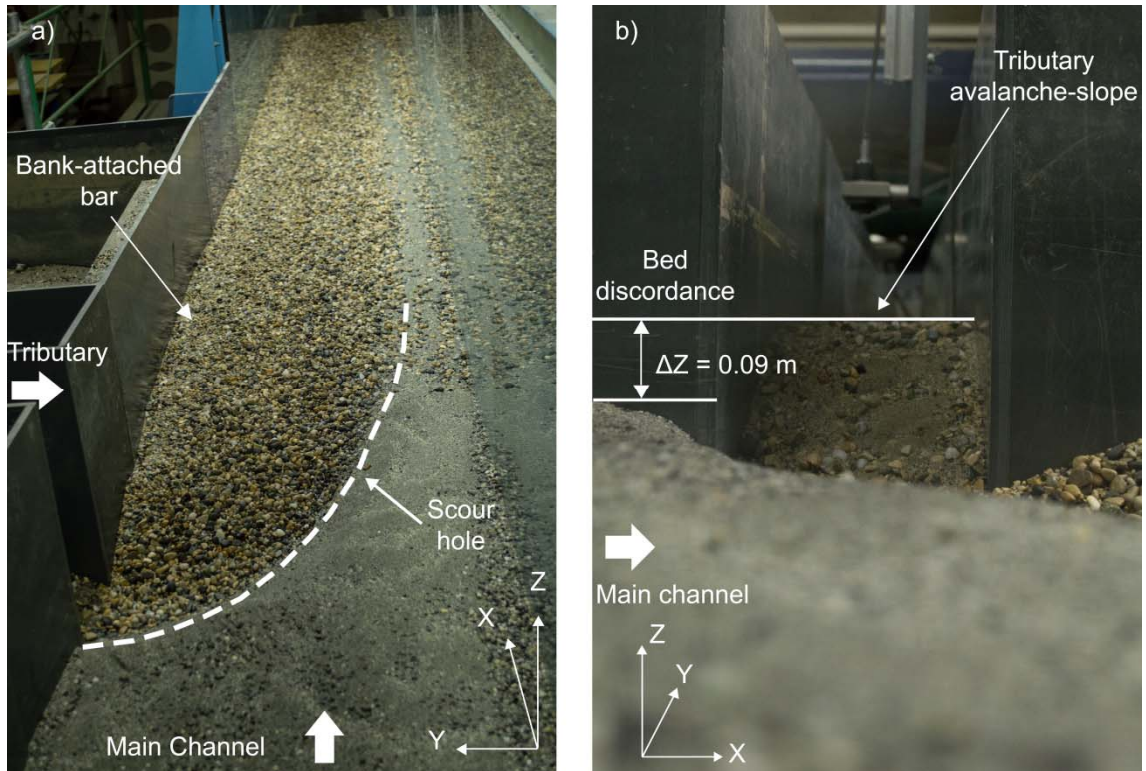
Figure 4.3 Bed morphology at equilibrium: a) downstream view from the main channel; b) frontal view of the tributary mouth.

At equilibrium, the tributary had a nearly constant longitudinal slope of approximately 1.6 % (Figure 4.2c and detail in Figure 4.3). The transition between the tributary and main channel was characterized by a steep wedge front or avalanche slope, with an average inclination of approximately 44 % that partially penetrated into the main channel (cf. Figures 4.3 and 4.4b). This morphological feature is herein considered as the inception of a tributary mouth-bar, which is commonly observed in river confluences (Best and Rhoads 2008).
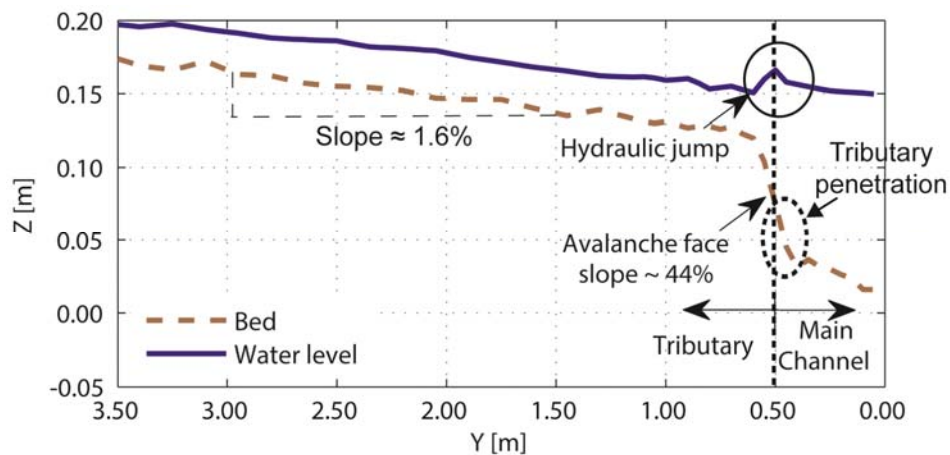
Figure 4.4 Bed level and water surface profiles along the tributary axis at equilibrium (t = 14 h).

At the inner bank of the main channel ($Y = 0.45$ m, Figure 4.2a and detail in Figure 4.5a) the bed remained nearly flat until reaching the confluence ($X \approx 0.00$ m), where the inception of the scour hole was observed at the tributary mouth as a small depression (Figure 4.5a). Downstream of the confluence, the bank-attached bar rapidly reached its maximum level ($Z = 0.108$ m at $X = 0.50$ m) through a steep slope (approximately 30%). Downstream of this maximum, the bar height gradually decreased through a slope of approximately 3 %. The steeper slope of the upstream face of the bank-attached bar is the result of the strong upwelling flow observed at the downstream junction corner (cf. Figure 4.6).
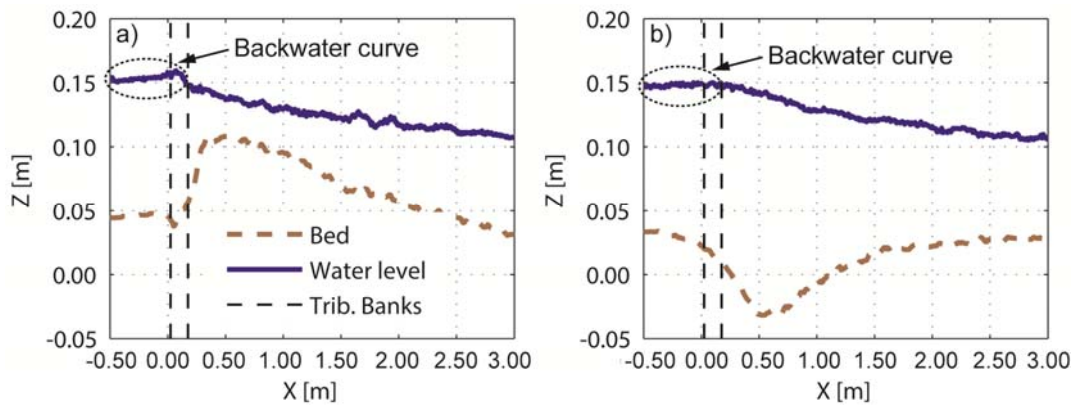
Figure 4.5 Bed level and water surface profiles at equilibrium ($t = 14$ h): a) along the inner bank ($Y = 0.45$ m); and b) along the outer bank of the main channel ($Y = 0.05$ m).
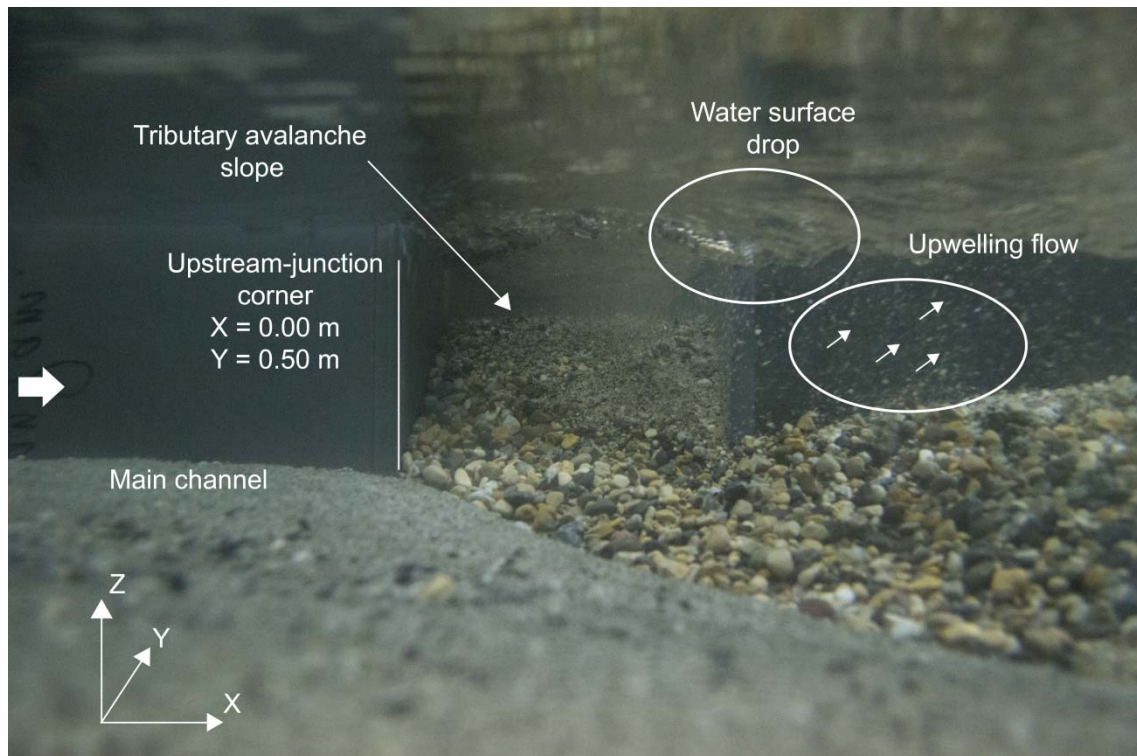
Figure 4.6 Frontal view of the tributary mouth. Notice the water surface drop and the upwelling flow at the downstream junction corner

At the outer bank ($Y = 0.05$ m, Figure 4.5b), upstream of the confluence, the bed level started to decrease progressively until reaching a minimum at $X \approx 0.70$ m. Downstream of this low point, the bed level increased, until converging to the same level as upstream of the confluence (cf. Figure 4.2c and detail in Figure 4.5b).

The water level profile measured in the tributary at equilibrium (see Figure 4.3) showed a steep and nearly constant slope until reaching the confluence. At the mouth, an abrupt increase in water surface elevation revealed the presence of a hydraulic jump. Moreover, in the tributary, the water level profile was parallel to the bed, indicating that the flow was nearly uniform.

In the main channel, at the inner bank ($Y = 0.45$ m) upstream of the confluence ($X < 0.00$ m), the water level profile (Figure 4.5a) exhibited an upstream-oriented slope. At a distance of $X = 0.08$ m, the water surface reached a maximum level ($Z = 0.160$ m). This water level profile corresponds to a M1-type backwater curve (Chow, 1959) induced by the tributary inflow. The local water level increase may be associated with the presence of a stagnation zone, which was visually observed at the upstream corner of the confluence. At the downstream junction corner ($X = 0.15$ m in Figure 4.5a), the water surface exhibited a drop revealing a low pressure zone, which was caused by the abrupt change of direction of the tributary flow (90°). Downstream of the confluence, due to the flow constriction exerted by the bank-attached bar and the fixed lateral banks, the flow accelerated and the slope of the water surface increased.

At the outer bank of the main channel ($Y = 0.05$ m), upstream of the confluence ($X < 0.00$ m), the water level profile (Figure 4.5b) was nearly horizontal, which again corresponds to a M1-type backwater curve (Chow, 1959) induced by the tributary inflow. As observed at the inner bank, the water level gradient increased downstream of the confluence, corresponding to flow acceleration.

Figure°4.7 depicts the cross-sectional average (CSA) values of bed elevation, water level and water depth along the main channel at equilibrium. Upstream of the confluence ($X < 0.00$ m), the water depth increased until reaching its maximum at $X \sim 0.08$ m. Such an increase confirms the presence of a M1-type water curve in the upstream region. Consequently, the mean velocity in the main channel decreased. Downstream of the confluence, between $0.15 < X < 1.50$, the water depth rapidly decreased because of the flow acceleration; and for $X > 1.50$ m, the flow became nearly uniform, as confirmed by the constant CSA water depth.
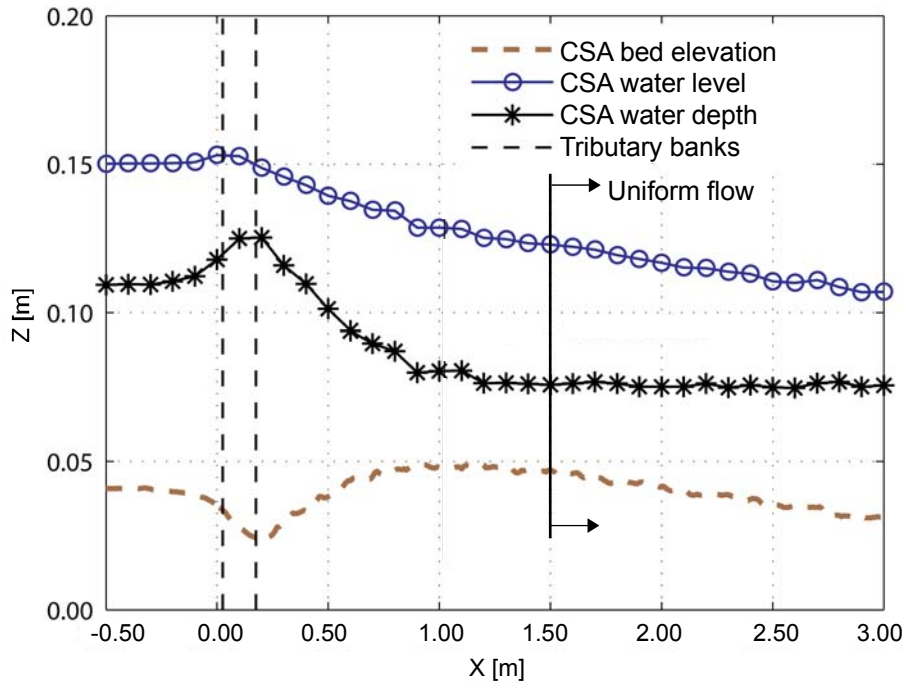
Figure°4.7 Cross-sectional average (CSA) values of bed elevation, water surface elevation and water depth along the main channel at equilibrium.

4.3.2   Velocities

At equilibrium, using the CSA water depths, the mean velocities were computed upstream of the confluence at X = -0.25 m for the main channel (U_{mu}), at Y = 2.00 m for the tributary (U_t), and downstream of the confluence in the main channel (X = 2.50 m, U_{md}). The obtained values are shown in Table 4.2 together with their respective water depths and Froude numbers.

Table 4.2 Main hydraulic variables for the confluence physical system at equilibrium.

y_{mu}	y_{md}	y_t	U_{mu}	U_{md}	U_t	Fr_{mu}	Fr_{md}	Fr_t
[m]	[m]	[m]	[m/s]	[m/s]	[m/s]	[-]	[-]	[-]
0.109	0.075	0.028	0.50	0.80	0.72	0.48	0.93	1.37

where y_{xx}, U_{xx}, and Fr_{xx} refer to the CSA values of water depth, flow velocity and Froude number, respectively. Subscripts mu, md and t refer to main channel upstream, main channel downstream and tributary, respectively.

Froude numbers show the existence of two different flow regimes in the confluence. In the main channel upstream of the confluence, flow is subcritical ($Fr < 1$), whereas downstream of the confluence, the flow was trans-critical ($0.7 < Fr < 1.0$). Supercritical flow ($Fr > 1$) occurred in the tributary. These differences in flow regimes, which were also observed by Leite Ribeiro *et al*. (2012a), resulted in a hydraulic jump at the junction, which can be observed in Figure 4.3 by an abrupt increase of the water level, at approximately Y = 0.50 m, in the transition between the tributary and the main channel.

The point-velocity values measured at equilibrium in the main channel upstream of the confluence (V_7 to V_9 in Figure 4.8) reveal a fairly uniform distribution of the flow velocity across the section, which is in agreement with the observation of a fairly uniform bed and water surface across the section (see Figure 4.5) and with the computed CSA velocity (U_{mu}) shown in Table 4.2. The nearest point-velocity value to the upstream junction corner (V_7 in Figure 4.8) was measured 12 cm upstream of the confluence and thus does not show any evidence of a stagnation zone, although the existence of a stagnation zone was inferred from the local water level increase at $X = 0.60$ m (Figure 4.5a).
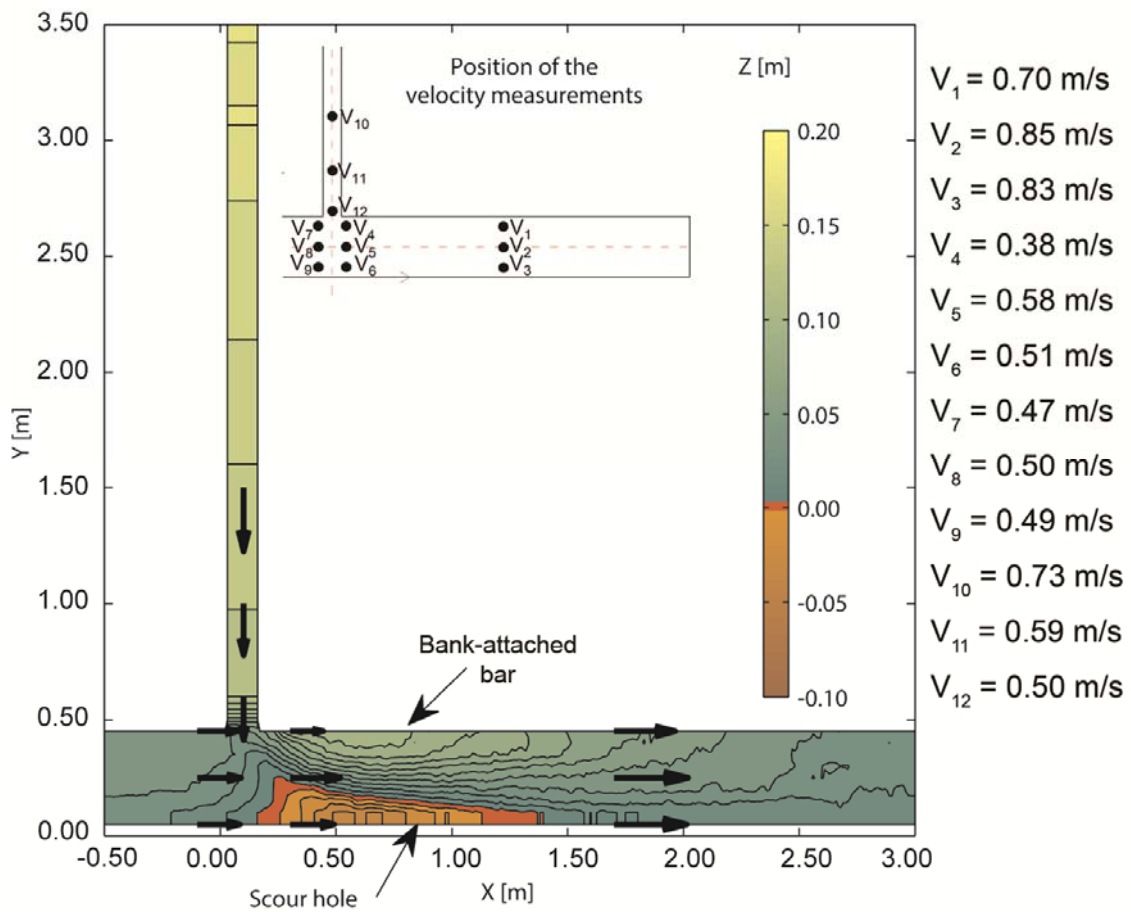
Figure 4.8 Point velocity measurements over the bed topography at equilibrium (see Figure 3.18 for measuring position).

At the downstream corner of the junction (V_4 in Figure 4.8), the presence of a zone of reduced velocities, which favored the deposition and growth of the bar, was observed. The positive velocity value at this point, together with the steep slope of the water surface (see Figure 4.5a), indicates the absence of a recirculation zone at equilibrium. At the outer bank downstream of the confluence, the flow was concentrated in the region of the main scour hole (V_5 and V_6 in Figure 4.8).

Farther downstream, where the scour hole and the bank-attached bar vanished, flow velocities increased, indicating a general convective acceleration of the flow between $X = 0.80$ m and $X = 2.20$ m, and trending again toward a uniform distribution

of the velocity across the section. These velocities (V_1 to V_3 Figure 4.8) are representative of the recovery zone, and they are close to the computed cross-average velocity $U_{md} = 0.80$ m/s.

In the tributary, the velocity measured at the point V_{10} (see Figure 4.8) is similar to the value U_t computed in Table 4.2. However, V_{11} to V_{12} appear to be unreliable because the low values of velocity at these locations are not consistent with the constant water depth observed in the longitudinal profile depicted in Figure 4.3. The poor quality of these velocity readings may be due to the shallow water depth ($y_t = 0.028$ m) compared with the size of the micro-propeller.

4.3.3 Sediment transport

Observations during the experiments provide insight into the dynamics of bedload in the confluence (Figure 4.9). At equilibrium, the spatial distribution of bed sediments downstream of the confluence reveals segregation between those coming from the tributary and those from the main channel. The tributary bed load was conveyed along the inner part of the main channel, whereas the sediment supplied to the main channel was transported along the outer bank (see Figure 4.9). Selective paths for the sediment originating from the tributary were observed: the finer portion of sediment coming from the tributary moved through a corridor along the crest of the bank-attached bar, whereas the coarser sediment was transported along the avalanche face of this bar (Figure 4.9).
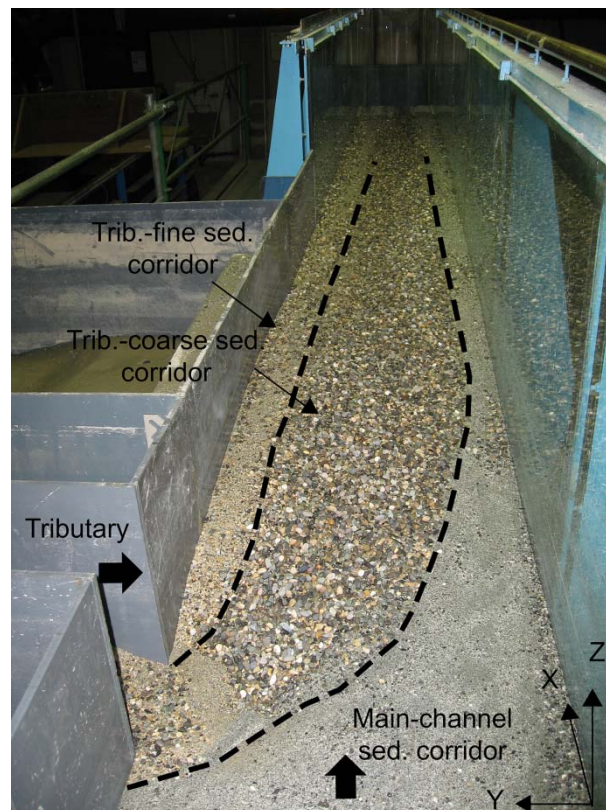
Figure 4.9 Upstream view of the main channel bed at equilibrium. Notice the sediment segregation between the tributary sediments (inner bank) and those originating from the main channel (outer bank).

The GSD of the bed surface was analyzed by four representative samples taken at different places within the confluence system (Figure 4.10). In the main channel, the GSD of S1 indicates a slight coarsening ($d_{50} \sim 1$ mm) with respect to the initial bed ($d_{50} = 0.8$ mm) as shown in Figure 4.11. In the tributary bed (S2), the bed surface was covered by a coarse armor layer with a $d_{50} \sim 1.5$ mm (cf. Figure 4.10a), which was considerably larger than the initial mixture ($d_{50} = 0.8$ mm). A lack of the small size fractions in the sediment mixture was particularly evident for sizes smaller than 2 mm (see Figure 4.11).
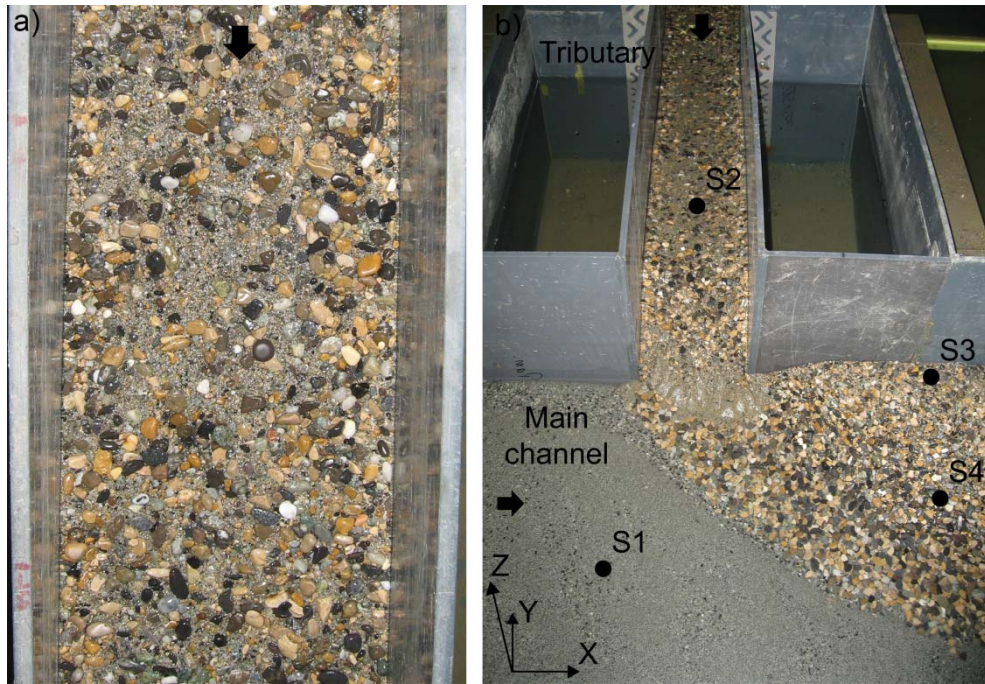
Figure 4.10 a) Bed surface of the tributary at equilibrium. Notice the armouring of the surface. b) Bed surface of the main channel at equilibrium. The black points indicate the position of the samples for the GSD analysis.
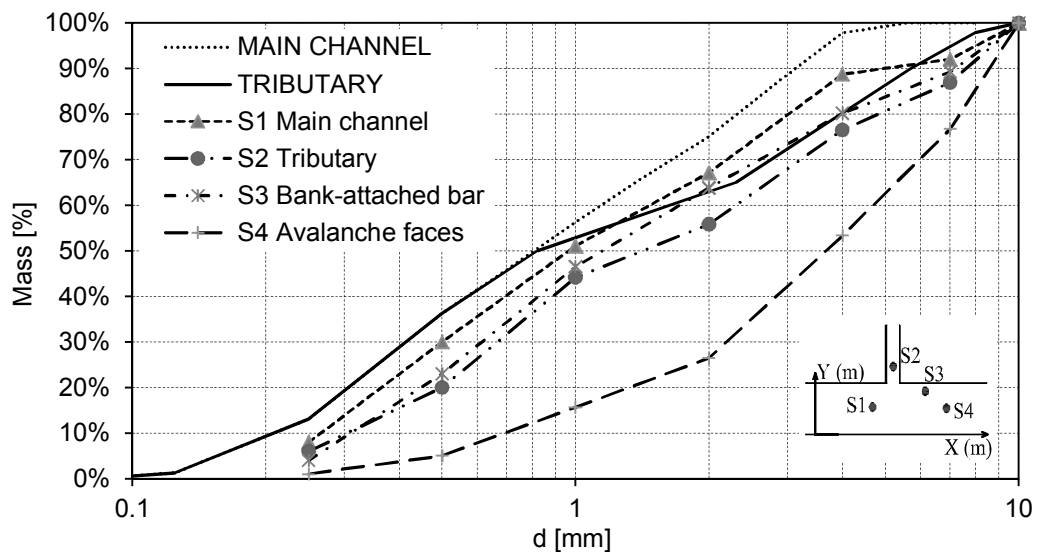
Figure 4.11 GSD of the initial sediments and samples at different position after equilibrium was reached (see Figure 4.10b for sample positions)

The GSD corresponding to S3, taken at the top of the bank-attached bar, fits well with the GSD of the tributary bed surface (S2), indicating that the bar was fed mainly by the tributary. The larger amount of fine sediment in sample S3 than in sample S4 confirms the presence of a corridor of fine sediment at the top of the bank-attached bar.

At the lateral slope of the bank-attached bar (S4), the GSD reveals armoring ($d_{50} \sim 3.7$ mm) with respect to the initial sediment supplied into the tributary ($d_{50} \sim 0.8$ mm). This armoring is in agreement with the observation of a coarse sediment corridor at this position (cf. Figure 4.9).

4.4 Discussion

4.4.1 On the bed morphology

The initial state ($t = 0$ h) corresponds to a fairly planar channel bed for the main channel and a relatively steep bed for the tributary (slope ~ 0.5 %).

After one hour ($t = 1$ h), a scour hole at the channel junction was observed (Figures 4.1b and 4.2a). This scour hole was eroded in the initial bed of the main channel because the front of the sediment wedge from the tributary had not yet reached the confluence. This initial scour hole is a typical feature observed either in symmetrical or asymmetrical concordant confluences (Mosley, 1976). Similar confluence scour holes were also reported by other authors such as Ashmore & Parker (1983); Best (1988) and Ghobadian & Bajestan (2007). That initial scour hole was progressively filled with sediment coming from the tributary until reaching equilibrium, whereas the tributary bed increased in elevation above the bed of the main channel.

The discordance between the tributary and main channel beds, observed at equilibrium, was due to the dominant sediment load in the tributary compared to that of the main channel, and it was considerably larger than the one initially imposed. The avalanche slope observed in the tributary mouth enhances the transport of coarse tributary sediment into the confluence. Best & Roy (1991), Biron *et al*. (1993), Biron *et al*. (1996a), Biron *et al*. (1996b), Boyer *et al*. (2006), Best & Rhoads (2008) and Leite Ribeiro *et al*. (2012a) documented the important influence of the bed height discordance on the bed morphology and flow dynamics within the confluence.

The bank-attached bar is associated with the reduced velocity zone observed at the downstream junction corner. This feature was also observed by Mosley (1976), Best (1988), Biron *et al*. (1993), Rhoads & Kenworthy (1995), Leite Ribeiro *et al*. (2012a), and Leite Ribeiro *et al*. (2012b) in asymmetrical confluences. Although the bar is typically associated with flow separation at the downstream junction corner, it may also form in regions of flow deceleration without actual flow separation (Best and Rhoads 2008).

At equilibrium, a final scour hole formed in the main channel whose alignment bisected the junction angle (Mosley, 1976; Ashmore and Parker, 1983). The scour became parallel to the outer bank (see Figures 4.1d and Figure 4.3b). This erosion is

mainly motivated by net outward flow in the main channel. Due to lateral deflection of the main-channel flow by the tributary and by the bank-attached bar, the flow in the main channel is confined to the outer bank, where it accelerates and erodes the bed. The tributary inflow affects the upper-part of the main flow because of the bed discordance, whereas the near-bed flow of the main channel is steered to the outer bank by the bank-attached bar. When both deflected flows (upper and lower) converge in the outer bank, the unitary flow discharge increases, leading to flow acceleration. Moreover, the turbulence associated with the shear/mixing layer (Best, 1987) present at the flow deflection zone contributes to this erosion. A similar scour hole, confined to the outer bank of the main stream, was observed by (Rhoads, 2006) in a natural concordant confluence with $M_r > 1$. In this case, the deflection of the flow of the main channel, along with the consequent flow concentration at the outer bank, was mostly caused by the tributary inflow. Biron *et al*. (1993) noted an absence of marked scour holes at discordant confluences and Leite Ribeiro *et al*. (2012a), who also studied discordant confluences, reported only weak erosion associated with the convective flow acceleration at the outer bank. In the case of Biron *et al*. (1993), the absence of a marked scour hole at the Bayonne-Berthier confluence in Canada may be a consequence of weak flow deflection exerted by both the tributary inflow and the bank-attached bar. In the case of Leite Ribeiro *et al*. (2012a), though the bank-attached bar considerably reduced the effective flow section in the main channel, the acceleration experienced by the flow did not produce significant erosion, possibly due to armoring.

4.4.2 On the hydrodynamics

The flow patterns observed in this study agree with the two-layer flow structure reported by Leite Ribeiro *et al*. (2012a), Biron *et al*. (1993), and Biron *et al*. (1996). In discordant confluences, the tributary flow deflects the upper part of the main channel flow towards the outer bank, whereas the lower part of the main flow, protected by the bed discordance, flows unimpeded downstream until reaching the bank-attached bar. This bar steers the flow toward the outer bank of the channel producing flow convergence and acceleration.

The hydrodynamic features inferred from the present experiment at equilibrium consisted of: i) a reduced-velocity zone instead of a flow separation zone at the downstream junction corner; ii) the presence of upwelling flow also at the downstream junction corner; iii) a flow deflection zone associated with a shear layer; iv) an acceleration zone created by the flow-constriction exerted by the bank-attached bar and the lateral banks of the main channel; v) a zone of flow recovery downstream of the confluence where the flow tends to recover a uniform distribution along the cross-section (see V_1 to V_3 in Figure 4.8); and vi) a hydraulic jump at the tributary mouth, which was also observed by Leite Ribeiro *et al*. (2012a) and Leite Ribeiro *et al*. (2012b).

The absence of flow separation and the presence of upwelling flow at the downstream junction corner were identified by Biron *et al*. (1993), Biron *et al*. (1996a),

and Biron *et al*. (1996b) as typical flow patterns in discordant confluences. The low-pressure zone observed at the downstream junction corner (X = 0.15 m in Figure 4.8a) attracted the non-deflected near-bed flow of the main channel, which upwelled towards the surface (cf. Figure 4.6). This flow-upwelling inhibited the formation of flow recirculation (Biron *et al*. 1996b).

Additionally, the local water level increase observed at the upstream junction corner (see Figure 11a) may correspond to the stagnation zone that Leite Ribeiro *et al*. (2012a) and Rhoads and Sukhodolov (2001) observed at the same location. This local water level increase, caused by the tributary inflow, induced an M1 backwater curve (Chow, 1959) in the main channel upstream of the confluence .

The water surface profile along the tributary, where the flow was supercritical, exhibited an abrupt elevation increase in the water surface at the junction with the main channel (Y = 0.50 m in Figure 4.3). This abrupt increase in the water surface elevation corresponds to a hydraulic jump as supercritical flow joins the subcritical flow of the main channel. Thus a change of flow regime occurred as tributary flow entered the main channel flow. Supercritical flow regime in the tributary at equilibrium was also observed by Leite Ribeiro *et al*. (2012a). This regime seems to be the result of the hydrodynamic adjustment to the imposed sediment load to the tributary.

4.4.3   On the sedimentology

The sediment segregation observed in the main channel at equilibrium is consistent with data from Best (1988) that indicates that segregation becomes more pronounced with the increase of the junction angle, the flow deflection and the depth of the scour hole.

Despite the different discharge ratios between this study and that of Best (1988) (0.11 in this study and 0.93 to 1.08 in Best, 1988) and the different junction angles (90º in this study and 70º and 105º in Best, 1988), the patterns of sediment transport observed in this study are quite similar to those reported by Best (1988). The sediment movement originated in the main channel concentrated at the outer bank, whereas the load from the tributary was conveyed along the bank-attached bar, which occupied the inner part of the main channel.

Bed morphology and sediment patterns observed in this study at equilibrium are in good agreement with those documented by Rhoads *et al*. (2009) for a natural asymmetrical concordant confluence under high discharge ratio conditions ($Q_r > 1$) where the tributary flow discharge and sediment flux are dominant over the main channel. Under these conditions, Rhoads *et al*. (2009) reported that the tributary flow and bed load penetrate into the confluence wrapping around the downstream junction corner, creating a bar along the inner bank of the main channel. The tributary flow penetration confines the main channel flow to the outer bank, where it accelerates and erodes the bed. The bed sediment mixture was composed of a coarse sediment bar along the inner bank of the main channel, a fine sediment corridor along the crest of the bar, and the presence of fine sediment from the main channel at the lateral slope of the bar

(Rhoads *et al*. 2009). This mixture of sediment from the tributary and main channel contrasts with the results observed in this study, in which inputs of sediment from each channel remained segregated downstream of the confluence (cf. Figure 4.9). This difference may be attributed to the absence of any curvature-induced helical cells from the tributary in this study because both flumes were straight. Rhoads *et al*. (2009) reported that these cells swept the fine sediment provided by the main channel towards the inner bank.

The similar bed morphology between this study (based on a discordant confluence with a low discharge ratio, $Q_r < 1$) and that of Rhoads *et al*. (2009) (based on a concordant confluence with a high discharge ratio, $Q_r > 1$), lies on the outward deflection of the main channel flow that leads to flow acceleration at the outer bank, where erosion occurs. In the concordant confluence (Rhoads *et al*. 2009), the outward flow deflection is strongly influenced by the tributary inflow due to the dominant tributary momentum ($Q_r > 1$), whereas in this study with a discordant bed, the tributary inflow deflects the upper part of the main channel flow, and the lower part is deflected by the bank-attached bar.

4.4.4 Comparison with Leite Ribeiro's *et al*. (2012a) results

To analyze the influence of the sediment supplied into the main channel, the results obtained in this study are compared with those obtained by Leite Ribeiro *et al*. (2012a), where sediment was supplied to only the tributary. Both studies were carried out in the same laboratory confluence, for the same discharge ratio ($Q_r = 0.11$) (Table 4.3), and supplying the same sediment mixture for the tributary.

To guarantee sediment transport capacity all along the main channel in this study, the total flow discharge (Q_{p-c}) was increased to 30 l/s, which contrasts with the 20 l/s adopted by Leite Ribeiro *et al*. (2012a). This increase in flow discharge leads to a reduction in the momentum ratio ($M_r = M_t / M_m$) from 0.22 to 0.16 (cf. Table 4.3).

Table 4.3 compares the discharge and momentum values, computed for the equilibrium state, for the present study with those of Leite Ribeiro *et al*. (2012a). Only the kinetic component of momentum was considered, i.e., for the tributary $M_t = \rho Q_t U_t$, and for the main channel $M_m = \rho Q_m U_{mu}$, where U_{mu} and U_t are the upstream mean velocities for the main channel and the tributary, respectively (see Table 4.2).

Table 4.3 Discharge and momentum ratios adopted in this study and by Leite Ribeiro *et al*. (2012a)

Research	Q_t [l/s]	Q_m [l/s]	Q_{p-c} [l/s]	Q_r [-]	$M_t = \rho Q_t U_t$ [N]	$M_m = \rho Q_m U_{mu}$ [N]	$M_r = M_t / M_m$ [-]
Present study	3.0	27.0	30.0	0.11	2.15	13.38	0.16
Leite Ribeiro (2012)	2.0	18.0	20.0	0.11	1.33	5.94	0.22

Subscripts *t*, *m* and *p-c* correspond to tributary, main and post-confluence channel values, respectively. ρ is the water density ($\rho = 1000$ kg/m³).

The larger discharges adopted in this study enhanced the sediment transport capacity in both channels, which may explain the difference in time required to reach equilibrium between this study (14 hours) and that of Leite Ribeiro *et al*. (2012a) (24 hours).

At equilibrium, the bed morphology obtained by both studies exhibited several common features such as the bank-attached bar downstream of the confluence, the avalanche slope at the tributary mouth and the discordance between the tributary and main channel beds (see Figure 4.12).

Similarities were also observed in the hydrodynamic features. For instance, the presence of a hydraulic jump at the tributary mouth, due to the different flow regimes between tributary and main channel, was observed in both studies.
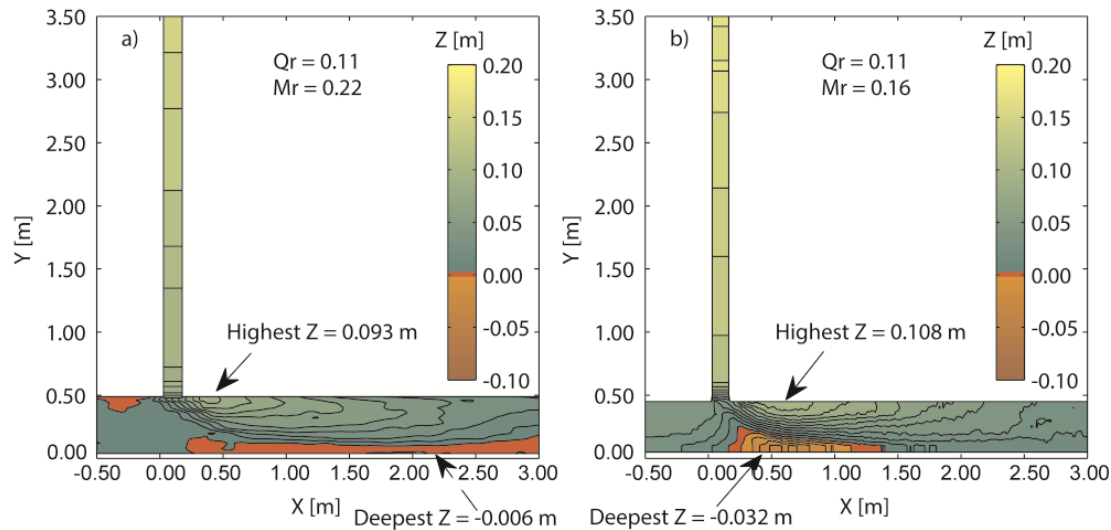
Figure 4.12 Bed topography at equilibrium: a) for Leite Ribeiro *et al*. (2012a) and b) for this study. The topographies correspond to the low discharge ratio ($Q_r = 0.11$). Contour lines are spaced by $\Delta Z = 0.01$ m.

Differences between the study by Leite Ribeiro *et al*. (2012a) and the present study were observed mainly in the main channel bed morphology. Deposition prevailed in the former study (see Figure 4.12a), whereas both erosion and deposition co-existed in the present study (see Figure 4.12b). The most relevant morphological differences in the present study consisted of a deeper scour hole at the outer bank of the main channel and a narrower and higher bank-attached bar at the inner bank. Leite Ribeiro *et al*. (2012a) reported only slight erosion of the bed at the outer bank of the main channel (see Figure 4.12).

The enhanced erosion might be a consequence of the larger discharges adopted in this study than those adopted by Leite Ribeiro *et al*. (2012a), though the discharge ratio was kept identical (see Table 4.3). These larger flow discharges, confined in the same channel width as Leite Ribeiro *et al*. (2012a), may have resulted in higher velocities and stronger acceleration in the confluence, causing the bed erosion and the width reduction of the bank-attached bar.

No armor effect was observed in the present study along the corridor of the sediment originating from the main channel, whose GSD is represented by S1 (see Figure 4.10). This is in contrast with the bed armoring reported by Leite Ribeiro *et al.* (2012a) in the same region. The d_{50} value corresponding to sample S1 was 1.8 mm for Leite Ribeiro *et al.* (2012a) and 1.0 mm for the present study, whereas the d_{50} value for the initial main channel bed sediment was 0.8 mm in both studies. In the present study, both the larger discharge of the main channel and the sediment discharge supplied into the main channel contributed to the maintaining of the texture of the sediment mixture during the experiment. In contrast, because Leite Ribeiro *et al.* (2012a) did not supply sediment into the main channel, the finer particles of the initial bed were washed out during the experiment and the coarse particles remained at the bed, constituting an armor layer.

In this study, the sediment supplied to the main channel during the experiment may have contributed to the bed erosion of the bed. The sediment discharge of the main channel maintained fairly constant the portion of finer particles in the bed sediment mixture, and this fine bed material reduced the critical shear stress for sediment motion enhancing the mobility of the bed, including relatively coarse particles (Wilcock, 1998; Wilcock *et al.*, 2001), which promoted bed erosion.

Segregation was also observed by Leite Ribeiro *et al.* (2012a) in the bed sediment at equilibrium as the sediment coming from the tributary was deposited at the inner bank of the main channel, downstream of the confluence (cf. Figure 15). In addition, as observed in this study, a fine sediment corridor was identified along the crest of the bank-attached bar, whereas the coarser particles were conveyed through the lateral slope of the bar (cf. Figure 15).

4.5 Conclusions

The hydro-morphodynamic evolution of an experimental right-angled discordant laboratory confluence with low momentum and discharge ratio conditions and with sediment supplied into both channels was studied herein. Interaction between flow dynamics and bed morphology was observed during the experiment through a simultaneous increase of the gradients of bed topography and water surface.

Once in equilibrium, the bed morphology presented typical features of discordant confluences, such as an avalanche face at the tributary mouth and a bank-attached bar along the inner bank of the post-confluence. In addition, a marked scour hole was observed at equilibrium, a finding that contrasts with previous work that noted the absence of marked scour holes in discordant confluences. The different erosion patterns are related to net deflection of flow toward the outer bank and the consequent acceleration.

The hydrodynamic features observed at equilibrium are consistent with those reported in previous investigations of discordant confluences. In particular, the upwelling flow at the downstream junction corner, which contributes to the presence of

a zone of reduced velocities instead of a recirculation zone therein, was identified as characteristic of discordant confluences. Moreover, the hydraulic jump observed at the tributary mouth is characteristics of discordant confluences with narrow steep tributaries that provide abundant sediment load to the confluence.

At equilibrium, the spatial distribution of the bed sediments exhibited segregation between the sediments provided by the tributary and main channel. This segregation is in good agreement with previous investigations that reported similar patterns for both discordant and concordant confluences.

The sediment discharge supplied to the main channel kept the portion of fine and coarse particles fairly constant throughout the experiment, avoiding bed armoring along the corridor followed by the sediments of the main channel. The lack of bed armoring may have facilitated scour of the bed of the main channel.

5

Influence of the junction angle and discharge ratio on the hydro-morphodynamics of the confluence

In this chapter the influence of the junction angle (α) and discharge ratio (Q_r) on the flow dynamics and bed morphology of the confluence is analyzed. For that purpose, six experiments were performed in a laboratory confluence, in which three discharge ratios were tested ($Q_r = 0.11$, 0.15, 0.23) with two different junction angles ($\alpha = 90°$ and 70°). Measurements consisted of systematic bed topography surveys during the experiments and water surface survey at equilibrium. The results show that for both junction angles, increasing discharge ratios yielded deeper scour holes and lower bank-attached bars in the main channel. In the tributary, the higher was the discharge ratio, the lower was the bed slope and the bed elevation. Regarding the hydrodynamics at equilibrium, the flow depth of both channels and the energy loss induced in the main channel by the tributary inflow increased with the discharge ratio. The lower junction angle ($\alpha = 70°$) facilitated the penetration of the tributary-mouth bar into the main channel, with respect to $\alpha = 90°$. This further penetration reduced the erosion at the tributary mouth and reinforced the topographic deflection of the main stream toward the outer bank, which in turn resulted in deeper erosion therein. Depending on the junction angle, the tributary adopted different flow regimes to convey the imposed sediment load. With $\alpha = 90°$ the tributary flow regime was critical or supercritical depending on the discharge ratio, whereas with $\alpha = 70°$ the tributary flow regime was always subcritical. The energy loss in the main channel caused by the tributary inflow, was lower with $\alpha = 90°$ than with $\alpha = 70°$ in the experiments with supercritical flow in the tributary. This pattern was due to the hydraulic jump formed at the tributary mouth, which reduced the velocity of the tributary before it entered the main channel.

Keywords: junction angle, discharge ratio, bed discordance, morphodynamics, supercritical flow.

5.1   Introduction

During the last two centuries, morphodynamics of alpine rivers have been highly constrained by human interventions, mainly motivated by flood safety reasons and agricultural and urban purposes. Often, these river training works have resulted in strongly channelized tributaries with steep slopes, which join the main channel at high junction angles.

Based on laboratory experiments performed in a right-angled confluence with low discharge ratio ($Q_r = 0.11$), Leite Ribeiro *et al.* (2012b) studied the effects of a local widening of the tributary mouth on confluence morphodynamics. The results show that the tributary flow adopted a natural angle of $\alpha \approx 65°$ to enter the main channel. Furthermore, Devauchelle *et al.* (2012) and Gutierrez *et al.* (2014) report that in nature, the junction angles of fluvial networks respond to a normal distribution with means of $\alpha \approx 72°$ and $82°$, respectively.

Based on these results, here the angles $\alpha = 90°$ and $70°$ were adopted as cases of study, with the purpose of analyzing the influence of the junction angle (α) and the discharge ratio (Q_r) on the hydro-morphodynamics of alpine river confluences. For that purpose six experiments were conducted in a laboratory confluence in which three discharge ratios were tested with each junction angle. The experiments were carried out under movable bed conditions and with continuous sediment supply to both channels. Systematic bed topography and water surface surveys show different hydrodynamic and morphodynamic patterns in the confluence for different discharge ratios and junction angles.

5.2   Experimental setup

The results presented herein correspond to the experimental sets I and II, performed in the experimental facility of the LCH-EPFL. The experimental setups are summarized in Table 5.1 and described in detail in Chapter 3.

Table 5.1 Overview of the experimental setup

Experimental set	α [°]	B_t/B_m [-]	σ [-]	Q_r [-]	Q_{sm} [Kg/min]	Q_{st} [Kg/min]	Measurements
Set I	90°	0.30	3.15 (main) 4.51 (trib.)	0.11 (LR) 0.15 (IR) 0.23 (HR)	0.3	0.5	Bed topo at $t = 0, 1, 7$ h, & equilibrium W. surf. at equilibrium
Set II	70°	0.30	3.15 (main) 4.51 (trib.)	0.11 (LR) 0.15 (IR) 0.23 (HR)	0.3	0.5	Bed topo at $t = 0, 1, 7$ h, & equilibrium W. surf. at equilibrium

5.3 Results

5.3.1.1 Bed morphology evolution common to all experiments

All the experiments started with a roughly flat bed in the main channel and a slight bed slope in the tributary (0.5%), with a small step ($\approx$ 0.03 m) imposed at the junction with the main channel. During the first hour of experiment, the sediments supplied to the tributary progressed downstream in form of a sediment wedge, increasing the slope and elevation of the tributary bed. Meanwhile, in the main channel, the flow resulting from the confluence eroded the bed locally at the tributary mouth, creating an initial scour hole there. When the tributary sediments reached the confluence, they filled the initial scour hole and were deposited at the downstream junction corner, thereby initiating the formation of a bar at the inner bank of the main channel, i.e. the so-called bank-attached bar (Best and Rhoads, 2008). The growth of this bar reduced the effective flow section in the main channel and confined most of the flow to the outer bank of the main channel. There, the flow accelerated and eroded the bed, creating a new scour hole that remained at equilibrium. In the tributary, the bed elevation and slope progressively increased during the experiments (cf. Figures 5.1 to 5.4). At equilibrium, the bed morphology presented common features in all the experiments: i) a bank-attached bar at the inner bank of the main channel, ii) a scour hole that extended from the tributary mouth to the outer bank, flanking the bar, iii) a steep bed slope in the tributary where $Y/B_m > 1.5$, and iv) a bed transition from the tributary to the main channel in the form of an avalanche slope that creates a marked bed discordance between the tributary and main channel (cf. Figures 5.1 to 5.4).

5.3.2 Bed morphology evolution with $\alpha = 90°$

This section presents an analysis of the influence of the discharge ratio on the bed morphology evolution in the experiments in which $\alpha = 90°$. Figure 5.1 illustrates the bed topography at times $t = 0, 1, 7$ and 14 h (equilibrium) corresponding the three discharge ratios, and Figure 5.2 depicts the longitudinal bed elevation at these same times and the water surface at equilibrium ($t = 14$ h). The plots in Figure 5.2 correspond to the longitudinal profiles along the inner and outer banks of the main channel ($Y/B_m = 0.9$ and 0.1, respectively) and to the axis of the tributary. X and Y were normalized by the width of the main channel $B_m = 0.50$ m and Z was normalized by the downstream flow depth ($y_d = 0.08$ m)

At $t = 1$ h, the initial scour hole was present at the tributary mouth at all discharge ratios (Figures 5.1a-c and 5.2a-c). The depth and size of this scour increased with the discharge ratio, indicating that the erosive capacity of the flow resulting from the confluence also increased with the discharge ratio. For the low and high discharge ratios the eroded material was deposited downstream of the confluence along the inner bank of the main channel (Figures 5.1d-e and 5.2a-b). For the intermediate discharge ratio the tributary sediments began to develop a bank-attached bar, by being deposited along the inner bank downstream of the confluence (Figures 5.1f and 5.2c).
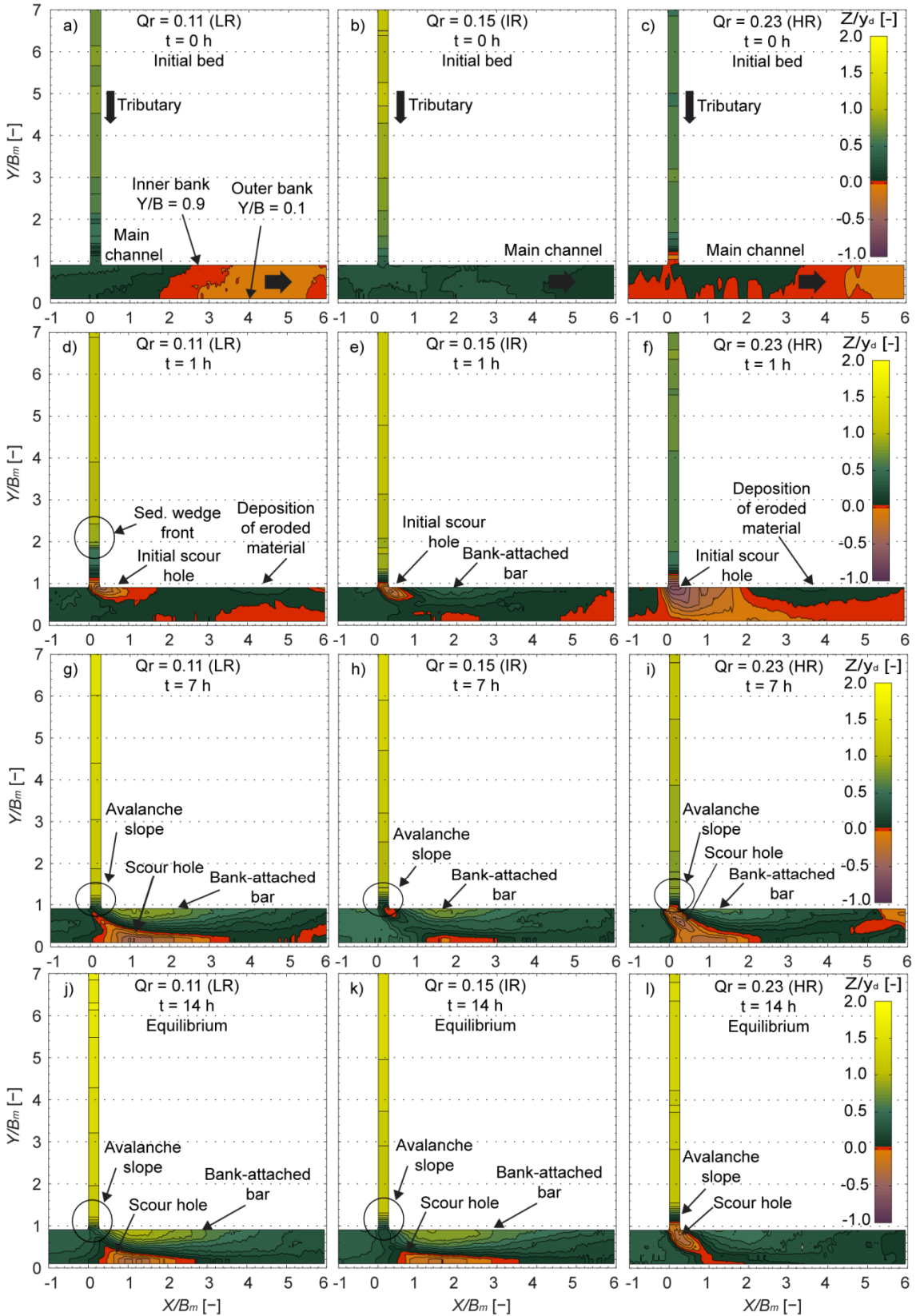
Figure 5.1 Evolution of the bed topography with a junction angle of $\alpha = 90°$. The bed elevation contours are spaced by $\Delta Z = 0.01$ m. Each row corresponds to a certain measurement time ($t = 0, 1, 7$ and 14 h), and each column correspond to a certain discharge ratio, i.e., $Q_r = 0.11$ (LR) (left), $Q_r = 0.15$ (IR) (center), and $Q_r = 0.23$ (HR) (right).
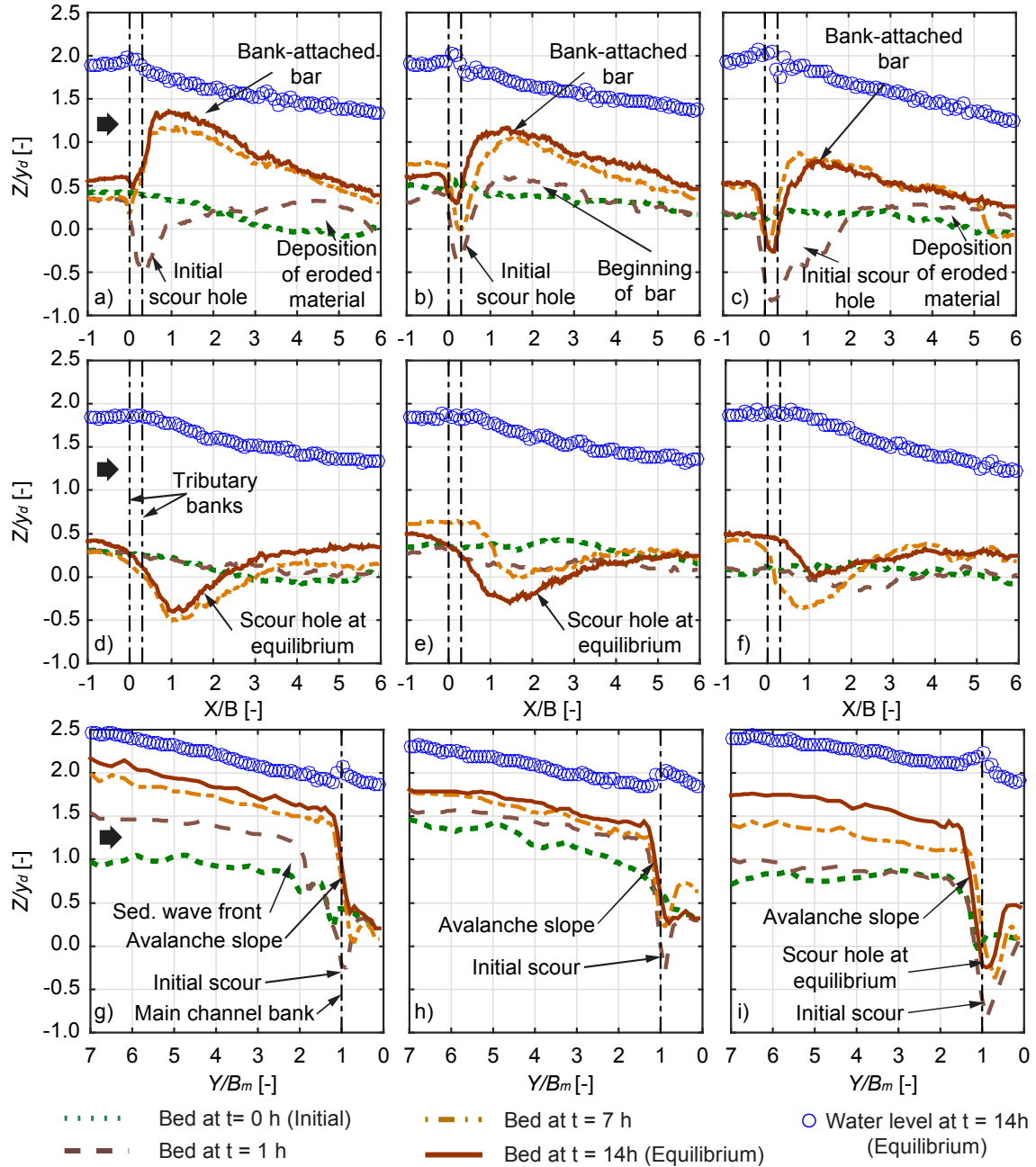
Figure 5.2 Longitudinal profiles of the bed topography evolution and water surface at equilibrium with $\alpha = 90°$. a) inner-bank of the main channel $Q_r = 0.11$ (LR), b) inner-bank of the main channel $Q_r = 0.15$ (IR), c) inner-bank of the main channel $Q_r = 0.23$ (HR), d) outer-bank of the main channel $Q_r = 0.11$ (LR), e) outer-bank of the main channel $Q_r = 0.15$ (IR), f) outer-bank of the main channel $Q_r = 0.23$ (HR), g) tributary axis $Q_r = 0.11$ (LR), h) tributary axis $Q_r = 0.15$ (IR), i) tributary axis $Q_r = 0.23$.

At $t = 7$ h and for the low discharge ratio, the initial scour hole was completely filled with tributary sediments (Figures 5.1g and 5.2a). In contrast, for the intermediate and high discharge ratios, the resultant flow from the confluence partially maintained the erosion at the tributary mouth (Figures 5.1h-i and 5.2b-c).

The experiments reached equilibrium after 14 hours. In these conditions, the height of the bank-attached bars and the depth of the scour holes at the outer bank decreased as the discharge ratio increased (Figure 5.2a-f). In addition, higher discharge

ratios led to deeper erosion due to the flow junction at the tributary mouth (Figure 5.2a c). This pattern implies that the erosional capacity of the resultant flow increased with the discharge ratio.

In the tributary, the front of the sediment wedge was present where $Y/B_m \approx 2.0$ at $t = 1$ h for the low discharge ratio (Figures 5.1d and 5.2g). For the intermediate discharge ratio, the tributary sediment wedge had already reached the main channel at $t = 1$h, thereby filling the scour hole (Figures 5.1e and 5.2h). For the high discharge ratio, only slight bed aggradation was observed where $Y/B_m > 4$ at $t = 1$ h, which indicates that the tributary sediments had not yet reached the confluence (Figure 5.2i).

At $t = 7$ h, the tributary presented a quasi-equilibrium bed morphology for all the discharge ratios, with a steep bed slope along the upstream reach ($Y/B_m > 1.5$) and a well-developed bed discordance (c.f. Figure 5.2g-i). This discordance was formed by the so-called tributary-mouth bar (Best and Rhoads, 2008), which barely extended into the main channel.

At equilibrium ($t = 14$ h), the penetration of the tributary-mouth bar into the main channel decreased as the discharge ratio increased (c.f. Figure 5.2g-i). The bed elevation and slope of the upstream reach of the tributary ($Y/B_m > 1.50$) decreased with the discharge ratio (cf. Figure 5.2g-i). The height of the bed discordance was nearly equivalent to the y_d (0.08 m) for the low and the intermediate discharge ratios, and approximately 1.75 y_d (0.14 m) for the high discharge ratio, due to erosion of the scour hole at the tributary mouth (cf. Figure 5.2g-i).

5.3.3 Bed morphology evolution with $\alpha = 70°$

This section presents an analysis of the variations in bed morphology observed in the experiments with $\alpha = 70°$ compared to the results obtained with $\alpha = 90°$. Figures 5.3 and 5.4 illustrate the bed topography evolution for the three discharge ratios and a junction angle of $\alpha = 70°$.

With $\alpha = 70°$, the bed morphology evolved similarly to that observed with the junction angle of $\alpha = 90°$. After the first hour of the experiments ($t = 1$ h), a small scour hole developed at the tributary mouth for the low discharge ratio (Figures 5.3d and 5.4a). This initial scour hole was considerably smaller than that observed with an angle of $\alpha = 90°$, indicating that the erosive capacity of the flow resulting from the junction was comparatively lower with $\alpha = 70°$. For the intermediate discharge ratio, no significant changes in the bed morphology were observed in the main channel at $t = 1$ h, with respect to the initial topography ($t = 0$ h). For the high discharge ratio, the bed topography exhibited deposition at the downstream junction corner, which constituted the inception of the bank-attached bar (Figures 5.3f and 5.4c). This deposition confined the flow to the outer bank, where the flow accelerated and created a scour hole ($0.0 < X/B_m < 2.0$ in Figures 5.3c and 5.4f).
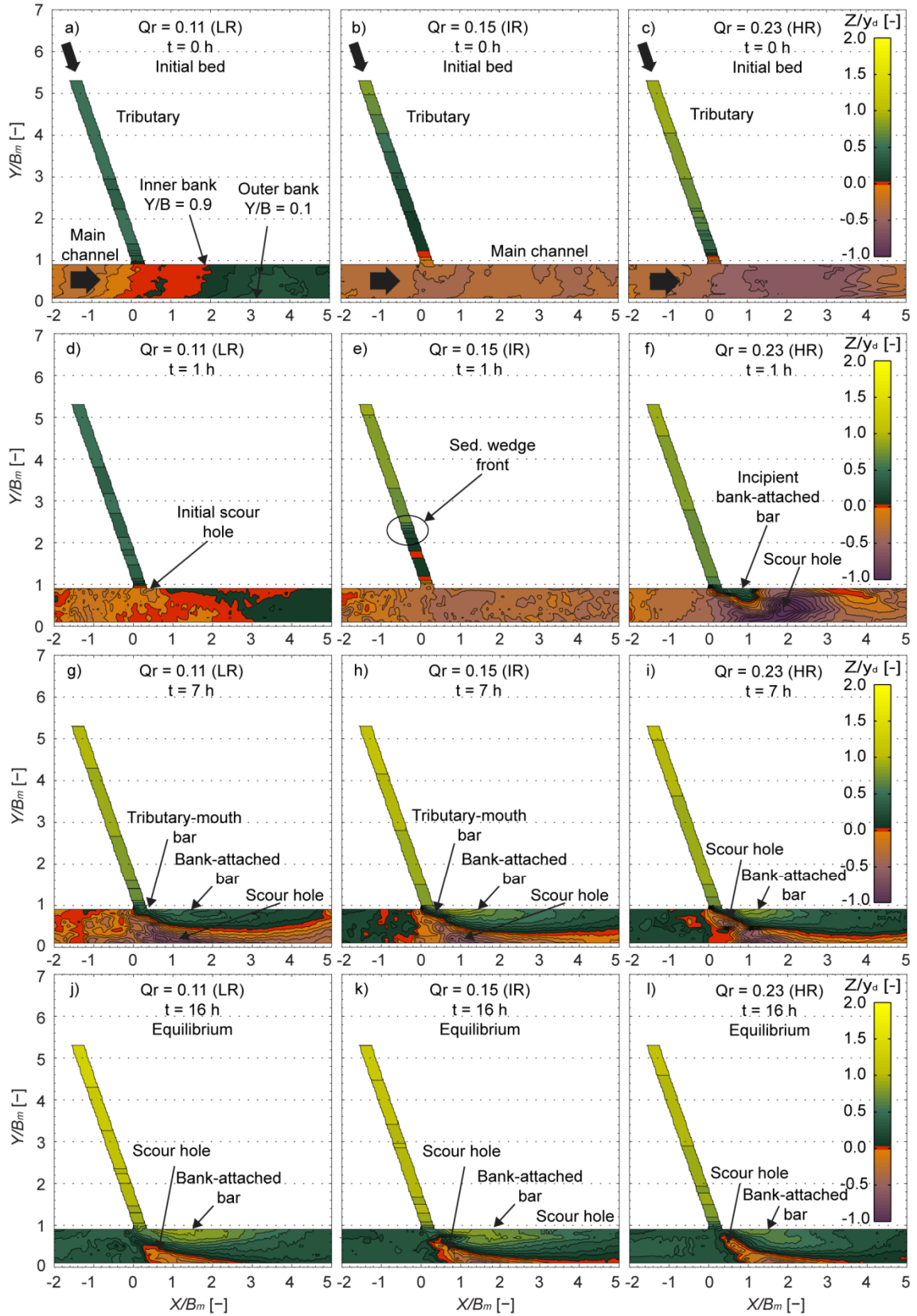
Figure 5.3 Evolution of the bed topography with a junction angle of α = 70°. The bed elevation contours are spaced by ΔZ = 0.01 m. Each row corresponds to a certain measurement time (t = 0, 1, 7 and 16 h), and each column correspond to a certain discharge ratio, i.e., Q_r = 0.11 (LR) (left), Q_r = 0.15 (IR) (center), and Q_r = 0.23 (HR) (right).
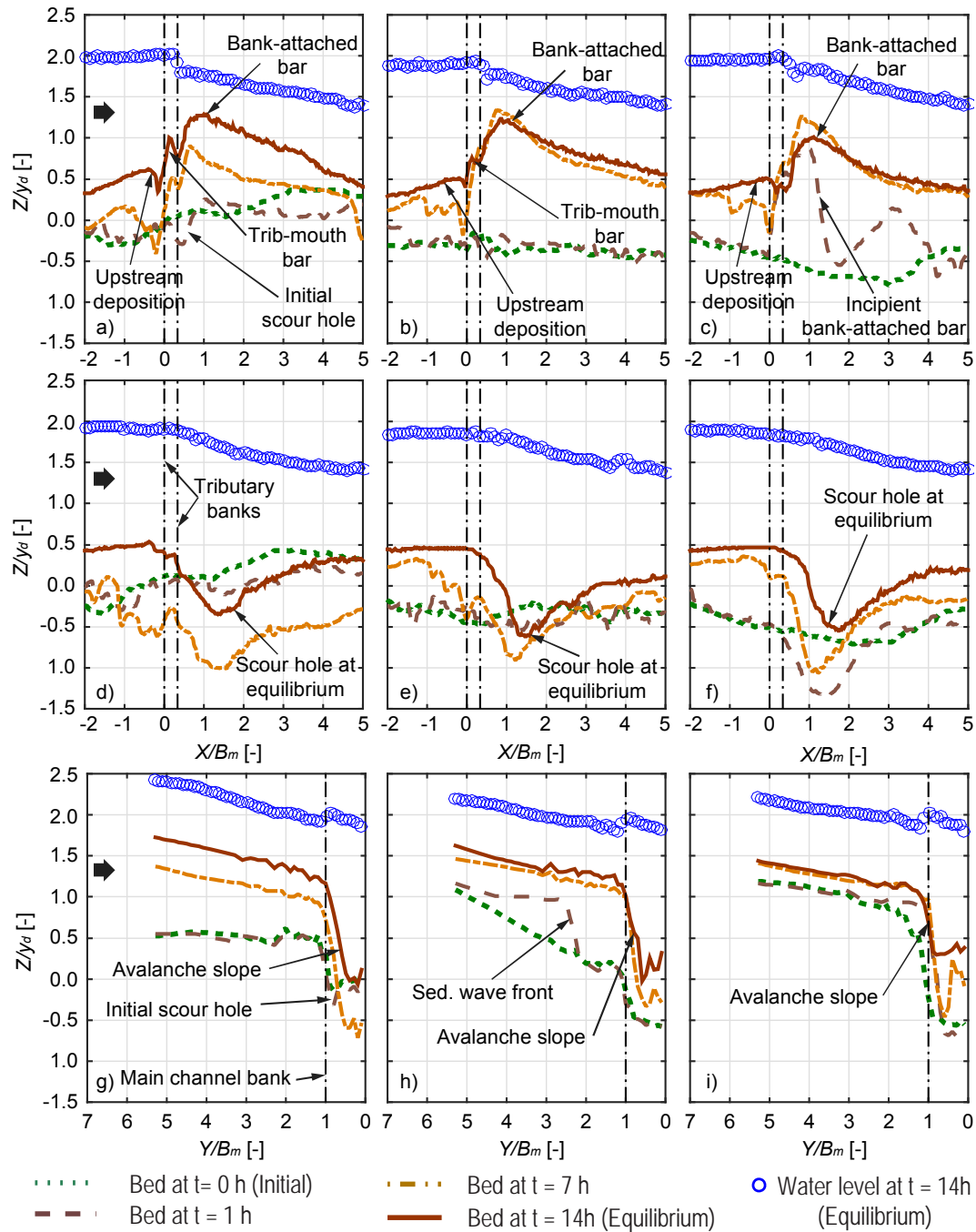
Figure 5.4 Longitudinal profiles of the bed topography evolution and water surface at equilibrium with $\alpha = 70°$. a) inner-bank of the main channel $Q_r = 0.11$ (LR), b) inner-bank of the main channel $Q_r = 0.15$ (IR), c) inner-bank of the main channel $Q_r = 0.23$ (HR), d) outer-bank of the main channel $Q_r = 0.11$ (LR), e) outer-bank of the main channel $Q_r = 0.15$ (IR), f) outer-bank of the main channel $Q_r = 0.23$ (HR), g) tributary axis $Q_r = 0.11$ (LR), h) tributary axis $Q_r = 0.15$ (IR), i) tributary axis $Q_r = 0.23$.

At $t = 7$ h and associated with all the discharge ratios, the bed morphology presented a well-developed bank-attached bar and a scour hole. This scour started at the tributary mouth and crosses the main channel until reaching the outer bank, where it became aligned with the bank (Figure 5.3g-i).

With $\alpha = 70°$, the experiments reached equilibrium conditions after 16 hours. Under these conditions, the effects of the discharge ratio on the morphological features

were similar to those observed with $\alpha = 90°$. Also with $\alpha = 70°$, increasing discharge ratios resulted in lower bank-attached bars and deeper scour holes at the tributary mouth (cf. Figures 5.3j-l and 5.4a-f). Aside from these morphological features, deposition was observed in the vicinity of the upstream junction corner $(- 2.0 < X/B_m < 0.0$ in Figure 5.4a-c), only in the experiments with $\alpha = 70°$. The size of this deposit decreased as the discharge ratio increased (cf. Figure 5.4a-c). This deposition was not observed with $\alpha = 90°$ and may be attributed to the presence of a stagnation zone at the upstream junction corner (Best and Rhoads, 2008).

In the tributary, the bed elevation for the low discharge ratio at $t = 1$ h did not present significant changes with respect to the initial bed ($t = 0$ h in Figure 5.4g). For the intermediate discharge ratio, the front of the sediment wedge was present at $Y/B_m \approx 2.5$ at $t = 1$ h (Figures 5.3e and 5.4b). For the high discharge ratio, the bed level rose during the first hour of the experiment in the reach where $1.0 < Y/B_m < 2.0$ (Figure 5.4i), indicating that the sediment wedge had reached the confluence by this time. At $t = 7$ h, the tributary presented a quasi-equilibrium bed morphology for the three discharge ratios, as was observed with $\alpha = 90°$. At equilibrium ($t = 16$ h), the bed elevation and slope of the upstream reach ($Y/B_m > 1.5$) together with the protrusion of the tributary-mouth bar decreased as the discharge ratio increased, as they did with $\alpha = 90°$. The bed discordance was approximately 1.25 y_d (0.10 m) for the low and intermediate discharge ratios and approximately 0.75 y_d (0.06 m) for the high discharge ratio. Moreover, the tributary-mouth bar extended farther into the main channel with $\alpha = 70°$ than with $\alpha = 90°$. This bar merged with the bank-attached bar in all the experiments with $\alpha = 70°$, whereas these features were separated with $\alpha = 90°$ (cf. Figure 5.5).

Figure 5.5 Perspective views of the tributary mouth at equilibrium corresponding to the low discharge ratio with a) $\alpha = 90°$ and b) $\alpha = 70°$

5.3.4 Hydrodynamics at equilibrium with the $\alpha = 90°$ and $70°$ configurations

5.3.4.1 Main channel

In the main channel, the water surface at equilibrium presented similar features for all the discharge ratios and with both junction angles. At the inner bank, the level of the water surface rose as it approached the confluence. This local rise of the water surface was due to the tributary inflow and may be associated with the presence of a stagnation zone at the upstream junction corner (Rhoads and Sukhodolov, 2001; Leite Ribeiro *et al.*, 2012a). This local rise was more pronounced with $\alpha = 90°$ than with $\alpha = 70°$ (cf. Figure 5.6a-b). With both junction angles, the highest rises in the water level were observed for the low and high discharge ratios (cf. Figure 5.6a-b).

At the downstream junction corner ($X/B_m \approx 0.30$ and $Y/B_m \approx 1.0$), the water surface presented a drop associated with a low pressure zone, which was caused by the abrupt change in direction of the tributary flow ($\alpha = 90°$ and $70°$). This water surface drop was more pronounced with greater discharge ratios and the greater junction angle. The low-pressure zone associated with the drop in the water surface was consistent with the presence of upwelling flow observed at the downstream junction corner (Figure 5.7) (Biron *et al.*, 1996a). This upwelling corresponded to the lower part of the main flow, which was not deflected outward because it was shielded from the tributary inflow by the bed discordance.
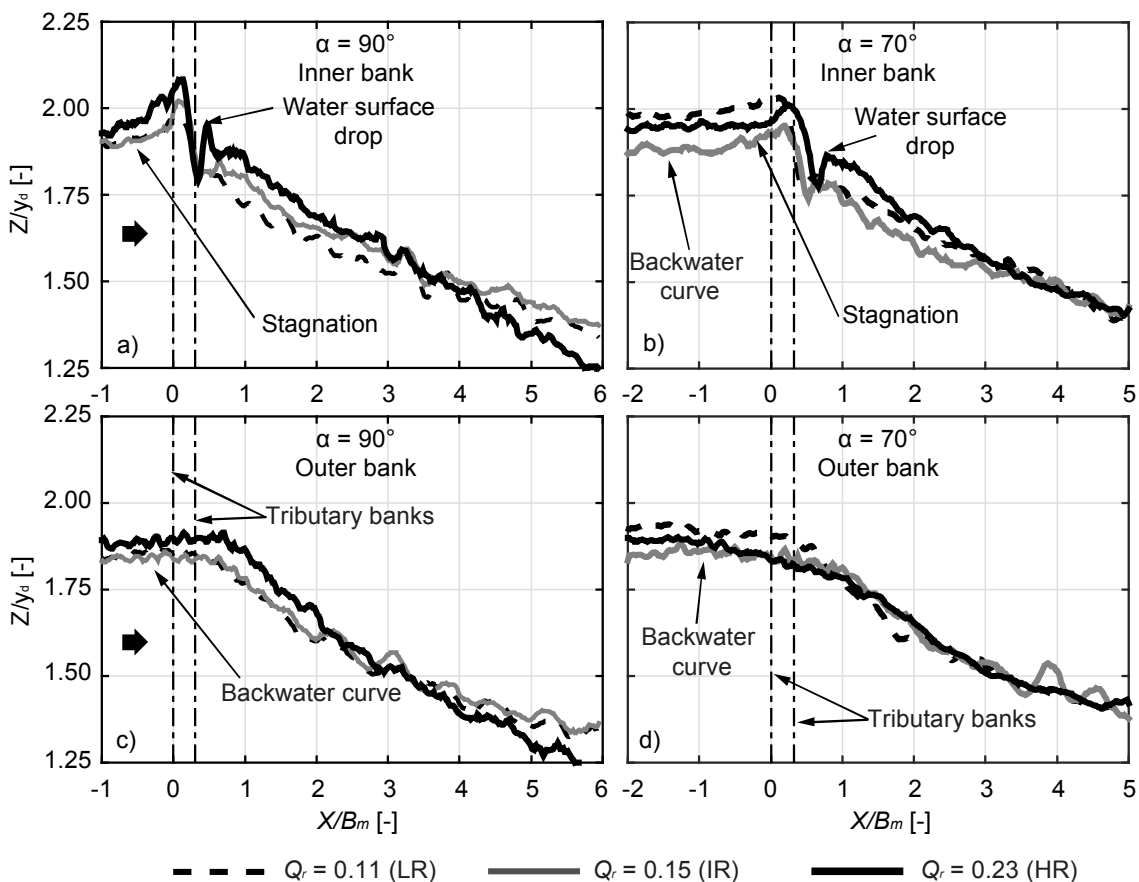
Figure 5.6 Water surface profiles along the inner and outer banks of the main channel at equilibrium with both junction angles. a) at the inner bank with $\alpha = 90°$, b) at the inner bank with $\alpha = 70$, c) at the outer bank with $\alpha = 90°$, and d) at the outer bank with $\alpha = 70°$.

Downstream of the confluence ($X/B_m > 0$) the flow accelerated over the bank-attached bar, and the slope of the water surface slope steepened (Figure 5.6a-b). This slope was similar for the low and intermediate discharge ratios but was steeper for the high ratio. This pattern indicates further flow acceleration for the high discharge ratio. No significant differences were observed in the water surface slopes associated with the two junction angle configurations.
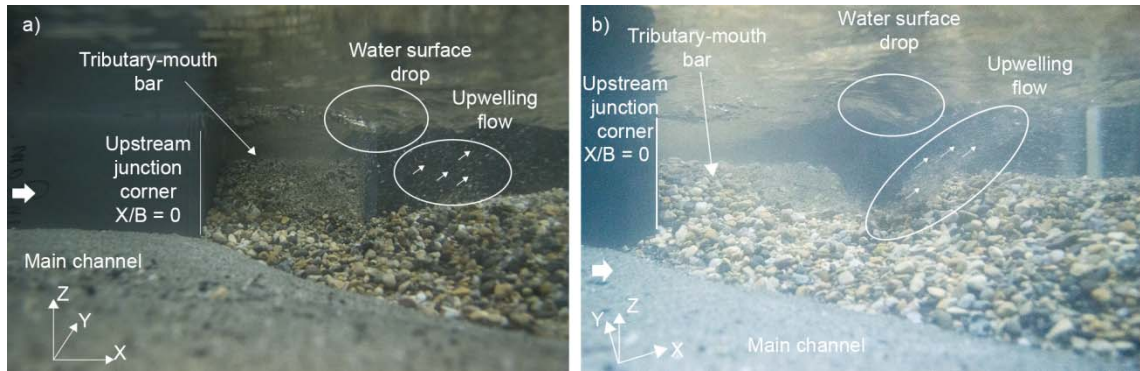
Figure 5.7 Frontal view of the tributary mouth corresponding to the low discharge ratio at equilibrium for a) $\alpha = 90°$, and b) $\alpha = 70°$.

At the outer bank and upstream of the confluence ($X/B_m < 0$), the water surface exhibited a nearly horizontal profile in all the experiments (Figure 5.6c-d). These quasi-horizontal profiles correspond to a M1-type backwater curve (Chow, 1959) induced by the tributary inflow. Downstream of the confluence ($X/B_m > 0$), the water surface steepened markedly reflecting flow acceleration along the outer bank of the main channel. With $\alpha = 90°$, the slope of the water surface downstream of the confluence for the high discharge ratio was steeper than that observed for the other discharge ratios, indicating further flow acceleration. In contrast, with $\alpha = 70°$, all the discharge ratios exhibited similar water surface slopes along the outer bank, which indicates similar flow acceleration along the outer bank.

Figure 5.8 shows the non-dimensional cross-sectional average values of flow depth (y/y_d), flow velocity (U/U_d) and Froude number (Fr) along the main channel for each experiment. Upstream of the confluence ($X/B_m < 0$), the flow depth was higher with $\alpha = 70°$ than with $\alpha = 90°$ for all the discharge ratios. In addition, higher discharge ratios were associated with higher flow depths where $X/B_m < 0$ with both junction angle configurations (Figure 5.8a-b). In the case of $\alpha = 90°$, the flow depth increased approaching the confluence, confirming the presence of the M1-type backwater curve. This increase observed with $\alpha = 90°$ contrasted with the nearly constant flow depth observed with $\alpha = 70°$ (Figure 5.8a-b).

Downstream of the confluence ($X/B_m > 0$), associated with the flow acceleration, the flow depth decreased until reaching a nearly constant value, indicating that the flow tended to become uniform. This downstream distance where the flow depth became uniform varied among the experiments. This distance was greater for increasing discharge ratios and in the experiments with $\alpha = 90°$ compared to those with $\alpha = 70°$ (Figure 5.8a-b). These results suggest that the effects of the tributary inflow in the main stream increased with the discharge ratios and the junction angle. With both junction

angles, the nearly constant flow depth measured downstream of the confluence increased as the discharge ratio increased.

The evolution of the flow depth along the main channel is reflected in the profiles of flow velocity (U/U_d) (Figure 5.8c-d) and Froude number (Fr) (Figure 5.8e-f). A pronounced decrease of velocity was observed upstream of the confluence with $\alpha = 90°$, particularly in the case of the high discharge ratio. With $\alpha = 70°$, the flow approached the confluence at a nearly constant flow velocity (Figure 5.8c-d).

The Froude number associated with each discharge ratio was calculated along the main channel, based on the cross-sectional average values of flow depth and flow velocity. Upstream of the confluence, the Froude number was in the range of 0.4 to 0.5 with $\alpha = 90°$, and 0.4 with $\alpha = 70°$. Downstream of the confluence, the Froude number increased due to the flow acceleration, reaching a nearly constant value of approximately 0.7 to 0.9. The 90° junction angle yielded significantly higher Froude numbers (max. $Fr \approx 0.91$) than did the 70° angle (max. $Fr \approx 0.85$).
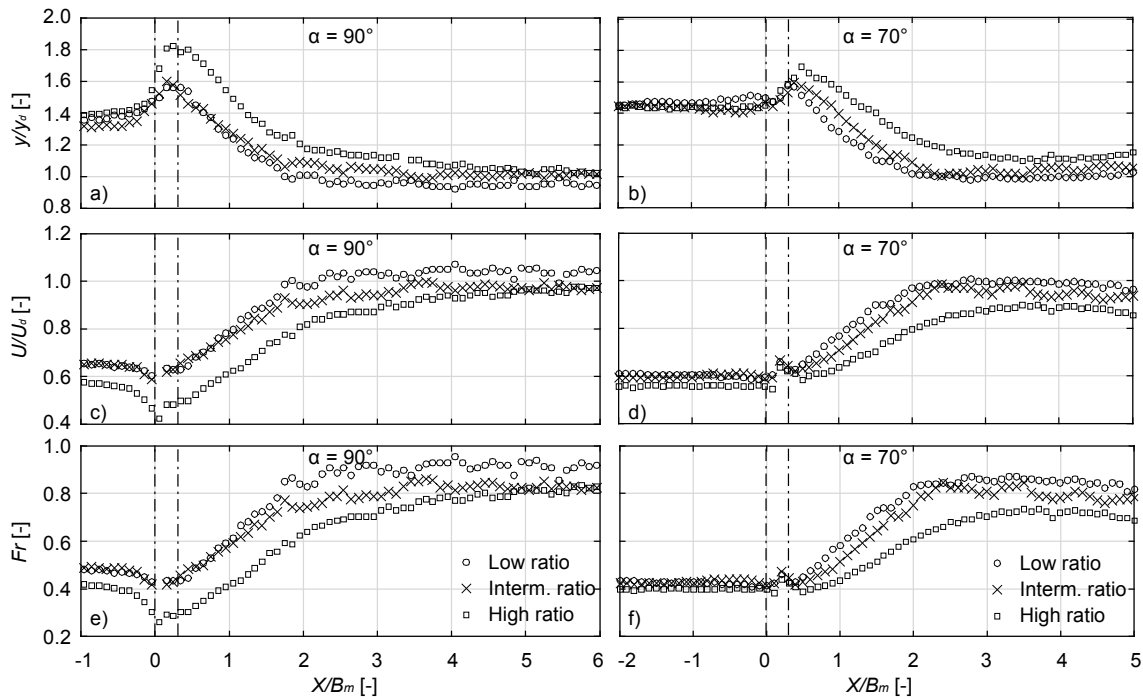
Figure 5.8 Variation in the normalized cross-sectional average values of flow depth (y/y_d), flow velocity (U/U_d), and Froude number (Fr). a) y/y_d with $\alpha = 90°$, b) y/y_d with $\alpha = 70°$, c) U/U_d with $\alpha = 90°$, d) U/U_d with $\alpha = 70°$, e) Fr with or $\alpha = 90°$, and f) Fr with $\alpha = 70°$.

The cross-sectional average values in Figure 5.8 indicate that the flow in the main channel at equilibrium tended toward subcritical uniform flow downstream of the confluence in all of the experiments. To verify this, the slope of the bedmodel

, water surface and total energy (J_b, J_{wl} and J_H respectively) were measured in the reach where the flow depth was nearly constant. The values of these slopes are given in Table 5.2 together with the flow depth (y), the flow velocity (U) and the Froude number (Fr) in each experiment. The values in the third column (X/B_m) indicate the reach where the flow depth was nearly constant.

Table 5.2 Main hydraulic variables in the main cannel at equilibrium with nearly uniform flow conditions.

α	Q_r	X/B_m	J_b	J_{wl}	J_H	y	U	Fr
[°]	[-]	[-]	[%]	[%]	[%]	[m]	[m/s]	[-]
	0.11 (LR)	> 3.0	1.1%	1.1%	1.1%	0.076	0.79	0.91
90	0.15 (IR)	> 4.0	1.0%	1.0%	1.0%	0.081	0.74	0.83
	0.23 (HR)	> 5.0	1.5%	1.6%	1.5%	0.081	0.74	0.82
	0.11 (LR)	> 2.0	1.2%	1.2%	1.2%	0.080	0.75	0.85
70	0.15 (IR)	> 3.0	1.3%	1.0%	1.2%	0.083	0.72	0.80
	0.23 (HR)	> 3.0	1.4%	1.2%	1.4%	0.087	0.69	0.75

5.3.4.2 Tributary

In all the experiments, the water surface in the tributary at equilibrium was characterized by a steep slope at $Y/B_m > 1.5$ and an abrupt rise at the junction with the main channel ($Y/B_m \approx 1.0$) (Figure 5.9). The slope of the water surface decreased with the discharge ratio with both junction angles. Moreover, in the experiments with $\alpha = 90°$, the water surface slope in the reach $Y/B_m > 1.5$ was more uniform than that with $\alpha = 70°$. The abrupt rise at the junction corresponded to a hydraulic jump in the experiments with low and intermediate discharge ratios and with $\alpha = 90°$.
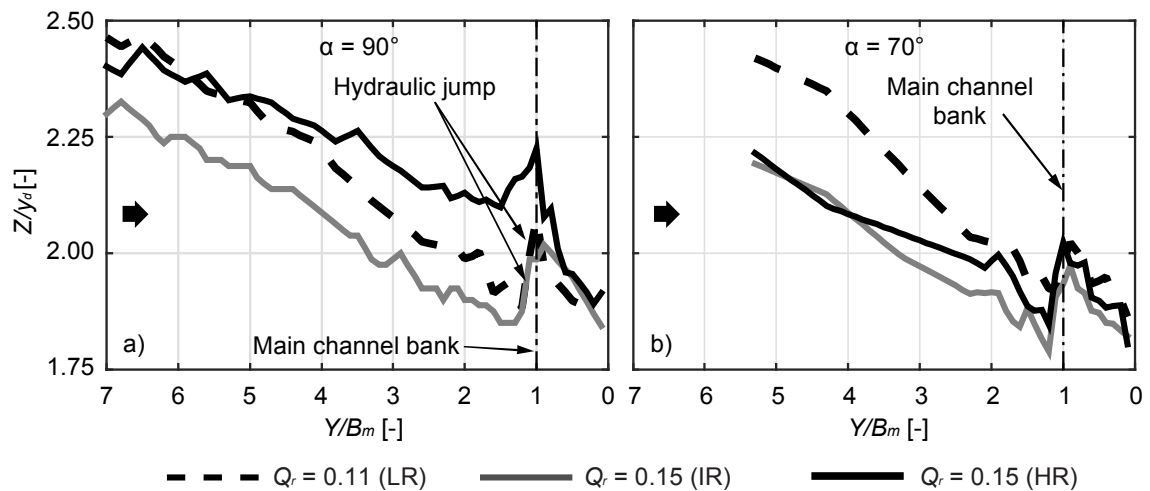
Figure 5.9 Water surface profiles along the tributary axis for the three discharge ratios at equilibrium with a) $\alpha = 90°$ and b) $\alpha = 90°$.

Figure 5.10 shows the tributary bed elevations and water surfaces at equilibrium associated with both junction angles and for each discharge ratio. At $Y/B_m > 1.5$, the flow depth was roughly constant in all the experiments. However, in the experiments with $\alpha = 90°$, the flow-depth was lower than in those with $\alpha = 70°$. This was partly due to the higher bed elevation observed with $\alpha = 90°$ compared to $\alpha = 70°$. With both junction angles, the flow depth increased with the discharge ratio.
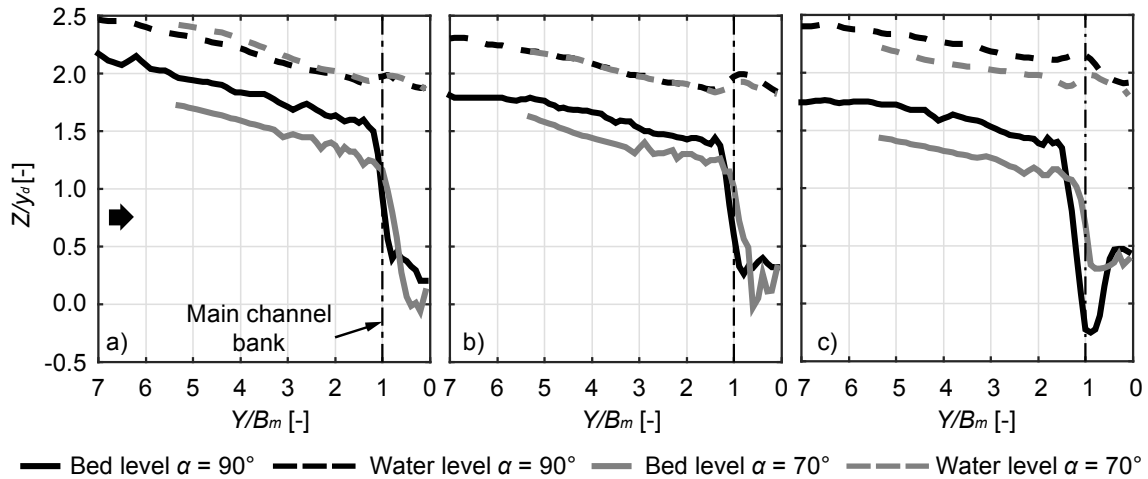
Figure 5.10 Profiles of bed elevation and water surface along the tributary axis at equilibrium with $\alpha = 90°$ and 70°. a) $Q_r = 0.11$ (LR), b) $Q_r = 0.15$ (IR); c) $Q_r = 0.23$ (HR).

In Table 5.3 the values of the main hydraulic variables measured in the upstream reach of the tributary ($Y/B_m > 1.5$) are shown. The measured flow depths (y), when compared to the critical value (y_c) indicate that with $\alpha = 90°$ the tributary flow at equilibrium was supercritical ($Fr > 1$) for the low and intermediate discharge ratios, whereas the flow was critical ($Fr \approx 1$) for the high discharge ratio. In the case of $\alpha = 70°$, the flow was always subcritical ($Fr < 1$) for all the discharge ratios.

To verify whether the tributary flow tended toward uniform flow conditions at equilibrium, the slopes of the bed, water surface and total energy (J_b, J_{wl} and J_H respectively) were also measured where $Y/B_m > 1.5$ (Table 5.3). In the case of $\alpha = 90°$, the three slopes were similar for each discharge ratio. This and the constant flow depth where $Y/B_m > 1.5$ indicate that the flow in the tributary (where $Y/B_m > 1.5$) corresponded to a quasi-uniform flow. With $\alpha = 70°$ the slopes of the bed, water surface and total energy exceeded those measured with $\alpha = 90°$, indicating that the flow at equilibrium corresponded to a subcritical varied flow rather than uniform flow.

Table 5.3. Mean values of the main hydraulic variables where $Y/B_m > 1.5$.

α	Q_r	Q_t	J_b	J_{wl}	J_H	y	y_c	U	Fr
[°]	[-]	[l/s]	[%]	[%]	[%]	[m]	[m]	[m/s]	[-]
	0.11 (LR)	3.0	1.7%	1.6%	1.7%	0.028	0.034	0.70	1.33
90	0.15 (IR)	3.9	1.3%	1.4%	1.4%	0.036	0.041	0.72	1.22
	0.23 (HR)	5.6	1.0%	1.0%	1.1%	0.052	0.052	0.72	1.01
	0.11 (LR)	3.0	1.8%	2.2%	2.0%	0.055	0.034	0.36	0.50
70	0.15 (IR)	3.9	1.5%	1.6%	1.5%	0.050	0.041	0.52	0.74
	0.23 (HR)	5.6	1.4%	1.0%	1.2%	0.063	0.052	0.59	0.75

5.3.5 Effects of the tributary on the hydro-morphodynamics of the main channel

The jet-like tributary inflow induced an energy loss in the flow in the main channel and affected the bed morphology at the confluence. These effects are analyzed and discussed below.

In each experiment, the normalized cross-sectional average bed elevation (Z/y_d), total energy (H/H_d) and total momentum (M/M_d) are shown in Figure 5.11 for the main channel at equilibrium. M is obtained using the equation 5.1:

$$M = \rho QU + \frac{1}{2}\gamma y^2 B_m \tag{5.1}$$

where ρ denotes the water density, Q is the flow discharge, U is the cross-sectional average flow velocity, γ is the specific weight of the water, y is the cross-sectional average flow depth, and B_m is the width of the main channel. M was normalized by using M_d, which corresponds to the total momentum at the downstream end of the main channel and it was calculated through the equation 5.1 and considering $Q = Q_{p-c} = 0.030$ m^3/s, $U = U_d = 0.75$ m/s, and $y = y_d = 0.08$ m.

R denotes the resultant of the external forces acting on the fluid, which are the weight component and the flow-resistance due to the friction and bedform. The value of R in each cross-section was obtained as the difference in total momentum (M) between two consecutive cross-sections (equation 5.2), where $\Delta X = 0.01$ m

$$R_{xi} = M_{xi+1} - M_{xi} \tag{5.2}$$

R was normalized using the term $\rho Q_{p-c} U_d$. The grey-shaded area in Figure 5.11 denotes the geomorphic work (W_g), which is the work made by the flow to build the bed morphology and to maintain it at equilibrium.

Figure 5.11 shows that bed aggradation decreased and erosion increased for increasing discharge ratios, with both junction angles. The total momentum increased in the junction area ($0 < X/B_m < 0.3$) because of the increased flow depth there. Downstream of the confluence, the total momentum decreased until reaching a constant value, which indicates that the flow had attained uniform conditions. The total energy profiles were quasi-horizontal upstream of the confluence ($X/B_m < 0$), which reveals that the flow approaching the confluence maintained constant total energy. In the junction area ($0 < X/B_m < 0.3$), the tributary inflow induced an energy loss in the main channel, which resulted in a step in the energy profile. Downstream of the confluence ($X/B_m > 0.3$), the energy slope progressively increased because of the flow acceleration until becoming parallel to the bottom, where the flow became uniform. The resultant force R was positive where $X/B_m < 0.3$ because the weight component (downstream-oriented) exceeded the flow-resistance, which acts opposite to the flow direction. On the contrary, R was positive where $X/B_m > 0.3$ because both the weight and flow-resistance components were oriented upstream. When the flow approached uniform conditions, R approached zero because the weight and flow-resistance components cancelled each other.
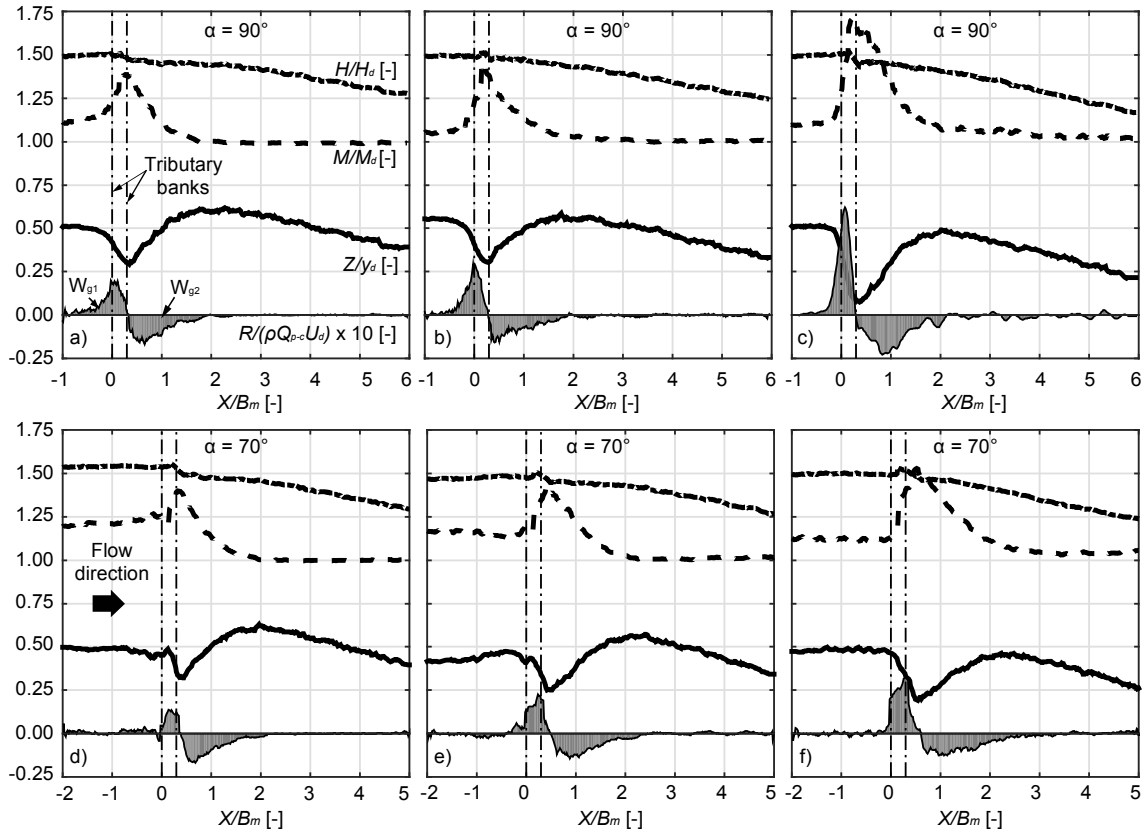
Figure 5.11 Cross-sectional average values of bed elevation (Z/y_d), total momentum (M/M_d), total energy (H/H_d), and flow resistance ($R/\rho Q_{p-c}U_d \times 10$), along the main channel at equilibrium with a) LR and $\alpha = 90°$; b) IR and $\alpha = 90°$; c) HR and $\alpha = 90°$; d) LR and $\alpha = 70°$; e) IR and $\alpha = 70°$; f) HR and $\alpha = 70°$.

To quantify the effects of the tributary on the main channel, total energy balance was calculated between cross-sections $X/B_m = -1$ (section I), $X/B_m = 1$ (section II), and $X/B_m = 5$ (section III). Additionally, the positive and negative geomorphic work (W_{g1} and W_{g2}, respectively in Figure 5.11) were determined in each experiment. The energy losses ΔH_{I-II} and ΔH_{I-III} were normalized by the value of total energy at the downstream end of the channel ($H_d = y_d + U_d^2/(2g)$), and the geomorphic work (W_{g1} and W_{g2}) was normalized by $\rho Q_{p-c}^2/B_m$. These values are shown in Table 5.4.

Table 5.4 Cross-sectional average values of normalized total energy losses and geomorphic work in the main channel at equilibrium

α	Q_r	$\dfrac{\Delta H_{I-II}}{H_d}$	$\dfrac{\Delta H_{I-III}}{H_d}$	$\dfrac{W_{g1}}{\rho Q^2/B_m}$	$\dfrac{W_{g2}}{\rho Q^2/B_m}$
[°]	[-]	[-]	[-]	[-]	[-]
	0.11 (LR)	0.040	0.188	0.06	0.08
90	0.15 (IR)	0.015	0.198	0.07	0.08
	0.23 (HR)	0.049	0.271	0.13	0.14
	0.11 (LR)	0.062	0.244	0.04	0.08
70	0.15 (IR)	0.027	0.204	0.06	0.09
	0.23 (HR)	0.038	0.260	0.09	0.10

$\Delta H_{I\text{-}II}$ and $\Delta H_{I\text{-}III}$ were higher with $\alpha = 70°$ than with $\alpha = 90°$ for the low and intermediate discharge ratios (Table 5.4). This pattern was consistent with the higher flow depth observed with $\alpha = 70°$ upstream of the confluence, with respect to that observed with $\alpha = 90°$ (Figure 5.8a-b). In contrast, for the high discharge ratio, the energy losses measured with $\alpha = 90°$ were higher than those measured with $\alpha = 70°$. With each junction angle, $\Delta H_{I\text{-}III}$ increased with the discharge ratio, with the exception of the intermediate ratio with $\alpha = 70°$. $\Delta H_{I\text{-}II}$ did not show any clear pattern as the discharge ratio varied (Table 5.4). The geomorphic work (W_{g1} and W_{g2}) increased with the discharge ratio with both junction angles, which is directly related to the greater scour holes observed for increasing discharge ratios (Figure 5.11).

5.4 Discussion

5.4.1 Bed morphology in the main channel

The initial scour hole observed at $t = 1$ h for all the discharge ratios and with $\alpha = 90°$, but only for the low discharge ratio with $\alpha = 70°$ is a common morphological feature in both symmetrical and asymmetrical confluences (Mosley, 1976; Ashmore and Parker, 1983; Best, 1988; Ghobadian and Bejestan, 2007; Rhoads et al., 2009). Mosley (1976) observed that such a scour formed before the arrival of the sediment wedges originating from each confluent channel, as was observed in this study for the low discharge ratio and with $\alpha = 90°$. This finding indicates that the scour was created by the flow patterns at the junction due to the erosive capacity of the resultant flow from the junction. Moreover, the increases in the depth and size of this initial scour for increasing discharge ratios and higher junction angles are consistent with the results reported by Mosley (1976), Ashmore and Parker (1983), Best (1988), and Ghobadian and Bejestan (2007).

The bed morphology observed in every experiment at equilibrium is similar to that describe by Best and Rhoads (2008) for asymmetrical confluences. This morphology consisted of a bank-attached bar downstream of the confluence, a scour hole in the main channel, and a tributary-mouth bar with a marked bed discordance between the tributary and main channel (cf. Figures 5.1 to 5.4). Aside from these features, deposition at the upstream junction corner was observed only in the experiments with $\alpha = 70°$.

The bank-attached bar was associated with a zone of reduced flow velocities (Section 5.4.3, and Chapter 4) at the downstream junction corner (Best and Rhoads, 2008). The height of this bar decreased for increasing discharge ratios and the higher junction angle (Figures 5.2a c and 5.4a-c). These patterns agree with the results of Leite Ribeiro et al. (2015) but they are in contrast with those of Best (1988) and Ghobadian and Bajestan (2007). According to these latter, the bank-attached bars should become higher as the discharge ratio and the junction angle increase. These differences may be attributed to, on the one side, the different discharge ratios and, on the other side, the bed discordance reported in this study and by Leite Ribeiro et al. (2015), which was not observed in the studies by Best (1988) and Ghobadian and Bajestan (2007).

The scour hole in the main channel at equilibrium was associated both with the turbulence resulting from the flow junction (Best, 1987, and Bristow *et al.*, 1993), and with the acceleration of the flow that was deflected and confined to the outer bank (Rhoads *et al.*, 2009; Leite Ribeiro *et al.*, 2012a; and Chapter 4). In this study, the erosion at the tributary mouth at equilibrium increased with the discharge ratio with both junction angles, indicating an increase in the turbulence associated with the flow junction (Figures 5.1j-l and 5.3j-l). The erosion at the outer bank was more pronounced with $\alpha = 70°$ than with $\alpha = 90°$, especially for the intermediate and high discharge ratios (Figures 5.2a-c and 5.4a-c). This was due to the larger bank-attached bars observed with $\alpha = 70°$, which reinforced the outward flow deflection and acceleration along the outer bank. Scour holes confined to the outer bank of the main channel were observed by Rhoads (2006) and Rhoads *et al.* (2009) in a natural concordant confluence for high discharge ratios ($Q_r > 1$). The similarity with the scour holes observed in this study for lower discharge ratios ($Q_r < 1$) consists on the fact that in both cases, there was a great deflection and confinement of flow to the outer bank. For $Q_r > 1$ the deflection was mainly caused by the tributary inflow, whereas for $Q_r < 1$ the flow deflection was mainly caused by the bank-attached bar. In contrast, Biron *et al.* (1993) and De Serres *et al.* (1999) suggested the absence of marked scour holes at the discordant bed of the Bayonne-Berthier confluence for $0.4 < Q_r < 2.5$, and Leite Ribeiro *et al.* (2012a, 2015) only reported weak scour at the outer bank for $0.11 < Q_r < 0.23$. The absence of significant scour holes at the confluence observed by Biron *et al.* (1993) and De Serres *et al.* (1999) may be explained by a low unit discharge produced by both weak flow deflection and wide effective flow section. In the case of Leite Ribeiro *et al.* (2012a), although the bank-attached bar considerably reduced the effective flow cross-section in the main-channel, the acceleration of flow may not have been sufficient to produce significant bed erosion. In addition, the bed was armored due to the lack of sediment supply to the main channel during the experiment (see Chapter 4).

5.4.2 Bed morphology in the tributary

The dominant tributary sediment load led to a marked bed discordance between the tributary and main channel (Leite Ribeiro *et al.*, 2012a). The different bed elevations and slopes observed in the tributary at equilibrium represented the morphological response to the imposed flow discharges and sediment rate. Therefore, morphodynamics of the confluence evolved toward the required conditions and allowed for the transport of the imposed sediment load by the flow discharge in each discharge ratio scenario. To convey the imposed bed load, the tributary bed adopted steep bed slopes that were similar with both junction angles at equilibrium (see Table 5.3). This pattern indicates that the imposed sediment discharge exerted a major influence on the tributary bed slopes. With $\alpha = 90°$ and compared to $\alpha = 70°$, the tributary adopted a higher bed elevation which results in lower flow depth and higher flow velocity (see *U* in Table 5.3). The higher flow velocity enhanced the transport capacity of the tributary with $\alpha = 90°$, which delivered the bed load into the main channel by dumping it over the tributary-mouth bar. With $\alpha = 70°$, the tributary flow component parallel to the main flow eased the penetration of the tributary-mouth bar into the main channel, by which the bed load was delivered into the main stream. The further penetration of the

tributary-mouth bar with $\alpha = 70°$ with respect to $\alpha = 90°$ agrees with the results reported by Best (1988) and Best and Rhoads (2008).

In this study and that of Leite Ribeiro *et al.* (2015), the penetration of the tributary-mouth bar decreased as the discharge ratio increased. This finding contrasts with those of previous authors (Ashmore and Parker, 1983; Best, 1988; Biron *et al.*, 1993; Leclair and Roy, 1997; Rhoads, 2006; Rhoads *et al.*, 2009; Riley *et al.*, 2015) in which, the penetration of the tributary-mouth bar increased with the discharge ratio. This discrepancy may be due to the turbulence associated with the flow junction, which increased with the discharge ratio and eroded the front of the tributary-mouth bar.

5.4.3 Hydrodynamics at equilibrium

The hydrodynamics of the main channel at equilibrium in all the experiments exhibited most of the features reported by Best (1987). At the upstream junction corner, the local rise in the water surface may be associated with the presence there of a stagnation zone, as reported by Rhoads and Sukhodolov (2001), who investigated a concordant confluence, and by Leite Ribeiro *et al.* (2012a), who investigated a discordant confluence. With $\alpha = 70°$, the deposition observed in the vicinity of the upstream junction corner corroborates the presence of a stagnation zone therein (Best and Rhoads, 2008). The flow deflection zone and the associated shear layer can be related to the scour hole observed at equilibrium in all the experiments. Downstream of the confluence, the increase in the slope of the water surface indicates flow acceleration due to the reduction of the effective flow section by the bank-attached bar. In all the experiments the flow approached to uniform flow farther downstream, which may have been associated with the recovery zone reported by Best (1987).

At the downstream junction corner, a zone of reduced flow velocities developed, promoting the deposition of the tributary sediments and the aggradation of the bank-attached bar. This zone, where no flow-recirculation was observed, contrasts with the flow separation or recirculation zone reported by Best (1987). The absence of flow recirculation and the presence of flow upwelling were identified as typical hydrodynamic features of discordant confluences by Biron *et al.* (1993, 1996a).

The morphological differences observed in the main channel for the different discharge ratios and junction angles reveal that the flow patterns were modified by the bed morphology evolution and were controlled by the discharge ratio. Specifically, for the low and the intermediate discharge ratios and with $\alpha = 90°$, the aggradation of the bank-attached bar modified the flow patterns by concentrating the erosion at the outer bank of the main channel, where an elongated scour hole developed. For the high discharge ratio and $\alpha = 90°$, the intensity of the resulting flow from the junction maintained the scour hole that initially formed at the tributary mouth throughout the experiments (Figure 5.1a-c), whereas for the low and intermediate ratios this scour hole was filled with sediments from the tributary.

At equilibrium, the tributary flow regime was different depending on the discharge ratio. With $\alpha = 90°$ the flow regime corresponded to a critical or supercritical quasi-uniform flow ($Fr \geq 1$), whereas for $\alpha = 70°$ the flow was a subcritical spatially

varied flow ($Fr < 1$). The results corresponding to $\alpha = 90°$ agree with those of Leite Ribeiro *et al*. (2012a; 2015), since they also reported critical and supercritical flows in the tributary for the same discharge ratios and with $\alpha = 90°$. The steep tributary bed slope and high bed elevation at equilibrium result in supercritical or critical flow with $\alpha = 90°$, since the main channel did not impose a downstream boundary condition. The transition from the tributary to the main flow was via a hydraulic jump for the low and intermediate discharge ratios. In the case of $\alpha = 70°$, the lower angle eased the conveyance of the tributary bed load to the main channel, which resulted in a lower tributary bed elevation compared with the $\alpha = 90°$ case. With this configuration, the main flow imposed the downstream boundary condition on the tributary flow, which resulted in a subcritical spatially varied flow for all the discharge ratios.

5.4.4   Effects of the tributary on the main channel

The tributary inflow to the main channel can be described as a jet entering a main stream (Ashmore and Parker, 1983; Leite Ribeiro *et al*., 2012b). This jet-like inflow induced an energy loss that increased with the discharge ratio for both junction angles (see $\Delta H_{I\text{-}III}$ in Table 5.4), which is in good agreement with the results of Webber and Greated (1966), Lin and Soong (1979), and Hsu *et al*. (1998b). In the case of the low and intermediate discharge ratios, the head loss was higher with $\alpha = 70°$ than with $\alpha = 90°$, whereas the opposite was observed for the high discharge ratio. This finding may be explained by the hydraulic jump observed at the junction with the main channel associated with the low and intermediate discharge ratios and with $\alpha = 90°$. The hydraulic jump dissipated a portion of the energy of the tributary flow before entering the main channel. Thus, the tributary inflow induced a lower head loss in the main flow with $\alpha = 90°$ in comparison with the case of $\alpha = 70°$, in which no hydraulic jump occurred. On the contrary, for the high discharge ratio, the higher energy loss associated with $\alpha = 90°$ with respect to $\alpha = 70°$ was due to the absence of a hydraulic jump in both angle configurations and the better alignment of tributary and main channel with $\alpha = 70°$, which eased the tributary inflow to the main channel. Other effects induced by the jet-like tributary inflow in the main channel were the reduced flow velocity of the main channel upstream of the confluence and the flow acceleration downstream. These patterns may be related to a change in the momentum balance of the main stream induced by the tributary inflow (Ramamurthy *et al*., 1988, 1994).

Regarding to the bed morphology, the turbulence associated with the flow resulting from the junction eroded the bed, thereby creating a scour hole and preserving it after equilibrium. The size and depth of this scour was directly related to the intensity of the resultant flow, and all increased with the discharge ratio (cf. Figure 5.11). The intensity of the resultant flow was related to the geomorphic work, which preserved the bed morphology. This geomorphic work increased with the discharge ratio and was higher with $\alpha = 90°$ than with $\alpha = 70°$ at a given discharge ratio.

5.5   Conclusions

The effects of the discharge ratio and junction angle on the morphodynamics of discordant confluences were analyzed in this chapter. The results indicate that these parameters greatly influenced the morphological and hydrodynamic features of the confluence. In general, the effects of the tributary on the morphodynamics of the main channel were amplified by higher discharge ratios and junction angles.

Regarding to bed morphology, higher discharge ratios resulted in lower deposition and greater erosion in the main channel bed. A lower junction angle ($\alpha = 70°$) attenuated the erosion at the tributary mouth and favored the penetration of the tributary-mouth bar. This penetration reinforced the topographic flow deflection and consequently the erosion at the outer bank.

Regarding to hydrodynamics, increasing discharge ratios resulted in a greater energy loss induced by the tributary inflow in the main channel. In addition, the downstream distance to where the flow became uniform increased with the discharge ratio and the junction angle. With $\alpha = 70º$, the flow regime in the tributary was subcritical for all the discharge ratios, whereas with $\alpha = 90º$, the flow regime was supercritical or critical depending on the discharge ratio. The hydraulic jump observed for the low and the intermediate discharge ratios with $\alpha = 90º$ reduced the tributary velocity before it entered the main channel. This led to a lower energy loss in the main channel for these discharge ratios and $\alpha = 90º$, when compared with $\alpha = 70º$. For the high discharge ratio the energy loss was higher with $\alpha = 90º$ than with $\alpha = 70º$, due to the better alignment between the tributary and main streams with $\alpha = 70°$ and the absence of hydraulic jump in both angle configurations.

The geomorphic work produced by the flow resulting from the junction was the responsible for building the confluence bed morphology during the experiments and for maintaining it at equilibrium. This work correlated with the intensity of the resultant flow and it was increased for increasing discharge ratios and at the higher junction angle.

6

Influence of the gradation of bed material on the hydro-morphodynamics of the confluence

This chapter analyzes the influence of the gradation of the bed sediments on the bed morphology and hydrodynamics of open-channel confluences. For that purpose six experiments were conducted in two experimental facilities to which different sediment mixtures were supplied. In the first experimental facility (LCH-EPFL), poorly sorted sand-gravel mixtures were supplied to the main channel and tributary ($\sigma = 3.15$ and 4.51, respectively), for three different discharge ratios ($Q_r = 0.11, 0.15, 0.23$). In the second facility (IST-UL), uniform sand ($\sigma = 1.35$) was supplied both to the tributary and main channel for the same discharge ratios. The sediment rates were the same for all the experiments, 0.5 and 0.3 *kg/min* for the tributary and main channel respectively. The experiments were run until reaching equilibrium, which means that the outgoing sediment rate approximates the incoming, and the bed morphology attained a quasi-steady state. Bed topography and water surface surveys were recorded at equilibrium. The results show, that with non-uniform sediments, the flow dynamics and bed morphology need to evolve in order to achieve enough transport capacity to convey the imposed sediment load. The evolution of the bed morphology consisted of an increase in the topographic gradient by means of a developed bar and scour hole in the main channel, a marked bed discordance between the tributary and main channel, and a steep bed slope in the tributary. In parallel to the bed morphological evolution, the hydrodynamics also developed high flow velocity gradients between the upstream and downstream parts of the confluence. These velocity gradients were reflected in the water surface by means of abrupt changes of its slope. With uniform sediments, the bed morphology and water surface displayed attenuated features with respect to those with non-uniform sediments, indicating a higher transport capacity of the flow. The relative excess of transport capacity along with the low gradation coefficient of the bed material created migrating dunes which masked the typical morphological features of the confluence (bank-attached bar and scour hole).

Keywords: River confluences, sediment gradation, bedforms, morphodynamics.

6.1 Introduction

In alpine river confluences, the bed material is composed of non-uniform sediment mixtures with high gradation coefficients (Leite Ribeiro, 2011). With this material, the sediment transport is selective and, in general, the finer particles are washed out by the flow whereas the coarser ones remain, which often results in an armored bed (Chiew, 1991).

The uniformity of a sediment mixture is assessed by means of the gradation coefficient σ defined as:

$$\sigma = \frac{1}{2}\left(\frac{d_{84}}{d_{50}} + \frac{d_{50}}{d_{16}}\right) \tag{6.1}$$

Where d_{84}, d_{50}, d_{16} are the particle sizes coarser than the 84%, 50%, and 16% by weight of the sediment mixture, respectively. A high value of σ indicates a non-uniform sediment mixture and, on the other hand, a low value of σ denotes a uniform sediment mixture.

Few studies exist, if any, which examine the role of the gradation of the bed material on the flow dynamics and bed morphology of open-channel confluences. For that purpose, six experiments were conducted in two experimental facilities at LCH-EPFL and IST-UL. In the LCH-EPFL experimental facility three discharge ratios were tested while non-uniform sediment mixtures were supplied to the tributary and main channel (σ = 4.51 and 3.15, respectively). The same discharge ratios were tested in the IST-UL experimental facility, but supplying uniform sand to both the tributary and the main channel (σ = 1.35). Bed topography and water surface surveys made after equilibrium was reached illustrate the differences in bed morphology and hydrodynamics of the confluence, between the different sediment mixtures.

6.2 Experimental setup

The results presented herein correspond to the experimental sets II and III, carried out in the experimental facilities of the LCH-EPFL and IST-UL, respectively. The experimental setups are summarized in Table 6.1 and described in detail in Chapter 3.

Table 6.1 Overview of the experimental setup

Experimental set	α [°]	B_t/B_m [-]	σ [-]	Q_r [-]	Q_{sm} [Kg/min]	Q_{st} [Kg/min]	Measurements
Set II	70°	0.30	3.15 (main) 4.51 (trib.)	0.11, 0.15, 0.23	0.3	0.5	Bed topo at equilibrium W. surf. at equilibrium
Set III	70°	0.30	1.35	0.11, 0.15, 0.23	0.3	0.5	Bed topo at equilibrium W. surf. at equilibrium

6.3 Results

6.3.1 Hydro-morphodynamics of the main channel

6.3.1.1 Experimental set II. Non-uniform sediments

The bed topography of the main channel at equilibrium for the three experiments performed with non-uniform sediments is depicted in Figure 6.1. For each discharge ratio, Figure 6.1 shows a plan view of the bed topography and the longitudinal profiles of the bed elevation and water surface at the inner and outer bank of the main channel ($Y/B_m = 0.9$ and 0.1, respectively). X and Y were normalized by the width of the main channel $B_m = 0.50$ m. Z was normalized by the downstream flow depth $y_d = 0.08$ m (see Section 3.4.5). The bed morphology of the main channel presented common features for all the discharge ratios. These features were: i) a bar attached to the inner bank, widely termed bank-attached bar; ii) a scour hole which extended from the tributary mouth to the outer bank, where it reached its deepest point; and iii) a bed elevation at the inner bank upstream of the confluence (cf. Figure 6.1). The bank-attached bar was associated with a zone of reduced flow velocity where the sediments coming from the tributary were deposited. This bar reduced the effective flow section and steered the flow toward the outer bank of the main channel. There the flow accelerated and eroded the bed, creating the scour hole. The rise in bed elevation observed at the upstream junction corner was associated with the presence of a stagnation zone induced by the tributary inflow, which promoted deposition.

These morphological features were affected by the distinct discharge ratios. Namely, the height of the bank-attached bar decreased as the discharge ratio increased (cf. Figure 6.1a2, b2, and c2). Also, the deepest point of the scour hole at the outer bank increased from the low to the intermediate ratio, whereas for the high ratio the depth of the scour is similar to that observed for the intermediate ratio (cf. Figure 6.1a3, b3, and c3). The inception of the scour hole observed at the inner bank, which coincided with the inception of the bar, moved farther downstream as the discharge ratio increased (cf. Figure 6.1a2, b2, and c2). Furthermore, the bed elevation observed at the inner bank upstream of the confluence became less pronounced as the discharge ratio increased (cf. Figure 6.1a2, b2 and c2). Additional to the aforementioned morphological features, small dunes were observed upstream of the confluence ($X/B_m < 0$) for the three discharge ratios (not shown in Figure 6.1). The heights of these dunes were of about $\Delta \approx 0.04\ y_d$ - $0.12\ y_d$, and their lengths approximately $\lambda \approx 1.25\ y_d - 1.88\ y_d$.

The water surface at equilibrium presented two well differentiated profiles that are visible in both the inner and outer bank of the main channel. These profiles are: i) a quasi-horizontal one upstream of the confluence ($X/B_m < 0.0$), corresponding to a M1-type backwater curve induced by the tributary inflow; and ii) a steeper profile associated with the acceleration experienced by the flow downstream of the confluence ($X/B_m > 0.0$) (cf. Figure 6.1). At the inner bank ($Y/B_m = 0.9$), the water surface presented a local elevation at the upstream junction corner ($X/B_m = 0.0$, $Y/B_m \approx 0.9$) associated with a stagnation zone observed therein. At the downstream junction corner ($X/B_m \approx 0.3$,

$Y/B_m \approx 0.9$), the water surface dropped, indicating the existence of a low-pressure zone due to the abrupt change of direction experienced by the tributary flow (cf. Figure 6.1a2, b2, and c2). Downstream of the confluence the flow accelerates and the water surface becomes steeper.
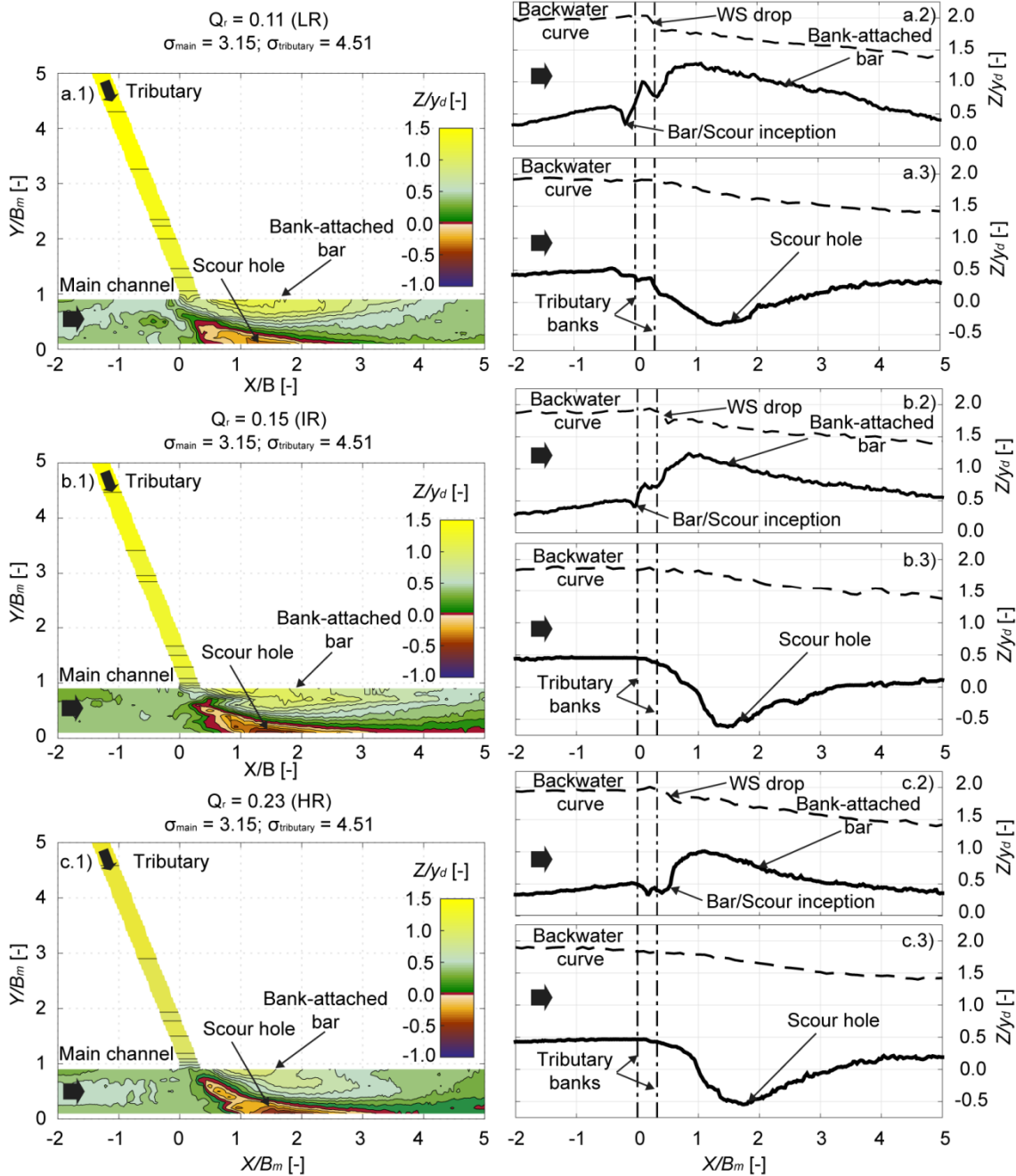
Figure 6.1 Bed topography and water surface profiles of the main channel at equilibrium corresponding to the experiments performed with non-uniform sediments (σ = 3.15 and 4.51). a.1) Bed topography with contour spaced ΔZ = 0.01 m for Q_r = 0.11 (LR); a.2) Longitudinal profile of the bed elevation and water surface measured at the inner bank of the main channel (Y/B_m = 0.9) for Q_r = 0.11 (LR); a.3) Longitudinal profile of the bed elevation measured at the outer bank of the main channel (Y/B_m = 0.1) for Q_r = 0.11 (LR). Similarly, plots b) and c) correspond to Q_r = 0.15 (IR) and Q_r = 0.23 (HR) respectively.

6.3.1.2 Experimental set III. Uniform sediments

In the case of the experiments performed with uniform sand, the aforementioned bank-attached bar and the scour hole co-existed with dunes in the bed morphology of the main channel at equilibrium. Figure 6.2 shows a plan view of the bed topography of the main channel at equilibrium for each discharge ratio. Figure 6.3 depicts the bed elevations and water levels along the inner and outer bank of the main channel ($Y/B_m = 0.9$; and 0.1, respectively).

From Figures 6.2 and 6.3, it is possible to infer that the length of the bank-attached bar and the size of the scour hole increased with the discharge ratio. Also, the erosion was more pronounced at the tributary mouth as the discharge ratio augmented. For the low discharge ratio, the erosion was concentrated at the outer bank, whereas for the intermediate and high discharge ratios the scour extended from the tributary mouth to the outer bank of the main channel (cf. Figures 6.2 and 6.3). Upstream of the confluence ($X/B_m < 0$) the bed aggradation increased with the discharge ratio.

Additionally to the bank-attached bar and the scour hole, migrating dunes were also observed in the bed of the main channel at equilibrium. For the low discharge ratio, seven dunes were observed upstream of the confluence for $-5 < X/B_m < 0$. These dunes had an average wave length of $\lambda \approx 3.5\ y_d$ ($y_d = 0.10$ m in set III, see Section 3.4.5). Their height was between $\Delta \approx 0.1\ y_d$ and $\Delta \approx 0.3\ y_d$ (cf. Figures 6.2a and 6.3a). For the intermediate discharge ratio, seven dunes were also observed for $-5 < X/B_m < -1$ (Figures 6.2b and 6.3b), whose average wave length was $\lambda \approx 3.0\ y_d$ and height about $\Delta \approx 0.1\ y_d$ - 0.3 y_d. The high discharge ratio resulted in an approximately plane bed upstream of the confluence (cf. Figures 6.2c and 6.3c).

For every discharge ratio, the dunes downstream of the confluence were generally higher and longer than those observed upstream. For the low discharge ratio, the length of the downstream dunes was about $\lambda \approx 5 - 12.5\ y_d$, and the height was about $\Delta \approx 0.1$ - 0.5 y_d (cf. Figures 6.2a and 6.3a). For the intermediate and high discharge ratios, the dunes alternated between the outer and inner banks of the main channel. For the intermediate discharge ratio, the length and height of the dunes at the inner bank were about $\lambda \approx 5 - 10\ y_d$ and $\Delta \approx 0.4$ - 0.7 y_d, respectively (cf. Figure 6.3b.1). At the outer bank $\lambda \approx 10 - 12.5\ y_d$ and $\Delta \approx 0.5\ y_d$ (cf. Figure 6.3b.3). For the high discharge ratio, the dunes at the inner bank presented a length of $\lambda \approx 7.5\ y_d$ and a height of $\Delta \approx 0.3\ y_d$ (cf. Figure 6.3c.1). At the outer bank, $\lambda \approx 12.5\ y_d$ and $\Delta \approx 3.5\ y_d$ (cf. Figure 6.3c.3). The alternation of dunes may be due to the meandering flow induced by the tributary inflow and the bank-attached bar.
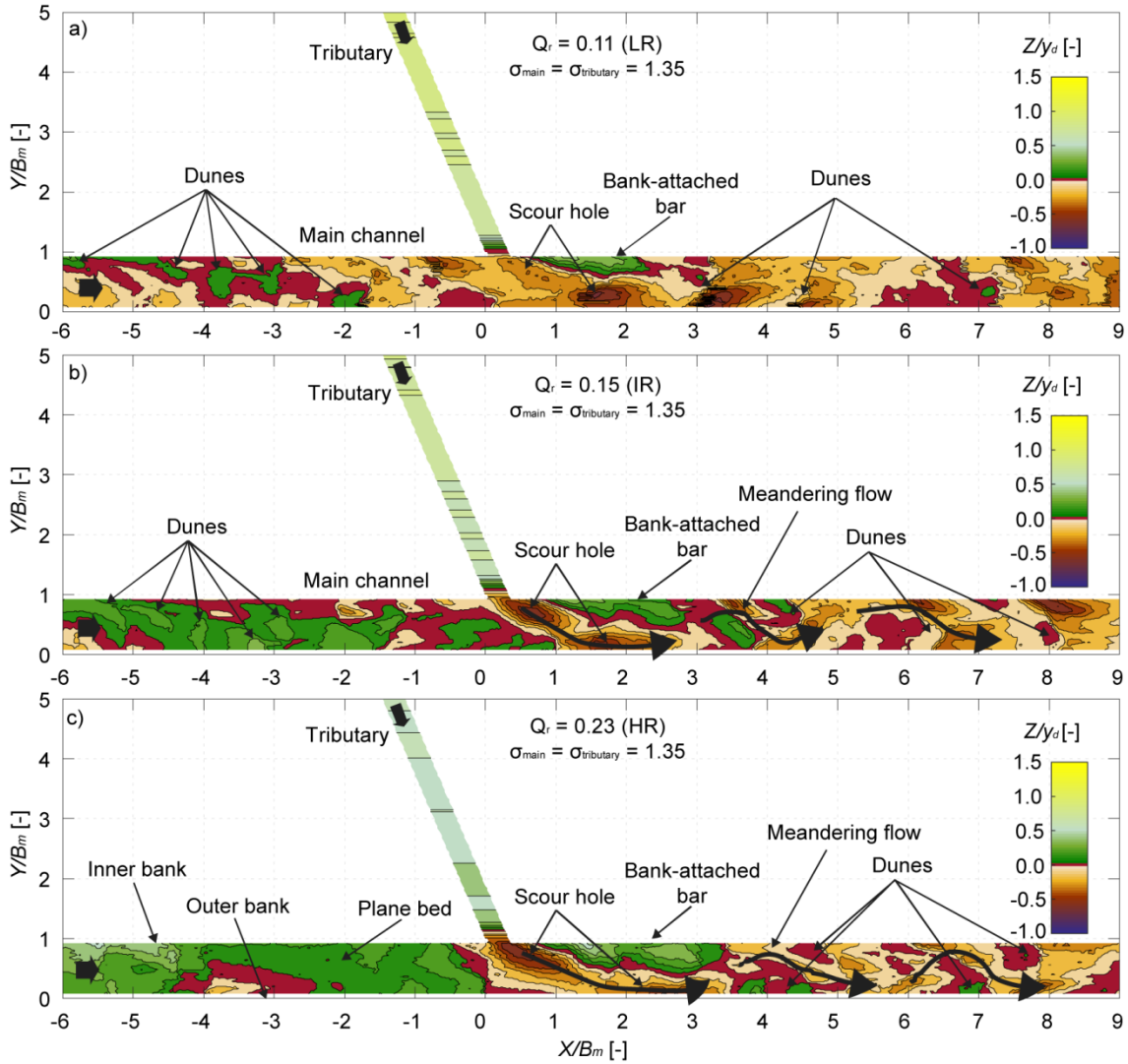
Figure 6.2 Plan view of the bed topography of the main channel at equilibrium, corresponding to the experiments performed with uniform sediments (σ = 1.35). Bed-contours spaced ΔZ = 0.01 m. a) Q_r = 0.11 (LR); b) Q_r = 0.15 (IR); c) Q_r = 0.23 (HR).

The water surface measured at equilibrium presented similar features to those reported for the experiments with non-uniform sediments, i.e. a M1-type backwater curve upstream of the confluence, a local raise at the upstream junction corner, a drop of the water surface at the downstream junction corner, and a steeper slope downstream of the confluence. Aside from such features, the water surface of these experiments was wavier and presented lower slopes than those measured with non-uniform sediments (cf. Figure 6.3).
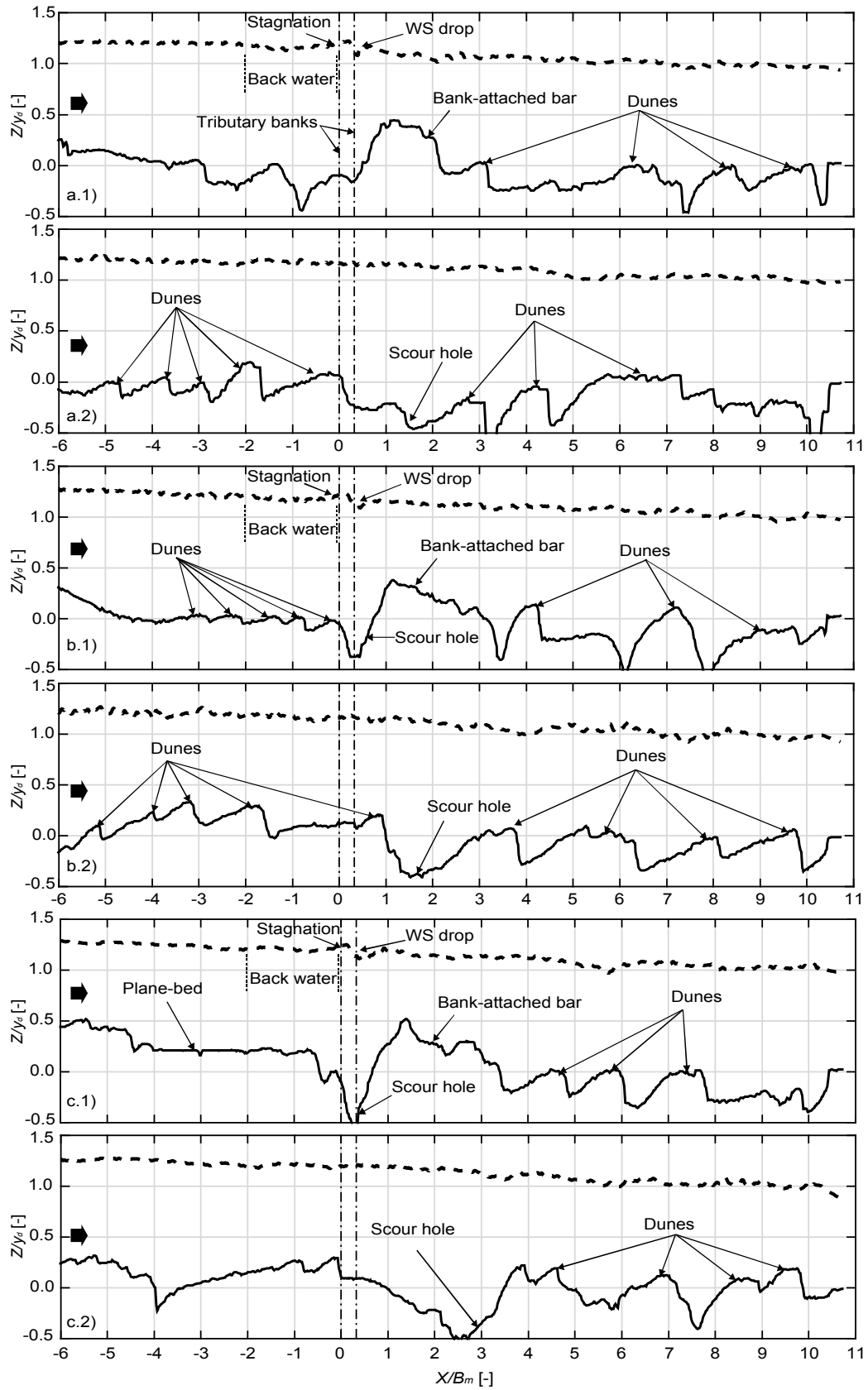
Figure 6.3 Longitudinal profiles of the bed elevation and water surface at equilibrium, corresponding to the experiments performed with uniform sediments (experimental set III). The letters a, b and c refer to the low, intermediate and high discharge ratios, respectively. The numbers 1 and 2 correspond to the inner and outer banks of the main channel ($Y/B_m = 0.9$; and 0.1 respectively), respectively.

6.3.1.3 On the flow regime of the main channel

The flow regime of the main channel was classified based on the mean values of the flow depth (y), flow velocity (U) and Froude number (Fr). Also, the van Rijn's (1984) method was applied upstream and downstream of the confluence to predict and classify the bedforms of the main channel. This method characterizes the bed material and the sediment transport capacity by D_* and T, respectively. Both are defined as follows:

$$D_* = d_{50} \left[\frac{(s-1)g}{v^2} \right]^{1/3} \tag{6.2}$$

$$T = \frac{(u_*)^2 - (u_{*,cr})^2}{(u_{*,cr})^2} \tag{6.3}$$

In this study, the mean diameter d_m is adopted to characterize the bed material instead of the median diameter d_{50}. The reason of this modification is that the supplied sediment mixtures have approximately the same d_{50} values (0.82 and 0.85), which do not reflect the differences between them. Therefore in equation 6.2 d_{50} is substituted by the mean diameter d_m, s denotes the specific density, g is the gravity acceleration, v is the kinematic viscosity coefficient. In equation 6.3 u_* denotes the bed-shear velocity, and $u_{*,cr}$ is the critical bed-shear velocity (Shields, 1936). u_* and $u_{*,cr}$ were obtained as follows:

$$u_* = U(g^{0.5}/C') \tag{6.4}$$

$$u_{*,cr} = \sqrt{\tau_{cr}(s-1)d_m} \tag{6.5}$$

Where C' is the Chézy roughness coefficient and τ_{cr} denotes the critical shear stress. These were obtained according to van Rijn (1984a):

$$C' = 18 \log(12R_h/3d_{90}) \tag{6.6}$$

$$\tau_{cr} = 0.013 \, (D_*)^{0.29} \; for \quad 20 \leq D_* \leq 150 \tag{6.7}$$

Where R_h denotes the hydraulic radius and d_{90} is the particle size coarser than 90% by weight of the bed material.

In the experimental set II (non-uniform sediments), the bed material of the main channel upstream of the confluence was characterized by the GSD of the sediment mixture supplied to the main channel ($d_m = 1.4$ mm and $d_{90} = 3.0$ mm). The bed material of the tributary and that of the main channel downstream of the confluence were characterized by the GSD of the sediment mixture supplied to the tributary ($d_m = 2.3$ mm and $d_{90} = 5.7$ mm). In the experimental set III (uniform sediments), the bed material of both flumes was approached by the GSD of the sediment mixture supplied to them ($d_m = 0.85$ mm and $d_{90} = 1.40$ mm)

Table 6.2 shows the normalized mean values of flow depth (y/y_d) and flow velocity (U/U_d) for the main channel upstream and downstream of the confluence. These values were normalized by the downstream flow depth y_d and the concomitant flow velocity U_d (see Section 3.4.5), respectively. Also, the Froude number (Fr) and the dimensionless parameters of van Rijn (1984) (D_* and T) are shown in Table 6.2. Sub-indexes *up* and *dw* refer to upstream and downstream of the confluence, respectively.

Table 6.2 Normalized mean values of the main hydraulic variables for the main channel at equilibrium.

Experimental set	Q_r	Upstream ($X/B_m < 0$)					Downstream ($X/B_m > 0$)				
		y_{up}/y_d	U_{up}/U_d	Fr_{up}	D_{*up}	T_{up}	y_{dw}/y_d	U_{dw}/U_d	Fr_{dw}	D_{*dw}	T_{dw}
	[-]	[-]	[-]	[-]	[-]	[-]	[-]	[-]	[-]	[-]	[-]
Set II (non-uniform sediments)	0.11	1.47	0.61	0.43	35	0.89	1.00	1.00	0.85	58	3.08
	0.15	1.45	0.60	0.42	35	0.82	1.04	0.96	0.80	58	2.71
	0.23	1.44	0.57	0.40	35	0.61	1.09	0.92	0.75	58	2.34
Set III (uniform sediments)	0.11	1.07	0.84	0.55	22	2.28	1.02	0.98	0.59	22	3.46
	0.15	1.05	0.83	0.55	22	2.19	1.04	0.97	0.57	22	3.33
	0.23	1.04	0.78	0.52	22	1.83	1.05	0.95	0.56	22	3.21

The Froude numbers obtained for main channel upstream and downstream of the confluence reveal that the flow regime was subcritical ($Fr < 1$) for all experiments. Upstream of the confluence ($X/B_m < 0$) the flow depth and flow velocity decreased for increasing discharge ratios, in both experimental sets (Table 6.2). The decrease in flow velocity was associated with a decrease in the sediment transport capacity, which was assessed by T_{up} in Table 6.2. The values of D_{*up} reflected the differences of bed material between both experimental sets, i.e., the coarse bed material in the experimental set II was associated with a higher value of D_{*up}, whereas the fine bed material in set III was associated with a lower value of D_{*up} (Table 6.2)

In both experimental sets, the flow depth increased and the flow velocity decreased for increasing discharge ratios downstream of the confluence ($X/B_m > 0$). This resulted in a decrease of sediment transport capacity for increasing discharge ratios (T_{dw} in Table 6.2). The values of D_{*dw} downstream of the confluence differed substantially between experimental sets (Table 6.2). This difference reflected the coarse bed of the main channel in the experimental set II, which was in contrast with the fine bed in the experimental set III (Figure 6.4).

In both experimental sets and for every discharge ratio, the sediment transport capacity increased from upstream to downstream of the confluence (Table 6.2). This increase was associated with the increase in flow velocity that was due to the increase in flow discharge. In the experimental set II, the increase in sediment transport capacity from upstream to downstream of the confluence was more pronounced than in the set III. This contrast may be attributed to the different bed materials observed upstream and downstream of the confluence in the experimental set II, whereas in set III the bed material was uniform all along the main channel Figure 6.4.
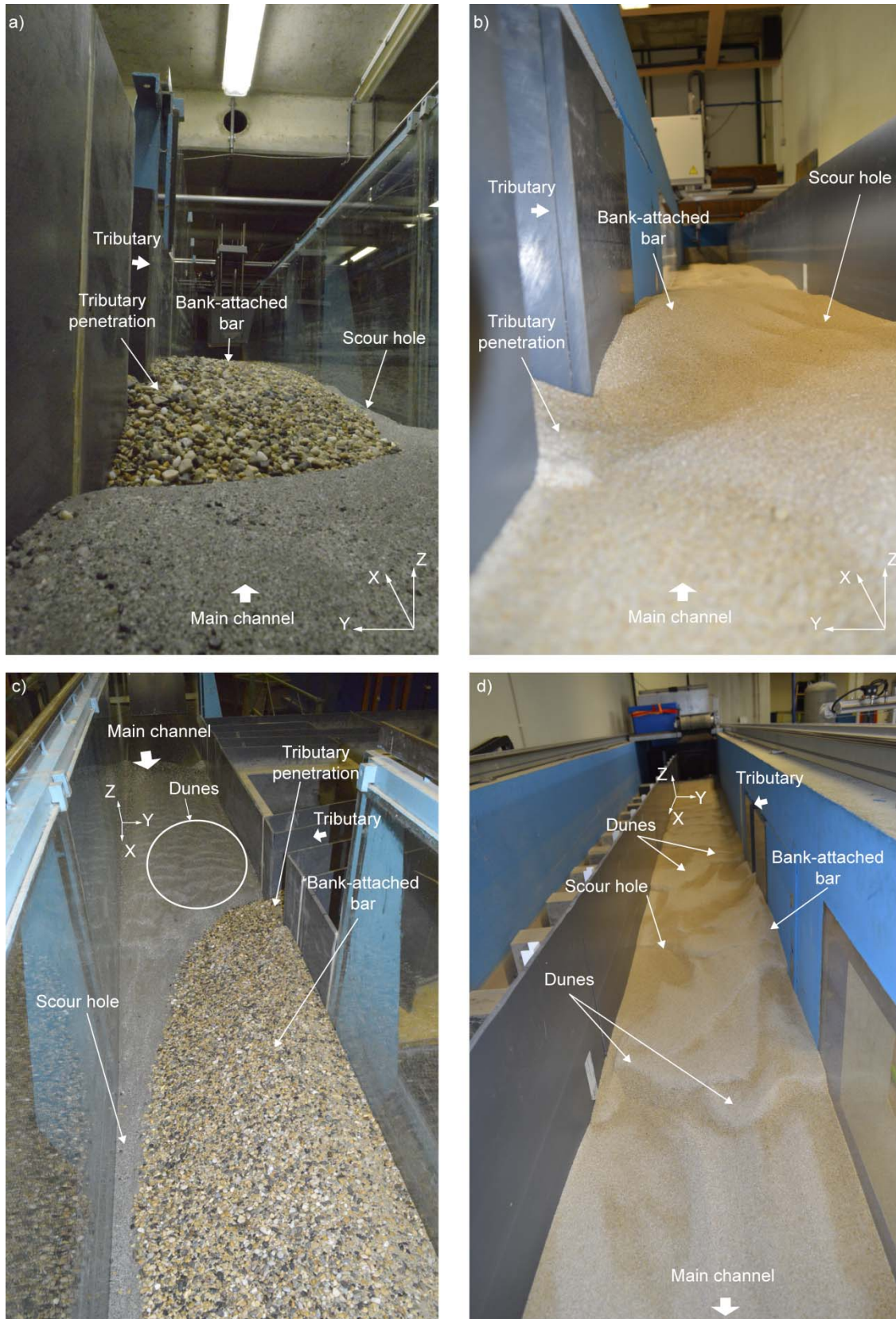
Figure 6.4 Bed morphology at equilibrium corresponding to the low discharge ratio (Q_r= 0.11) for set II and set III. a) View of the tributary mouth from the upstream junction corner corresponding to the experiment performed with non-uniform sediments (set II). b) Analogous to a) but with uniform sediments (set III). c) Upstream view of the confluence corresponding to the experiment performed with non-uniform sediments (set II). d) Analogous to c) but with uniform sediments (set III).

The dune-type bedforms observed in both experimental sets were in agreement with the observations made by van Rijn (1984) for each pair of values $\{D_*, T\}$. Also, the absence of bedforms downstream of the confluence for the experimental set II may be attributed to the coarse bed material. This corresponded to a high value of D_{*dw} (Table 6.2), for which van Rijn (1984) did not observe bedforms neither. In the experimental set III and for the high discharge ratio, the plane bed observed in the main channel upstream of the confluence was due to a lower sediment transport capacity (T_{up} in Table 6.2), compared to the other discharge scenarios. This plane bed was not consistent with the observations made by van Rijn (1984) for the associated pair of values $\{D_*, T\}$, for which dunes were reported.

6.3.2 Hydro-morphodynamics of the tributary

The profiles of bed elevation and water surface of the tributary at equilibrium are depicted in Figure 6.4 for each experiment. The bed morphology of the tributary at equilibrium presented common features for all the experiments. These features were: i) a reach with a nearly constant slope upstream of the confluence ($Y/B_m > 1.5$) and ii) a tributary-mouth bar with an avalanche slope at the junction with the main channel, which created a marked bed discordance between the tributary and main channel.
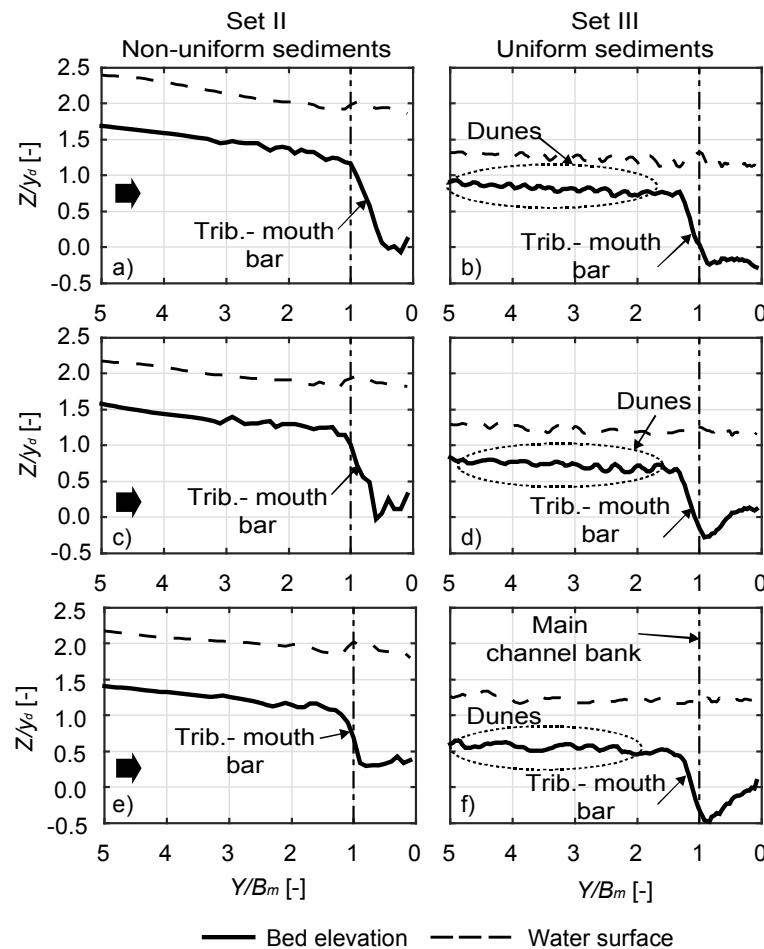
Figure 6.5 Longitudinal profiles of the bed elevation and water surface measured at equilibrium along the tributary axis. a) $Q_r = 0.11$ (LR) in set II; b) $Q_r = 0.11$ (LR) in set III; c) $Q_r = 0.15$ (IR) in set II; d) $Q_r = 0.15$ (IR) in set III; e) $Q_r = 0.23$ (HR) in set II; and d) $Q_r = 0.23$ (HR) in set III.

In both experimental sets, the bed slope and bed elevation of the upstream reach ($Y/B_m > 1.5$) decreased as the discharge ratio increased. The bed discordance was similar for the low and intermediate discharge ratios in both experimental sets. For the high discharge ratio, the bed discordance was higher with uniform sediments (set III) due to the deeper scour hole formed at the tributary mouth. The bed slope where $Y/B_m > 1.5$ and the penetration of the tributary-mouth bar into the main channel were more pronounced with non-uniform sediments (set II) than with uniform sediments (set III) (Figure 6.4a and b).

The water surface of the tributary at equilibrium presented an upstream reach with an approximately constant slope where $Y/B_m > 1.5$, and a local rise at the entry of the main channel ($Y/B_m \approx 1$). As observed for the bed, the water surface exhibited steeper slopes with non-uniform sediments (set II) than with uniform sand (set III).

With non-uniform sediments (set II), the bed of the tributary was armored. This inhibited the formation of bedforms (see Figure 6.6a). In contrast, dunes were observed in the tributary bed for all the discharge ratios tested with uniform sand (set III) (Figure 6.6b). For the low discharge ratio, the dunes observed in the reach where $5 > Y/B_m > 2$ presented a height of about $\Delta \approx 0.05y$ and a wave-length of approximately $\lambda \approx 3y$, where y denotes the the mean flow depth where $Y/B_m > 1.5$. For the intermediate discharge ratio, the height of the dunes observed where $3 > Y/B_m > 1.5$ increased from $\Delta \approx 0.12y$ to $\Delta \approx 0.20y$ as approached the confluence. The length of these dunes was of approximately $\lambda \approx 3.2y - 3.6y$. For the high discharge ratio, the height of the dunes observed where $5 > Y/B_m > 2$ was $\Delta \approx 0.09y$ - $0.14y$, and the wave-length value of $\lambda \approx 2.6y - 3.6y$.
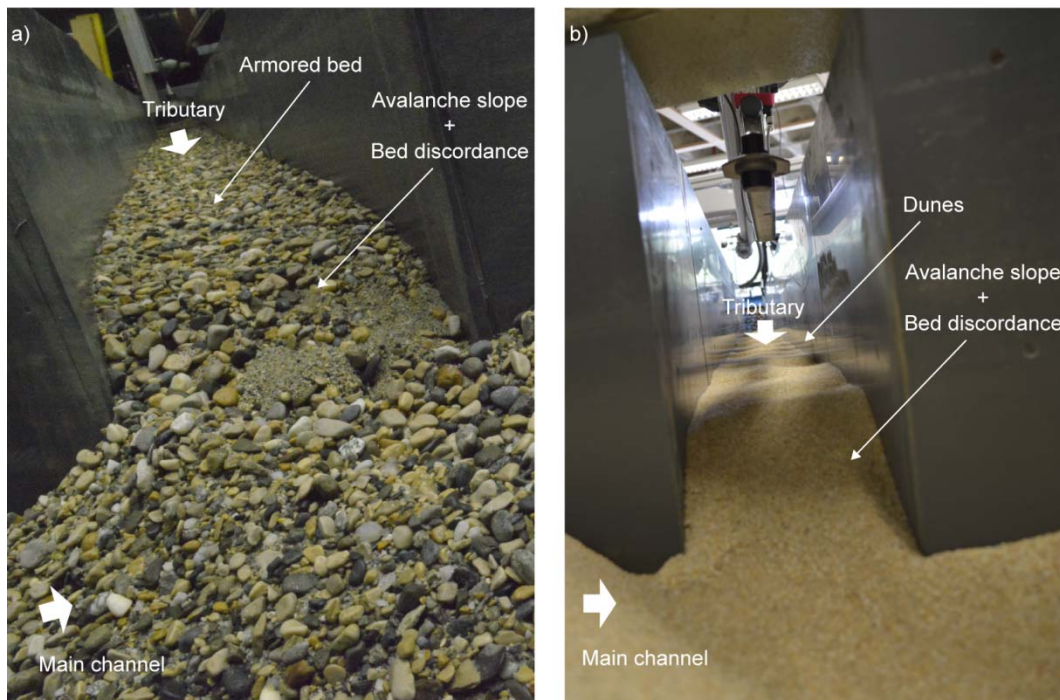
Figure 6.6 a) Tributary bed at equilibrium for $Q_r = 0.11$ with non-uniform sediments (set II). b) Tributary bed at equilibrium for $Q_r = 0.11$ with uniform sediments (set III).

Table 6.3 shows the normalized values of flow depth (y/y_d) and flow velocity (U/U_d), corresponding to the upstream reach of the tributary at equilibrium ($Y/B_m > 1.5$). Also, the Froude number (Fr), and the particle and transport stage parameters of van Rijn (1984) (D_* and T) are given in Table 6.3. These values reveal that the flow regime was subcritical ($Fr < 1$) for all the experiments. Also, the flow depth and flow velocity increased with the discharge ratio in both sets of experiments.

Table 6.3 Normalized values of the main hydraulic variables of the tributary for $Y/B_m > 1.5$.

Experimental set	Q_r	Fr	y/y_d	U/U_d	D_*	T
	[-]	[-]	[-]	[-]	[-]	[-]
Set II (non-uniform sediments)	0.11	0.50	0.69	0.48	58	0.40
	0.15	0.74	0.63	0.69	58	1.97
	0.23	0.75	0.79	0.79	58	2.55
Set III (uniform sediments)	0.11	0.70	0.44	0.77	22	3.09
	0.15	0.74	0.50	0.86	22	4.01
	0.23	0.65	0.69	0.90	22	3.98

The armored bed observed in the tributary in all the experiments of set II agreed with the high value of D_* obtained for those experiments (Table 6.3). In the experimental set III, the dunes observed in the tributary bed were in agreement with the observations made by van Rijn (1984) for the pair of values {D_*, T} obtained for each discharge ratio (Table 6.3).

6.4 Discussion

The bed morphology observed in both experimental sets at equilibrium presented common features that are characteristic of river confluences. These were a bank-attached bar at the inner bank of the main channel, a scour hole which extended from the tributary mouth to the outer bank, and a marked bed discordance between the tributary and main channel. Such features were influenced by the gradation coefficient (σ) of the sediment mixtures supplied to the flumes during the experiments.

The bank-attached bar is typically associated with a zone of flow recirculation at the downstream junction corner of concordant confluences (Best, 1987, 1988; Bristow *et al.*, 1993). Nevertheless, in discordant confluences where flow recirculation may not occur (Biron *et al.*, 1993, 1996a; Boyer *et al.*, 2006, Chapter 4), the bar can develop in a zone of reduced flow velocities but not necessarily with flow recirculation (Best & Rhoads, 2008). The size of the bank-attached bars formed with non-uniform sediments (set II) decreased with the discharge ratio. On the contrary, the bar became larger as the discharge ratio increased with uniform sediments (set III) (cf Figures 6.1 to 6.4). Between both experimental sets, the bank-attached bars formed with non-uniform sediments (set II) were considerably larger than those formed with uniform sand (set III) (cf. Figure 6.4). With non-uniform sediments (set II), the coarser particles provided by the tributary to the confluence could not be conveyed downstream. They consequently tended to deposit at the downstream junction corner, building the bar. During the experiments, the size of the bar increased, which reduced the effective flow section and

accelerated the flow until the necessary conditions to transport the bedload imposed from upstream were met. In contrast, the finer sediments supplied to the confluence for the experimental set III, were conveyed more easily by the resultant flow, yielding smaller bars.

The scour hole is associated both with the turbulence resulting from the flow junction and with the flow acceleration experienced by the flow deflected and confined to the outer bank. The turbulence is mostly responsible for the erosion at the tributary mouth (Best, 1987, 1988; Bristow *et al.*, 1993), while the deflected and accelerated flow erodes the bed along the outer bank (Rhoads, 2006; Rhoads *et al.*, 2009). In this study, the erosion at the tributary mouth increased with the discharge ratio (cf Figures 6.1 to 6.4) in both experimental sets. This is because the turbulence resulting from the flow junction was more intense for increasing discharge ratios. The erosion at the outer bank of the main channel also increased with the discharge ratio, which indicates that the outward flow deflection was enhanced for increasing discharge ratios (cf Figures 6.1 to 6.4). In the experimental set II, the erosion was mostly concentrated at the outer bank, whereas for the experimental set III the scour hole extended from the tributary mouth to the outer bank. The comparatively deeper scour holes at the tributary mouth observed with uniform sediments (set III) can be justified as the fine particles were transported more easily than the coarse ones supplied in the experimental set II, promoting more erosion. The deeper erosion observed at the outer bank of the main channel with non-uniform sediments (set II), compared with the results of set III, may be attributed to a stronger flow concentration and acceleration at that location. This major concentration and acceleration of the flow was caused by the larger bank-attached bars that were formed with non-uniform sediments (set II). In contrast, the smaller bars formed with uniform sediments (set III) led to less flow deflection, resulting in fewer erosion at the outer bank.

In the tributary and with non-uniform sediments, the bed morphology at equilibrium presented steeper bed slopes upstream of the confluence and further penetration of the tributary-mouth bar in the main channel, with respect to the results obtained with uniform sediments (Figure 6.5a and b). To convey the wide range of particle sizes supplied to the tributary in the experimental set II, the bed adopted a steep slope increasing the available shear stress. In contrast, the bed evolved toward comparatively flatter slopes in the experimental set III, since the sediment load was composed of finer particles. The fine sediments of set III were easily eroded by the turbulence associated with the flow junction and thus, the tributary bed did not penetrate into the main channel as far as it did with coarser sediments (set II). The bed discordance was related to the different sediment rates transported by each flume (Leite Ribeiro *et al.*, 2012a). The similar bed discordance observed for the low and intermediate discharge ratios in both experimental sets may be attributed to the fact that the sediment rates were the same in all the experiments. In the case of the high ratio, the turbulence associated to the flow junction eroded the fine bed increasing the discordance, whereas for the experiment performed with non-uniform sediments, the flow resulting from the junction was not able to erode the bed at the tributary mouth because it was composed of coarse particles.

The morphodynamics differences observed between both set of experiments may be qualitatively explained through the Lane's (1955) balance:

$$Q \times J \sim Q_s \times d \tag{6.8}$$

Where Q and J denote the flow discharge and bed slope, and Q_s and d denote the rate and characteristic grain size of the sediment supplied from upstream. Lane (1955) stated that the river regime requires a balance between the sediment supply and the transport capacity. The idea consists on that if any of the variables is altered, at least any one other will change to maintain the regime. In this study, the sediment rates (Q_s) and the flow discharges (Q) were fixed for the experiments run with the same discharge ratio, and the characteristic grain diameter of the supplied sediments (d) was coarser for the experimental set II than for set III. This implies that the variable which must compensate the variation in d is the bed slope (J). In this line, the coarser sediments supplied to the experiments of set II led to an increase of the bed slope, which in turn was reflected in a steeper slope of the water surface.

In the experiments performed with non-uniform sediments (set II), the morphodynamics of the confluence seemed to be governed by the imposed sediment loads. In these experiments, the bed morphology evolved as to enhance the sediment transport capacity of the flow and thus convey the coarser sediments provided by the tributary. The development of the bank-attached bar, the scour hole, and the steep bed slope of the tributary were evidences of this morphological evolution. In the experiments performed with uniform sediments (set III), the dunes observed in both flumes at equilibrium revealed a relative excess of transport capacity (Dey, 2014), which led to attenuated morphological features that were masked by the migrating dunes. The differences in bed morphology were reflected in the water surface. In the experimental set II, the water surface exhibited an abrupt change of slope from upstream to downstream of the confluence, revealing a high velocity gradient. In the experimental set III only minor changes were observed in the slope of the water surface (cf. Figures 6.1, 6.3, and 6.5), indicating a smoother flow acceleration.

The high gradation coefficient of the tributary sediments supplied in the experimental set II resulted in an armored bed which inhibited the formation of bedforms (Chiew, 1991). On the contrary, the uniform sediments supplied for the experimental set III led to the formation of bedforms in the tributary and main channel. These bedforms were dunes, agreeing with the bedform predictors of van Rijn (1984) and Yalin (1992). The length of these dunes differed from what is proposed by them ($\lambda \approx 2\pi y$ and $\lambda \approx 7.3y$ respectively), being shorter upstream of the confluence $1.25\, y_d < \lambda < 3.5\, y_d$) and longer downstream ($5\, y_d < \lambda < 12.5\, y_d$). In addition, the length of the dunes downstream of the confluence was larger at the outer bank than at the inner. Similar streamwise and lateral increases in the length of the dunes were reported by Rosier *et al.* (2011) in a straight sand-bedded channel with lateral water withdrawal. Such increases were attributed to the augmented shear stress, associated with flow acceleration. The augmented shear stress contributed to a flattening of the dunes. Similarly, in this study the streamwise increase in the length of the dunes may be attributed to the increased shear stress, due to the overall flow acceleration experienced

downstream of the confluence. The lateral increase may be justified by the acceleration experienced by the flow deflected to the outer bank, much greater than that of the inner. Moreover, for the intermediate and high discharge ratios with uniform sediments, the tributary inflow induced a meandering flow in the main channel downstream of the confluence (Figure 6.2) similar to that reported by Rosier *et al.* (2011).

6.5 Conclusions

The effects of the sediment gradation coefficient (σ) on the bed morphology and hydrodynamics of open-channel confluences were analyzed and discussed, based on the results of six laboratory experiments.

With non-uniform sediments (high σ), the confluence morphodynamics evolved until the sediment transport capacity necessary to transport the wide range of particle sizes was attained. This evolution resulted in a bed morphology characterized by a high topographic gradient with a large bank-attached bar, a deep scour hole at the outer bank of the main channel, and a steep and armored tributary bed that notably penetrated into the main channel. Also, the high value of σ promoted bed armoring, which inhibited the formation of bedforms.

The lack of coarse particles in the uniform sediment mixture (low σ) facilitated the transport of the imposed sediment load. This resulted in a bed morphology with an attenuated bank-attached bar and scour hole, a flatter bed slope in the tributary and a slight penetration of the tributary-mouth bar into the main channel. Also, the migrating dunes observed in both channels masked the typical morphological features of the confluence.

With uniform sediments, the flow acceleration downstream of the confluence and that experienced by the flow deflected to the outer bank of the main channel increased the available shear stress. This augmented shear stress increased the length of the dunes in the streamwise direction and laterally.

7

Influence of the width ratio on the confluence morphodynamics

In this chapter, the influence of the ratio between the tributary and main channel widths (B_t/B_m) on the confluence morphodynamics is analyzed. The results of six experiments, in which three unit-discharge ratios were tested (q_r = 0.37, 0.50 and 0.77) with two different width ratios (B_t/B_m = 0.30 and 0.15) are presented and discussed herein. These experiments were conducted in the experimental facility located at IST-UL. This confluence was composed of a 0.15 m wide tributary that joined with a 0.50 or 1.00 m wide main channel at an angle of α = 70º. The experiments were performed under movable bed conditions with continuous sediment supply to both flumes during the experiments. The sediment consisted of a 0.4 – 2.0 mm uniform sand (σ = 1.35), which was supplied at a constant rate of Q_{st} = 0.50 kg/min for the tributary, whereas for the main channel the rates were Q_{sm} = 0.30 kg/min with B_t/B_m = 0.30 and Q_{sm} = 0.60 kg/min with B_t/B_m = 0.15. Bed topography and water surface surveys were measured after reaching equilibrium. These measurements confirm the role of the width ratio as an influence on confluence morphodynamics. Namely, with B_t/B_m = 0.15 the size of the bank attached bar and the depth of the scour hole at the tributary mouth were increased when compared to the same unit-discharge ratio but with B_t/B_m = 0.30. Also, incipient meandering patterns were observed with B_t/B_m = 0.30 but not with B_t/B_m = 0.15.

Keywords: Open-channel confluences, width ratio, momentum-flux ratio, bed morphology, uniform sediments

7.1 Introduction

The ratio of tributary to main channel width (B_t /B_m) has been identified as an influence on the morphodynamics of open-channel confluences (Benda *et al.*, 2004; Bejestan and Hemmati, 2008; Gutierrez *et al.*, 2014). Nevertheless, few studies have examined the influence of the width ratio on the confluence morphodynamics by means of systematic laboratory experiments, in which the effects of the width ratio can be isolated from those produced by other factors.

The aim of this chapter is to analyze the influence of the width ratio on the morphodynamics of an open-channel confluence. For that purpose, six experiments were conducted in a laboratory confluence, in which three unit-discharge ratios were tested with two different width ratios. The experiments were performed under movable bed conditions and with continuous sediment supply to both flumes. The results show the differences in bed morphology at equilibrium for the distinct unit-discharge and width ratios.

7.2 Experimental setup

The results presented herein correspond to the experimental sets III and IV, carried out in the experimental facility of the IST-UL. The experimental setups are summarized in Table 7.1 and described in detail in Chapter 3.

Table 7.1. Overview of the experimental setup

Experimental set	α [°]	B_t/B_m [-]	σ [-]	q_r [-]	Q_{sm} [Kg/min]	Q_{st} [Kg/min]	Measurements
Set III	70°	0.30	1.35	0.37 (LR) 0.50 (IR) 0.77 (HR)	0.3	0.5	Bed topo at equilibrium W. surf. at equilibrium
Set IV	70°	0.15	1.35	0.37 (LR) 0.50 (IR) 0.77 (HR)	0.6	0.5	Bed topo at equilibrium W. surf. at equilibrium

7.3 Results

The bed topography at equilibrium of each discharge ratio with $B_t/B_m = 0.30$ and 0.15 is shown in Figures 7.1 and 7.2, respectively. Qualitatively, the experiments presented similar bed morphology composed of: i) a bank-attached bar at the inner bank of the main channel, downstream of the confluence; ii) a scour hole which extended from the tributary mouth to the outer bank of the main channel, flanking the bar; iii) a marked bed discordance between the tributary and main channel; and iv) migrating dunes on the bed of both confluent channels.
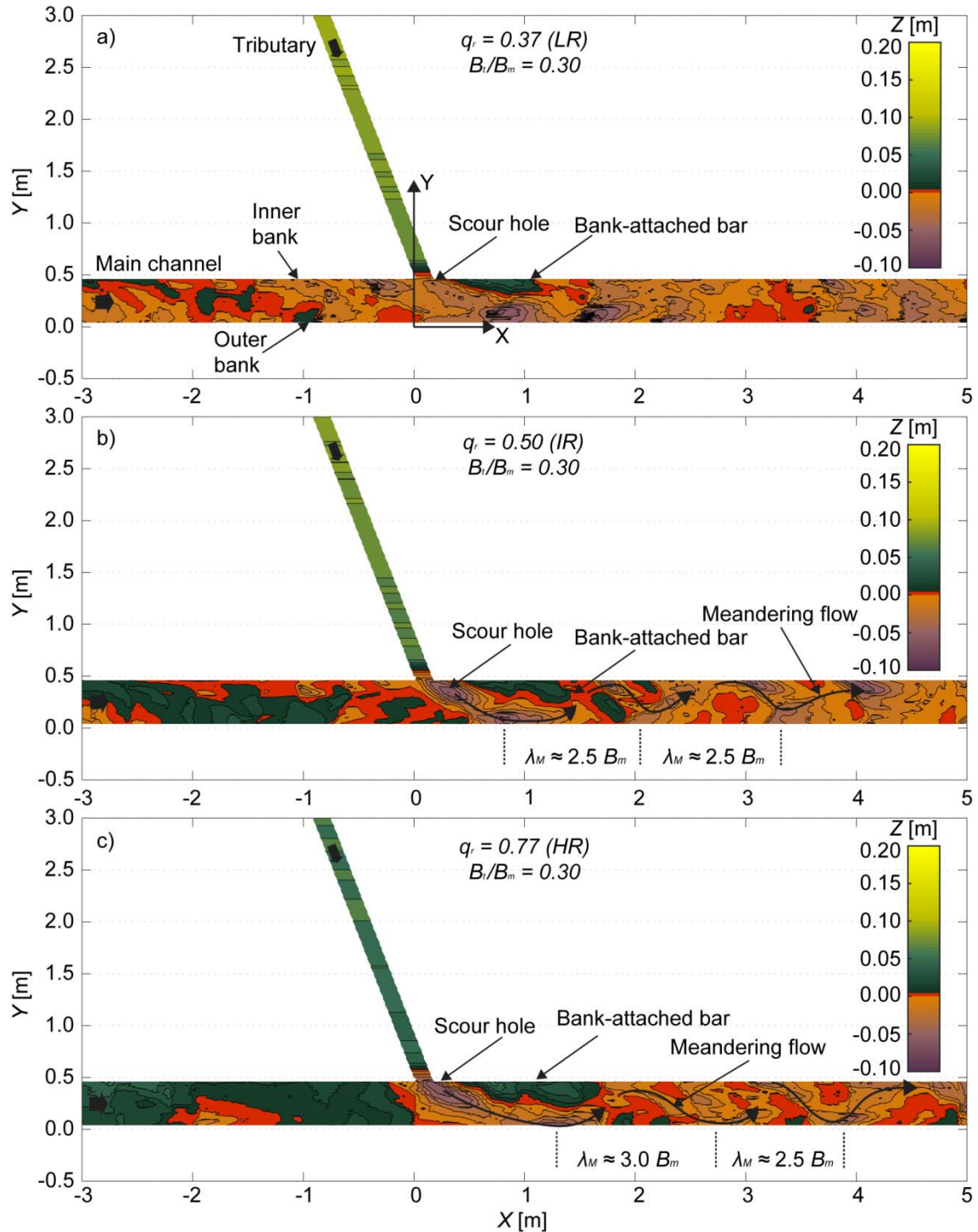
Figure 7.1 Bed topography at equilibrium with $B_t/B_m = 0.30$ and a) $q_r = 0.37$ (LR), b) $q_r = 0.50$ (IR), c) $q_r = 0.77$ (HR). The bed-level contours are spaced by $\Delta Z = 0.01$ m.

With $B_t/B_m = 0.30$, increasing discharge ratios resulted in longer, wider and higher bank-attached bars and deeper scour holes at the tributary mouth (cf. Figure 7.1). Furthermore, for $q_r = 0.50$ and 0.77 (IR and HR respectively) the tributary inflow induced meandering flow downstream of the confluence (Figures 7.1b-c). The wavelength of this meandering flow was approximately $\lambda_M \approx 2.5\ B_m$ for $q_r = 0.50$, and slightly larger for $q_r = 0.77$ ($2.5\ B_m < \lambda_M < 3.0\ B_m$). With $B_t/B_m = 0.15$, the depth of the

scour at the tributary mouth also increased with the discharge ratio (cf. Figure 7.2) and the length and width of the bank-attached bar increased from the intermediate to the high discharge ratios. For the $q_r = 0.37$ (LR) the bank-attached bar was longer than for the other unit-discharge ratios (cf. Figure 7.2). With $B_t/B_m = 0.15$, no meandering flow patterns were observed for any of the unit-discharge ratios, which is in contrast with the observations made with $B_t/B_m = 0.30$.
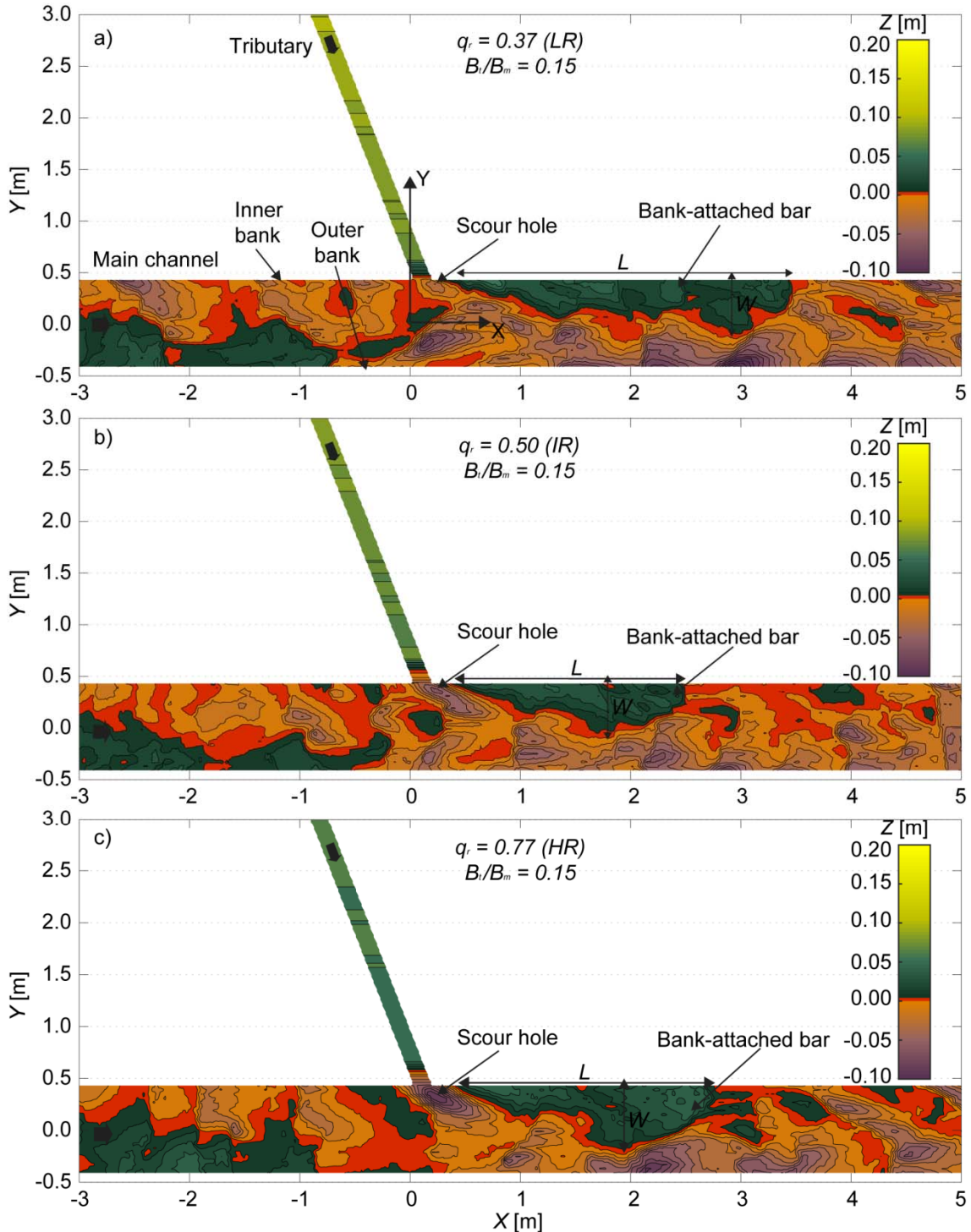
Figure 7.2 Bed topography at equilibrium with bed-level contours spaced by $\Delta Z = 0.01$ m, for $B_t/B_m = 0.15$. a) $q_r = 0.37$ (LR), b) $q_r = 0.50$ (IR), c) $q_r = 0.77$ (HR).

The length (L), width (W) and maximum height (H) of the bank attached bar together with the maximum depth (D) of the scour hole at the tributary mouth are given in Table 7.2 for each experiment. For a given unit-discharge ratio (q_r), the length and width of the bank-attached bar were significantly larger with $B_t/B_m = 0.15$ than with $B_t/B_m = 0.30$. For $q_r = 0.37$ and 0.50 (LR and IR respectively), the depth of the scour hole at the tributary mouth (D in Table 7.2) was similar between both width ratios, whereas for $q_r = 0.77$ (HR) the scour was significantly deeper with $B_t/B_m = 0.15$ than with $B_t/B_m = 0.30$.

Table 7.2 Values of maximum length, width and height of the bank-attached bar and maximum depth of the scour hole at the tributary mouth.

B_t/B_m	q_r	L	W	H	D
[-]	[-]	[m]	[m]	[m]	[m]
	0.37 (LR)	0.85	0.20	0.044	-0.032
0.30	0.50 (IR)	0.98	0.26	0.045	-0.060
	0.77(HR)	1.32	0.30	0.053	-0.064
	0.37 (LR)	3.16	0.59	0.059	-0.030
0.15	0.50 (IR)	2.12	0.55	0.044	-0.062
	0.77(HR)	2.34	0.67	0.049	-0.089

In the tributary, the bed morphology was quite similar with both width ratios. It consisted of a steep slope upstream of the confluence ($Y > 0.75$ m) and an incipient tributary-mouth bar that barely penetrated into the main channel. Migrating dunes were also observed in the tributary bed, for every experiment at equilibrium. The bed elevation and water surface of the tributary at equilibrium associated with both width ratios are depicted in Figure 7.3, for each unit-discharge ratio.

With both width ratios, the slopes of the bed and water surface upstream of the confluence ($Y > 0.75$ m) decreased as the discharge ratio increased. In addition, with both width ratios the bed elevation increased as the discharge ratio increased, reducing the flow depth in the tributary (Figure 7.3). As mentioned above, the depth of the scour hole at the tributary mouth was higher with $B_t/B_m = 0.15$ than with $B_t/B_m = 0.30$ in the case of the high unit-discharge ratio, whereas for the low and intermediate ratios the depth was similar with both width ratios (Figure 7.3). Notice that the depth values observed directly in Figure 7.3 may differ slightly from those shown in Table 7.2 since the maximum-depth points were not aligned with the tributary axis (see Figures 7.1 and 7.2).
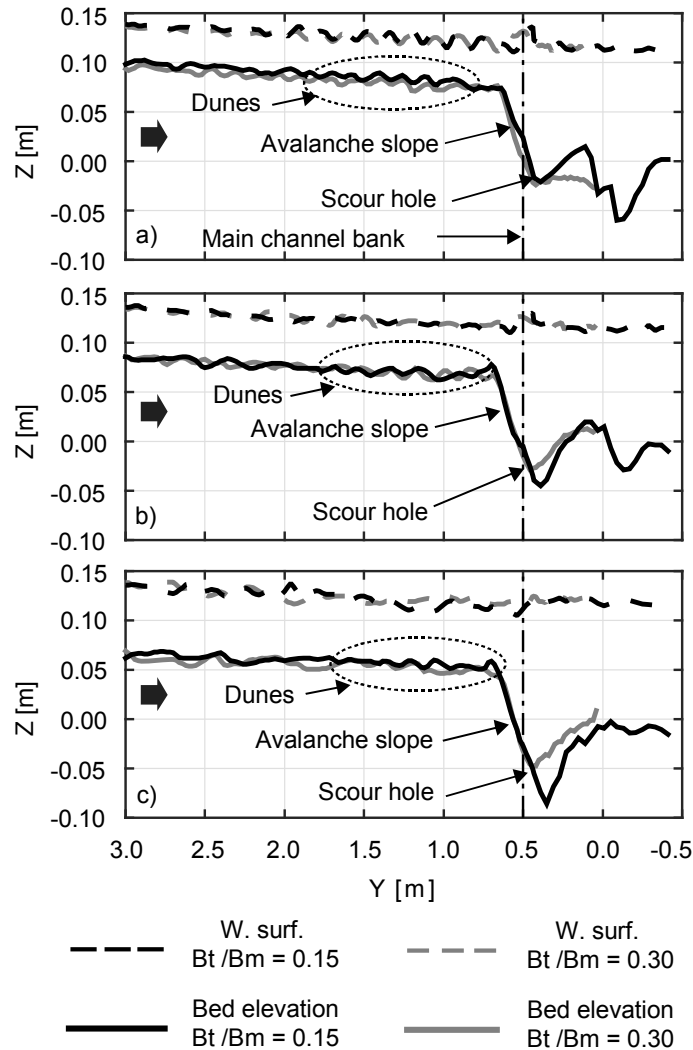
Figure 7.3 Bed elevation and water surface profiles along the tributary axis with both width ratios and for a) $q_r = 0.37$ (LR), b) $q_r = 0.50$ (IR), c) $q_r = 0.77$ (HR).

7.4   Discussion

The bed morphology of each experiment at equilibrium was composed of most of the features described by Best (1988) and Best and Rhoads (2008) and in chapters 4 to 6, i. e. a bank-attached bar, a scour hole and a tributary-mouth bar with an avalanche slope which dipped into the scour hole. The sediment load supplied to the tributary, dominant with respect to that supplied to the main channel, resulted in a marked bed discordance between the tributary and main channel (Leite Ribeiro *et al*., 2012a). The bed discordance influenced the morphodynamics of the confluence by inducing a two-layer flow structure (Biron *et al*., 1993, 1996a; Leite Ribeiro *et al*., 2012a). This consists on a double outward deflection of the main channel flow; one by the tributary inflow affecting the near-surface flow, and the other by the bank-attached bar which affects the near-bed flow. At the confluence, the flow junction produced a strong turbulence that eroded the bed at the tributary mouth, forming a scour hole therein (Best, 1987, 1988; Bristow *et al*., 1993). The higher was the discharge ratio, the

deeper was the erosion at the tributary mouth (Best, 1988 and Chapters 5 and 6). When both deflected flows converged at the outer bank of the main channel, the resultant flow accelerated and eroded the bed extending the scour hole along the outer bank (Rhoads, 2006; Rhoads *et al*., 2009). The depth of the scour at the outer bank was directly related to the size of the bank-attached bar (see Figures 7.1, 7.2, and Chapters 5 and 6).

In concordant confluences the bank-attached bar is typically associated with a zone of flow separation or recirculation at the downstream junction corner (Best, 1987, 1988; Best and Rhoads, 2008). In discordant confluences in which flow recirculation may not occur (Biron *et al*., 1993, 1996a; Boyer *et al*., 2006, and Chapters 4 and 5), the bank-attached bar is rather associated with a zone of reduced flow velocities (Best and Rhoads, 2008). The results shown in this chapter reveal that in general, for increasing discharge ratios the size of the bar increased (Table 7.2), which is in agreement with the results of Best (1988) and Ghobadian and Bajestan (2007). In addition, for a given unit-discharge ratio, the length and width of the bank attached bar were larger with $B_t/B_m = 0.15$ than with $B_t/B_m = 0.30$ (Table 7.2). This pattern indicates that the zone of reduced flow-velocities was larger with $B_t/B_m = 0.15$, with respect to that with $B_t/B_m = 0.30$. Between both width ratios, the size of the bank-attached bar was significantly larger with $B_t/B_m = 0.15$ when compared to $B_t/B_m = 0.30$. This pattern was possibly due to the wider main channel, which with $B_t/B_m = 0.15$ allowed a further development of the zone of reduced flow-velocities, which in turn promoted the deposition. Conversely, with $B_t/B_m = 0.30$ the flow was confined in the narrower main channel, increasing the flow velocity and reducing the deposition at the inner bank of the main channel.

The erosion at the tributary mouth is associated with the local flow structure resulting from the flow junction. This erosion was more pronounced with $B_t/B_m = 0.15$ when compared to $B_t/B_m = 0.30$, and the differences in depth increased for increasing unit-discharge ratios (Figure 7.3 and Table 7.2). These results are consistent with those of Bejestan and Hemmati (2008) based on experiments in discordant confluences, who also reported deeper scour holes for decreasing width ratios. To analyze these patterns, the momentum-flux ratio (M_r) and the unit momentum-flux ratio (m_r) were calculated as follows:

$$M_r = M_t/M_m = \frac{\rho\, Q_t U_t}{\rho\, Q_m U_m} \tag{7.1}$$

$$m_r = m_t/m_m = \frac{\rho\, Q_t U_t B_m}{\rho\, Q_m U_m B_t} \tag{7.2}$$

where Q and U denote the flow discharge and the mean flow velocity upstream of the confluence respectively, q stands for the unit-flow discharge upstream of the confluence, and the sub-indexes t and m refer to the tributary and main channel respectively.

Table 7.3 contains the values of the flow discharge, average flow depth, mean flow velocity, momentum-flux and unit momentum-flux measured in the main channel and tributary upstream of the confluence. Also, the momentum-flux ratio and the unit momentum-flux ratio of each experiment are given in Table 7.3.

Table 7.3 Values of the main hydraulic variables of the main channel and tributary, measured upstream of the confluence.

B_t/B_m	q_r	Q_m	y_m	U_m	M_m	m_m	Q_t	y_t	U_t	M_t	m_t	M_r	m_r
[-]	[-]	[l/s]	[m]	[m/s]	[N]	[N/m]	[l/s]	[m]	[m/s]	[N]	[N/m]	[-]	[-]
	0.37 (LR)	27.0	0.107	0.50	13.63	27.25	3.0	0.044	0.45	1.36	9.09	**0.10**	**0.33**
0.30	0.50 (IR)	26.1	0.105	0.50	12.98	25.95	3.9	0.050	0.52	2.03	13.52	**0.16**	**0.52**
	0.77 (HR)	24.4	0.104	0.47	11.45	22.90	5.6	0.069	0.54	3.03	20.20	**0.26**	**0.88**
	0.37 (LR)	54.0	0.116	0.47	25.16	25.16	3.0	0.041	0.49	1.48	9.88	**0.06**	**0.39**
0.15	0.50 (IR)	52.2	0.116	0.45	23.53	23.53	3.9	0.049	0.53	2.05	13.68	**0.09**	**0.58**
	0.77 (HR)	48.8	0.116	0.42	20.58	20.58	5.6	0.065	0.57	3.20	21.31	**0.16**	**1.04**

Table 7.3 shows that for all the unit-discharge ratios (q_r), the momentum flux ratio (M_r) was higher with $B_t/B_m = 0.30$ than with $B_t/B_m = 0.15$. The decrease in the width ratio (B_t/B_m) from 0.30 to 0.15 resulted in higher unit momentum-flux ratio (m_r) for each discharge scenario. These higher unit momentum-flux ratios observed for $B_t/B_m = 0.15$ may be related to the deeper scour holes that occurred at the tributary mouth for $B_t/B_m = 0.15$, compared to those occurred for $B_t/B_m = 0.30$.

The incipient meandering flow observed with $B_t/B_m = 0.30$ but not with $B_t/B_m = 0.15$, is in good agreement with the statement of Gutierrez *et al.* (2014), according to which increasing width ratios are associated with instabilities in the planimetric configuration.

7.5 Conclusions

The influence of the width ratio on the confluence morphodynamics was analyzed by means of six laboratory experiments, in which three unit-discharge ratios were tested with two different width ratios.

With $B_t/B_m = 0.15$, the wider main channel promoted a larger bank attached bar probably due to a more developed zone of reduced flow velocities at the downstream junction corner. With $B_t/B_m = 0.30$, the narrower main channel constrained the flow which accelerated, reducing the deposition at the downstream junction corner and thus, the size of the bank-attached bar. The deeper scour holes observed with $B_t/B_m = 0.15$ with respect to $B_t/B_m = 0.30$ correlate with the values of the unit momentum-flux ratio, which were also higher with $B_t/B_m = 0.15$ than with $B_t/B_m = 0.30$.

The higher width ratio ($B_t/B_m = 0.30$) promoted the formation of meandering flow induced by the tributary inflow in the post-confluence channel, whereas with the lower width ratio ($B_t/B_m = 0.15$) no meandering patterns were observed.

8

Conclusions and recommendations

The present research concerns the hydro-morphodynamics of mountain river confluences and it is based on experimental data obtained with systematic laboratory experiments. This research study builds on the previous work of Leite Ribeiro (2011), inspired in confluences of mountain rivers such as those of the Upper-Rhone river basin. The goal is to widen the sparse knowledge of the hydrodynamic, morphological and sedimentary processes involved in this type of river confluence. The results presented herein contribute to a better understanding of these processes.

The experiment by Leite Ribeiro (2011) provided valuable insights on the influence of the discharge ratio and the local tributary widening on the dynamics of high-mountain river confluences. These insights are now complemented with the assessment of factors such as sediment supply in the main channel, discharge ratio, junction angle, sediment gradation and width ratio, and their influence on the confluence dynamics.

This investigation constitutes indeed a novelty in the study of the dynamics of open-channel confluences since:

- It focuses on a particular type of confluence that, with the exception of Leite Ribeiro (2011), none studied previously through systematic laboratory experiments.

- It approaches the natural sediment dynamics by considering sediment feeding in both the tributary and main channel.

- It assesses a wide range of parameters as potential controls of the confluence dynamics.

8.1   General

Mountain river confluences are characterized by narrow and steep tributaries that provide important sediment load to the confluence, whereas the main channel supplies the dominant flow discharge. This means that the unit sediment load provided by the tributaries is proportionately higher, given the low discharge ratio ($Q_r < 1$), than the sediment load provided by the main river. In these confluences, the sediment is composed of poorly sorted sand-gravel mixtures with high gradation. The present research revealed that, despite the differences caused by the variation of the physical parameters, common characteristics were found in this type of confluence. In this type of confluence, the bed morphology at equilibrium consisted of:

- A bank-attached bar along the inner bank of the main channel downstream of the confluence. This bar was mostly composed of the tributary sediments.

- A scour hole which extended from the tributary mouth to the outer bank of the main channel, flanking the bar.

- A tributary-mouth bar which imposed a marked bed discordance between the tributary and main channel. This discordance was a consequence of the dominant sediment load provided by the tributary.

- The high sediment load in the tributary yielded a steep bed slope upstream of the confluence. The tributary adopted such a slope to be capable to convey the high sediment load with the low flow discharge.

In terms of hydrodynamics, the following features were common in all the experiments:

- A M1-type backwater curve induced by the tributary inflow in the main channel upstream of the confluence.

- A stagnation zone in the vicinity of the upstream junction corner, characterized by a local increase of the water surface and eventual deposition at the inner bank of the main channel upstream of the confluence.

- A flow deflection zone where both confluent flows become aligned with the post-confluence channel. The tributary flow was deflected by the main stream. In the case of the main channel, the near-surface flow was deflected outward by the tributary inflow, whereas the near-bed flow was protected by the bed discordance. When the near-bed flow reached the bank-attached bar, it steered the flow toward the outer bank.

- A zone of reduced flow-velocity at the downstream junction corner, caused by the abrupt change of direction of the tributary flow.

- Flow-upwelling associated with a low pressure zone at the downstream junction corner.

- A shear layer which separated the tributary flow from the outward deflected main channel flow.

- An acceleration zone downstream of the confluence, where the flow accelerated due to, on the one side, the reduction of the effective flow section caused by the bank-attached bar and, on the other side, the flow concentration at the outer bank because of the flow deflection.

- A recovery zone, where the flow tended to uniform conditions by adopting a nearly constant flow-depth.

- Eventually, the steep bed slope and high sediment load of the tributary resulted in supercritical flow (Fr > 1), which yielded a hydraulic jump at the tributary mouth.

  The bed surface was characterized by:

- A clear segregation between the sediment originating from the tributary and main channel. The tributary sediments remained at the inner half of the post-confluence channel, forming the bank-attached bar. The sediments provided by the main channel remained at the outer bank flanking the bar.

- The existence of three corridors: i) on top of the bar at the inner bank of the main channel for the finer tributary sediments; ii) along the lateral slope of the bank-attached bar for the coarser tributary sediments; and iii) along the outer bank of the main channel for the sediments provided by the main channel.

- Armoring of the tributary bed and lateral slope of the bank-attached bar.

The continuous supply of sediments to the main channel inhibited the armoring of the bed and may have been contributed to erosion. On the contrary, the absence of sediment discharge in the main channel promoted the bed armoring, making the bed less erodible.

8.2   Influence of discharge ratio

In this research study three discharge ratios were tested in each of the four experimental sets. The influence of the discharge ratio on the confluence dynamics can be summarized through the following conclusions:

- Increasing discharge ratios amplified the intensity of the flow resulting from the junction, producing deeper scour at the tributary mouth.

- In the experiments performed with non-uniform sediments, the size of the bank-attached bar decreased as the discharge ratio increased. Conversely, with uniform sediments, the bank-attached bar was larger as the discharge ratio increased.

- The distance to where the flow became uniform downstream of the confluence increased with the discharge ratio.

- The sediment transport capacity of the tributary increased with the discharge ratio. Therefore, increasing discharge ratios resulted in lower bed slope and higher flow depth in the tributary upstream of the confluence.

- The energy loss induced in the main channel by the tributary inflow increased with the discharge ratio.

- The geomorphic work of the flow resulting from the confluence increased also with the discharge ratio.

8.3   Influence of the junction angle

Two junction angles were compared in this thesis $\alpha = 90°$ and $\alpha = 70°$. The results showed that both the bed morphology and hydrodynamics of the confluence are highly influenced by the junction angle. The main conclusions are listed below:

- The lower angle ($\alpha = 70°$) corresponds to a better alignment between both confluent streams, with respect to $\alpha = 90°$. This better alignment facilitated the penetration of the tributary-mouth bar into the main channel, which in turn eased the delivery of the tributary sediment load to the main stream. The further penetration of the tributary-mouth bar with $\alpha = 70°$ reduced the erosion at the tributary mouth and enlarged the bank-attached bar with respect to $\alpha = 90°$.

- With $\alpha = 70°$ the larger bank-attached bar reinforced the topographic outward flow deflection with respect to $\alpha = 90°$. This resulted in larger scour holes along the outer bank of the main channel, compared to those observed with $\alpha = 90°$.

- In the tributary, the bed elevation was lower with $\alpha = 70°$ than with $\alpha = 90°$, which resulted in higher flow depths with $\alpha = 70°$ than with $\alpha = 90°$. With $\alpha = 90°$, the steep bed slope together with the lower flow depth resulted in supercritical or critical flow regimes in the tributary, depending on the discharge ratio. In contrast, with $\alpha = 70°$ the higher flow depth led to a subcritical flow regime, in spite of the steep bed slope.

- With $\alpha = 90°$, the hydraulic jump formed at the tributary mouth when the tributary flow regime was supercritical, reduced the flow velocity of the tributary before it entered the main channel. This "weaker" tributary inflow induced an energy loss in the main channel lower than that induced for the equivalent discharge ratio but with $\alpha = 70°$.

- Since the flow regime in the main channel was subcritical, the greater energy loss induced by the tributary in the main channel with $\alpha = 70°$ resulted in higher flow depths in the main channel upstream of the confluence, compared to those measured with $\alpha = 90°$.

8.4 Influence of sediment gradation

The influence of the sediment gradation on the confluence dynamics was analyzed by means of the results of six experiments in which two different sediment mixtures were supplied. One was composed of a non-uniform sand-gravel mixture with high gradation coefficients ($\sigma = 3.15$ and 4.51), and the other consisted of uniform sand with low gradation coefficient ($\sigma = 1.35$). Based on the results of these experiments, the following conclusions can be drawn:

- With non-uniform sediments, the bed morphology was forced to evolve to attain the necessary sediment transport capacity to convey the wide range of particle sizes. This evolution resulted in a bed morphology with a high topographic gradient, i. e., a large bank-attached bar, a deep scour hole and a steep bed slope in the tributary.

- With uniform sediments, the relative excess of sediment transport capacity resulted in a bed morphology with a more attenuated bed morphology when compared with that obtained with non-uniform sediments. Thus, with uniform sediments the bank-attached bar was smaller, the scour hole was less pronounced and the tributary bed slope was flatter with respect to those features obtained with non-uniform sediments.

- The differences in bed morphology were reflected in the water surface that with non-uniform sediments displayed a great change of slope from the upstream part to downstream part of the confluence, whereas with uniform sediments this change was smoother.

- The wide range of particle sizes of the non-uniform mixture promoted the armoring of the bed, which in turn inhibited the formation of bedforms.

- The low gradation of the uniform sediment mixture together with the relative excess of sediment transport resulted in migrating dunes which masked the typical morphological features of a confluence, i.e. the bank-attached bar and the scour hole.

8.5 Influence of the width ratio

Two width ratios were compared in this research study: $B_t/B_m = 0.30$ and $B_t/B_m = 0.15$. With each one of them three unit-discharge ratios were tested, making a total of six experiments. The following conclusions summarize the inferred knowledge about the influence of the width ratio on the confluence morphodynamics:

- A lower width ratio resulted in larger bank-attached bars and deeper scour holes of the bank-attached bar and the depth of the scour hole in the main channel, with respect to a higher width ratio. These morphological variations were related with the variation of unit-momentum flux ratio, which was higher with $B_t/B_m = 0.15$ than with $B_t/B_m = 0.30$.

- A higher width ratio promoted the instability in the planimetric configuration, namely by forming a meandering flow downstream of the confluence.

8.6 Practical recommendations for restoration of river confluences

In this section a few recommendations inferred from the results of the present research are given for potential projects of restoration of river confluences:

- Parameters such as the discharge and momentum-flux ratios, the junction angle, the sediment transport rates in each channel, the sediment gradation, and the width ratio are parameters that should be considered for each case of study.

- Concerning the sediment transport rates in each channel, the suppression or reduction of the sediment transport rate in any of the confluent channels may result in bed armoring. Conversely, the existence of sediment transport in both channels may inhibit the armoring of the bed, facilitating to the bed erosion.

- Concerning flood safety, a reduction of the junction angle may result in higher head losses in the confluence and higher water levels in both channels upstream of the confluence.

- Concerning bed morphology, low sediment gradation may promote the formation of bedforms and attenuate the depth of the scour hole and the size of the bank-attached bar. In addition, a reduction of the width ratio may result in larger bank-attached bars and deeper scour holes. An increase of the width ratio may induce meandering flow downstream of the confluence.

8.7 Recommendations for future research

The present investigation is inherently limited to a relatively small number of configurations that partially covers the broad range of influent factors on the dynamics of river confluences. The experiments presented herein were conducted under laboratory conditions and the results only refer to steady flow discharges and to an unique and constant sediment rate for each flume. Nevertheless, this research study contributes to widen the current knowledge on the hydraulic, morphological and sedimentary processes of river confluences. To deepen the knowledge about the dynamics of this type of confluence, the following topics are proposed for future laboratory investigations:

- Systematic laboratory experiments with sediment rates that vary with respect to the sediment transport capacity may be conducted to study the influence of this parameter on the confluence morphodynamics, and especially on the bed discordance.

- Other configurations in terms of discharge ratio, junction angle, sediment gradation and width ratio would be useful to enlarge the existing experimental database.

- Experiments with variable flow discharges and sediment rates would represent better the conditions observed in nature during flood events.

- The detailed characterization of the three dimensional velocity field of the confluence would provide very valuable insights on the turbulence involved in the confluence dynamics.

Most of the existent knowledge about dynamics of river confluences comes from the study of two low-land river confluences. Unfortunately, these confluences are not appropriate to validate the experimental data presented herein, since for example, they cover a different range of discharge and momentum ratios, width ratios, sediment gradation and rates and junction angles. For that reason, field measurements in high-mountain river confluences with low discharge and momentum ratios, high junction angles and with dominant tributary supply of poorly sorted sediments will contribute significantly to the validation of the experimental data. A first step could be the monitoring of variables such as flow discharge, sediment rates, bed topography, water surface topography.

Finally, the study of the dynamic processes involved in the confluence through numerical simulation constitutes a quite challenging and interesting topic, which would provide an excellent tool for predicting the evolution of the confluence dynamics under any variation of the governing parameters.

Bibliography

Ashmore, P. E. (1982). Laboratory modelling of gravel braided stream morphology. *Earth Surface Processes and Landforms*, *7*(3), 201–225. doi:10.1002/esp.3290070301

Ashmore, P. E., Ferguson, R. I., Prestegaard, K. L., Ashworth, P. J., and Paola, C. (1992). Secondary flow in anabranch confluences of a braided, gravel-bed stream. *Earth Surf. Process. Landforms*, *17*(3), 299–311. doi:10.1002/esp.3290170308

Ashmore, P., and Parker, G. (1983). Confluence scour in coarse braided streams. *Water Resources Research*, *19*(2), 392–402. doi:10.1029/WR019i002p00392

Baranya, S., and Józsa, J. (2007). Numerical and laboratory investigation of the hydrodynamic complexity of a river confluence. *Periodica Polytechnica Civil Engineering*, *51*(1), 3. doi:10.3311/pp.ci.2007-1.01

Bejestan, M. S., and Hemmati, M. (2008). Scour depth at river confluence of unequal bed level. *Journal of Applied Sciences*, *8*(9), 1766–1770. doi:10.3923/jas.2008.1766.1770

Benda, L., Andras, K., Miller, D., and Bigelow, P. (2004). Confluence effects in rivers: Interactions of basin scale, network geometry, and disturbance regimes. *Water Resources Research*, *40*(5). doi:10.1029/2003WR002583

Bernhardt, E. S., Palmer, M. A., Allan, J. D., Alexander, G., Barnas, K., Brooks, S., … Sudduth, E. (2005). Ecology. Synthesizing U.S. river restoration efforts. *Science (New York, N.Y.)*, *308*(5722), 636–637. doi:10.1126/science.1109769

Best, J. L. (1987). Flow dynamics at river channel confluences: Implications for sediment transport and bed morphology. In F. G. Ethridge, R. M. Flores, & M. D. Harvey (Eds.), *Recent Developments in Fluvial Sedimentology* (pp. 27–35). SEPM (Society for Sedimentary Geology). doi:10.2110/pec.87.39.0027

Best, J. L. (1988). Sediment transport and bed morphology at river channel confluences. *Sedimentology*, *35*(3), 481–498. doi:10.1111/j.1365-3091.1988.tb00999.x

Best, J. L., and Reid, I. (1984). Separation Zone at Open-Channel Junctions. *Journal of Hydraulic Engineering*, *110*(11), 1588–1594. doi:10.1061/(ASCE)0733-9429(1984)110:11(1588)

Best, J. L., and Rhoads, B. L. (2008). Sediment transport, bed morphology and the sedimentology of river channel confluences. In S. P. Rice, A. G. Roy, & B. L.

Rhoads (Eds.), *River Confluences, Tributaries and the Fluvial Network* (pp. 45–72). Chichester, UK: John Wiley & Sons, Ltd. doi:10.1002/9780470760383.ch4

Best, J. L., and Roy, A. G. (1991). Mixing-layer distortion at the confluence of channels of different depth. *Nature*, *350*(6317), 411–413. doi:10.1038/350411a0

Biron, P. M., Best, J. L., and Roy, A. G. (1996a). Effects of Bed Discordance on Flow Dynamics at Open Channel Confluences. *Journal of Hydraulic Engineering*. doi:10.1061/(ASCE)0733-9429(1996)122:12(676)

Biron, P. M., and Lane, S. N. (2008). Modelling hydraulics and sediment transport at river confluences. In S. P. Rice, A. G. Roy, & B. L. Rhoads (Eds.), *River Confluences, Tributaries and the Fluvial Network* (pp. 17–43). John Wiley & Sons, Ltd.

Biron, P. M., Ramamurthy, A. S., and Han, S. (2004). Three-Dimensional Numerical Modeling of Mixing at River Confluences. *Journal of Hydraulic Engineering*, *130*(3), 243–253. doi:10.1061/(ASCE)0733-9429(2004)130:3(243)

Biron, P. M., Richer, A., Kirkbride, A. D., Roy, A. G., and Han, S. (2002). Spatial patterns of water surface topography at a river confluence. *Earth Surface Processes and Landforms*, *27*(9), 913–928. doi:10.1002/esp.359

Biron, P. M., Roy, A. G., and Best, J. L. (1996b). Turbulent flow structure at concordant and discordant open-channel confluences. *Experiments in Fluids*. doi:10.1007/BF00189046

Biron, P. M., Roy, A. G., Best, J. L., and Boyer, C. J. (1993). Bed morphology and sedimentology at the confluence of unequal depth channels. *Geomorphology*, *8*(2-3), 115–129. doi:10.1016/0169-555X(93)90032-W

Boyer, C., Roy, A. G., and Best, J. L. (2006). Dynamics of a river channel confluence with discordant beds: Flow turbulence, bed load sediment transport, and bed morphology. *Journal of Geophysical Research: Earth Surface*, *111*(F4), F04007. doi:10.1029/2005JF000458

Bradbrook, K. F., Biron, P. M., Lane, S. N., Richards, K. S., and Roy, A. G. (1998). Investigation of controls on secondary circulation in a simple confluence geometry using a three-dimensional numerical model. *Hydrological Processes*, *12*(8), 1371–1396. doi:10.1002/(SICI)1099-1085(19980630)12:8<1371::AID-HYP620>3.0.CO;2-C

Bradbrook, K. F., Lane, S. N., and Richards, K. S. (2000). Numerical simulation of three-dimensional, time-averaged flow structure at river channel confluences. *Water Resources Research*, *36*(9), 2731. doi:10.1029/2000WR900011

Bradbrook, K. F., Lane, S. N., Richards, K. S., Biron, P. M., and Roy, A. G. (2001, May). Role of Bed Discordance at Asymmetrical River Confluences. *Journal of Hydraulic Engineering*. doi:10.1061/(ASCE)0733-9429(2001)127:5(351)

Bristow, C. S., Best, J. L., and Roy, A. G. (1993). Morphology and facies models of channel confluences. In M. Marzo & C. Puigdefábregas (Eds.), *Alluvial Sedimentation* (pp. 91–100). Ltd, Oxford, Uk. doi:10.1002/9781444303995.ch8

Chiew, Y. M. (1991). Bed Features in Nonuniform Sediments. *Journal of Hydraulic Engineering, 117*(1), 116–120. doi:10.1061/(ASCE)0733-9429(1991)117:1(116)

Chow, V. Te. (1959). *Open-Channel Hydraulics*. New York: McGraw-Hill Book Company,Inc.

D'Oria, M., and Tanda, G. M. (2006). Physical and Numerical Modeling of a River Confluence Reshaping. In *Proceeding of 32nd Congress of IAHR, Venice*. Retrieved from http://hdl.handle.net/11381/2437096

De Serres, B., Roy, A. G., Biron, P. M., and Best, J. L. (1999). Three-dimensional structure of flow at a confluence of river channels with discordant beds. *Geomorphology, 26*(4), 313–335. doi:10.1016/S0169-555X(98)00064-6

Devauchelle, O., Petroff, A. P., Seybold, H. F., and Rothman, D. H. (2012). Ramification of stream networks. *Proceedings of the National Academy of Sciences of the United States of America, 109*(51), 20832–20836. doi:10.1073/pnas.1215218109

Duan, J. G., and Schwar, M. T. (2003). Modeling of Flow and Sediment Transport at a River Confluence with the EnSed2D Model. In *World Water and Environmental Resources Congress 2003* (pp. 1–10). doi:10.1061/40685(2003)170

Ghobadian, R., and Bejestan, M. S. (2007). Investigation of Sediment Patterns at River Confluence. *Journal of Applied Sciences, 7*(10), 1372–1380. doi:10.3923/jas.2007.1372.1380

Ghostine, R., Mose, R., Vazquez, J., Ghenaim, A., and Grégoire, C. (2010). Two-Dimensional Simulation of Subcritical Flow at a Combining Junction: Luxury or Necessity? *Journal of Hydraulic Engineering*. doi:10.1061/(ASCE)HY.1943-7900.0000230

Guillén-Ludeña, S., Franca, M. J., Cardoso, A. H., and Schleiss, A. J. (2015). Hydro-morphodynamic evolution in a 90° movable bed discordant confluence with low discharge ratio. *Earth Surface Processes and Landforms*, n/a–n/a. doi:10.1002/esp.3770

Gutierrez, R. R., Abad, J. D., Choi, M., and Montoro, H. (2014). Characterization of confluences in free meandering rivers of the Amazon basin. *Geomorphology*, *220*, 1–14. doi:10.1016/j.geomorph.2014.05.011

Hager, W. H. (1989). Transitional Flow in Channel Junctions. *Journal of Hydraulic Engineering*, *115*(2), 243–259. doi:10.1061/(ASCE)0733-9429(1989)115:2(243)

Havinga, H., Jagers, H. R. A., and Sloff, C. J. (2005). Knowledge requirements for sustainable fairway management. In *Proceedings RCEM 2005, Oct 4-7, Urbana, Illinois, USA* (p. 10). doi:10.1201/9781439833896.ch127

Hsu, C.-C., Lee, W.-J., and Chang, C.-H. (1998a). Subcritical Open-Channel Junction Flow. *Journal of Hydraulic Engineering*. doi:10.1061/(ASCE)0733-9429(1998)124:8(847)

Hsu, C.-C., Wu, F.-S., and Lee, W.-J. (1998b). Flow at 90° Equal-Width Open-Channel Junction. *Journal of Hydraulic Engineering*. doi:10.1061/(ASCE)0733-9429(1998)124:2(186)

Huang, J., Weber, L. J., and Lai, Y. G. (2002). Three-Dimensional Numerical Study of Flows in Open-Channel Junctions. *Journal of Hydraulic Engineering*, *128*(3), 268–280. doi:10.1061/(ASCE)0733-9429(2002)128:3(268)

Kantoush, S. A., Bollaert, E., Cesare, G. D. E., Boillat, J., and Schleiss, A. J. (2008). Flow field investigation in a rectangular shallow reservoir using UVP, LSPIV and numerical model. *Flow Measurement and Instrumentation*, *19*, 129–133.

Kennedy, B. A. (1984). On Playfair's law of accordant junctions. *Earth Surface Processes and Landforms*, *9*(2), 153–173. doi:10.1002/esp.3290090207

Khan, A. A., Cadavid, R., and Wang, S. S.-Y. (2000). Simulation of channel confluence and bifurcation using the CCHE2D model. *Proceedings of the ICE - Water and Maritime Engineering*. doi:10.1680/wame.2000.142.2.97

Lane, S. N., Bradbrook, K. F., Richards, K. S., Biron, P. a., and Roy, A. G. (1999a). The application of computational fluid dynamics to natural river channels: three-dimensional versus two-dimensional approaches. *Geomorphology*, *29*(1-2), 1–20. doi:10.1016/S0169-555X(99)00003-3

Lane, S. N., Bradbrook, K. F., Richards, K. S., Biron, P. M., and Roy, a. G. (1999b). Time-averaged flow structure in the central region of a stream confluence: A discussion. *Earth Surface Processes and Landforms*, *24*(4), 361–367. doi:10.1002/(SICI)1096-9837(199904)24:4<361::AID-ESP982>3.0.CO;2-5

Lane, S. N., Bradbrook, K. F., Richards, K. S., Biron, P. M., and Roy, A. G. (2000). Secondary circulation cells in river channel confluences: measurement artefacts or coherent flow structures? *Hydrological Processes*, *14*(11-12), 2047–2071. doi:10.1002/1099-1085(20000815/30)14:11/12<2047::AID-HYP54>3.0.CO;2-4

Lane, S. N., and Richards, K. S. (1998). High resolution, two-dimensional spatial modelling of flow processes in a multi-thread channel. *Hydrological Processes*, *12*(8), 1279–1298. doi:10.1002/(SICI)1099-1085(19980630)12:8<1279::AID-HYP615>3.0.CO;2-E

Leclair, S. F., and Roy, A. G. (1997). Variabilité de la morphologie et des structures sédimentaires du lit d'un confluent de cours d'eau discordant en période d'étiage. *Géographie Physique et Quaternaire*, *51*(2), 125–139. doi:10.7202/033114ar

Leite Ribeiro, M. (2011). *Influence of Tributary Widening on Confluence Morphodynamics*. *Ecole Polytechnique Fédérale de Lausanne, Lausanne, Switzerland*. EPFL.

Leite Ribeiro, M., Blanckaert, K., Roy, A. G., and Schleiss, A. J. (2012a). Flow and sediment dynamics in channel confluences. *Journal of Geophysical Research*, *117*(F1), F01035. doi:10.1029/2011JF002171

Leite Ribeiro, M., Blanckaert, K., Roy, A. G., and Schleiss, A. J. (2012b). Hydromorphological implications of local tributary widening for river rehabilitation. *Water Resources Research*, *48*(10), n/a–n/a. doi:10.1029/2011WR011296

Leite Ribeiro, M., Blanckaert, K., and Schleiss, a. J. (2015). Local tributary widening for river rehabilitation. *Ecohydrology*. doi:10.1002/eco.1588

Lin, J. D., and Soong, H. K. (1979). Junction losses in open channel flows. *Water Resources Research*, *15*(2), 414–418. doi:10.1029/WR015i002p00414

Liu, T. huan, Chen, L., and Fan, B. ling. (2012). Experimental study on flow pattern and sediment transportation at a 90° open-channel confluence. *International Journal of Sediment Research*, *27*(2), 178–187. doi:10.1016/S1001-6279(12)60026-2

McLelland, S. J., Ashworth, P. J., and Best, J. L. (1996). The origin and downstream development of coherent flow structures at channel junctions. In P. J. Ashworth, S. J. Bennett, J. L. Best, & S. J. McLelland (Eds.), *Coherent Flow Structures in Open Channels* (pp. 459–490). Wiley & Sons Ltd, Chichester.

Miller, J. P. (1958). High mountain streams; effects of geology of channel characteristics and bed material. *Memoir - New Mexico, Bureau of Mines and*

Mineral Resources, 53. Retrieved from http://search.proquest.com/docview/53085097?accountid=14244

Mosley, M. P. (1976). An experimental study of channel confluences. *Journal of Geology*, *84*(5), 535–562. Retrieved from http://www.jstor.org/stable/30066212

Nakamura, K., Tockner, K., and Amano, K. (2006). River and Wetland Restoration: Lessons from Japan. *BioScience*. doi:10.1641/0006-3568(2006)056[0419:RAWRLF]2.0.CO;2

Parsons, D. R. (2003). Discussion of "Three-Dimensional Numerical Study of Flows in Open-Channel Junctions" by Jianchun Huang, Larry J. Weber, and Yong G. Lai. *Journal of Hydraulic Engineering*. doi:10.1061/(ASCE)0733-9429(2003)129:10(822)

Parsons, D. R., Best, J. L., Lane, S. N., Orfeo, O., Hardy, R. J., and Kostaschuk, R. (2007). Form roughness and the absence of secondary flow in a large confluence-diffluence, Rio Paraná, Argentina. *Earth Surface Processes and Landforms*, *32*(1), 155–162. doi:10.1002/esp.1457

Peter, A. (2006). Rehabilitation – to What Extent , and Why ? *Eawag News*, *61e*(November), 4–8.

Ramamurthy, A. S., Carballada, L. B., and Tran, D. M. (1988). Combining Open Channel Flow at Right Angled Junctions. *Journal of Hydraulic Engineering*, *114*, 1449–1460. doi:10.1061/(ASCE)0733-9429(1988)114:12(1449)

Ramamurthy, A. S., Tran, D. M., and Carballada, L. B. (1994). Increased hydraulic resistance in combining open channel flows. *Water Research*, *28*(6), 1505–1508. doi:10.1016/0043-1354(94)90319-0

Reichert, P., Borsuk, M., Hostmann, M., Schweizer, S., Spörri, C., Tockner, K., and Truffer, B. (2007). Concepts of decision support for river rehabilitation. *Environmental Modelling and Software*, *22*(2), 188–201. doi:10.1016/j.envsoft.2005.07.017

Rezaur, R. B., Jayawardena, A. W., and Hossain, M. M. (1999). Factors affecting confluence scour. In A. W. Jayawardena, J. H. W. Lee, & Z. Y. Wang (Eds.), *River Sedimentation: Theory and Applications* (pp. 187–192). Balkema: Rotherdam.

Rhoads, B. L. (1996). Mean structure of transport-effective flows at an asymmetrical confluence when the main stream is dominant. In P. J. Ashworth, S. J. Bennett, J. L. Best, & S. J. McLelland (Eds.), *Coherent Flow Structures in Open Channels* (pp. 491–517). Chichester, UK: Wiley.

Rhoads, B. L. (2006). Scaling of confluence dynamics in river systems: some general considerations. In G. Parker & M. García (Eds.), *Proceedings of the 4th IAHR Symposium on River, Coastal and Estuarine Morphodynamics (RCEM 2005, Urbana, Illinois, USA, 4-7 October 2005)* (pp. 378–387). London: Taylor & Francis. doi:10.1201/9781439833896

Rhoads, B. L., and Kenworthy, S. T. (1995, March). Flow structure at an asymmetrical stream confluence. *Geomorphology*. doi:10.1016/0169-555X(94)00069-4

Rhoads, B. L., and Kenworthy, S. T. (1998). Time-averaged flow structure in the central region of a stream confluence. *Earth Surface Processes and Landforms*, *23*(2), 171–191. doi:10.1002/(SICI)1096-9837(199802)23:2<171::AID-ESP842>3.0.CO;2-T

Rhoads, B. L., Riley, J. D., and Mayer, D. R. (2009). Response of bed morphology and bed material texture to hydrological conditions at an asymmetrical stream confluence. *Geomorphology*, *109*(3-4), 161–173. doi:10.1016/j.geomorph.2009.02.029

Rhoads, B. L., and Sukhodolov, A. N. (2001). Field investigation of three-dimensional flow structure at stream confluences: 1. Thermal mixing and time-averaged velocities. *Water Resources Research*, *37*(9), 2393–2410. doi:10.1029/2001WR000316

Rhoads, B. L., and Sukhodolov, A. N. (2004). Spatial and temporal structure of shear layer turbulence at a stream confluence. *Water Resources Research*. doi:10.1029/2003WR002811

Rice, S. P., Roy, A. G., and Rhoads, B. L. (2008). *River Confluences, Tributaries and the Fluvial Network*. (S. P. Rice, A. G. Roy, & B. L. Rhoads, Eds.). Chichester, UK: John Wiley & Sons, Ltd.

Riley, J. D., Rhoads, B. L., Parsons, D. R., and Johnson, K. K. (2015). Influence of junction angle on three-dimensional flow structure and bed morphology at confluent meander bends during different hydrological conditions. *Earth Surface Processes and Landforms*, *40*(2), 252–271. doi:10.1002/esp.3624

Roca, M., Martín-Vide, J. P., and Moreta, P. J. M. (2009). Modelling a torrential event in a river confluence. *Journal of Hydrology*, *364*(3-4), 207–215. doi:10.1016/j.jhydrol.2008.10.020

Roy, A., and Bergeron, N. (1990). Flow and particle paths at a natural river confluence with coarse bed material. *Geomorphology*. doi:10.1016/0169-555X(90)90039-S

Rusconi, M. (2012). *Etude morphologique d'une confluence Application à la jonction de la Lizerne et du Rhône*. Master Thesis at École polytechnique fédérale de Lausanne.

Shabayek, S., Steffler, P., and Hicks, F. E. (2002). Dynamic Model for Subcritical Combining Flows in Channel Junctions. *Journal of Hydraulic Engineering, 128*(9), 821–828. doi:10.1061/(ASCE)0733-9429(2002)128:9(821)

Shakibainia, A., Tabatabai, M. R. M., and Zarrati, A. R. (2010). Three-dimensional numerical study of flow structure in channel confluences. *Canadian Journal of Civil Engineering, 37*(5), 772–781. doi:10.1139/L10-016

Shields, A. (1936). Application of similarity principles and turbulence research to bed-load movement. In W. P. Ott & J. C. van Uchelen (Eds.), *Hydrodynamics Laboratory Publ. No. 167*. Berlin: U.S. Dept. of Agr., Soil Conservation Service Cooperative Laboratory, California Institute of Technology, Pasadena, Calif.

Smart, G. M. (1984). Sediment Transport Formula for Steep Channels. *Journal of Hydraulic Engineering, 110*(3), 267–276. doi:10.1061/(ASCE)0733-9429(1984)110:3(267)

Sukhodolov, A. N., and Rhoads, B. L. (2001). Field investigation of three-dimensional flow structure at stream confluences 2. Turbulence. *Water Resources Research, 37*(9), 2411–2424. doi:10.1029/2001WR000317

Taylor, E. H. (1944). Flow characteristics at rectangular open-channel junctions. *American Society of Civil Engineers1, 70*, 119–121.

Van Rijn, L. C. (1984a). Sediment Transport, Part I: Bed Load Transport. *Journal of Hydraulic Engineering, 110*(10), 1431–1456. doi:10.1061/(ASCE)0733-9429(1984)110:10(1431)

Van Rijn, L. C. (1984b). Sediment Transport, Part III: Bed forms and Alluvial Roughness. *Journal of Hydraulic Engineering*. doi:10.1061/(ASCE)0733-9429(1984)110:12(1733)

Webber, N. B., and Greated, C. A. (1966). An investigation of flow behaviour at the junction of rectangular channels. *Proceedings of Institute of Civil Engineers, 34*(3), 321–334. doi:10.1680/iicep.1966.8925

Weber, L. J., Schumate, E. D., and Mawer, N. (2001). Experiments on Flow at a 90° Open-Channel Junction. *Journal of Hydraulic Engineering, 127*(5), 340–350. doi:10.1061/(ASCE)0733-9429(2001)127:5(340)

Wilcock, P. R. (1998). Two-Fraction Model of Initial Sediment Motion in Gravel-Bed Rivers. *Science*, *280*(5362), 410–412. doi:10.1126/science.280.5362.410

Wilcock, P. R., Kenworthy, S. T., and Crowe, J. C. (2001). Experimental study of the transport of mixed sand and gravel. *Water Resources Research*, *37*(12), 3349–3358. doi:10.1029/2001WR000683

Yalin, M. S. (1992). *River mechanics*. Pergamon Press Ltd.

Acknowledgements

I would like to manifest my sincerest thanks and appreciation to Professors Anton J. Schleiss and António H. Cardoso, who trusted in my capacity to perform this research in such a challenging and interesting topic and accepted to guide my work. I want to praise also the great investment in the experimental facility of IST-UL and the compromise of Prof. Cardoso to make everything work. Very especial thanks to Mário J. Franca for the inestimable help and support and for the guidance provided during this PhD. Muito obrigado Mário!.

I would like to thank the members of the Jury for accepting to evaluate the contents of this research. Prof. Ian Smith, thank you so much for accepting to chair the PhD defense. Prof. Ramiro Neves, thank you for agreeing to come from Lisbon to discuss the research. I want to express all my gratitude to Prof. Stuart Lane and Prof. Annunziato Siviglia for accepting to discuss this work.

All my gratitude to Michael Rusconi, Pedro M. Abreu, Nadia Pena and Javier Ludeña Nicolás for helping me during the experiments with great commitment. Prof. Francisco Alegria, thank you very much for your incredibly nice work in the facility of the IST-UL. Especial thanks to Marc-Eric Pantillon, Michel Teucher, Grégory and Stephan who were always willing for the construction, modification and reparation of the confluence. In addition, I want to thank to Dr. Marcelo Leite Ribeiro the advices to improve the facility and the experimental methodology.

During two years, I have had the great opportunity of being a member of the LCH-team, where I met very motivated and responsible people and at the same time fun and friendly. I want to thanks the first LCH generation for the great times we shared together and their contribution to the great atmosphere of the group. This *crew* was composed by Raphaël Sprenger, Violaine Dugué, Mohammad Javad Ostad Mirza, Tamara Ghilardi, Mona-*mie* Jafarnejad, Milad Daneshvari, Elena Battisacco, Rafael Duarte, Stephan Terrier, Michael Müller, and Javier García. Thanks also to the new amazing generation of the LCH formed by Irene Samora, Reyhaneh Sadat, Paloma Furlan, Jessica Zordan, Sabine Chamoun, Sebastian Schwindt, Alex Pachoud, Gaetano Crispino, Davide Würthrich, Nicolas Adam, Severin Stähly, Adamczyk Mikolaj, and Fränz Zeimetz, for maintaining the great atmosphere at the LCH. Thanks to Giovanni De Cesare, Michael Pfister, and Pedro Manso for the good advices and for their availability to discuss many technical issues of this thesis. I could also meet the administrative stuff of the LCH formed by Scarlett Monnin, Caroline Etter and Gesualdo Casciana, thank you very much for your efficiency and your sympathy.

In Lisbon, where I passed the other two years of this PhD, I met also incredibly nice people who really made me enjoy that period in Portugal. They are: Artur Silva,

A1

Experimental set I

In this appendix, graphical representations of the measurements performed in the experimental set I are displayed for every experiment. The following information is shown for each experiment:

- Bed topography at the times $t = 0$ h, $t = 1$ h, $t = 7$ h, and at equilibrium.
- Grain size distribution of the bed surface characterized by four samples obtained from different locations of the confluence.
- Profiles of the bed elevation and water surface measured during the experiment along the inner bank of the main channel, outer bank of the main channel and tributary axis.
- Evolution of the bed elevation measured at the checkpoints P_1 to P_5 (Figure 3.17a) during the experiments to assess the equilibrium condition.
- Outgoing sediment rates measured at the downstream end of the main channel to assess the equilibrium condition during the experiments.
- Value of the point velocity measurements measured at equilibrium at 12 different locations.

The values of the discharge ratio (Q_r), unit-discharge ratio (q_r), junction angle (α), sediment gradation coefficient (σ), and width ratio (B_t/B_m) adopted in each experiment of the experimental set I are given in Table A1.1

Table A1.1. Summary of the main parameters adopted in experimental set I

| Experiment	Q_r [-]	q_r [-]	α [°]	σ [-]	B_t/B_m [-]	Results discussed in chapter
Low discharge ratio (LR)	0.11	0.37	90°	3.15 (main channel) 4.51 (tributary)	0.30	4 - 5
Intermediate discharge ratio (IR)	0.15	0.50	90°	3.15 (main channel) 4.51 (tributary)	0.30	5
High discharge ratio (HR)	0.23	0.77	90°	3.15 (main channel) 4.51 (tributary)	0.30	5

1.1 Low discharge ratio ($Q_r = 0.11$, $q_r = 0.37$)
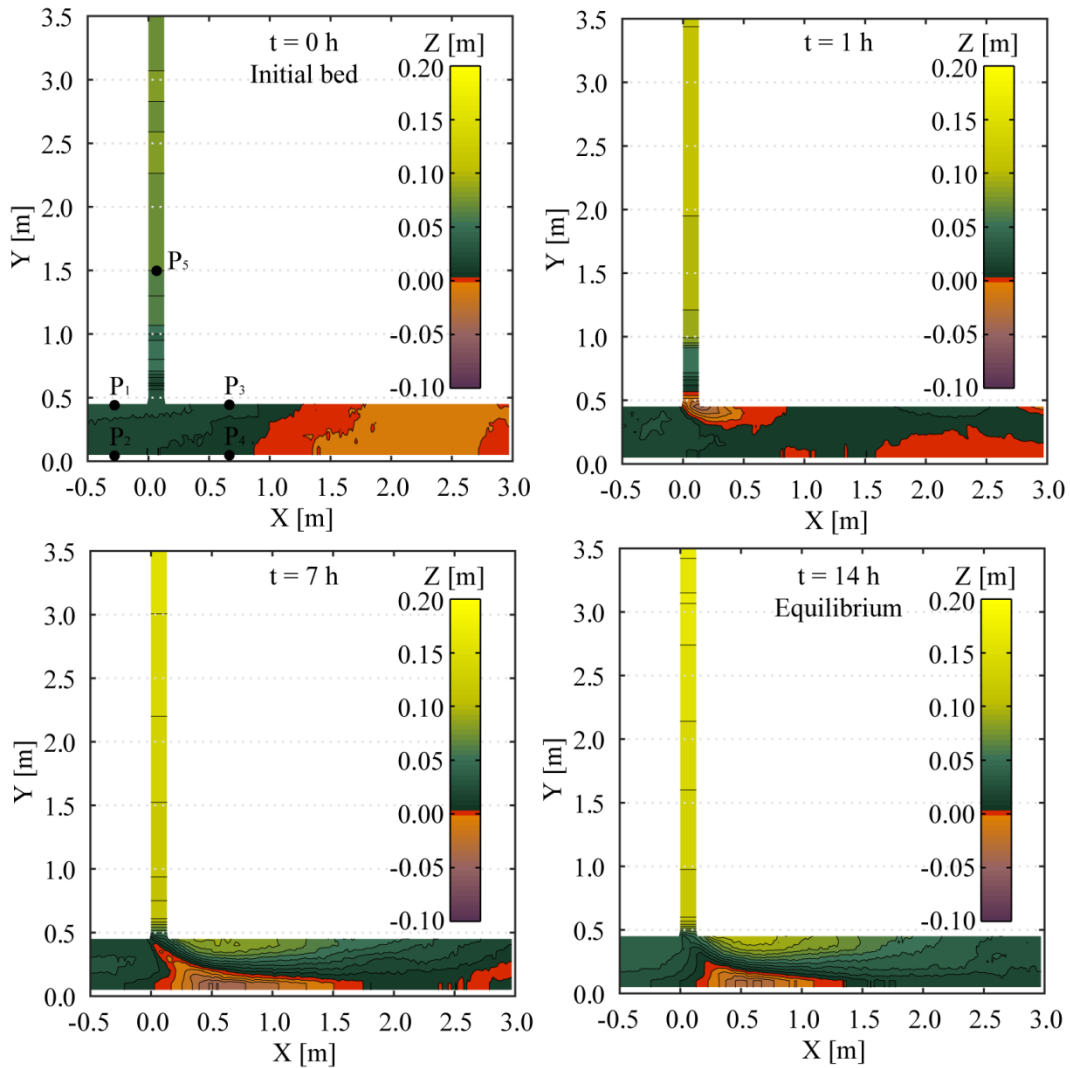
Figure A1.1 Bed topography for the low discharge ratio with $\alpha = 90°$ at the measuring times: a) $t = 0$ h, b) $t = 1$ h, c) $t = 7$ h, and d) $t = 14$ h (equilibrium). P_1 to P_5 indicate the position of the checkpoints to assess equilibrium.
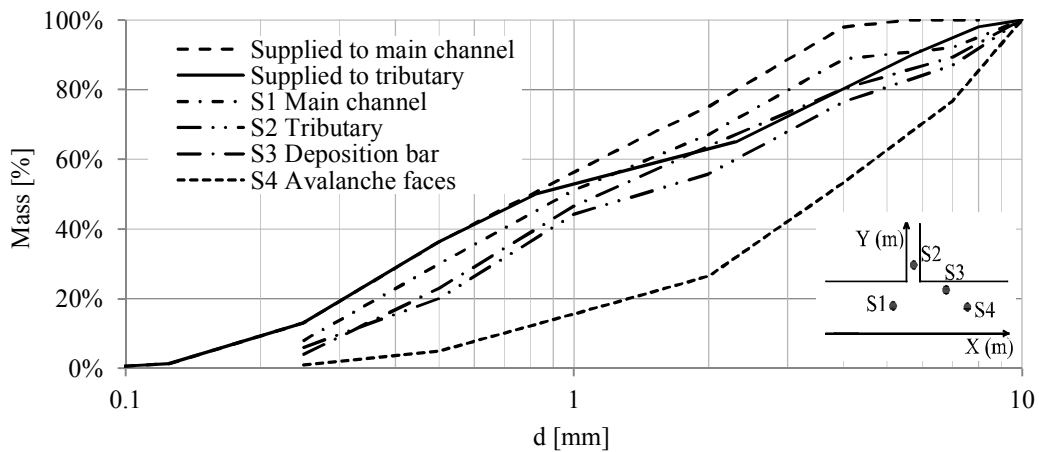

Figure A1.2 Grain size distribution of the bed surface at equilibrium and of the supplied sediment mixtures, for the low discharge ratio with $\alpha = 90°$.
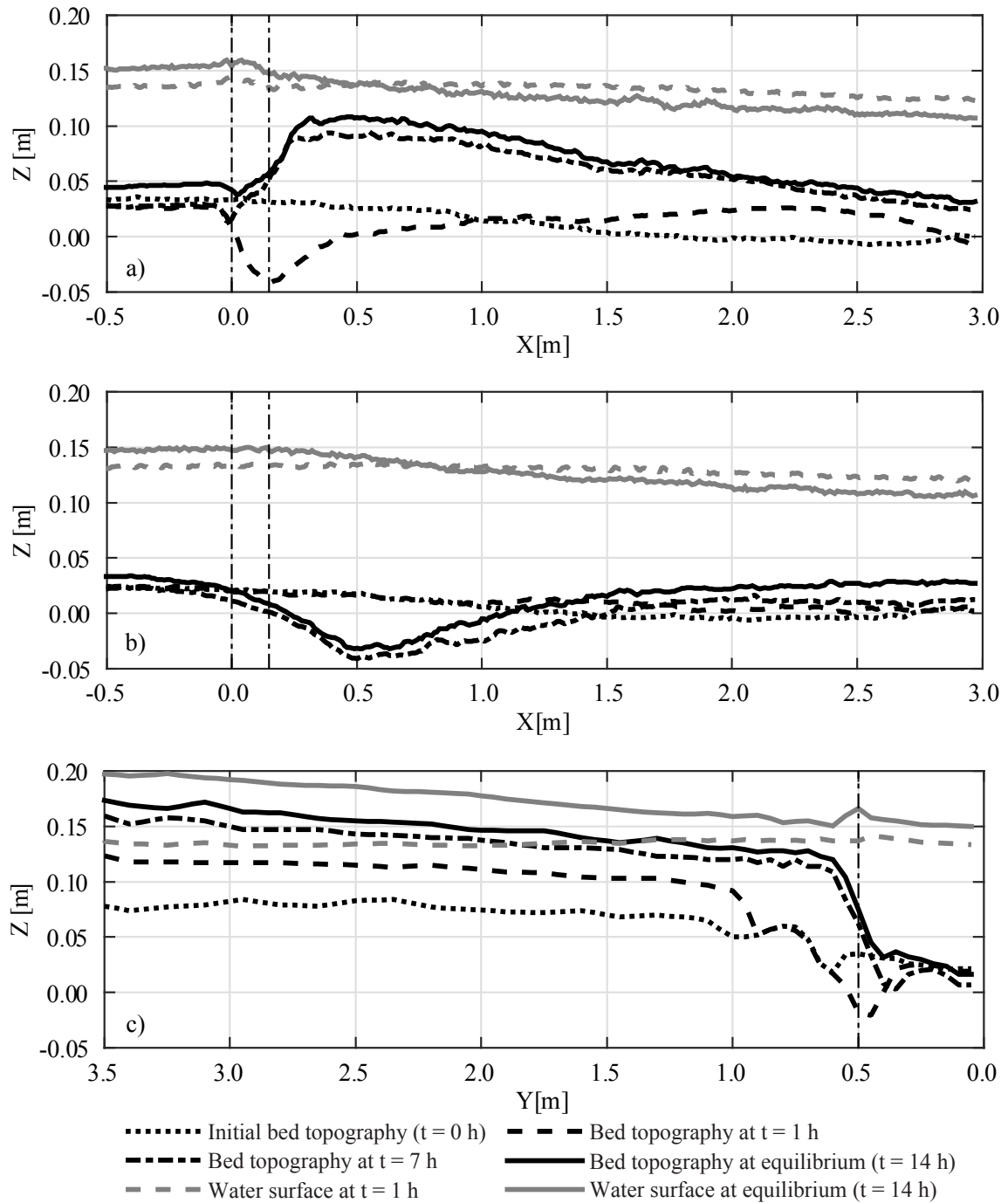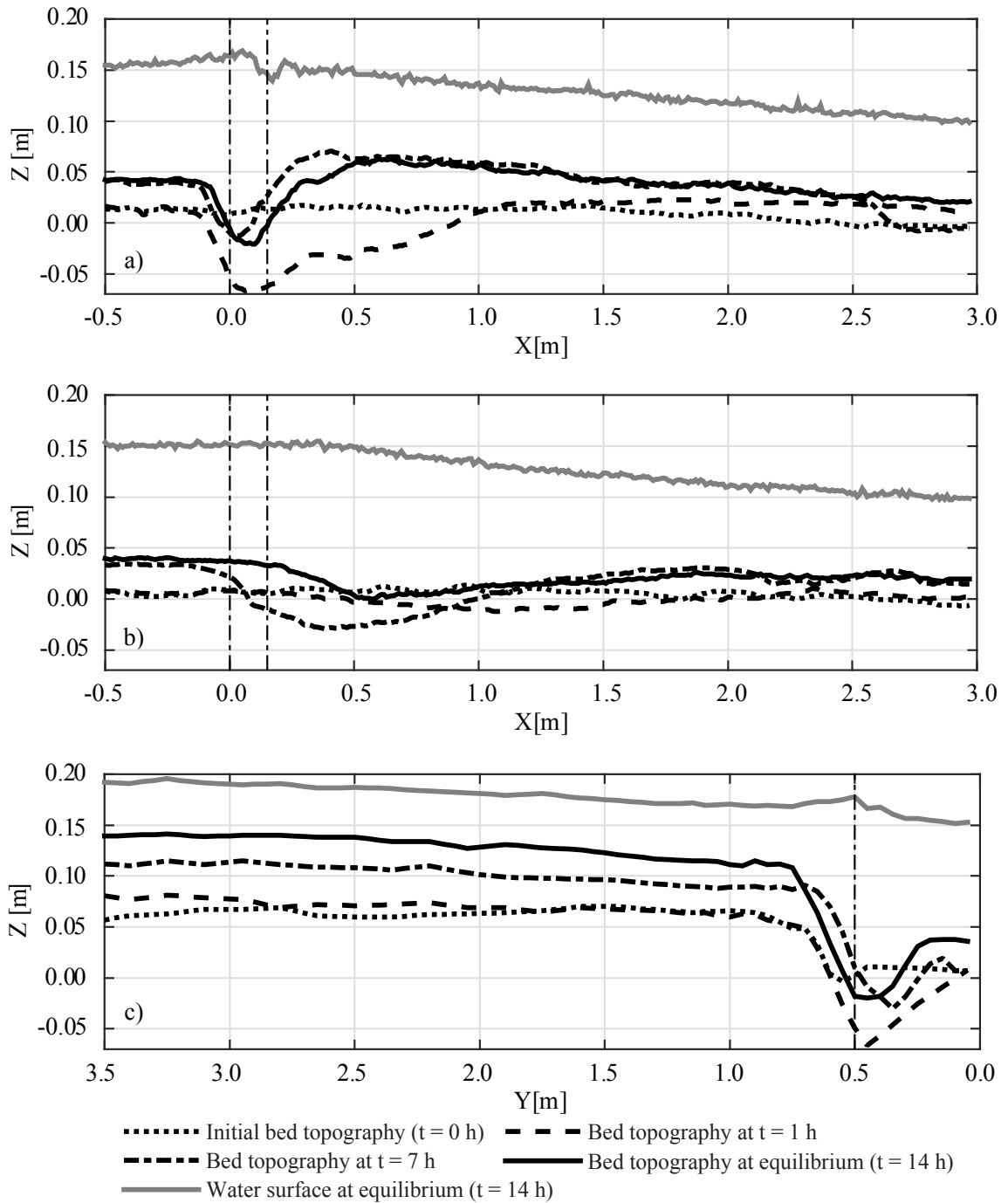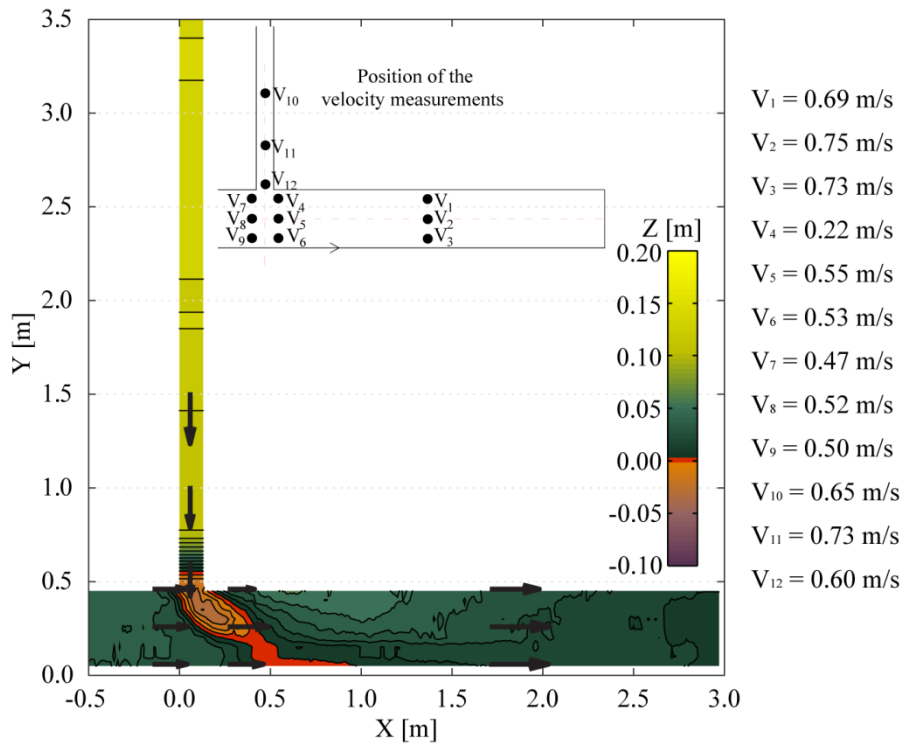
Figure A1.3 Profiles of the bed elevation and water surface during the experiment along the a) inner bank of the main channel ($Y = 0.45$ m), b) outer bank of the main channel ($Y = 0.05$ m), and c) tributary axis ($X = 0.60$ m). The values correspond to the low discharge ratio with $\alpha = 90°$.
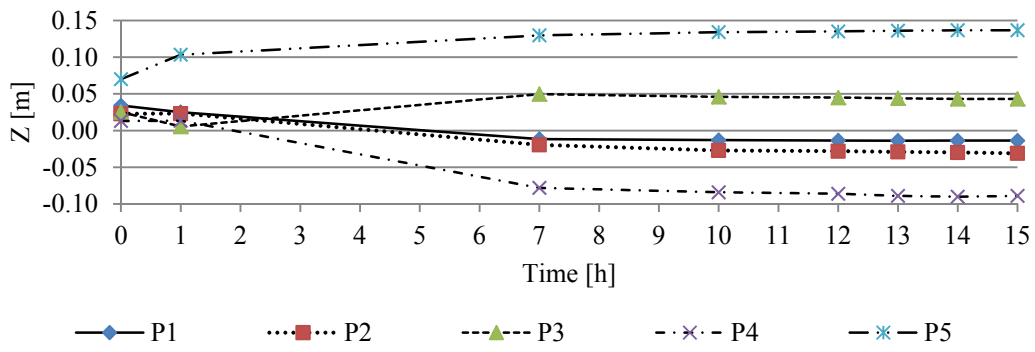
Figure A1.4 Evolution of the bed elevation at the checkpoints P_1 to P_5 during the experiment corresponding to the low discharge ratio with $\alpha = 90°$.
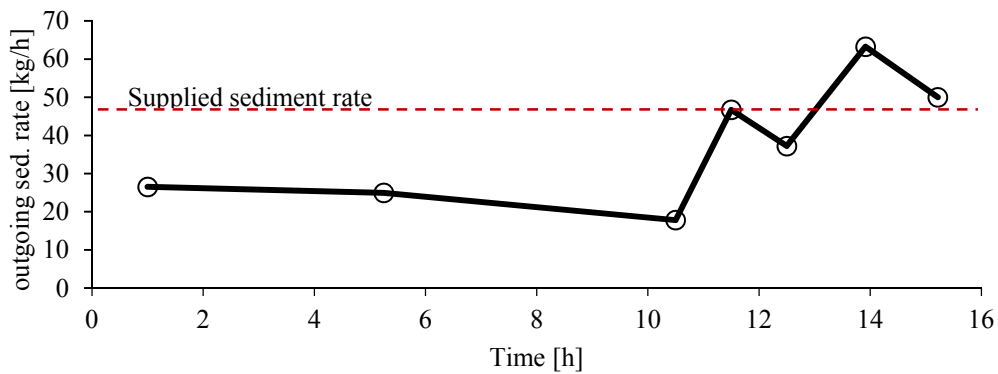
Figure A1.5 Outgoing sediment rates measured during the experiment corresponding to the low discharge ratio with $\alpha = 90°$. Dashed line represents the supplied sediment rate.
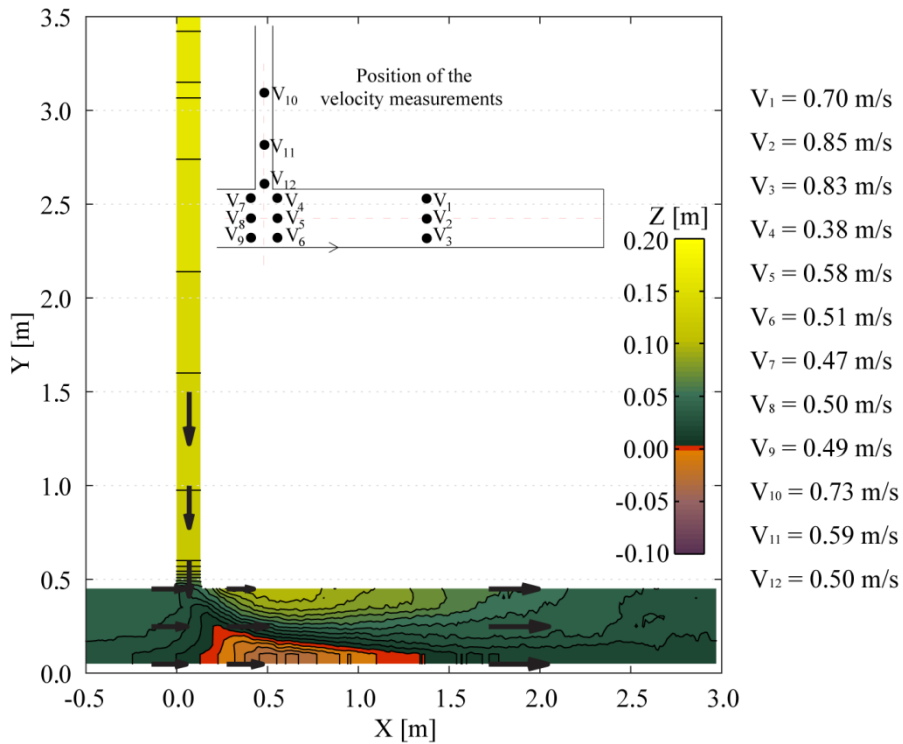
Figure A1.6 Point velocity measurements at equilibrium (t = 14 h) for the low discharge ratio with $\alpha = 90°$.

1.2 Intermediate discharge ratio ($Q_r = 0.15$ $q_r = 0.50$)
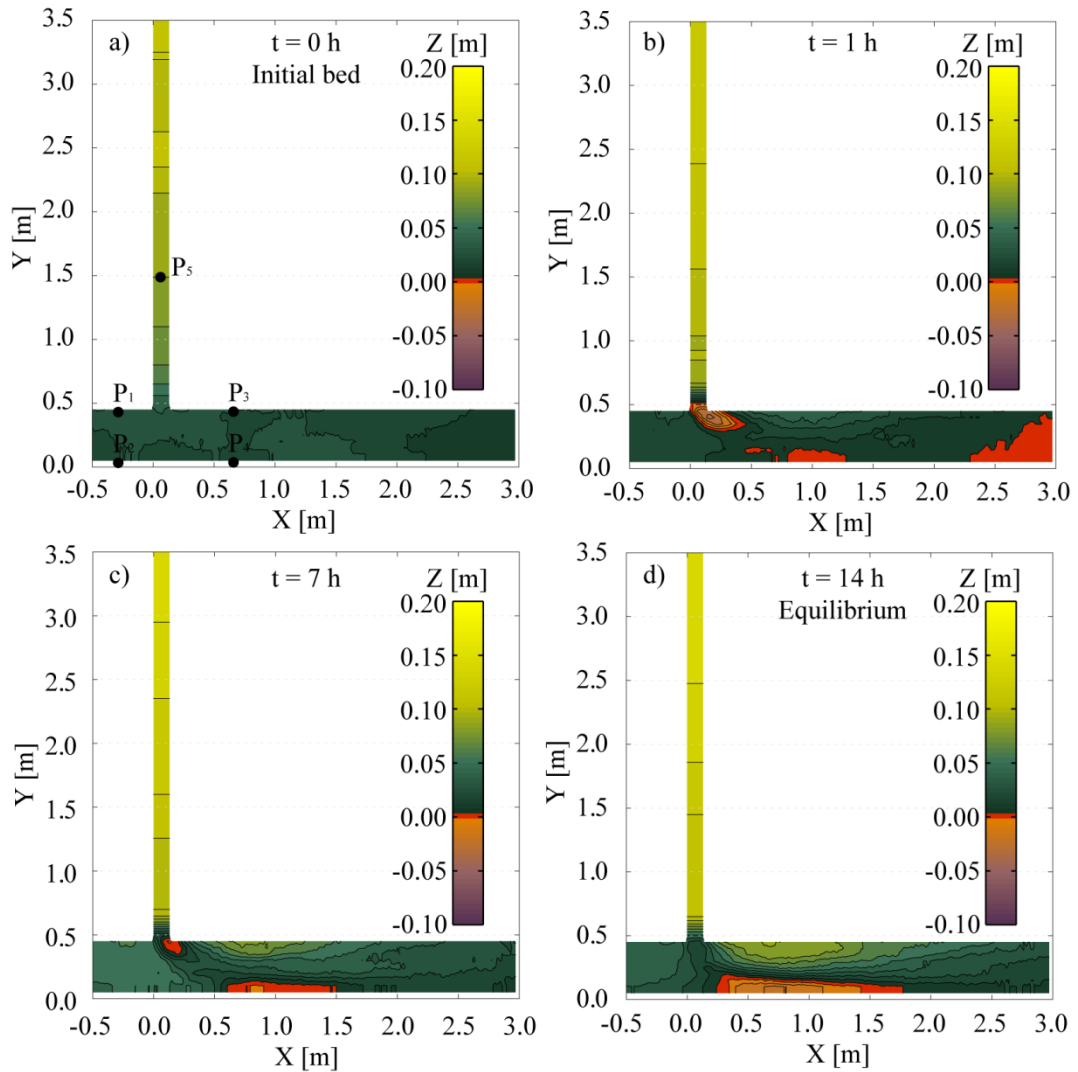
Figure A1.7 Bed topography for the intermediate discharge ratio with $\alpha = 90°$ at the measuring times a) $t = 0$ h, b) $t = 1$ h, c) $t = 7$ h, and d) $t = 14$ h (equilibrium). P_1 to P_5 indicate the position of the checkpoints to assess equilibrium.
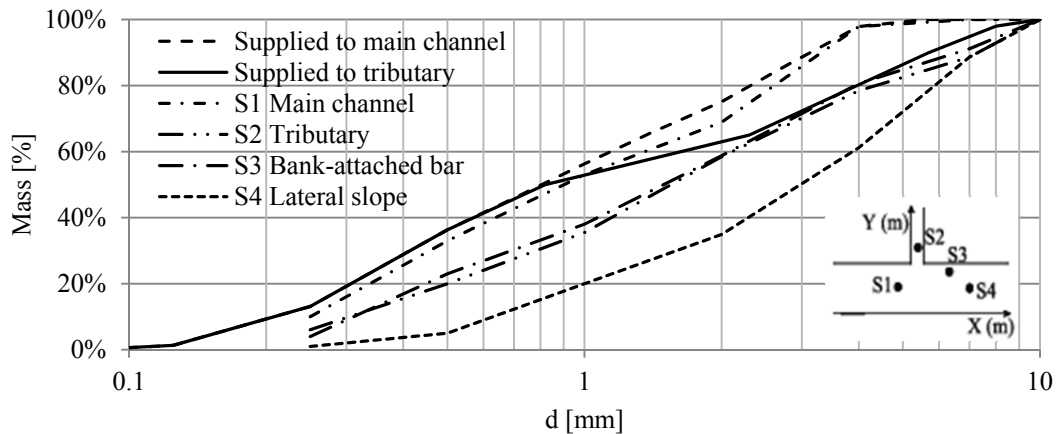
Figure A1.8 Grain size distribution of the bed surface at equilibrium and of the supplied sediment mixtures, for the intermediate discharge ratio with $\alpha = 90°$.
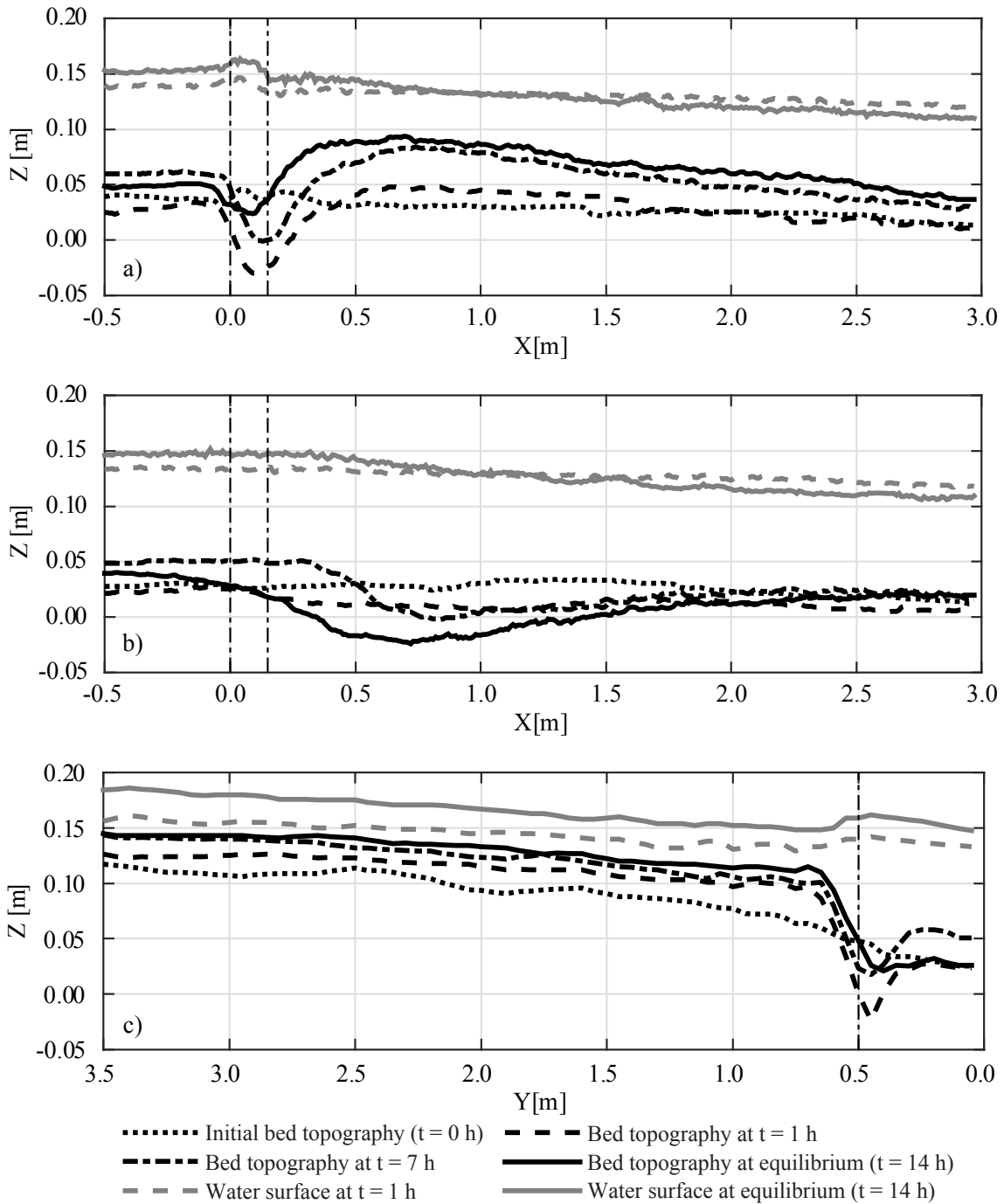
Figure A1.9 Profiles of the bed elevation and water surface during the experiment along the a) inner bank of the main channel ($Y = 0.45$ m), b) outer bank of the main channel ($Y = 0.05$ m), and c) tributary axis ($X = 0.60$ m). The values correspond to the intermediate discharge ratio with $\alpha = 90°$.
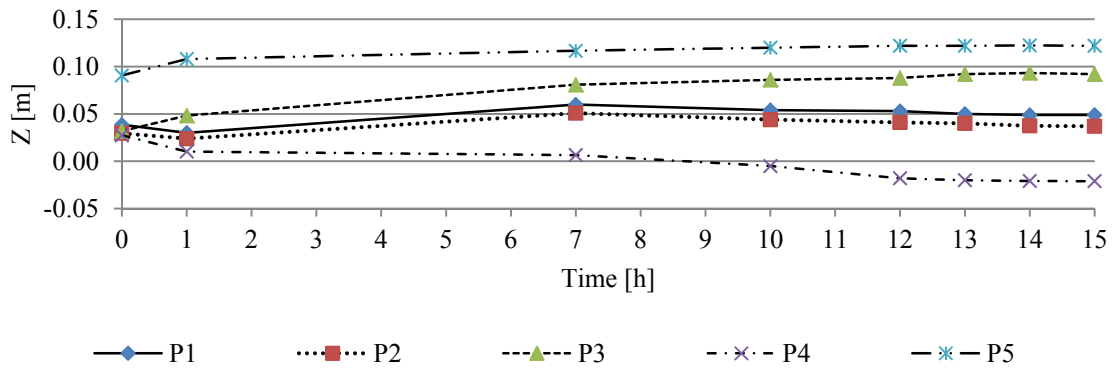
Figure A1.10 Evolution of the bed elevation at the checkpoints P_1 to P_5 during the experiment corresponding to the intermediate discharge ratio with $\alpha = 90°$.
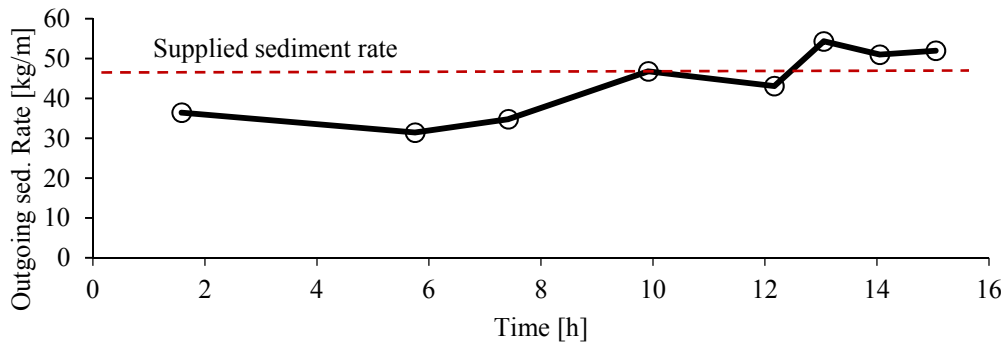
Figure A1.11 Outgoing sediment rates measured during the experiment corresponding to the intermediate discharge ratio with $\alpha = 90°$. Dashed line represents the supplied sediment rate.
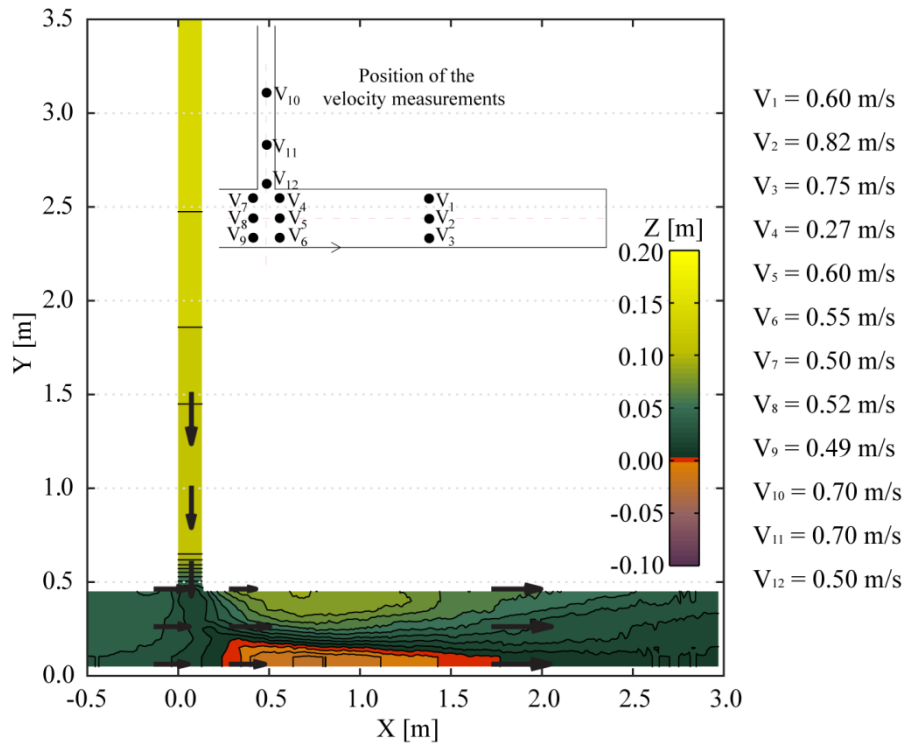
Figure A1.12 Point velocity measurements at equilibrium (t = 14 h) for the intermediate discharge ratio with $\alpha = 90°$.

127

1.3 High discharge ratio ($Q_r = 0.23$, $q_r = 0.77$)
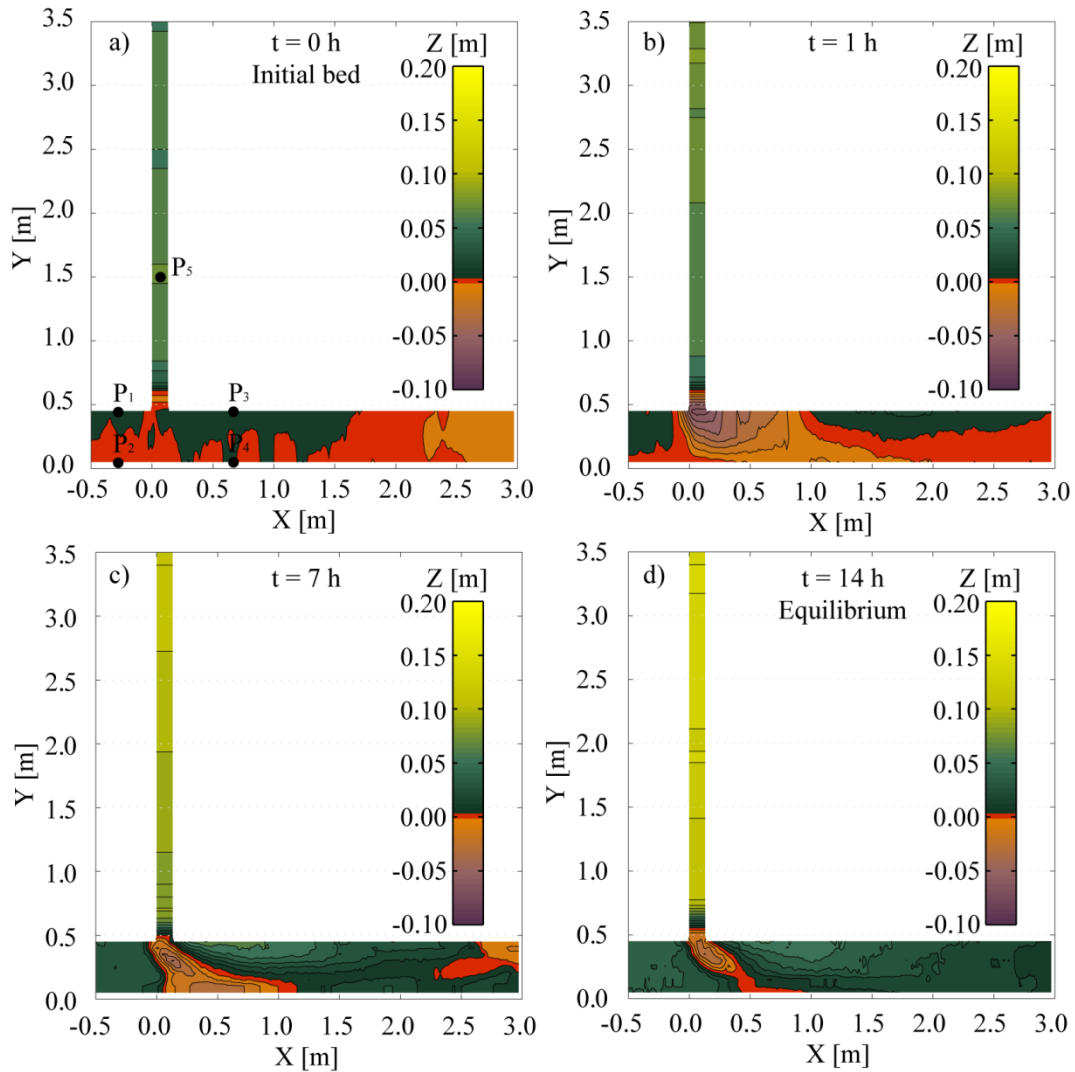
Figure A1.13 Bed topography for the high discharge ratio with $\alpha = 90°$ at the measuring times a) $t = 0$ h, b) $t = 1$ h, c) $t = 7$ h, and d) $t = 14$ h (equilibrium). P_1 to P_5 indicate the position of the checkpoints to assess equilibrium.
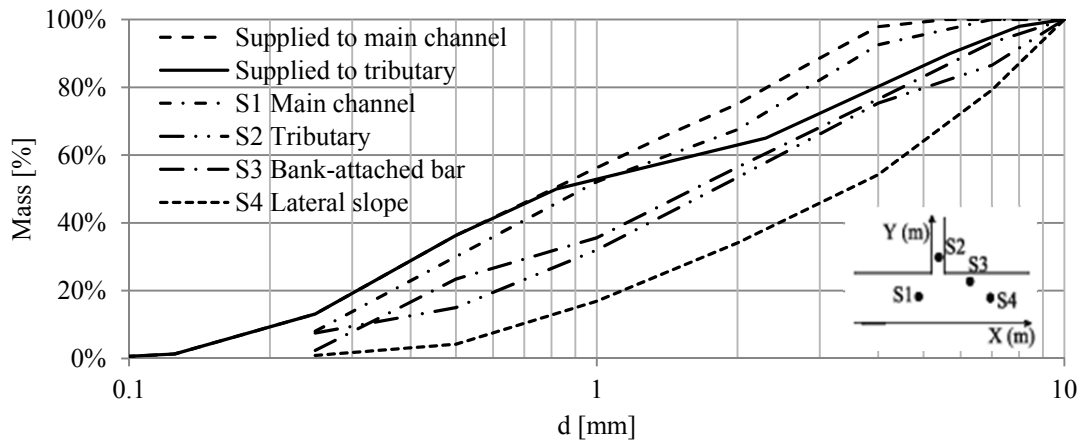
Figure A 1.14 Grain size distribution of the bed surface at equilibrium and of the supplied sediment mixtures, for the high discharge ratio with $\alpha = 90°$.

Figure A1.15 Profiles of the bed elevation and water surface during the experiment along the a) inner bank of the main channel ($Y = 0.45$ m), b) outer bank of the main channel ($Y = 0.05$ m), and c) tributary axis ($X = 0.60$ m). The values correspond to the high discharge ratio with $\alpha = 90°$.
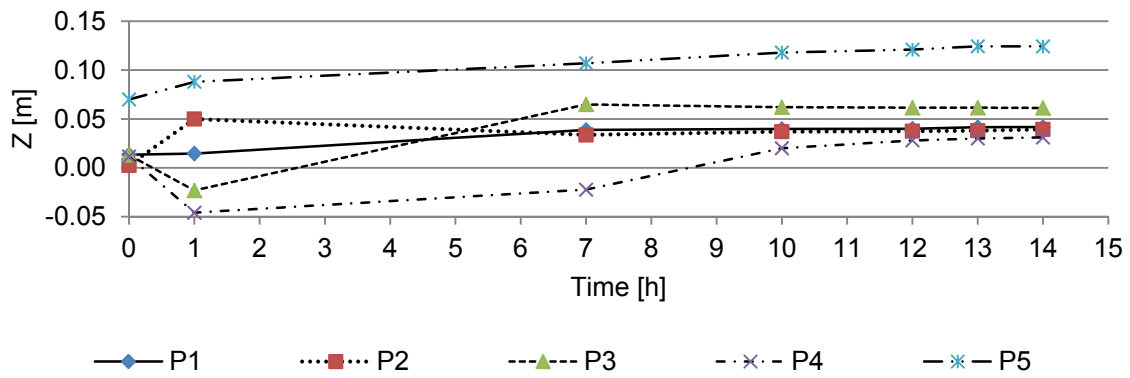
Figure A1.16 Evolution of the bed elevation at the checkpoints P_1 to P_5 during the experiment corresponding to the high discharge ratio with $\alpha = 90°$.
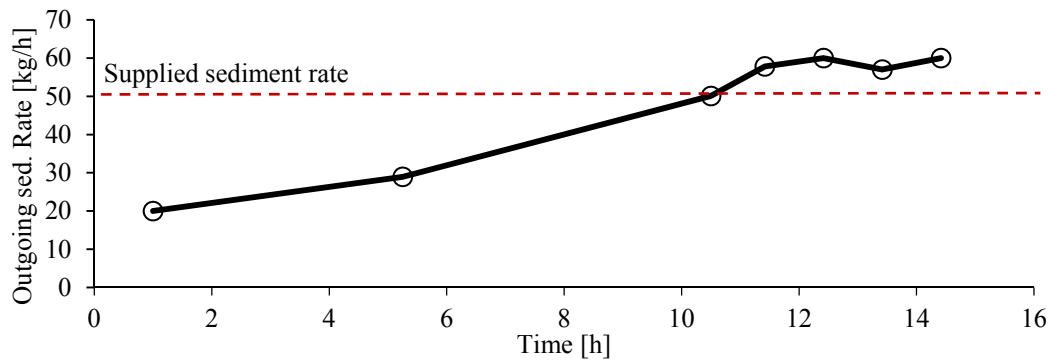
Figure A1.17 Outgoing sediment rates measured during the experiment corresponding to the high discharge ratio with $\alpha = 90°$. Dashed line represents the supplied sediment rate.

Figure A1.18 Point velocity measurements at equilibrium (t = 14 h) for the high discharge ratio with $\alpha = 90°$.

A2

Experimental set II

In this appendix, graphical representations of the measurements performed in the experimental set II are displayed for every experiment. The following information is shown for each experiment:

- Bed topography at the times $t = 0$ h, $t = 1$ h, $t = 7$ h, and at equilibrium.
- Profiles of the bed elevation and water surface measured during the experiment along the inner bank of the main channel, outer bank of the main channel and tributary axis.
- Evolution of the bed elevation measured at the checkpoints P_1 to P_5 (Figure 3.17b) during the experiments to assess the equilibrium condition.
- Outgoing sediment rates measured at the downstream end of the main channel to assess the equilibrium condition during the experiments.

The values of the discharge ratio (Q_r), unit-discharge ratio (q_r), junction angle (α), sediment gradation coefficient (σ), and width ratio (B_t/B_m) adopted in each experiment of the experimental set II are given in Table A2.1

Table A2.1. Summary of the main parameters adopted in experimental set II

Experiment	Q_r [-]	q_r [-]	α [°]	σ [-]	B_t/B_m [-]	Results discussed in chapter
Low discharge ratio (LR)	0.11	0.37	70°	3.15 (main channel) 4.51 (tributary)	0.30	5 - 6
Intermediate discharge ratio (IR)	0.15	0.50	70°	3.15 (main channel) 4.51 (tributary)	0.30	5 – 6
High discharge ratio (HR)	0.23	0.77	70°	3.15 (main channel) 4.51 (tributary)	0.30	5 - 6

2.1   Low discharge ratio ($Q_r = 0.11$, $q_r = 0.37$)
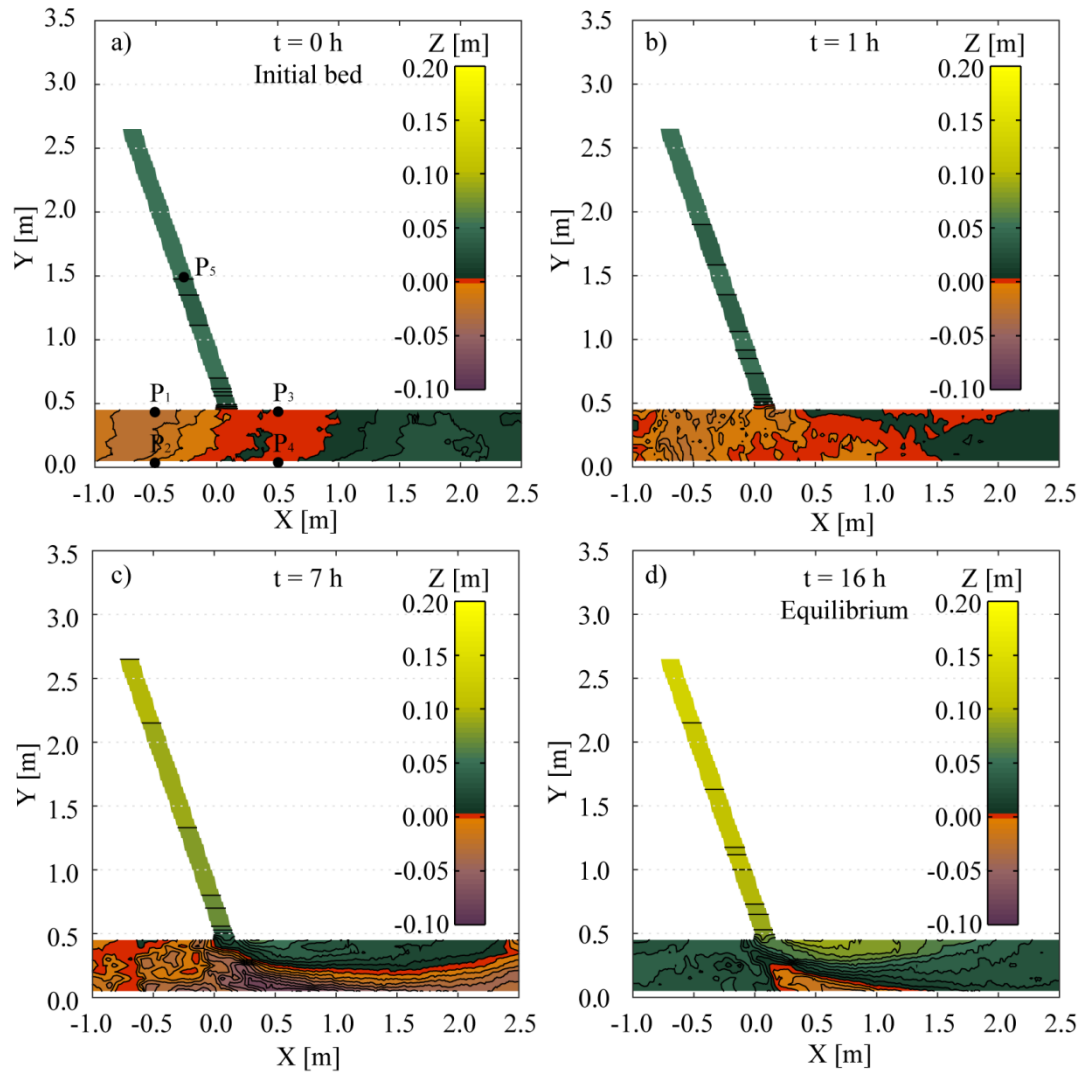
Figure A2.1 Bed topography for the low discharge ratio with $\alpha = 70°$ at the measuring times a) $t = 0$ h, b) $t = 1$ h, c) $t = 7$ h, and d) $t = 16$ h (equilibrium). P_1 to P_5 indicate the position of the checkpoints to assess equilibrium.
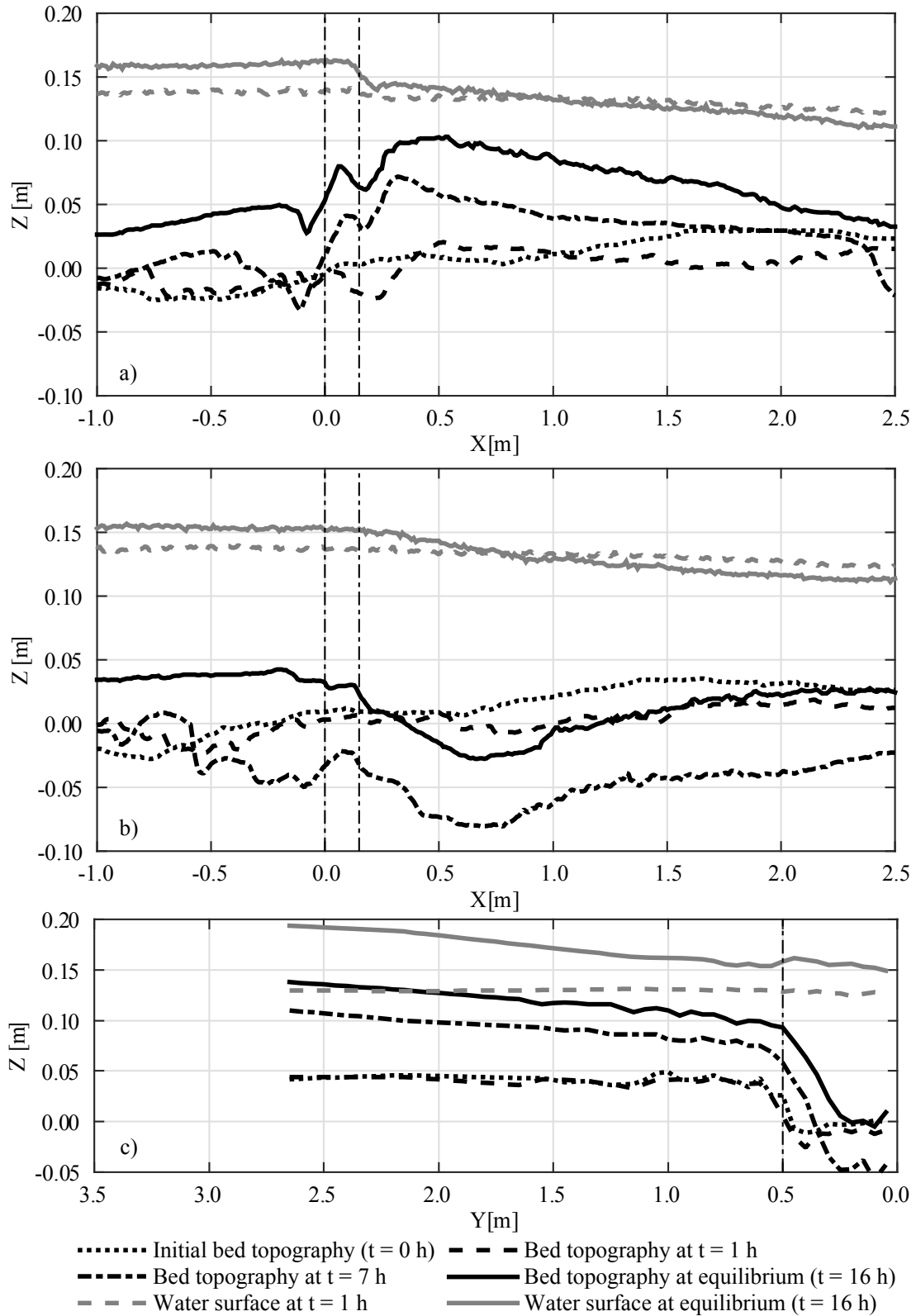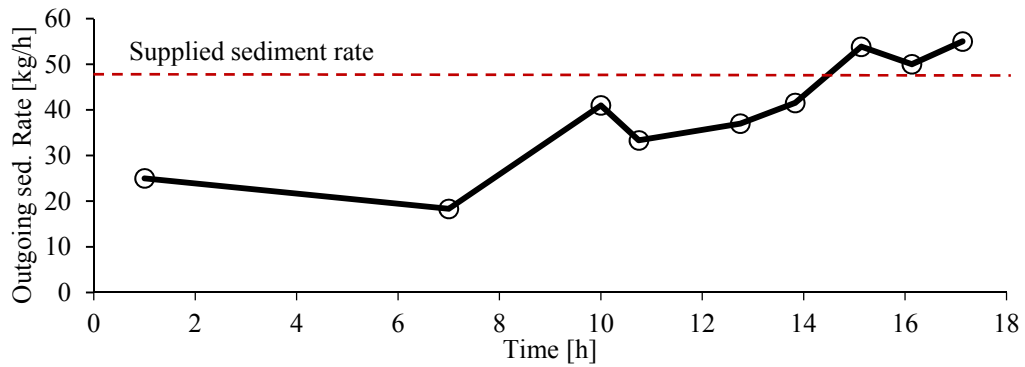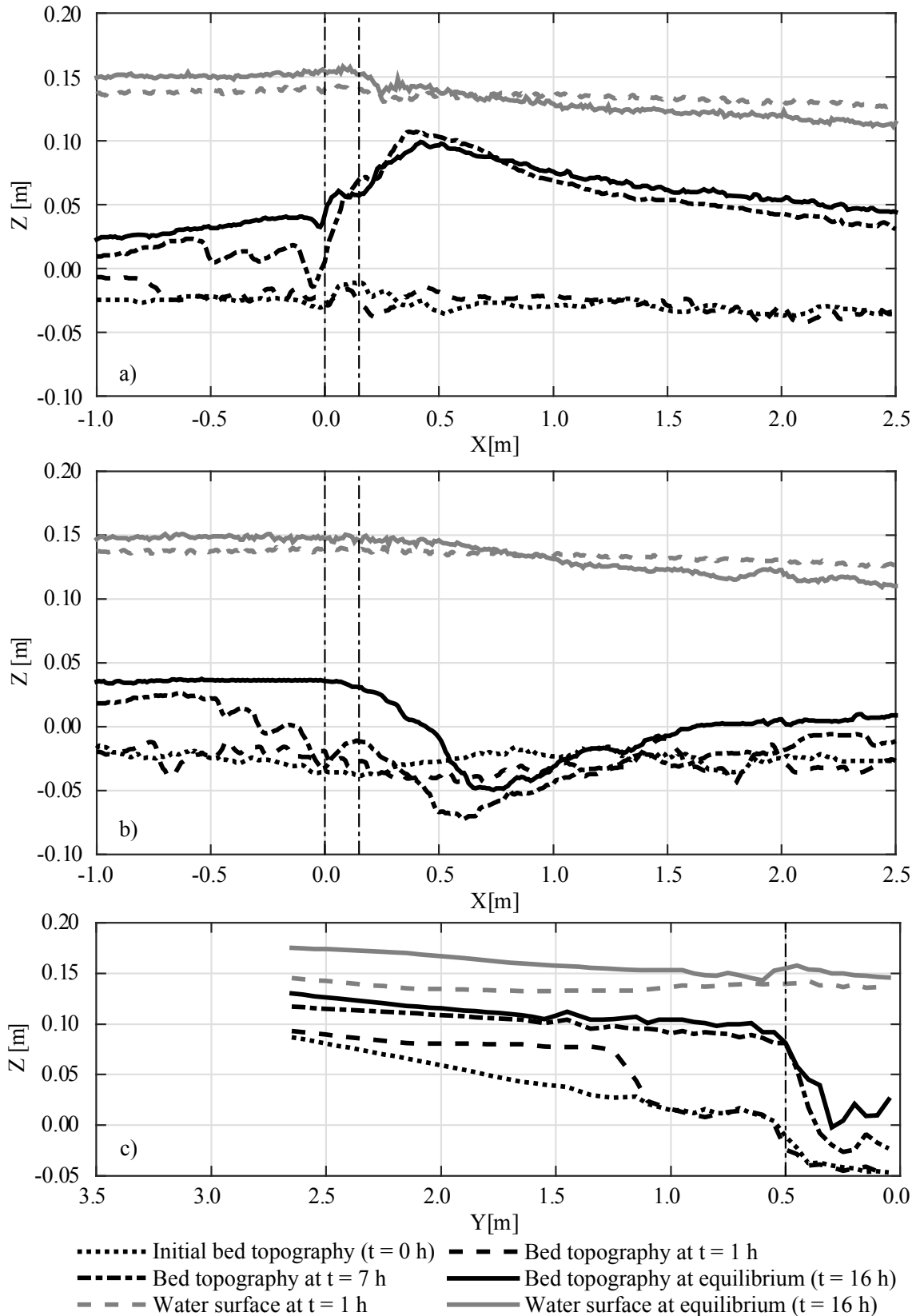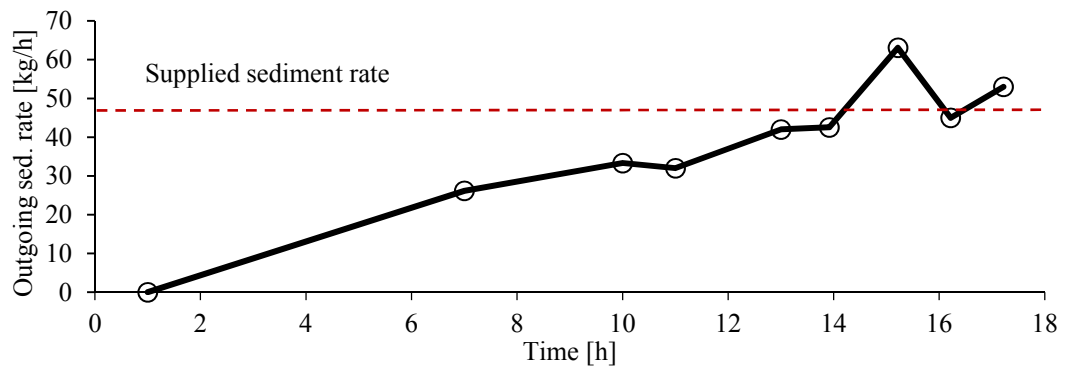
Figure A2.2 Profiles of the bed elevation and water surface during the experiment along the a) inner bank of the main channel ($Y = 0.45$ m), b) outer bank of the main channel ($Y = 0.05$ m), and c) tributary axis. The values correspond to the low discharge ratio with $\alpha = 70°$.
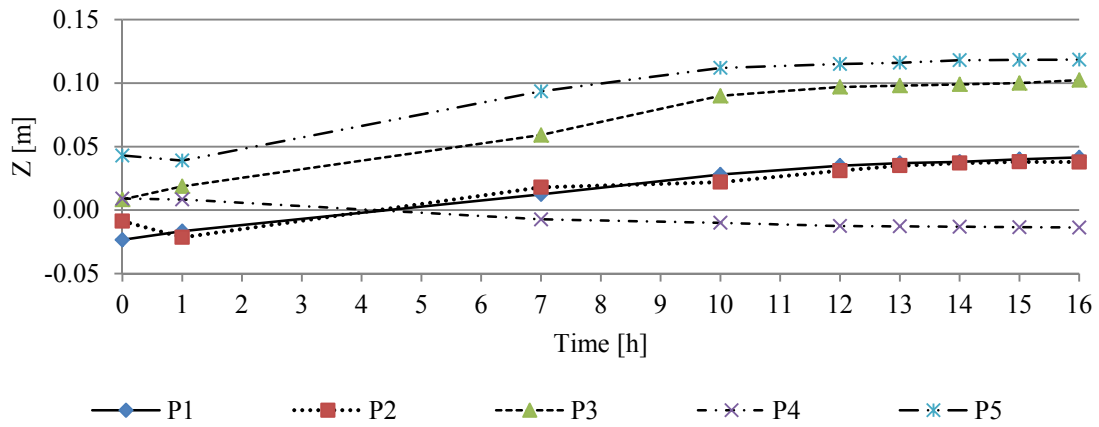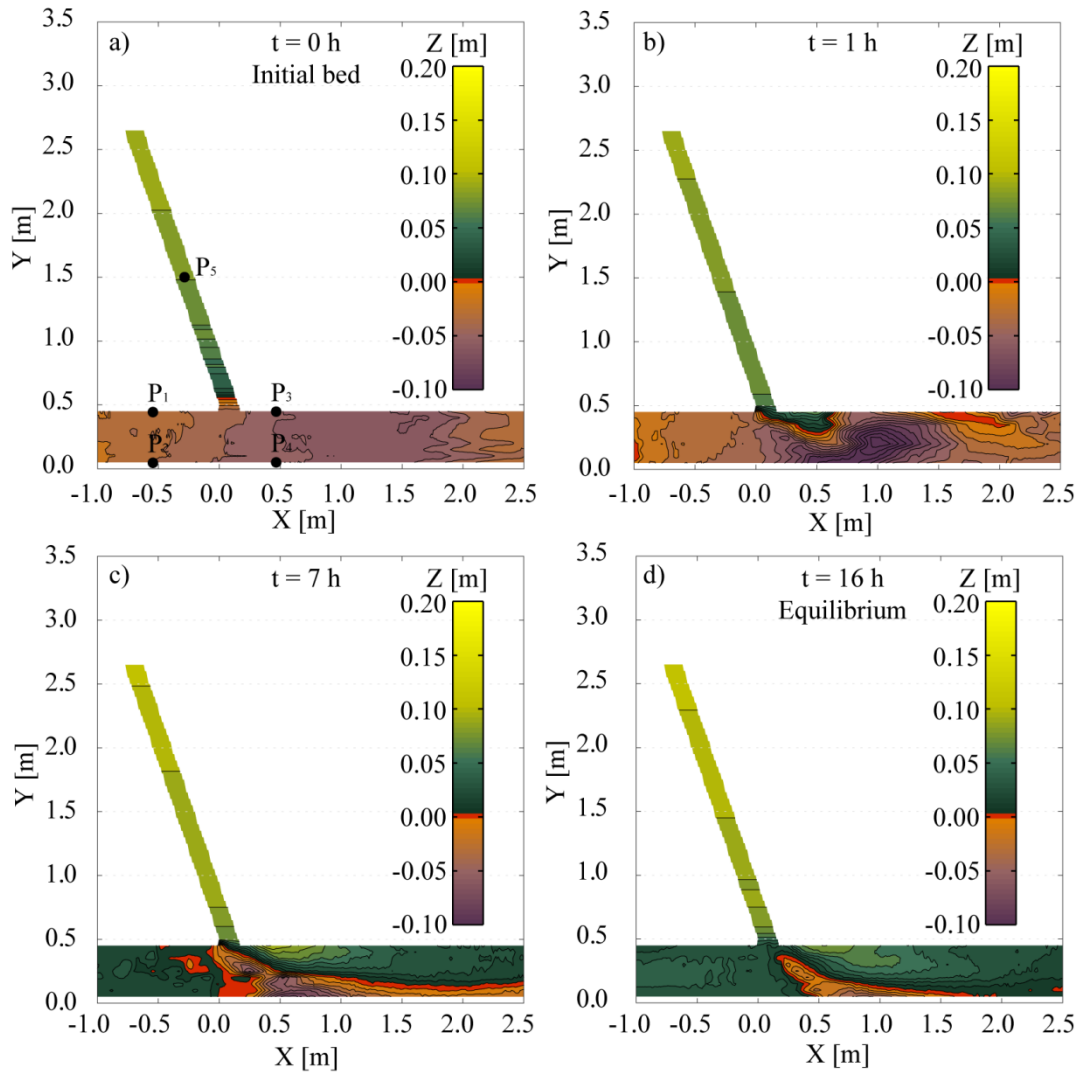
Figure A2.3 Evolution of the bed elevation at the checkpoints P_1 to P_5 during the experiment corresponding to the low discharge ratio with $\alpha = 70°$.
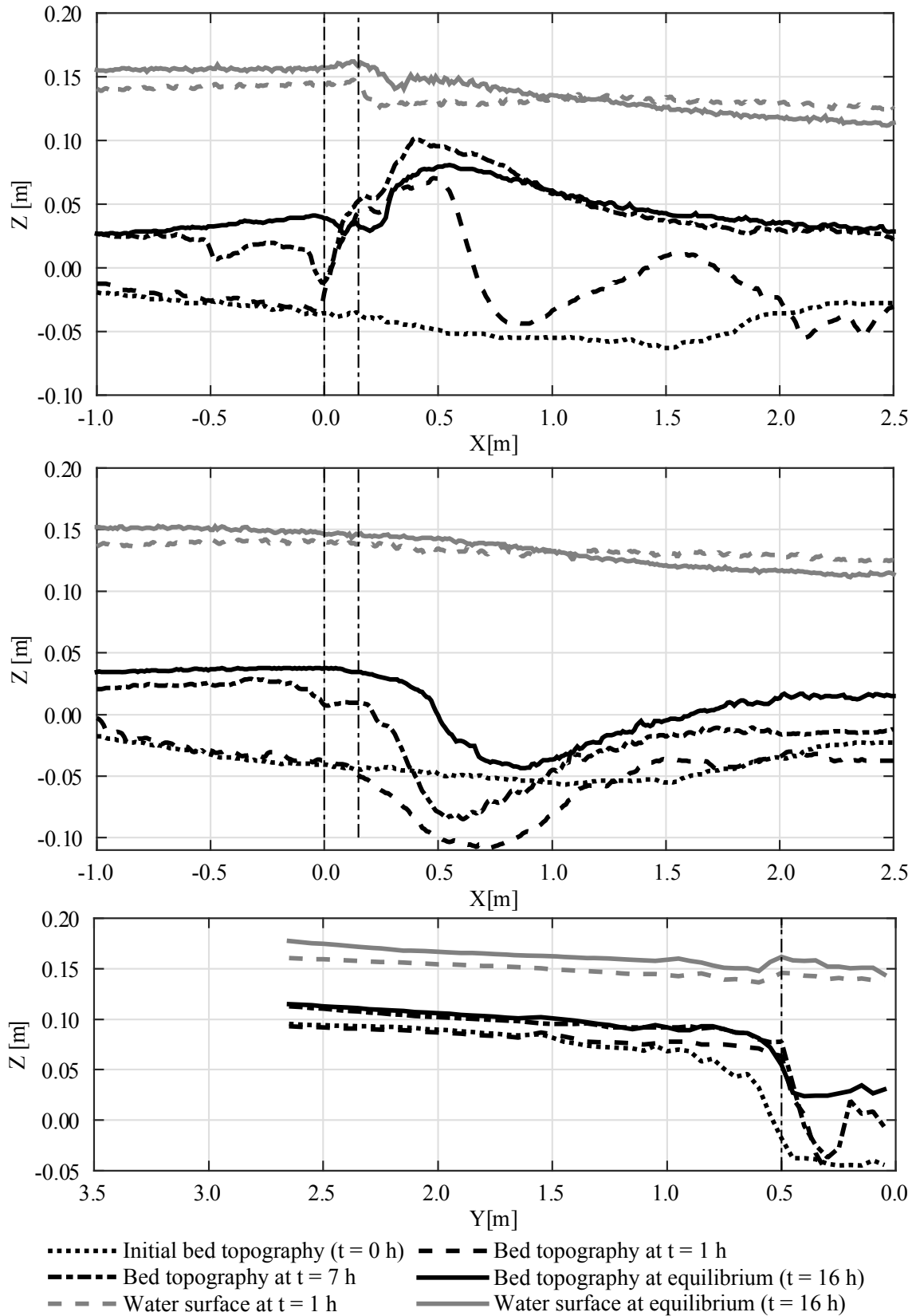

Figure A2.4 Outgoing sediment rates measured during the experiment corresponding to the low discharge ratio with $\alpha = 70°$. Dashed line represents the supplied sediment rate.

## 2.2 Intermediate discharge ratio ($Q_r = 0.15$, $q_r = 0.50$)
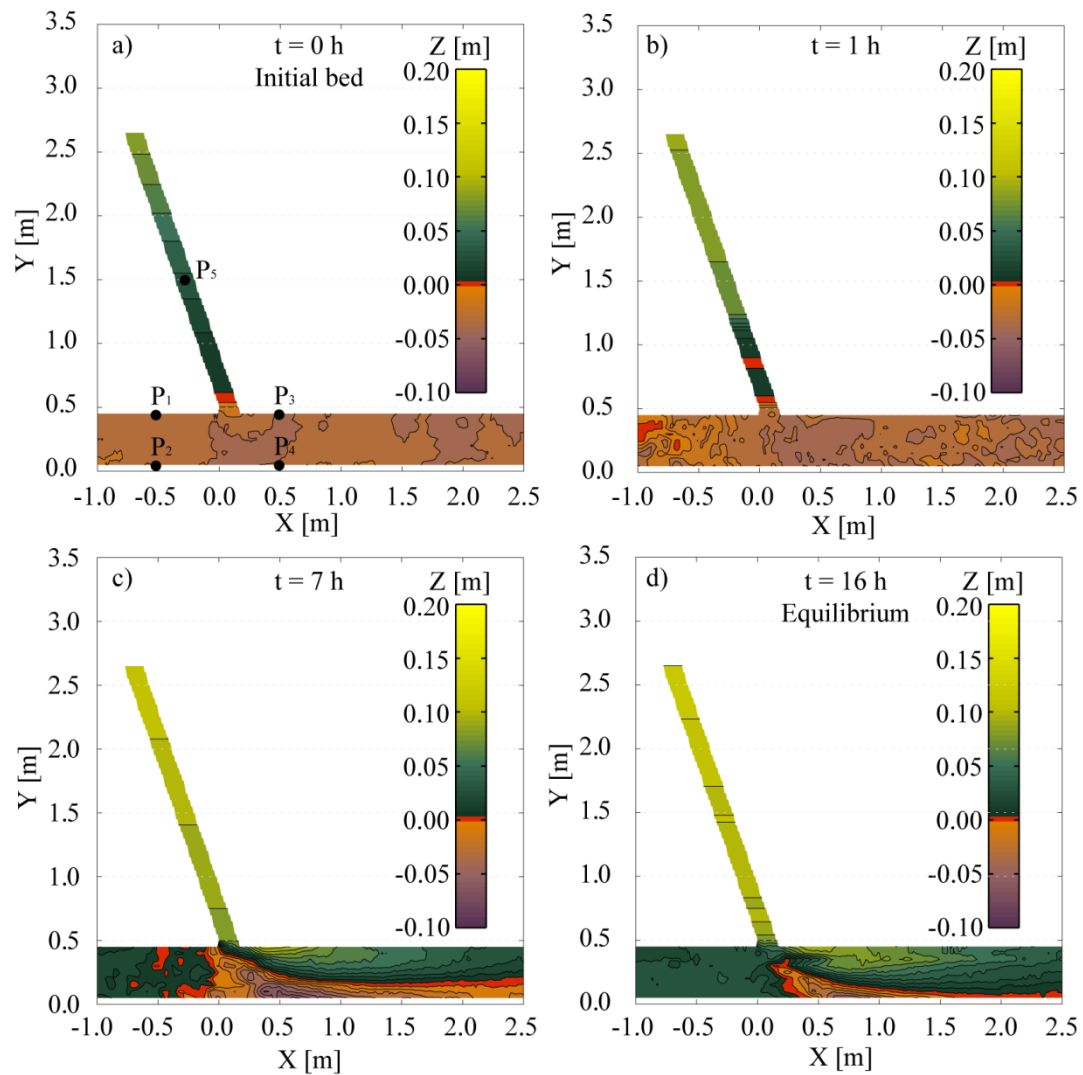
Figure A2.5 Bed topography for the intermediate discharge ratio with $\alpha = 70°$ at the measuring times a) $t = 0$ h, b) $t = 1$ h, c) $t = 7$ h, d) and $t = 16$ h (equilibrium). P_1 to P_5 indicate the position of the checkpoints to assess equilibrium.

Figure A2.6 Profiles of the bed elevation and water surface during the experiment along the a) inner bank of the main channel (Y = 0.45 m), b) outer bank of the main channel (Y = 0.05 m), and c) tributary axis. The values correspond to intermediate discharge ratio with α = 70°.
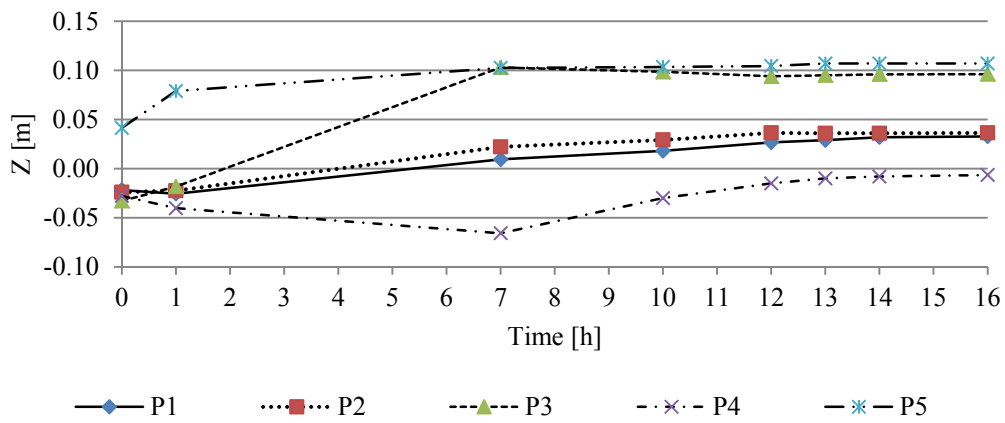
Figure A2.7 Evolution of the bed elevation at the checkpoints P_1 to P_5 during the experiment corresponding to the intermediate discharge ratio with $\alpha = 70°$.

Figure A2.8 Outgoing sediment rates measured during the experiment corresponding to the intermediate discharge ratio with $\alpha = 70°$. Dashed line represents the supplied sediment rate.

2.3 High discharge ratio ($Q_r = 0.23$, $q_r = 0.77$)

Figure A2.9 Bed topography for the high discharge ratio with $\alpha = 70°$ at the measuring times a) $t = 0$ h, b) $t = 1$ h, c) $t = 7$ h, and d) $t = 16$ h (equilibrium). P_1 to P_5 indicate the position of the checkpoints to assess equilibrium.

Figure A2.10 Profiles of the bed elevation and water surface during the experiment along the a) inner bank of the main channel (Y = 0.45 m), b) outer bank of the main channel (Y = 0.05 m), and c) tributary axis. The values correspond to high discharge ratio with α = 70°.
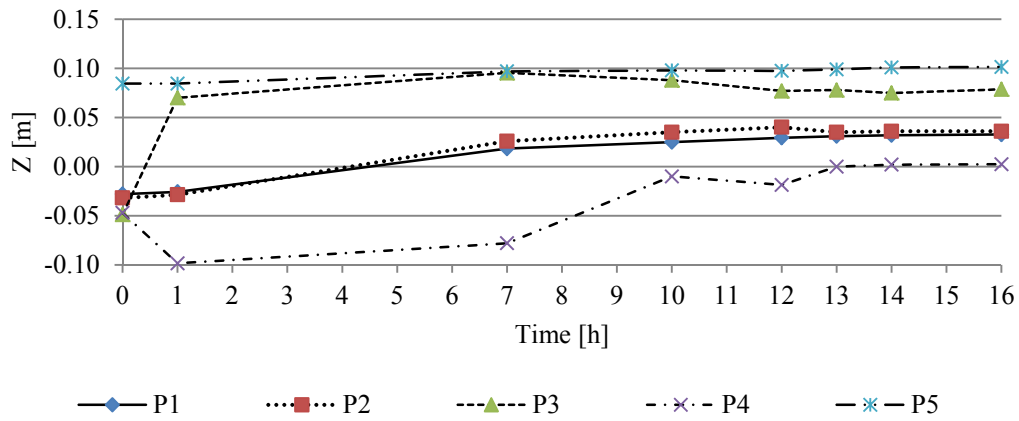
Figure A2.11 Evolution of the bed elevation at the checkpoints P_1 to P_5 during the experiment corresponding to the high discharge ratio with $\alpha = 70°$.
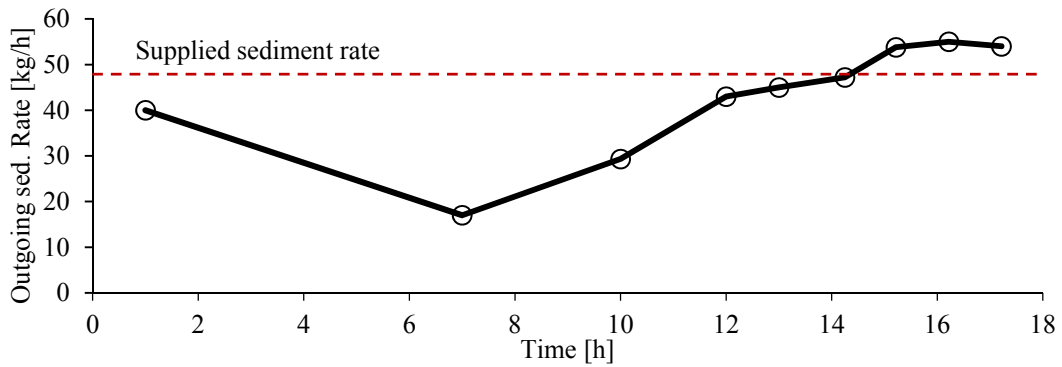
Figure A2.12 Outgoing sediment rates measured during the experiment corresponding to the high discharge ratio with $\alpha = 70°$. Dashed line represents the supplied sediment rate.

A3

Experimental set III

In this appendix, graphical representations of the measurements performed in the experimental set III are displayed for every experiment. The following information is shown for each experiment:

- Bed topography at the times $t = 0\ h$, $t = 1\ h$, $t = 7\ h$, and at equilibrium.
- Profiles of the bed elevation and water surface measured during the experiment along the inner bank of the main channel, outer bank of the main channel and tributary axis.
- Outgoing sediment rates measured at the downstream end of the main channel to assess the equilibrium condition during the experiments.

The values of the discharge ratio (Q_r), unit-discharge ratio (q_r), junction angle (α), sediment gradation coefficient (σ), and width ratio (B_t/B_m) adopted in each experiment of the experimental set III are given in Table A3.1

Table A3.1. Summary of the main parameters adopted in experimental set III

| Experiment	Q_r [-]	q_r [-]	α [°]	σ [-]	B_t/B_m [-]	Results discussed in chapter
Low discharge ratio (LR)	0.11	0.37	70°	1.35	0.30	6 - 7
Intermediate discharge ratio (IR)	0.15	0.50	70°	1.35	0.30	6 - 7
High discharge ratio (HR)	0.23	0.77	70°	1.35	0.30	6 - 7

3.1   Low discharge ratio ($Q_r = 0.11$, $q_r = 0.37$)
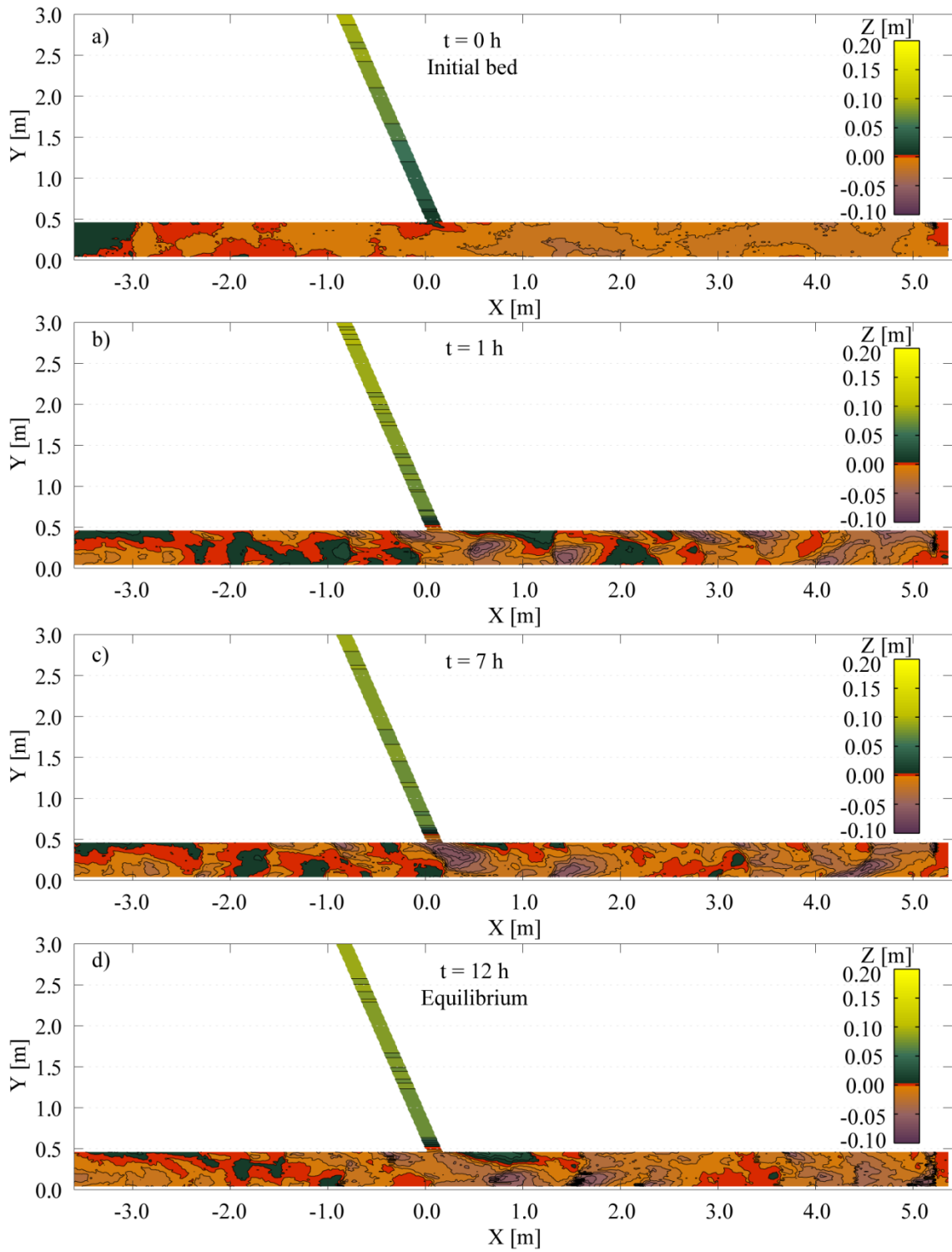
Figure A3.1 Bed topography for the low discharge ratio with $\alpha = 70°$ at the measuring times a) $t = 0$ h, b) $t = 1$ h, c) $t = 7$ h, and d) $t = 12$ h (equilibrium). P_1 to P_5 indicate the position of the checkpoints to assess equilibrium.
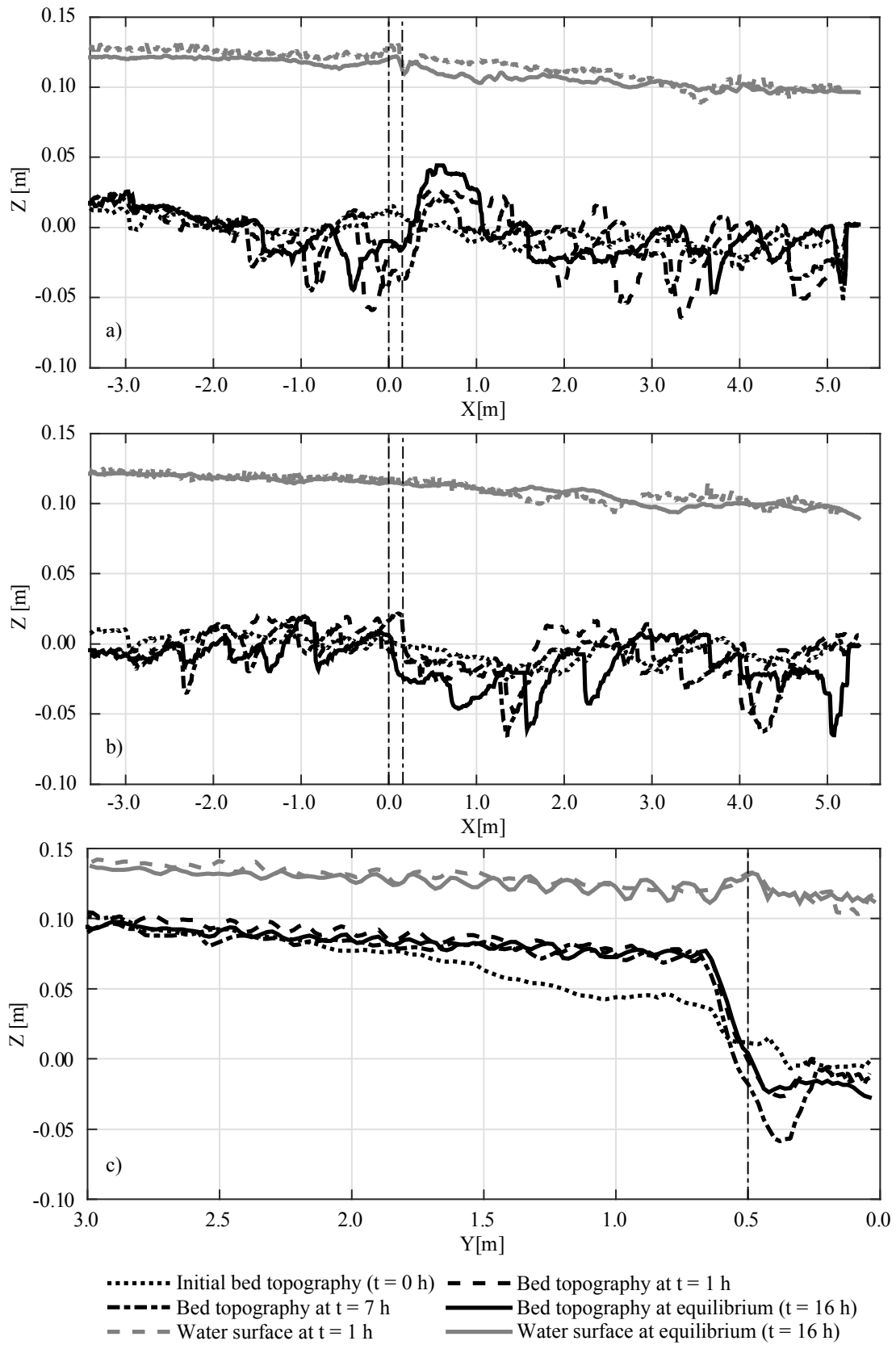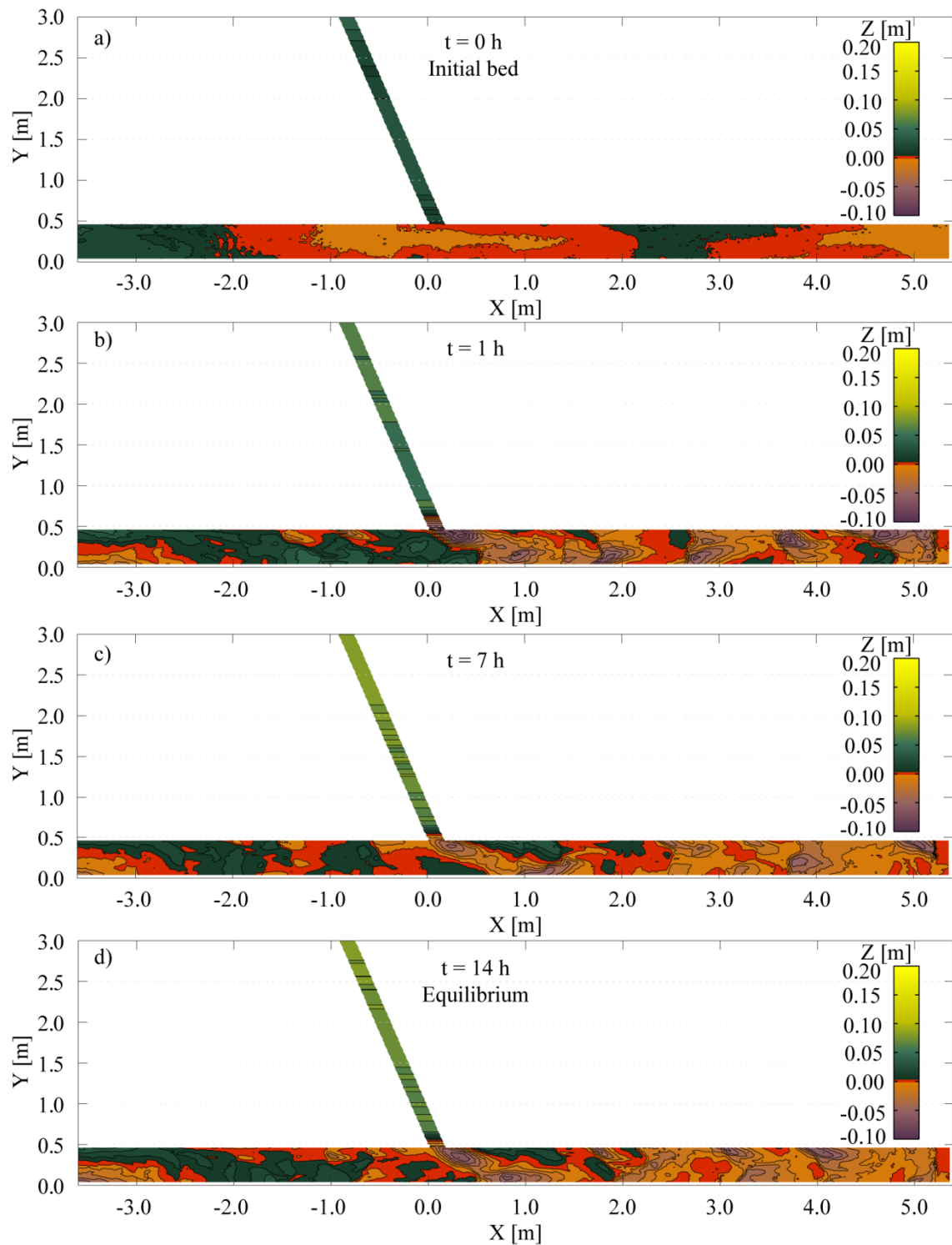
Figure A3.2 Profiles of the bed elevation and water surface during the experiment along the a) inner bank of the main channel ($Y = 0.45$ m), b) outer bank of the main channel ($Y = 0.05$ m), and c) tributary axis. The values correspond to the low discharge ratio with $\alpha = 70°$.
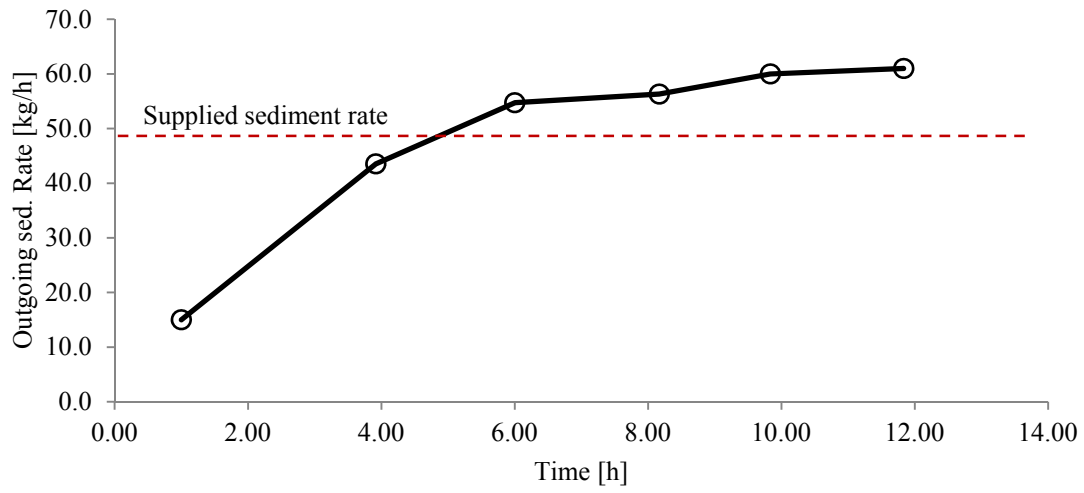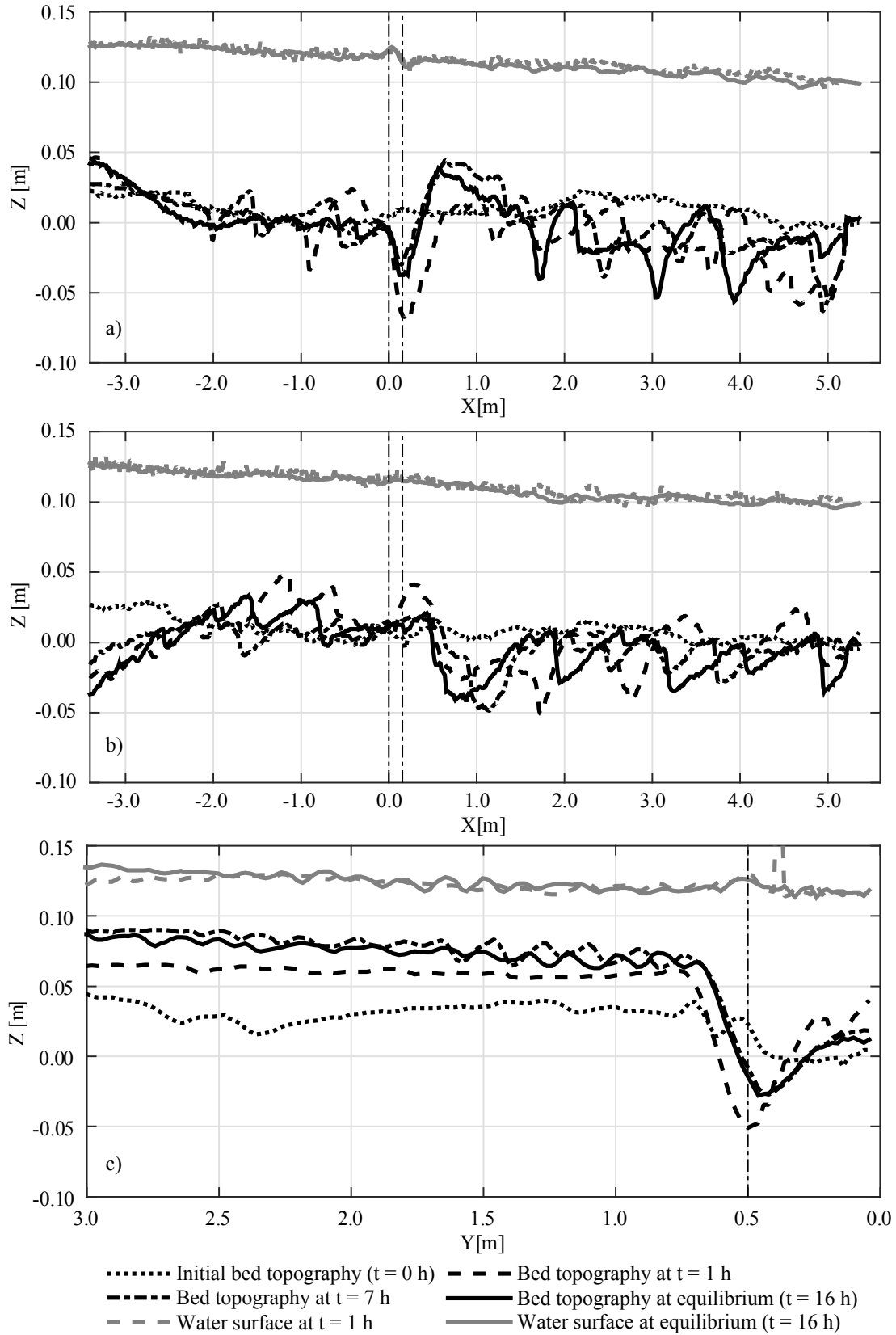
Figure A3.3 Outgoing sediment rates measured during the experiment corresponding to the low discharge ratio with $\alpha = 70°$. Dashed line represents the supplied sediment rate.
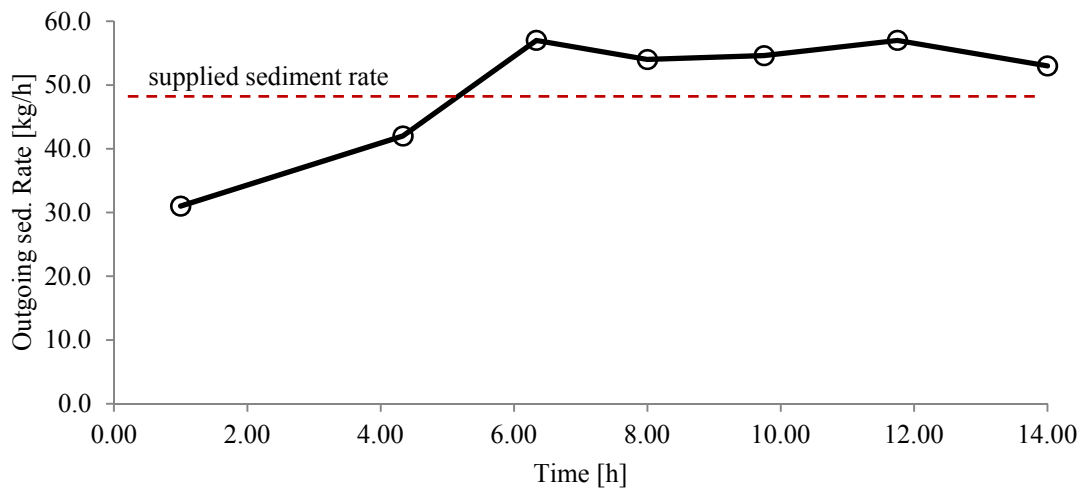
3.2 Intermediate discharge ratio ($Q_r = 0.15$, $q_r = 0.50$)

Figure A3.4 Bed topography for the intermediate discharge ratio with $\alpha = 70°$ at the measuring times a) $t = 0$ h, b) $t = 1$ h, c) $t = 7$ h, and d) $t = 14$ h (equilibrium). P_1 to P_5 indicate the position of the checkpoints to assess equilibrium.
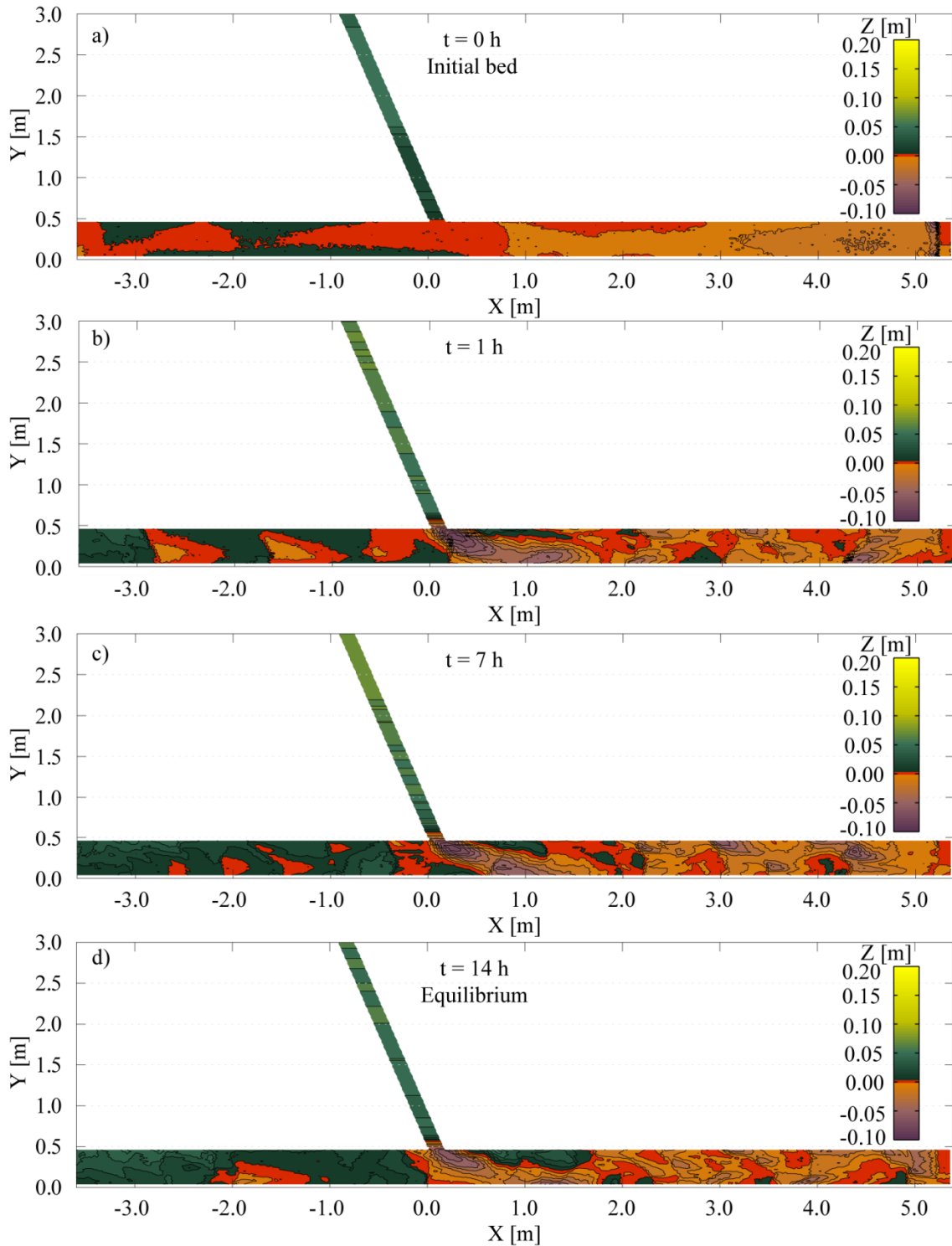
Figure A3.5 Profiles of the bed elevation and water surface during the experiment along the a) inner bank of the main channel (Y = 0.45 m), b) outer bank of the main channel (Y = 0.05 m), and c) tributary axis. The values correspond to the intermediate discharge ratio with α = 70°.
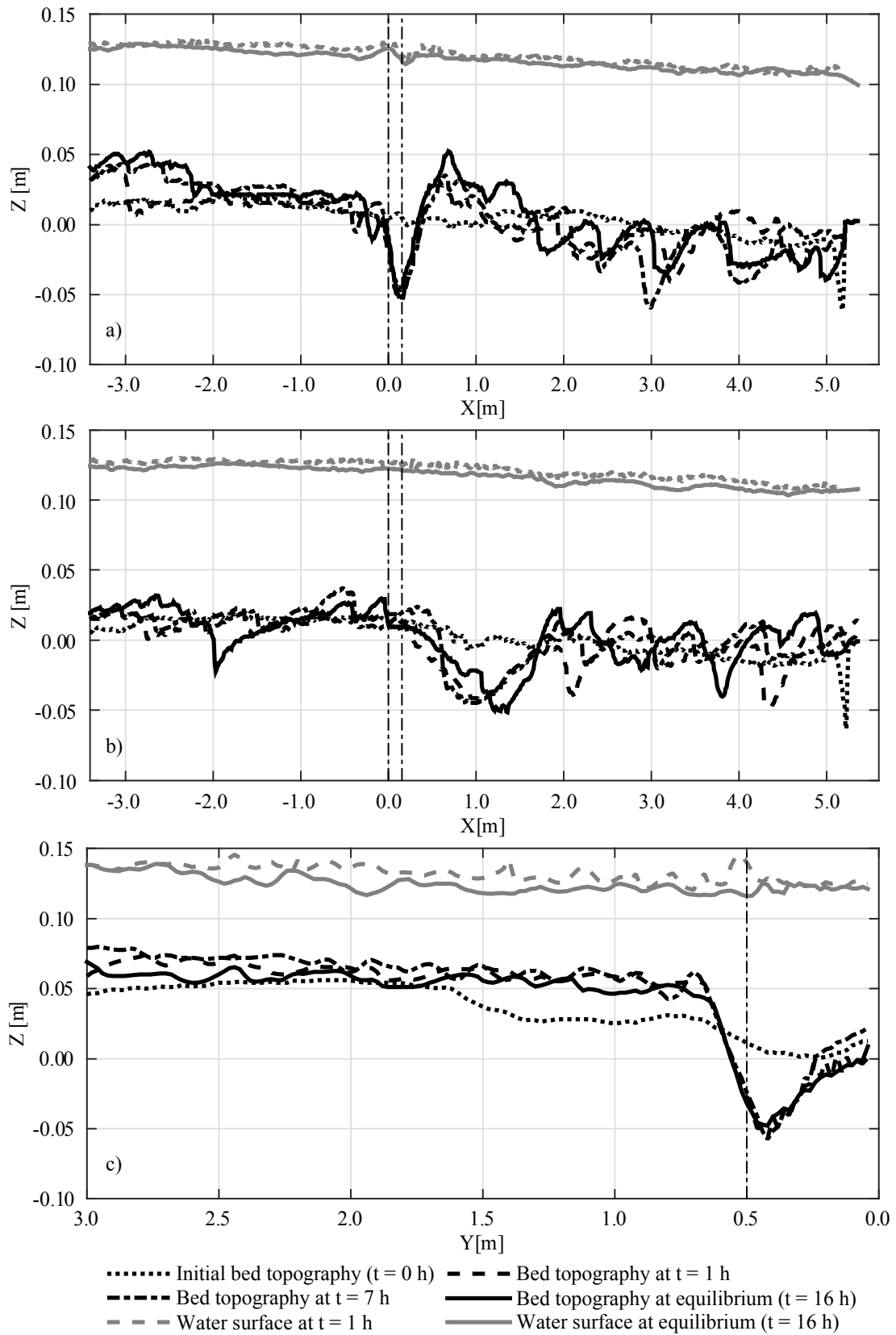
Figure A3.6 Outgoing sediment rates measured during the experiment corresponding to the intermediate discharge ratio with $\alpha = 70°$. Dashed line represents the supplied sediment rate.

3.3 High discharge ratio ($Q_r = 0.23$, $q_r = 0.77$)

Figure A3.7 Bed topography for the high discharge ratio with $\alpha = 70°$ at the measuring times a) $t = 0$ h, b) $t = 1$ h, c) $t = 7$ h, and d) $t = 14$ h (equilibrium). P_1 to P_5 indicate the position of the checkpoints to assess equilibrium.

Figure A3.8 Profiles of the bed elevation and water surface during the experiment along the a) inner bank of the main channel (Y = 0.45 m), b) outer bank of the main channel (Y = 0.05 m), and c) tributary axis. The values correspond to the high discharge ratio with α = 70°.
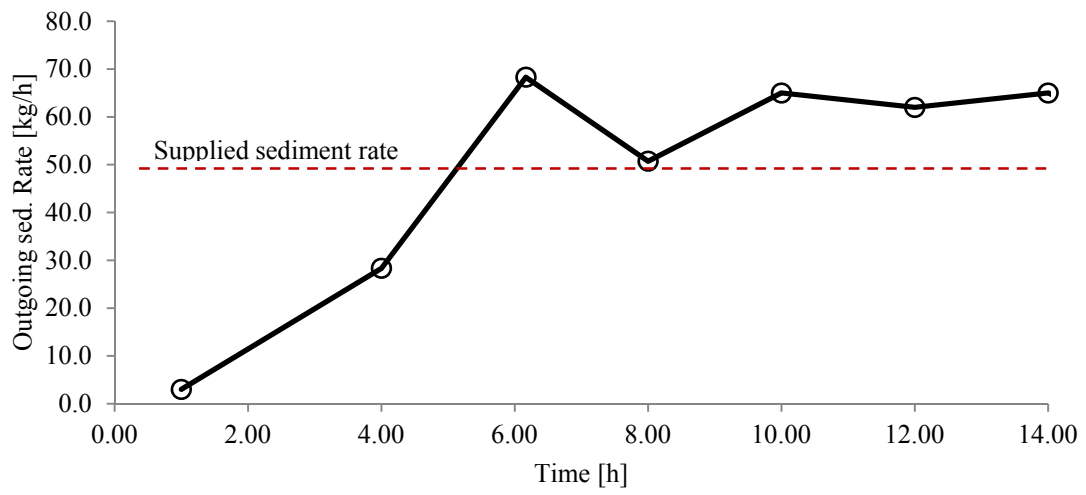
Figure A3.9 Outgoing sediment rates measured during the experiment corresponding to the high discharge ratio with $\alpha = 70°$. Dashed line represents the supplied sediment rate.

A4

Experimental set IV

In this appendix, graphical representations of the measurements performed in the experimental set IV are displayed for every experiment. The following information is shown for each experiment:
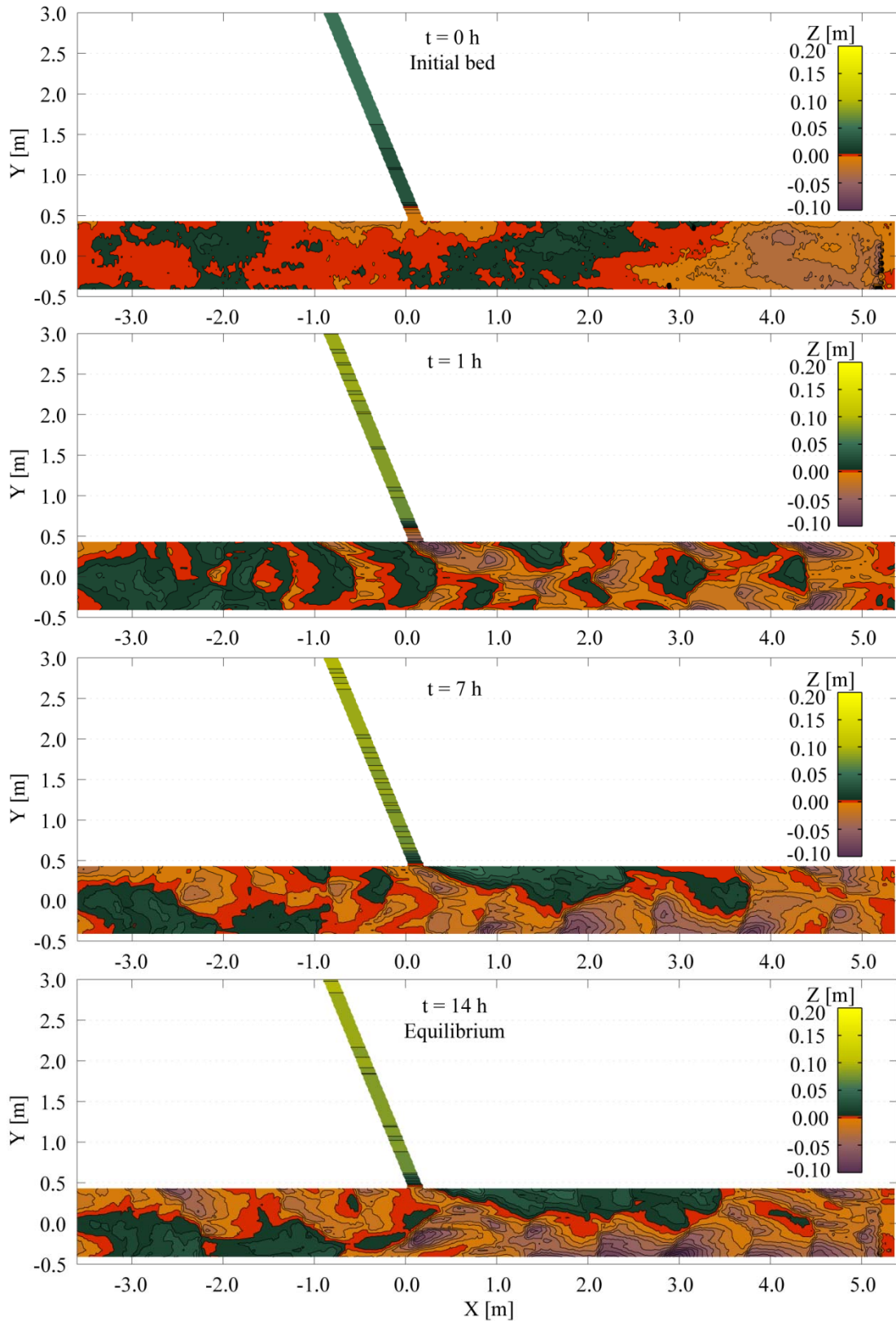
- Bed topography at the times $t = 0$ h, $t = 1$ h, $t = 7$ h, and at equilibrium.
- Profiles of the bed elevation and water surface measured during the experiment along the inner bank of the main channel, outer bank of the main channel and tributary axis.
- Outgoing sediment rates measured at the downstream end of the main channel to assess the equilibrium condition during the experiments.

The values of the discharge ratio (Q_r), unit-discharge ratio (q_r), junction angle (α), sediment gradation coefficient (σ), and width ratio (B_t/B_m) adopted in each experiment of the experimental set IV are given in Table A4.1

Table A4.1. Summary of the main parameters adopted in experimental set IV

| Experiment	Q_r [-]	q_r [-]	α [°]	σ [-]	B_t/B_m [-]	Results discussed in chapter
Low discharge ratio (LR)	0.06	0.37	70°	1.35	0.15	7
Intermediate discharge ratio (IR)	0.07	0.50	70°	1.35	0.15	7
High discharge ratio (HR)	0.11	0.77	70°	1.35	0.15	7

4.1 Low discharge ratio ($Q_r = 0.06$, $q_r = 0.37$)

Figure A4.1 Bed topography for the low discharge ratio with $\alpha = 70°$ at the measuring times a) $t = 0$ h, b) $t = 1$ h, c) $t = 7$ h, and d) $t = 14$ h (equilibrium). P_1 to P_5 indicate the position of the checkpoints to assess equilibrium.
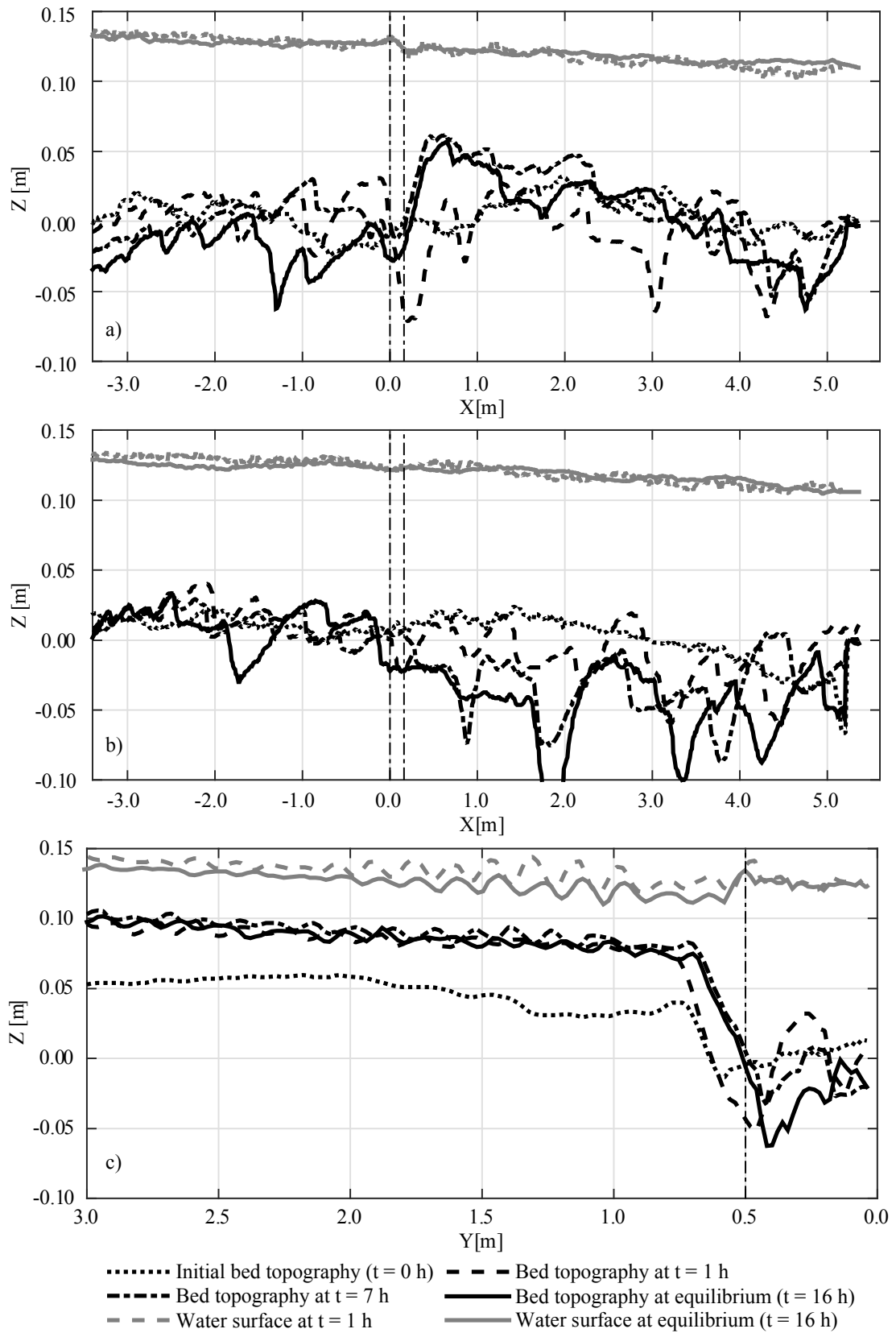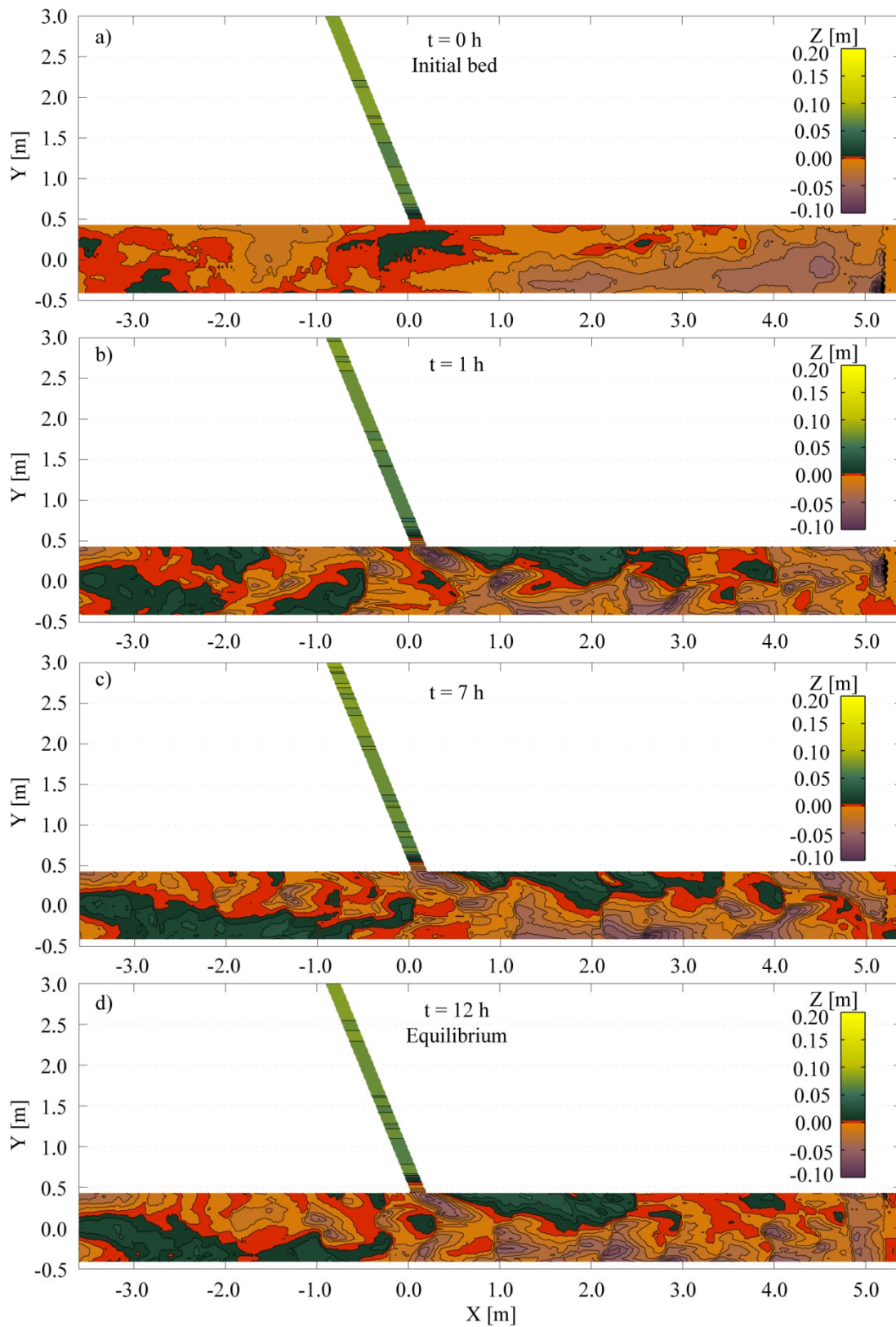
Figure A4.2 Profiles of the bed elevation and water surface during the experiment along the a) inner bank of the main channel ($Y = 0.45$ m), b) outer bank of the main channel ($Y = - 0.45$ m), and c) tributary axis. The values correspond to the low discharge ratio with $\alpha = 70°$.
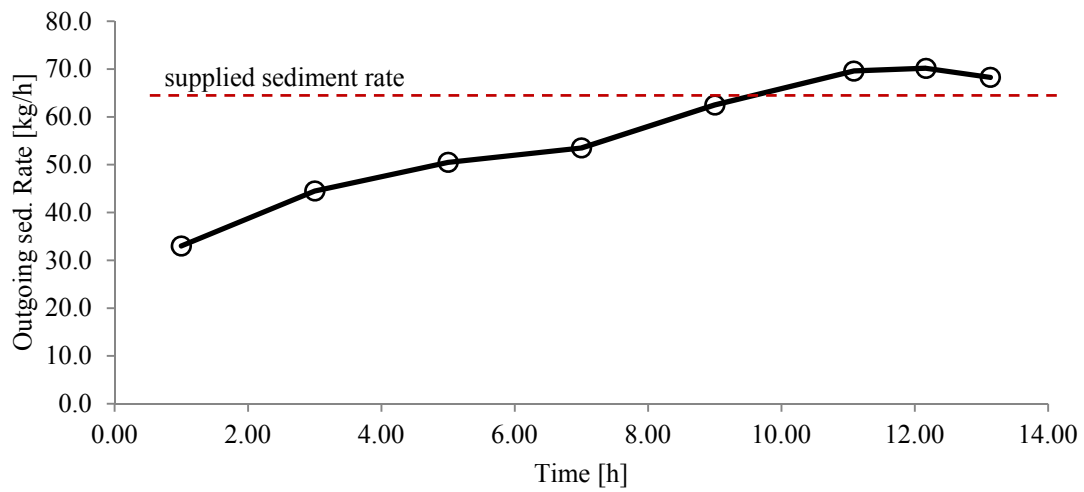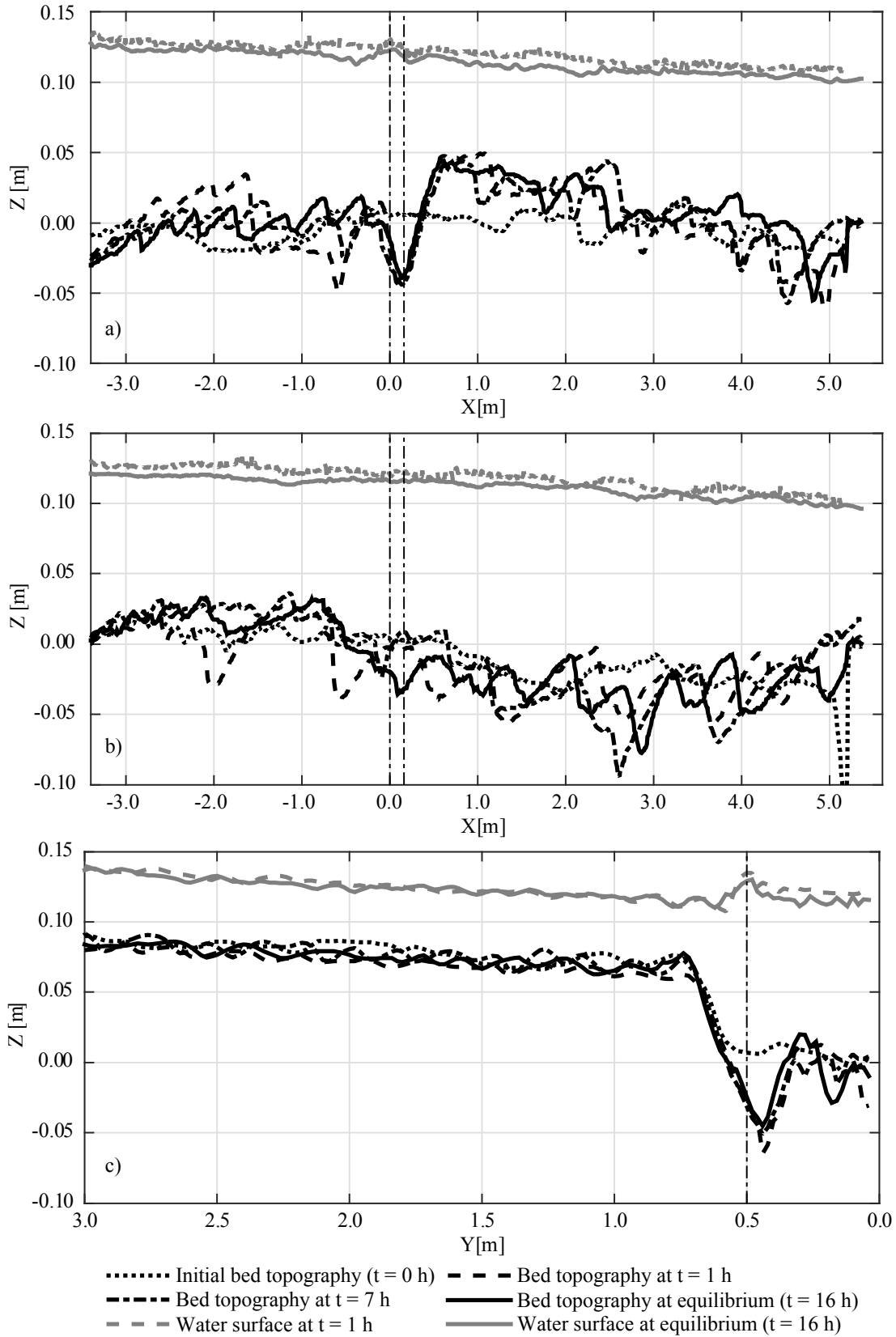
Figure A4.3 Outgoing sediment rates measured during the experiment corresponding to the low discharge ratio with $\alpha = 70°$. Dashed line represents the supplied sediment rate.

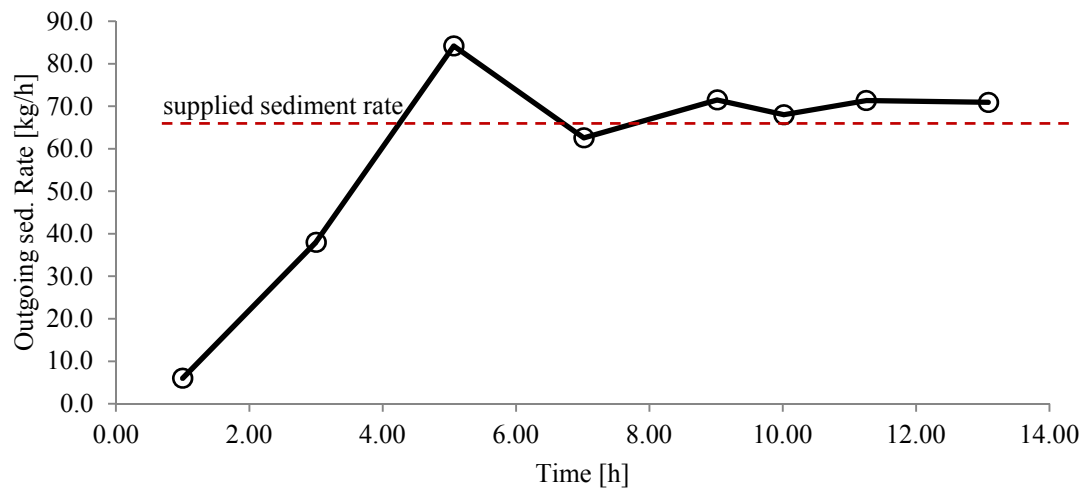## 4.2 Intermediate discharge ratio ($Q_r = 0.07$, $q_r = 0.50$)

Figure A4.4 Bed topography for the intermediate discharge ratio with $\alpha = 70°$ at the measuring times a) $t = 0$ h, b) $t = 1$ h, c) $t = 7$ h, and d) $t = 12$ h (equilibrium). P_1 to P_5 indicate the position of the checkpoints to assess equilibrium.

Figure A4.5 Profiles of the bed elevation and water surface during the experiment along the a) inner bank of the main channel ($Y = 0.45$ m), b) outer bank of the main channel ($Y = -0.45$ m), and c) tributary axis. The values correspond to the intermediate discharge ratio with $\alpha = 70°$.

Figure A4.6 Outgoing sediment rates measured during the experiment corresponding to the intermediate discharge ratio with $\alpha = 70°$. Dashed line represents the supplied sediment rate.

4.3 High discharge ratio ($Q_r = 0.11$, $q_r = 0.77$)

Figure A4.7 Bed topography for the high discharge ratio with $\alpha = 70°$ at the measuring times a) $t = 0$ h, b) $t = 1$ h, c) $t = 7$ h, and d) $t = 12$ h (equilibrium). P_1 to P_5 indicate the position of the checkpoints to assess equilibrium.
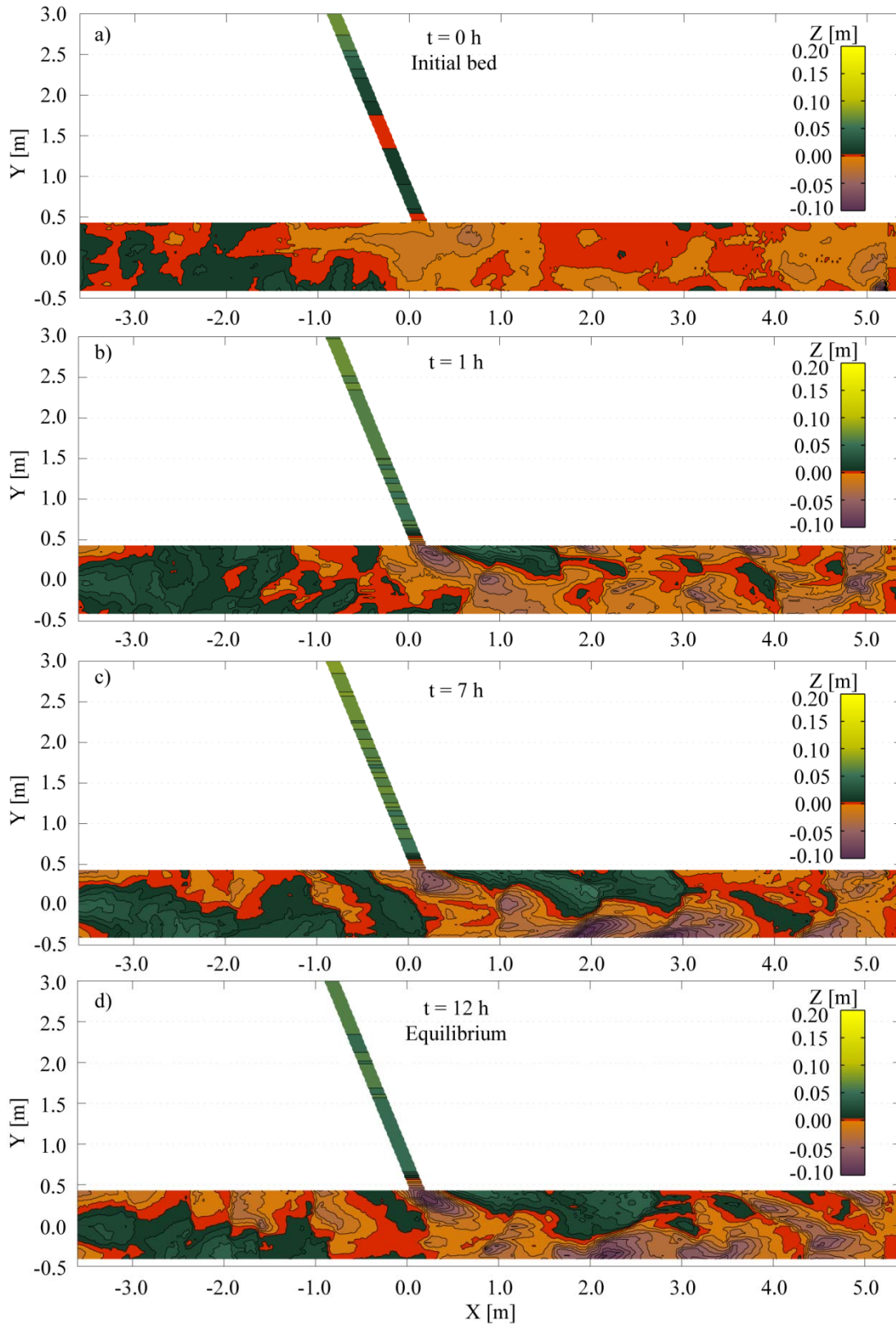
158

Figure A4.8 Profiles of the bed elevation and water surface during the experiment along the a) inner bank of the main channel ($Y = 0.45$ m), b) outer bank of the main channel ($Y = -0.45$ m), and c) tributary axis. The values correspond to the high discharge ratio with $\alpha = 70°$.
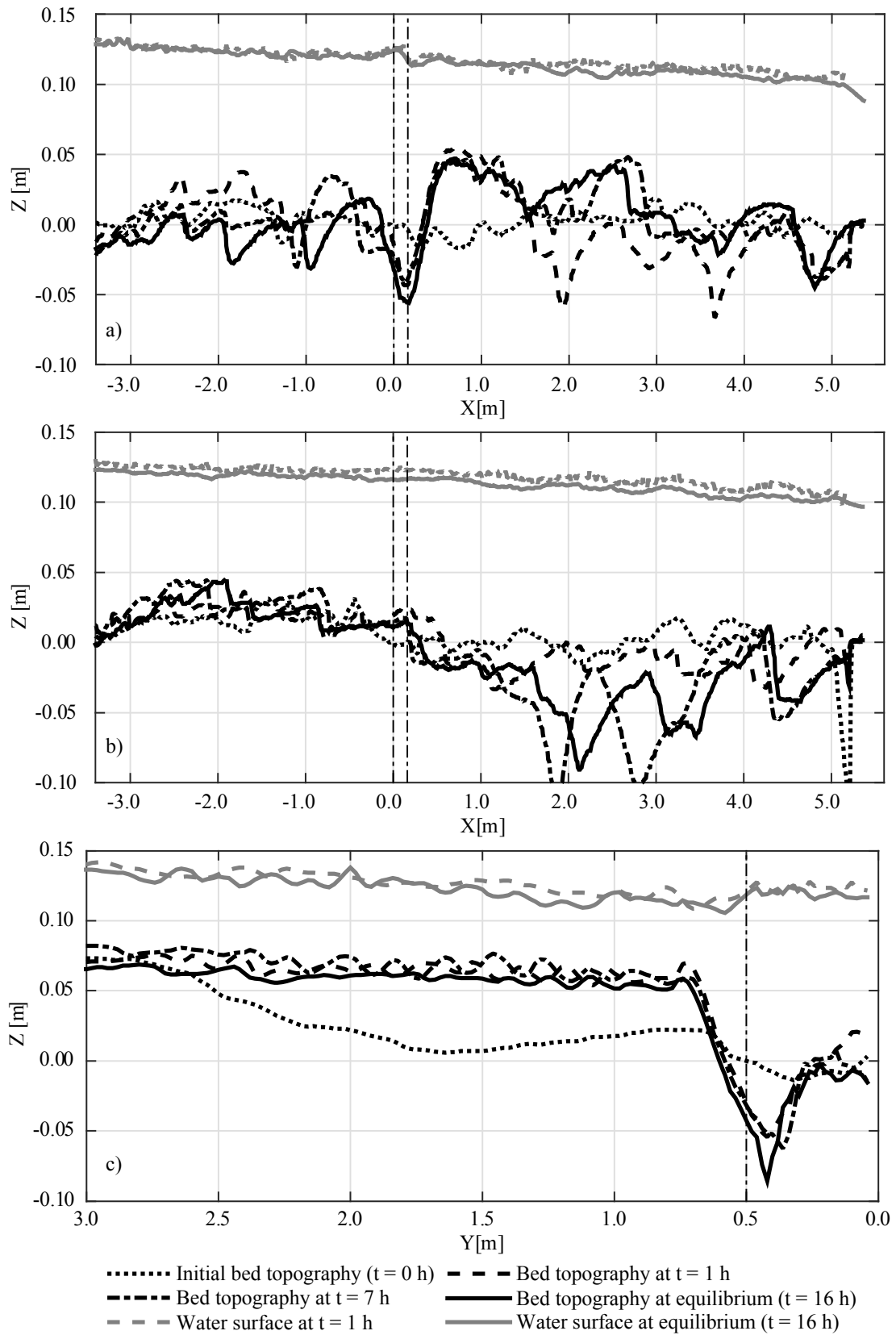
Figure A4.9 Outgoing sediment rates measured during the experiment corresponding to the high discharge ratio with $\alpha = 70°$. Dashed line represents the supplied sediment rate.

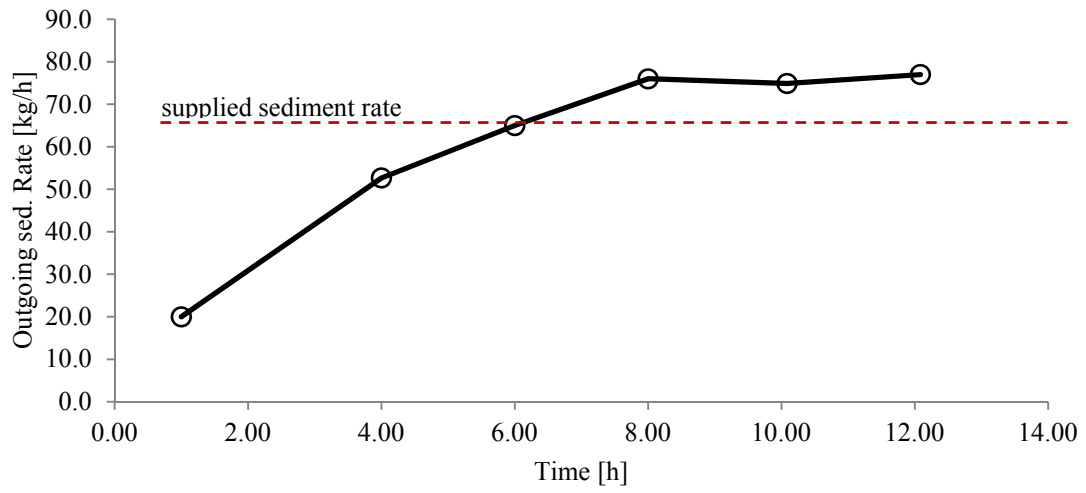# SEBASTIÁN GUILLÉN LUDEÑA

CIVIL ENGINEER

+ CONTACT

Mobile 1	+34 696722411
Mobile 2	+41 79 625 06 71
Email	sebastian.ludena@epfl.ch
Nationality	Spanish
Date of birth	December 10, 1981

+ EDUCATION

Aug. 2011 – Oct. 2015 IST-EPFL Joint Doctoral Initiative	**PhD** Thesis title: *Hydro-morphodynamics of open-channel confluences with low discharge ratio and dominant tributary sediment supply*
Feb. 2007 – Oct. 2010 Technical University of Madrid (Spain)	**Diploma of Advanced Studies (DEA)** Program of hydraulics and energy
Sept. 2000 – Sept. 2006 Technical University of Madrid (Spain)	**Civil Engineer** Specialized in hydraulics and energy

+ WORK EXPERIENCE

Aug. 2011 – Oct 2015 École Polytechnique Fédérale de Lausanne (Switzerland)	**Research Assistant** Thesis on dynamics of river confluences Experimental study of the hydrodynamic, morphodynamic and sedimentary processes involved in river confluences
May. 2008 – Jul. 2011 PROSER S.A. Madrid (Spain)	**Civil engineer** Design of irrigation networks, earth dams, pumping stations and hydropower plants. Numerical simulation of transient flows in complex pipe networks Numerical simulation of flood events with 1D and 2D hydrodynamic models
Aug. 2006 – Apr. 2008 GIS S.A. MADRID (Spain)	**Civil engineer** Supervision and technical assistance during the construction of a water treatment plant Supervision and technical assistance during the construction of a 3.5 MW hydropower plant.

+ RESEARCH ACTIVITIES

Nov. 2013 – Dec. 2014 LCH-EPFL, Lausanne (Switzerland)	**Research assistant** Numerical simulation of rock/ice avalanche impacts over glacier lakes. Client: NELAK-Project (UZH-EPFL)
Aug. 2013 – Dic. 2013 LCH-EPFL, Lausanne (Switzerland)	**Research assistant** Numerical simulation of the glacier-lake outburst in Laguna 513-Peru. Client: Proyecto Glaciares and COSUDE
Sept. 2012 – May 2013 LCH-EPFL, Lausanne (Switzerland)	**Research assistant** Physical modeling of the Kariba dam's plunge pool. Client: COYNE ET BELLIER – GDF SUEZ
Feb. 2008 – Dic. 2008 Technical University of Madrid (Spain)	**Research Grant Carlos González Cruz** Optimization of irrigation networks

+ LANGUAGES

Fluent	Spanish (mother tongue), English and Portuguese
Knowledge	French

+ IT. SKILLS

Operating systems	Windows
Computational tools	Office, CAD, GIS, Matlab, ClawPack, IBER, Basement, HEC-RAS, HEC-HMS

+ PUBLICATIONS IN SCIENTIFIC JOURNALS

Guillén-Ludeña, S*.,* Franca, M. J*.,* Cardoso, A. H*., and* Schleiss, A. J*. (*2015*) Hydro-morphodynamic evolution in a 90° movable bed discordant confluence with low discharge ratio.* Earth Surf. Process. Landforms*, doi:* 10.1002/esp.3770*.*

Schneider, D., Huggel, C., Cochachin, A., **Guillén, S**., and García, J.(2014) *Mapping hazards from glacier lake outburst floods based on modelling of process cascades at Lake 513, Carhuaz, Peru*, Adv. Geosci., 35, 145-155, doi:10.5194/adgeo-35-145-2014.

+ INTERNATIONAL CONFERENCES

Guillen-Ludeña, S. (2015). *Hydro-morphodynamic differences induced by different angles in an experimental discordant confluence*. In Proceedings of 36th IAHR World Congress. Deltas of the future. Delft - The Hage.

Birjukova, O., **Guillen-Ludeña, S.**, Alegria, F., and Cardoso, A. H. (2014). *Three dimensional flow field at confluent fixed-bed open channels*. In Proceeding River Flow. (pp. 1007–1014).

Guillén Ludeña, S., Franca, M. J., Schleiss, A. J., and Cardoso, A. H. (2014). *Morphodynamic differences induced by different confluence angles in widen confluence*s. In Proceedings River Flow 2014 (pp. 983–988). CRC Press 2014. doi:10.1201/b17133-133

Guillén-Ludeña, S., Franca, M. J., Schleiss, A. J., and Cardoso, A. H. (2014). *Bed topography evolution in a discordant bed channel confluence*. Proceedings of 3rd IAHR Europe Congress, (1), 1–10.

Guillén, S., Franca, M. J., Schleiss, A. J., and Cardoso, A. H. (2013). *Influence of the Convergence Angle on the Morphodynamics of Discordant Bed Confluence*s. Proceedings of 2013 IAHR World Congress. A10699, (1987), 1–12. Chengdu (China).